DISSERTATION | DOCTORAL THESIS

Titel | Title

Evaluating the effect of candidate prebiotics in the human gut microbiota by activity-based cell sorting and targeted isolation

verfasst von | submitted by

Dipl.-Ing. Hamid Rasoulimehrabani

angestrebter akademischer Grad | in partial fulfilment of the requirements for the degree of

Doctor of Philosophy (PhD)

Wien | Vienna, 2025

Studienkennzahl lt. Studienblatt | Degree programme code as it appears on the student record sheet:	UA 794 685 437
Dissertationsgebiet lt. Studienblatt | Field of study as it appears on the student record sheet:	Biologie
Betreut von | Supervisor:	Univ.-Prof. David Berry Privatdoz. PhD

To my wife and my son, who bear with my weariness.

Acknowledgements

Although acknowledgements appear at the beginning of this thesis, they are the very last part I have written. At first, I thought this would be the easiest section, but in reality it turned out to be one of the hardest, because looking back on this long journey as a PhD student and thinking about the past years, with all the failures and successes, and remembering the people who stood by me and supported me was not easy.

First and foremost, I want to express my deepest gratitude to David Berry for giving me the opportunity to join his lab and become part of the gut group. Coming from an engineering background, completely new to biology, there were many days when I felt frustrated, overwhelmed, and even close to giving up. What kept me going was David's constant support, guidance, and encouragement. Your openness, patience, and positivity motivated me to keep trying harder and harder. Especially during the writing phases of my papers, your advice was invaluable. Without your belief in me, I would not be here today finishing this thesis. Thank you for teaching me, guiding me, and giving me the chance to grow as a researcher. I also want to sincerely thank Georgi Nikolov, my very first trainer in the lab. You were the one who handed me my first pipette and patiently showed me the basics of experimental work. Thank you for all the time you spent teaching me, and for the friendship, morning coffees, and chats we shared. You made my first steps in biology possible and memorable. My thanks also go to Alessandra Riva, for your collaboration in designing these wonderful projects and for introducing me to so many exciting methods. I learned so much from you in the lab and always enjoyed working on these projects together. I am also grateful to Markus Schmid and Marton Palatinszky, my heroes in Raman spectroscopy, from whom I learned so much. A very special thanks to Kang Soo Lee for always being available, even from afar, to patiently explain RACS to me and troubleshoot countless problems over calls and video meetings. Without your help, I would not have understood the details of this technique, which remains one of the most fascinating methods I had the chance to use.

To all the postdocs of the gut group: Fatima Pereira, whose depth of knowledge always amazed me, Michaela Lang, Stephanie Schnorr, and Adnan Hodžić, thank you for your generosity, guidance, and for making me feel that I could always approach you with questions without hesitation. Working alongside you was an invaluable opportunity to learn and grow. I would also like to thank my students Sanaz Khadem and Deniz Inan for their dedication and hard work, and for generating valuable data for our projects. My gratitude also goes to Miriam Philipp, Norbert Hieger and all the other students who supported me in the lab. Thanks to Martin Kunert for his help with microscopy and for co-organizing many enjoyable and fun office meetings and lunches at the OAK pub. I also thank Marc Mußmann for his guidance on using the BD FACSMelody. To all members of the gut group, thank you for the scientific discussions, the laughter, and the many memorable moments we shared. I am especially grateful to my wonderful office mates, Paula Rojas, Huifeng Hu, Sarah Al-Ajeel, Marie Rutsch, and Alejandro Llanos Lizcano. You were not only colleagues but also close friends. Paula and Sara, you were always there during both the good times and the exhausting ones, listening to my endless complaints and making me feel better afterwards. You were also the first people I asked my basic biology questions before ChatGPT came into my life. Without you, this long road would have been much harder. My heartfelt thanks extend to everyone at DOME for their constant help, encouragement, and friendship over these years. This journey began just before the COVID pandemic and carried on through to today, and I am deeply grateful for all the support and positive energy I received along the way.

Outside of academia, my biggest thanks go to my family. To my wife Forough Soltanieh, your support during this journey has been incredible. Without your understanding, patience, and encouragement, I cannot imagine finishing this PhD. Thank you for standing by me, even during the stressful times when experiments failed, results did not meet expectations, or deadlines consumed my energy. Your love and belief in me carried me through. To my son Hamoun, your birth has been the most important and beautiful event of my life. Your smiles have already given me more motivation than anything else. You have changed my daily life into something richer

and more meaningful. I am sorry for the times when I was too tired to give you all the attention you deserved, but I am endlessly grateful for the joy you brought into my life. To my mother and my brother, thank you for always being the first readers of my papers and for supporting me unconditionally. Mom, your belief in me and your constant encouragement gave me strength whenever I felt stuck. Finally, to my father, whom I lost eight years ago. I have thought of you every single day during this journey. I know how proud you would have been to see this thesis completed, as education was always so important to you. Your photo was always on my desk while I was writing, reminding me of your smile and inspiring me to keep going. To all of you who supported me, taught me, and stood by me in different ways during these years, I thank you from the bottom of my heart.

Table of Contents

Summary

The human gut microbiota plays an important role in maintaining host health by influencing metabolism, immunity, and gut barrier integrity. The composition of the gut microbiota is strongly influenced by dietary habits, particularly through the action of prebiotics, which are non-digestible polysaccharides that can promote the selective growth of beneficial gut bacteria. However, the mechanisms by which distinct prebiotics exert selective effects on specific gut bacteria and drive functional changes remain incompletely understood.

This thesis addresses these knowledge gaps by developing and applying integrative single-cell and community-level approaches to comprehensively identify and functionally characterize prebiotic-responsive bacteria in the human gut. Focusing on xylooligosaccharides (XOS), lactulose, and arabinogalactan (AG) as model substrates, I combined high-resolution 16S rRNA gene sequencing with advanced cell sorting strategies including BONCAT-FACS and Raman-activated cell sorting (RACS) to profile bacterial responses at both the community and single-cell levels. In addition, pure culture and coculture growth experiments were conducted to measure substrate utilization and metabolic activity of isolated strains in response to each prebiotic compound.

The findings demonstrate that XOS exerts a robust bifidogenic effect, consistently increasing both *Bifidobacterium* and *Collinsella*. Lactulose selectively stimulated *Bifidobacterium*, *Collinsella*, and *Lactococcus*. Further analysis revealed cooperative metabolic interactions, where primary degraders supported the growth of non-degrading strains such as *Lactococcus*. Arabinogalactan treatment led to reproducible increases in *Gemmiger* and *Bifidobacterium* across all donors. Detailed analysis identified *Bifidobacterium longum* as a keystone species that promotes broader community benefits through metabolic cross-feeding.

Altogether, these studies provide new insights into how prebiotics differentially shape the gut microbiota, highlighting the importance of substrate specificity, keystone taxa, and microbial cooperation. The integrative experimental framework established here advances our understanding of how prebiotics influence gut microbial communities and serves as a model for designing targeted dietary strategies to promote gut and host health.

Zusammenfassung

Die menschliche Darmmikrobiota spielt eine wichtige Rolle für die Aufrechterhaltung der Gesundheit des Wirts, indem sie den Stoffwechsel, das Immunsystem und die Integrität der Darmbarriere beeinflusst. Die Zusammensetzung der Darmmikrobiota wird maßgeblich durch Ernährungsgewohnheiten beeinflusst, insbesondere durch den Einsatz von Präbiotika, bei denen es sich um nicht verdauliche Polysaccharide handelt, die das selektive Wachstum nützlicher Darmbakterien fördern können. Die Mechanismen, durch die verschiedene Präbiotika gezielte Effekte auf bestimmte Darmbakterien ausüben und funktionelle Veränderungen hervorrufen, sind jedoch noch nicht vollständig geklärt.

In dieser Arbeit wurden diese Wissenslücken durch die Entwicklung und Anwendung eines integrativen Ansatzes auf Einzelzell- und Gemeinschaftsebene adressiert, um präbiotika-reaktive Bakterien im menschlichen Darm umfassend zu identifizieren und funktionell zu charakterisieren. Im Fokus standen dabei Xylooligosaccharide (XOS), Lactulose und Arabinogalactan (AG) als Modellsusbstrate. Hierzu wurden hochauflösende 16S rRNA-Gen-Sequenzierungen mit fortschrittlichen Zellsortierungsverfahren, darunter BONCAT-FACS und Raman-aktivierte Zellsortierung (RACS), kombiniert, um bakterielle Reaktionen sowohl auf Gemeinschafts- als auch auf Einzelzellebene zu analysieren. Darüber hinaus wurden Reinkultur- und Kokultur-Experimente durchgeführt, um die Substratnutzung und die metabolische Aktivität isolierter Stämme als Reaktion auf die jeweiligen Präbiotika zu bestimmen.

Die Ergebnisse zeigen, dass XOS eine starke bifidogene Wirkung entfaltet und sowohl *Bifidobacterium* als auch Collinsella zuverlässig fördert. Lactulose stimulierte selektiv *Bifidobacterium, Collinsella* und *Lactococcus*. Weiterführende Analysen zeigten kooperative metabolische Interaktionen, bei denen primäre Abbauer das Wachstum nicht abbauender Stämme wie *Lactococcus* unterstützten. Die Behandlung mit Arabinogalactan führte bei allen Spendern zu einer reproduzierbaren Zunahme von *Gemmiger* und *Bifidobacterium*. Detaillierte Untersuchungen identifizierten Bifidobacterium longum als Schlüsselspezies, die durch metabolisches Cross-Feeding breitere Gemeinschaftsvorteile fördert.

Insgesamt liefern diese Studien neue Erkenntnisse darüber, wie Präbiotika die Darmmikrobiota unterschiedlich beeinflussen und unterstreichen die Bedeutung von Substratspezifität, Schlüsseltaxa und mikrobieller Kooperation. Der hier entwickelte integrative experimentelle Ansatz vertieft unser Verständnis darüber, wie Präbiotika die mikrobiellen Gemeinschaften im Darm beeinflussen, und dient als Modell für die Entwicklung gezielter Ernährungsstrategien zur Förderung der Darm- und Wirtsgesundheit.

Introduction

The Complex Role of Human Gut Microbiota

The human gut microbiota is a highly complex and dynamic ecosystem that plays a central role in host health (Clemente et al., 2012). It influences numerous physiological processes, including metabolism, immune function, and maintenance of the gut barrier (Jyoti & Dey, 2025). This diverse microbial community, consisting of millions of cells and hundreds of bacterial species, closely interacts with the host and adapts to changes in environment and diet (Rowland et al., 2018). The greatest microbial density and diversity are found in the large intestine, which is dominated by the bacterial phyla *Bacillota, Bacteroidota, Actinomycetota*, and *Pseudomonadota*. (He et al., 2022). The composition of the gut microbiota is influenced by several factors, with diet being an important determinant (Nova et al., 2022). Dietary patterns can alter the abundance of specific microbial groups, affecting metabolic activity and the overall functional potential of the microbiota (Nova et al., 2022). Other factors, such as age, genetics, medication use, and environment, also contribute to individual differences in microbiome structure and function (Ahn & Hayes, 2021).

The Role of Prebiotics in Shaping Gut Microbial Communities

A variety of strategies have been developed to modulate the gut microbiota for improved host health, including probiotics, synbiotics, antibiotics, fecal microbiota transplantation, and prebiotics(Ugwu et al., 2024). Prebiotics are substrates that resist digestion in the upper gastrointestinal tract and reach the colon intact, where they are metabolized by specific gut microbes (S. Ali et al., 2025). Through this selective fermentation, prebiotics stimulate the growth and activity of beneficial bacteria, leading to shifts in gut microbiota composition (S. Ali et al., 2025). These microbial changes are associated with increased production of short-chain fatty acids (SCFAs), which help maintain intestinal barrier integrity, modulate immune responses, and support metabolic health (Sankarganesh et al., 2025). By enhancing beneficial taxa and microbial

metabolite production, prebiotics contribute to better digestive function and may help protect against various gastrointestinal and systemic disorders (Kumar et al., 2025).

Inulin, fructooligosaccharides (FOS), and galactooligosaccharides (GOS) are well established prebiotics that have been shown to support beneficial gut bacteria (Carlson et al., 2018). In addition to these, compounds such as xylooligosaccharides (XOS), lactulose, and arabinogalactan (AG) have gained attention for their potential to selectively stimulate health associated members of the gut microbiota (Karakan et al., 2021; Y. Sun et al., 2021; Valladares-Diestra et al., 2023). Ongoing research continues to identify and characterize new prebiotic candidates, broadening our understanding of how different dietary substrates influence gut microbial communities.

Knowledge Gaps in Prebiotic Mechanisms and Microbial Interactions

Despite significant progress in prebiotic research, the mechanisms by which candidate prebiotics exert selective effects on specific gut bacteria and induce functional changes within the microbial community remain incompletely understood. The gut microbiota displays remarkable inter-individual variation, not only in community composition but also in metabolic potential and response to dietary intervention (Leeming et al., 2019). Understanding which taxa respond to particular prebiotics, and how these responses are mediated at the functional and ecological levels, is central to the rational design of targeted dietary interventions. Furthermore, the complex metabolic networks within the gut often involve cooperative interactions, such as metabolic cross-feeding, in which primary degraders of a substrate produce metabolites that support the growth of secondary consumers (Culp & Goodman, 2023). Characterizing these interactions requires approaches that go beyond conventional community profiling and incorporate both community-level and single-cell analyses (Shetty et al., 2022).

Research Approach and Methodological Advances

In this context, my doctoral research aimed to identify, isolate, and characterize gut bacteria that respond to specific prebiotic substrates, with a particular focus on three compounds: XOS, lactulose, and AG. These model prebiotics were chosen to reflect both naturally derived and synthetic substrates, and to explore differences in microbial selectivity, metabolic pathways, and

ecological interactions. To address the challenges of resolving functional responses within a highly diverse microbiota, we employed an integrative experimental framework that combined high-resolution 16S rRNA gene sequencing, advanced single-cell sorting technologies such as biorthogonal non-canonical amino acid tagging with fluorescence-activated cell sorting (BONCAT FACS) and Raman activated cell sorting (RACS), as well as targeted growth and coculture assays to directly measure substrate utilization and microbial interactions (Riva et al., 2023). This combined approach allowed us to directly identify both primary degraders, which are microbes capable of breaking down prebiotic substrates, and non-degrading taxa that benefit from the metabolic activities of others. It also enabled a detailed mapping of cooperative interactions between strains within the gut microbiota.

Xylooligosaccharides (XOS) and Bifidogenic Selectivity

Xylooligosaccharides (XOS) are short-chain oligosaccharides composed of xylose units. These units are connected by β-1,4-glycosidic bonds (K. Ali et al., 2025). These compounds are recognized for their ability to promote the growth of beneficial gut bacteria, especially *bifidobacteria* (Zhao et al., 2021). They are typically produced by the partial hydrolysis of xylan, a major hemicellulose found in plant cell walls of materials such as corncobs, wheat bran, rice bran, sugarcane bagasse, and certain hardwoods (K. Ali et al., 2025). In our study, we used XOS produced industrially from plant biomass to ensure consistency and purity for experimental purposes. XOS are produced through the enzymatic hydrolysis of xylan. In this process, endo-xylanases cleave the β-1,4-glycosidic linkages within the xylan backbone. This enzymatic action converts xylooligomers into shorter-chain xylooligosaccharides while minimizing the production of xylose (Manicardi et al., 2023). This method is efficient in producing XOS with a high degree of polymerization, which is desirable for their prebiotic effects (Manicardi et al., 2023).

In my first project, I focused on the ability of XOS to stimulate specific microbial groups using an activity-based cell sorting approach. The results demonstrated a consistent and pronounced enrichment of *Bifidobacterium* and *Collinsella aerofaciens* across donors, confirming previous

observations of XOS as a potent bifidogenic substrate (Z. Sun et al., 2022). The identification of metabolically active strains and their physiological validation in pure culture experiments underscored the selectivity of XOS and the importance of substrate structure in determining microbial responses. Notably, targeted isolation using RACS revealed not only established bifidogenic species but also previously unrecognized taxa capable of utilizing XOS, expanding the known diversity of responsive bacteria (Riva et al., 2023).

Lactulose Selective Stimulation and Cooperative Interactions

The second project focused on lactulose, a synthetic disaccharide composed of galactose and fructose (Vičič et al., 2024). Lactulose is not found naturally but is produced industrially by isomerizing lactose (Vičič et al., 2024). Clinically, it is widely used as a laxative for treating constipation and hepatic encephalopathy, where it helps reduce blood ammonia levels (Aït-Aissa & Aïder, 2014; Vilstrup et al., 2014). Beyond these medical uses, lactulose has gained attention at lower doses for its potential as a prebiotic, as research indicates it can selectively stimulate the growth of beneficial gut bacteria such as *bifidobacteria* (Karakan et al., 2021). This dual role makes lactulose a valuable candidate for both therapeutic and nutritional interventions that modulate the gut microbiota.

Despite these recognized benefits, the full range of bacterial groups responsive to lactulose and the ecological mechanisms underlying these effects have not been fully characterized. In my study, we found that lactulose is unique among prebiotics in its ability to promote the growth of specific gut bacteria, particularly *Bifidobacterium* and *Collinsella*, while also enhancing the metabolic activity of taxa such as *Lactococcus* (Rasoulimehrabani et al., 2025). Using an integrative workflow that combined BONCAT-FACS, RACS, and RNA sequencing, we were able to identify both primary lactulose degraders and non-degraders that benefited from cross-feeding interactions. Physiological and coculture experiments demonstrated that while *Lactococcus lactis* cannot degrade lactulose directly, its growth is enhanced by metabolic byproducts released from *Bifidobacterium adolescentis* and *Collinsella aerofaciens* (Rasoulimehrabani et al., 2025). These findings highlight the importance of cooperative interactions and ecological facilitation in shaping

prebiotic responses within the gut microbiota. Additionally, gene expression analysis identified a β-galactosidase gene that was highly upregulated in *B. adolescentis* when grown on both lactose and lactulose, providing mechanistic insight into the enzymatic basis of lactulose degradation.

Arabinogalactan Selectivity and Microbial Interactions in the Gut

Arabinogalactan is a complex plant-derived polysaccharide composed of arabinose and galactose that is naturally present in a variety of foods such as carrots, radishes, pears, and tomatoes, with particularly high concentrations in larch trees (Dion et al., 2016). This compound was the focus of my third project. While arabinogalactan has been proposed as a functionally selective prebiotic, the specific taxa involved in its metabolism and the dynamics of cooperative interactions remained incompletely defined. Research has shown that arabinogalactan is relatively selective in its prebiotic effects, favoring the growth of beneficial bacteria such as *Bifidobacterium* and *Faecalibacterium*, which are known to play key roles in maintaining gut health and immune function(He et al., 2022). Nevertheless, the complete spectrum of arabinogalactan degrading bacteria in the gut, including both primary degraders and secondary consumers, is still not fully understood. Further research is needed to identify a broader array of taxa capable of utilizing arabinogalactan and to clarify their distinct functional roles and interactions within the gut microbial ecosystem. Using a combination of community-level sequencing, single-cell Raman microspectroscopy, RACS, and coculture experiments, we showed that arabinogalactan supplementation consistently enriched *Bifidobacterium* and *Gemmiger* across all donors. *Bifidobacterium longum* emerged as a keystone species, efficiently degrading arabinogalactan and facilitating the growth of non-degrading strains via metabolic cross-feeding . Interestingly, while *Gemmiger* exhibited consistent enrichment at the community level, it was not recovered as a metabolically active isolate. This may reflect challenges in cultivation or specific growth requirements. Our experimental results also showed that the activity of *B. longum* provided broader benefits to the microbial community. This highlights the importance of keystone taxa like *B. longum* in facilitating cooperative interactions and supporting the stability and function of the gut ecosystem.

Significance and Impact of This Research

The research presented in this thesis demonstrates how an integrative, multi-method approach can uncover both compositional changes and functional dynamics within the human gut microbiota in response to selective prebiotics. We studied three different prebiotics: XOS, lactulose, and arabinogalactan. Our findings highlight that the structure of the substrate, microbial diversity at the strain level, and the presence of cooperative metabolic networks are key determinants of which bacteria are stimulated and how the overall function of the microbial community is altered. This work advances our understanding of how prebiotics selectively shape gut microbial communities by revealing the mechanisms underlying these effects. By integrating high-resolution molecular profiling, single-cell sorting, and physiological validation, the research goes beyond basic community descriptions to uncover the enzymatic pathways, ecological interactions, and cooperative networks that drive microbial responses to dietary substrates. The studies highlight how specific enzymes are upregulated during prebiotic use, and how cross-feeding interactions between microbial strains can support the growth of non-degrading species. Although the precise metabolites involved in these interactions were not identified, the research clearly demonstrates the importance of interspecies cooperation and the key role of certain bacterial taxa in structuring the gut microbiota. These findings clarify the selective interactions between prebiotics and the gut microbiota, which could inform the development of customized nutritional strategies for modulating the microbiome.

References

Ahn, J., & Hayes, R. B. (2021). Implications for Noncommunicable Disease. *Annu Rev Public Health.*, *47*, 277–292. https://doi.org/10.1146/annurev-publhealth-012420-105020.Environmental

Aït-Aissa, A., & Aïder, M. (2014). Lactulose: Production and use in functional food, medical and pharmaceutical applications. Practical and critical review. *International Journal of Food Science and Technology*, *49*(5), 1245–1253. https://doi.org/10.1111/ijfs.12465

Ali, K., Niaz, N., Waseem, M., Ashraf, W., Hussain, M., Khalid, M. U., Tahir, A. Bin, Raza, A., & Khan, I. M. (2025). Xylooligosaccharides: A comprehensive review of production, purification, characterization, and quantification. *Food Research International*, *201*(October 2024), 115631. https://doi.org/10.1016/j.foodres.2024.115631

Ali, S., Hamayun, M., Siraj, M., Khan, S. A., Kim, H. Y., & Lee, B. (2025). Recent advances in prebiotics: Classification, mechanisms, and health applications. *Future Foods*, *12*(February), 100680. https://doi.org/10.1016/j.fufo.2025.100680

Carlson, J. L., Erickson, J. M., Lloyd, B. B., & Slavin, J. L. (2018). Health effects and sources of prebiotic dietary fiber. *Current Developments in Nutrition*, *2*(3), 1–8. https://doi.org/10.1093/cdn/nzy005

Clemente, J. C., Ursell, L. K., Parfrey, L. W., & Knight, R. (2012). The impact of the gut microbiota on human health: An integrative view. *Cell*, *148*(6), 1258–1270. https://doi.org/10.1016/j.cell.2012.01.035

Culp, E. J., & Goodman, A. L. (2023). Cross-feeding in the gut microbiome: Ecology and mechanisms. *Cell Host & Microbe*, *31*(4), 485–499. https://doi.org/10.1016/j.chom.2023.03.016

Dion, C., Chappuis, E., & Ripoll, C. (2016). Does larch arabinogalactan enhance immune function? A review of mechanistic and clinical trials. *Nutrition and Metabolism*, *13*(1). https://doi.org/10.1186/s12986-016-0086-x

He, H., Sun, Y., Zhang, S., Zhang, H., Su, W., Guo, Z., Zhang, Y., Wen, J., Li, X., Hu, J., & Nie, S. (2022). Arabinogalactan, Bifidobacterium longum, and Faecalibacterium prausnitzii improve insulin resistance in high-fat diet-induced C57BL/6J mice. *EFood*, *3*(1–2), 1–19. https://doi.org/10.1002/efd2.1

Jyoti, & Dey, P. (2025). Mechanisms and implications of the gut microbial modulation of intestinal metabolic processes. *Npj Metabolic Health and Disease*, *3*(1), 1–19. https://doi.org/10.1038/s44324-025-00066-1

Karakan, T., Tuohy, K. M., & Janssen-van Solingen, G. (2021). Low-Dose Lactulose as a Prebiotic for Improved Gut Health and Enhanced Mineral Absorption. *Frontiers in Nutrition*, *8*(July), 1–15. https://doi.org/10.3389/fnut.2021.672925

Kumar, S., Mukherjee, R., Gaur, P., Leal, É., Lyu, X., Ahmad, S., Puri, P., Chang, C. M., Raj, V. S., &

Pandey, R. P. (2025). Unveiling roles of beneficial gut bacteria and optimal diets for health. *Frontiers in Microbiology*, *16*(February), 1–14. https://doi.org/10.3389/fmicb.2025.1527755

Leeming, E. R., Johnson, A. J., Spector, T. D., & Roy, C. I. L. (2019). Effect of diet on the gut microbiota: Rethinking intervention duration. *Nutrients*, *11*(12), 1–28. https://doi.org/10.3390/nu11122862

Manicardi, T., Baioni e Silva, G., Longati, A. A., Paiva, T. D., Souza, J. P. M., Pádua, T. F., Furlan, F. F., Giordano, R. L. C., Giordano, R. C., & Milessi, T. S. (2023). Xylooligosaccharides: A Bibliometric Analysis and Current Advances of This Bioactive Food Chemical as a Potential Product in Biorefineries' Portfolios. *Foods*, *12*(16). https://doi.org/10.3390/foods12163007

Nova, E., Gómez-Martinez, S., & González-Soltero, R. (2022). The Influence of Dietary Factors on the Gut Microbiota. *Microorganisms*, *10*(7). https://doi.org/10.3390/microorganisms10071368

Rasoulimehrabani, H., Riva, A., Inan, D., Hodžić, A., Hausmann, B., Nikolov, G., Khadem, S., Hieger, N., Wiesenbauer, J., Kaiser, C., Filz, V., Böttcher, T., & Berry, D. (2025). Lactulose selectively stimulates members of the gut microbiota, as determined by multi-modal activity-based sorting. *Gut Microbes*, *17*(1). https://doi.org/10.1080/19490976.2025.2525482

Riva, A., Rasoulimehrabani, H., Cruz-Rubio, J. M., Schnorr, S. L., von Baeckmann, C., Inan, D., Nikolov, G., Herbold, C. W., Hausmann, B., Pjevac, P., Schintlmeister, A., Spittler, A., Palatinszky, M., Kadunic, A., Hieger, N., Del Favero, G., von Bergen, M., Jehmlich, N., Watzka, M., … Berry, D. (2023). Identification of inulin-responsive bacteria in the gut microbiota via multi-modal activity-based sorting. *Nature Communications*, *14*(1), 8210. https://doi.org/10.1038/s41467-023-43448-z

Rowland, I., Gibson, G., Heinken, A., Scott, K., Swann, J., Thiele, I., & Tuohy, K. (2018). Gut microbiota functions: metabolism of nutrients and other food components. *European Journal of Nutrition*, *57*(1), 1–24. https://doi.org/10.1007/s00394-017-1445-8

Sankarganesh, P., Bhunia, A., Ganesh Kumar, A., Babu, A. S., Gopukumar, S. T., & Lokesh, E. (2025). Short-chain fatty acids (SCFAs) in gut health: Implications for drug metabolism and therapeutics. *Medicine in Microecology*, *25*(July), 100139. https://doi.org/10.1016/j.medmic.2025.100139

Shetty, S. A., Kuipers, B., Atashgahi, S., Aalvink, S., Smidt, H., & de Vos, W. M. (2022). Inter-species Metabolic Interactions in an In-vitro Minimal Human Gut Microbiome of Core Bacteria. *Npj Biofilms and Microbiomes*, *8*(1). https://doi.org/10.1038/s41522-022-00275-2

Sun, Y., Hu, J., Zhang, S., He, H., Nie, Q., Zhang, Y., Chen, C., Geng, F., & Nie, S. (2021). Prebiotic characteristics of arabinogalactans during in vitro fermentation through multi-omics analysis. *Food and Chemical Toxicology*, *156*(May), 112522. https://doi.org/10.1016/j.fct.2021.112522

Sun, Z., Yue, Z., Liu, E., Li, X., & Li, C. (2022). Assessment of the bifidogenic and antibacterial activities of xylooligosaccharide. *Frontiers in Nutrition*, *9*(August), 1–10. https://doi.org/10.3389/fnut.2022.858949

Ugwu, O. P. C., Alum, E. U., Okon, M. Ben, & Obeagu, E. I. (2024). Mechanisms of microbiota modulation: Implications for health, disease, and therapeutic interventions. *Medicine (United States)*, *103*(19), E38088. https://doi.org/10.1097/MD.0000000000038088

Valladares-Diestra, K. K., de Souza Vandenberghe, L. P., Vieira, S., Goyzueta-Mamani, L. D., de Mattos, P. B. G., Manzoki, M. C., Soccol, V. T., & Soccol, C. R. (2023). The Potential of Xylooligosaccharides as Prebiotics and Their Sustainable Production from Agro-Industrial by-Products. *Foods*, *12*(14). https://doi.org/10.3390/foods12142681

Vičič, V., Pandel Mikuš, R., & Ferjančič, B. (2024). Review of history and mechanisms of action of lactulose (4-O-β-D-Galactopyranosyl-β-D-fructofuranose): present and future applications in food. *Journal of Food Science and Technology*, *61*(11), 2036–2045. https://doi.org/10.1007/s13197-024-05997-z

Vilstrup, H., Amodio, P., Bajaj, J., Cordoba, J., Ferenci, P., Mullen, K. D., Weissenborn, K., & Wong, P. (2014). Hepatic encephalopathy in chronic liver disease: 2014 Practice Guideline by the American Association for the Study Of Liver Diseases and the European Association for the Study of the Liver. *Hepatology*, *60*(2), 715–735. https://doi.org/10.1002/hep.27210

Zhao, S., Zhang, G. L., Chen, C., Yang, Q., Luo, X. M., Wang, Z. B., Wu, A. M., & Feng, J. X. (2021). A combination of mild chemical pre-treatment and enzymatic hydrolysis efficiently produces xylooligosaccharides from sugarcane bagasse. *Journal of Cleaner Production*, *291*, 125972. https://doi.org/10.1016/j.jclepro.2021.125972

nature communications

Article

https://doi.org/10.1038/s41467-023-43448-z

Identification of inulin-responsive bacteria in the gut microbiota via multi-modal activity-based sorting

Received: 24 September 2023

Accepted: 9 November 2023

Published online: 14 December 2023

Check for updates

Alessandra Riva[1,13], Hamid Rasoulimehrabani[1,2], José Manuel Cruz-Rubio[3], Stephanie L. Schnorr[1], Cornelia von Baeckmann[4], Deniz Inan[1], Georgi Nikolov[1], Craig W. Herbold[1], Bela Hausmann[5,6], Petra Pjevac[1,5], Arno Schintlmeister[1], Andreas Spittler[7], Márton Palatinszky[1], Aida Kadunic[1], Norbert Hieger[1], Giorgia Del Favero[8], Martin von Bergen[9], Nico Jehmlich[9], Margarete Watzka[10], Kang Soo Lee[11], Julia Wiesenbauer[2,10], Sanaz Khadem[1], Helmut Viernstein[3], Roman Stocker[11], Michael Wagner[1,12], Christina Kaiser[10], Andreas Richter[10], Freddy Kleitz[4] & David Berry[1,5]

Prebiotics are defined as non-digestible dietary components that promote the growth of beneficial gut microorganisms. In many cases, however, this capability is not systematically evaluated. Here, we develop a methodology for determining prebiotic-responsive bacteria using the popular dietary supplement inulin. We first identify microbes with a capacity to bind inulin using mesoporous silica nanoparticles functionalized with inulin. 16S rRNA gene amplicon sequencing of sorted cells revealed that the ability to bind inulin was widespread in the microbiota. We further evaluate which taxa are metabolically stimulated by inulin and find that diverse taxa from the phyla *Firmicutes* and *Actinobacteria* respond to inulin, and several isolates of these taxa can degrade inulin. Incubation with another prebiotic, xylooligosaccharides (XOS), in contrast, shows a more robust bifidogenic effect. Interestingly, the *Coriobacteriia Eggerthella lenta* and *Gordonibacter urolithinfaciens* are indirectly stimulated by the inulin degradation process, expanding our knowledge of inulin-responsive bacteria.

Chapter 1

Widespread and novel inulin-responsive bacteria in the gut microbiota as revealed by multi-modal activity-based sorting

Alessandra Riva[1#], **Hamid Rasoulimehrabani[1]**, José Manuel Cruz-Rubio[2], Stephanie L. Schnorr[1], Cornelia von Baeckmann[3], Deniz Inan[1], Georgi Nikolov[1], Craig W. Herbold[1], Bela Hausmann[4,5], Petra Pjevac[1,4], Arno Schintlmeister[1], Andreas Spittler[6], Márton Palatinszky[1], Aida Kadunic[1], Norbert Hieger[1], Giorgia Del Favero[7], Martin von Bergen[8], Nico Jehmlich[8], Margarete Watzka[9], Kang Soo Lee[10], Julia Wiesenbauer[9], Sanaz Khadem[1], Helmut Viernstein[2], Roman Stocker[10], Michael Wagner[1,11], Christina Kaiser[9], Andreas Richter[9], Freddy Kleitz[3] and David Berry[1,4*]

[1]Centre for Microbiology and Environmental Systems Science, Department of Microbiology and Ecosystem Science, Division of Microbial Ecology, University of Vienna, Vienna, Austria.

[2]Department of Pharmaceutical Technology and Biopharmaceutics, University of Vienna, Vienna, Austria.

[3]Department of Inorganic Chemistry-Functional Materials, Faculty of Chemistry, University of Vienna, Vienna, Austria.

[4]Joint Microbiome Facility of the Medical University of Vienna and the University of Vienna, Vienna, Austria.

[5]Department of Laboratory Medicine, Medical University of Vienna, Vienna, Austria.

[6]Core Facility Flow Cytometry and Surgical Research Laboratories, Medical University of Vienna, Vienna, Austria.

[7]Department of Food Chemistry and Toxicology, Faculty of Chemistry, University of Vienna, Vienna, Austria.

[8]Helmholtz Centre for Environmental Research, Department of Molecular Systems Biology, Leipzig, Germany.

[9]Centre for Microbiology and Environmental Systems Science, Department of Microbiology and Ecosystem Science, Division of Terrestrial Ecosystem Research, University of Vienna, Vienna, Austria.

[10]Institute for Environmental Engineering, Department of Civil, Environmental and Geomatic Engineering, ETH Zurich, Zurich, Switzerland.

[11]Center for Microbial Communities, Department of Chemistry and Bioscience, Aalborg University, Aalborg, Denmark.

Abstract

Prebiotics are defined as non-digestible dietary components that promote the growth of beneficial gut microorganisms. In many cases, however, this capability is not systematically evaluated. Here, we develop a methodology for determining prebiotic-responsive bacteria using the popular dietary supplement inulin. We first identified microbes with a capacity to bind inulin using mesoporous silica nanoparticles functionalized with inulin. 16S rRNA gene amplicon sequencing of sorted cells indicated that the ability to bind inulin was widespread in the microbiota. We further evaluated which taxa were metabolically stimulated by inulin and we found that diverse taxa from the phyla *Firmicutes* and *Actinobacteria* responded to inulin, and several isolates of these taxa were able to degrade inulin. Incubation with another prebiotic, xylooligosaccharides (XOS), in contrast, showed a more robust bifidogenic effect. Interestingly, the *Coriobacteriia Eggerthella lenta* and *Gordonibacter urolithinfaciens* were identified to be stimulated by the inulin degradation process, expanding our knowledge of inulin-responsive bacteria.

Introduction

Non-digestible fibers are dietary components important for maintaining gut microbiome diversity and metabolic function[1,2]. Some dietary fibers have been shown to confer a variety of health benefits, which has led to their classification as prebiotics[2]. The original definition of prebiotics, introduced in 1995, was “non-digestible food ingredients that beneficially affect the host by selectivity stimulating the growth and/or activity of one or a limited number of bacterial species already resident in the colon, and thus attempt to improve host health”[3]. The initial concept underwent many revisions, and a consensus was achieved in 2016, defining a prebiotic as “a substrate that is selectively utilized by host microorganisms conferring a health benefit”[4]. Although all currently recognized prebiotics are fibers, not all fibers are prebiotics. Classification of a food ingredient as a prebiotic requires scientific demonstration that the ingredient: (i) resists gastric acidity, hydrolysis by mammalian enzymes, and absorption in the upper gastrointestinal

tract, (ii) is fermented by the intestinal microbiota, and (iii) selectively stimulates the growth and/or activity of intestinal bacteria potentially associated with health and well-being of the host[5,6]. Inulin, one of the most popular prebiotics in the food and supplement industry, is a non-structural polysaccharide produced by plants consisting of <60 linearly β-1,2-linked D-fructosyl residues with a terminal α-1,2-linked D-glucose moiety. Inulin is abundant in foods such as banana, chicory root, Jerusalem artichoke, wheat, barley, rye, onions, leeks, and garlic[7]. Inulin consumption from natural sources is estimated to be approximately 2-11 g/d in most European countries and 2-8 g/d in the United States[8,9]. Positive effects on human health ascribed to inulin include reduction in insulin resistance[10,11], anti-inflammatory activity[11,12], and anti-carcinogenic properties[13].

Inulin is not digestible by humans, and after ingestion it enters the large intestine where it is degraded and fermented by the gut microbiota[6]. Microbial inulinases catalyze the hydrolysis of inulin, producing fructooligosaccharides (FOS) and glucose and fructose monomers. Most characterized inulinases are of fungal origin and are used for industrial food production[14]. Information on gut bacterial inulinases is scarce, and thus-far only members of the genera *Bacteroides*, *Lactobacillus* and *Bifidobacterium*, and *Arabiibacter massiliensis* have experimentally validated inulinase activity[15-18]. An increase of the relative abundance of *Bifidobacterium* upon inulin consumption has been reported in human intervention studies[19-22]. Although dietary intervention with prebiotics is a promising strategy for modulating the gut microbiota, gaps in knowledge regarding the microbial metabolic pathways involved in the utilization of prebiotics[23], inter-individual variability[19,24,25] and strain-level diversity has made the design of rational interventions challenging[23].

Due to its health benefits as well as its popularity, a better understanding of inulin metabolism by the gut microbiota is of great importance. At the same time, in-depth knowledge about the interaction between gut microbiota and inulin would enhance our understanding of prebiotic function and the development of science-based dietary interventions. To assess which bacterial taxa interact with inulin or are stimulated by it or its breakdown products, we employed *ex vivo* gut microbiota incubations and a multi-modal sorting approach that relies on measurement of

fluorescence and Raman signals followed by 16S rRNA gene amplicon sequencing and targeted isolation of microbial strains. We validated our findings with physiological experiments, fluorescence *in situ* hybridization (FISH), and whole genome sequencing and analysis (Supplementary Figure 1). This revealed that a diverse set of bacteria were able to interact with or use inulin, including previously unrecognized species, thereby demonstrating its properties as a broadly stimulating microbial nutritional substrate.

Results

Detection of inulin-binding bacteria in the gut microbiota

Many polysaccharides are too large to be directly imported into the cell, so they must either first be partially hydrolyzed by secreted enzymes or captured by cell surface proteins with carbohydrate-binding modules[26-29], although import of fructans without surface pre-digestion by *Bacteroides* spp. has also been described[23].

In order to identify members of the gut microbiota with inulin-binding characteristics, we employed fluorescently-labeled mesoporous silica nanoparticles (MSNs) grafted with inulin[30,31] to capture and sort inulin-bound bacteria. We performed anaerobic incubations of freshly collected human stool samples from six different donors and incubated them for one hour in the presence of inulin-grafted or ungrafted MSNs (Figure 1a). One hour was chosen to allow sufficient time for attachment but to minimize the possibility of complete degradation of inulin. Two different formulations of MSNs - one hydrophilic and the other hydrophobic - were used to maximize capture of bacteria with different cell surface properties. Structured illumination confocal microscopy (SIM) confirmed that inulin-grafted MSNs possessed high affinity for bacteria (Figure 1a). Specific binding of bacteria to inulin-grafted MSNs was quantified by flow cytometry, which showed an increase in the number of DAPI-stained bacteria bound to inulin-grafted MSNs compared to ungrafted controls (hydrophilic MSNs: mean increase ± sd,70 ± 4.4%, Student's t-test: $p<0.0001$, hydrophobic MSNs: mean increase ± sd, 24 ± 2.5%, Student's t-test: $p=0.0003$; Supplementary Figure 2).

We next performed fluorescence-activated cell sorting (FACS) of inulin-grafted and ungrafted MSNs followed by 16S rRNA gene amplicon sequencing to determine which bacterial taxa were bound to MSNs. Stool samples had a microbial composition typical for the healthy adult gut[32] (Figure 1b). Microbiome profiles of sorted MSNs had high technical reproducibility, with technical replicates only contributing to 1.1% of the variation in the dataset (PerMANOVA, p=0.576). The largest source of variability in the dataset was due to host inter-individual differences, which accounted for 69.1% of total variation (PerMANOVA, p=0.001). This was also the main driver of clustering of unsorted and sorted samples in principal coordinate ordination (Bray-Curtis distances, ANOSIM: p=0.001; Supplementary Figure 3, 4a-d). Despite this inter-individual host variability, jackknife-based diversity estimates indicated that we had identified ~80% of amplicon sequence variants (ASVs) and 99% of all genera that would be found if stool from additional donors were to be analyzed (Supplementary Figure 4e,f). This suggests that the inulin-binding fraction of the microbiota is, like the entire microbiota, individualized to a certain degree. However, much of this variation appears to be due to differences in frequency, as we also find that 40% of identified genera were detected in all six samples and 77% were present in at least half the samples (Supplementary Figure 4g). Bacterial genera significantly enriched in inulin-grafted MSNs compared to ungrafted MSNs belonged to the families *Lachnospiraceae* (*Blautia*, *Roseburia*, and *Lachnospira*), *Ruminococcaceae* (*Ruminococcus*, *Agathobaculum*, and *Dysosmobacter*), *Lactobacillaceae* (*Lactobacillus*), *Veillonellaceae* (*Dialister*), *Selenomonadaceae* (*Mitsuokella*), *Bacteroidaceae* (*Phocaeicola*), and *Eggerthellaceae* (*Raoultibacter*) (Wald test, $p<0.05$, n=156) (Figure 1b; Supplementary Table 1).

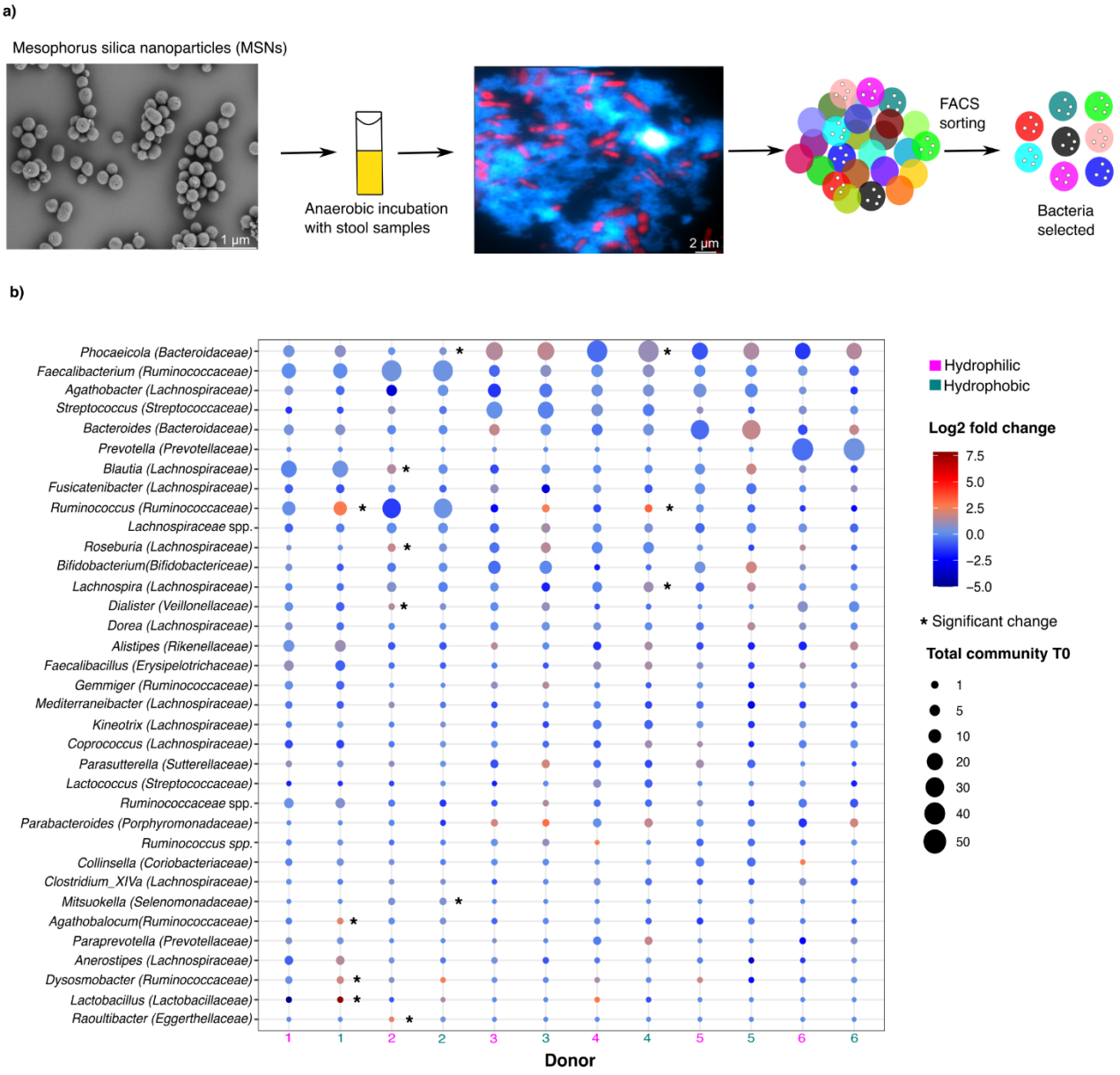

Figure 1. Inulin-binding taxa in the gut microbiota. (**a**) Experimental design: After 1 h of anaerobic incubation of human stool samples with mesoporous silica nanoparticles (MSNs, scanning electron microscopy micrograph of MSNs is shown on the left), structured illumination microscopy fluorescence image revealed the interaction between bacteria (DAPI=red) and MSNs (rhodamine=blue). Subsequently the bacteria bound to MSNs were sorted with fluorescence activated cell sorting (FACS) and profiled with 16S rRNA gene amplicon sequencing. Colors refers to different bacterial taxa. (**b**) Log2 fold changes for each donor are shown at the genus-level. Bubble size indicates relative abundance in the starting sample. Asterisks indicate significantly enriched taxa after supplementation with inulin-grafted MSN, as calculated with the Wald test ($p<0.05$, $n=108$). Genera with relative abundance > 0.5% were considered. Hydrophobic and hydrophilic refers to the type of MSNs used.

Translationally-active microbiota after inulin amendment

As not all bacteria that benefit from inulin might bind to it - either because they secrete extracellular inulinases or because they cross-feed on liberated sugars or metabolic products of inulin degraders, we next sought to identify gut microbes that display increased translational activity in the presence of inulin. We performed 6 h anaerobic incubations[33] of freshly-collected stool samples from eleven different donors supplemented with 2 mg/ml inulin, a level similar to reasonable dietary intake[5,34], as well as the cellular activity marker L-Azidohomoalanine (AHA). The 6 h time point was chosen based on an optimization of incubation time in a previous study[33]. The presence of translationally-active cells was detected following incubation using bioorthogonal non-canonical amino acid tagging (BONCAT)[35], and fluorescently-labeled cells were sorted by FACS[36]. For analysis, we divided the samples into total community (samples submitted to anaerobic incubation only without FACS sorting) and active fraction (samples submitted to anaerobic incubation and BONCAT-labeled cells sorted by FACS) (Figure 2a). The taxonomic composition of the stool microbiota was typical for that of healthy adults[32] (Figure 2b). We confirmed that the technical variability associated with the BONCAT procedure was much smaller than the observed biological variability [(technical variation: 0.2%, PerMANOVA, p=0.83; biological variation: 57%, PerMANOVA: p=0.001)], indicating the reproducibility and accuracy of the method.

Translationally-active cells were detected in all inulin-amended samples after incubation with inulin, while there was only minimal activity observed in incubations without inulin amendment (Supplementary Figure 5). The diversity and the composition of the total microbial community did not change significantly during the incubations (PerMANOVA, p=0.591, Supplementary Figure 6), indicating that these experimental conditions did not appreciably modify the composition of the microbiota. However, inulin degradation was detected in all the stool samples (mean ± sd: 31.7 ± 13%) (Supplementary Figure 5c) and a substantial fraction of cells were BONCAT-labeled (mean ± sd: 51.3 ± 24.3%) (Supplementary Figure 5d). Donor 12 was the only participant with a low percentage of labeled cells, which could be due to a less abundant but extremely active inulin-

degrading population. The most abundant genera in the BONCAT-positive fraction belonged to the families *Bacteroidaceae* (*Phocaeicola* and *Bacteroides*), *Lachnospiraceae* (*Blautia* and *Eubacterium*), *Ruminococcaceae* (*Faecalibacterium* and *Ruminococcus*), *Rikenellaceae* (*Alistipes*), and *Prevotellaceae* (*Prevotella*). Taxa that were enriched in the BONCAT-positive fraction compared to the total community for each participant belonged to the *Erysipelotrichaceae* (*Faecalibacillus* and *Clostridium*_XVIII), *Coriobacteriaceae* (*Collinsella), Corynebacteriaceae* (*Corynebacterium*), *Lachnospiraceae* (*Blautia*, *Anaerostipes, Anaerobutyricum, Roseburia, Agathobacter,* and *Enterocloster*), *Bifidobacteriaceae* (*Bifidobacterium*), *Sutterellaceae* (*Parasutterella*), *Ruminococcaceae* (*Ruminococcus*), *Streptococcaceae* (*Streptococcus*) (Wald test, $p<0.05$, $n=33$). The most consistent enrichments across donors were found for *Blautia*, *Collinsella* and *Faecalibacillus* (Figure 2b; Supplementary Table 2). Similarly to the MSN experiments, there was substantial inter-individual variability in the BONCAT-enriched fraction due to variations in the frequency of different taxa and, to a lesser extent to variations in taxon presence/absence, though jackknife-based diversity estimates (Supplementary Figure 7a-d) indicated that we had identified ~76% of ASVs and 99% of all genera that would be found if stool from additional donors were to be analyzed (Supplementary Figure 7e,f), and 30% of identified genera were detected in all eleven samples and 86% were present in at least half the samples (Supplementary Figure 7g). In addition to evaluating the response to native inulin with a degree of polymerization (DP) of more than 10, the same experimental approach was applied to the inulin breakdown products fructooligosaccharides (FOS, <10 monomeric units) and fructose. Comparing the active fraction and the total community after inulin, FOS, and fructose supplementations, inulin activated the largest number of ASVs, and this activation pattern had only partial overlap with the one observed after addition of smaller compounds (Supplementary Figure 8, Supplementary Tables 2-5), suggesting that DP is an important factor in the gut microbiota response to fructans.

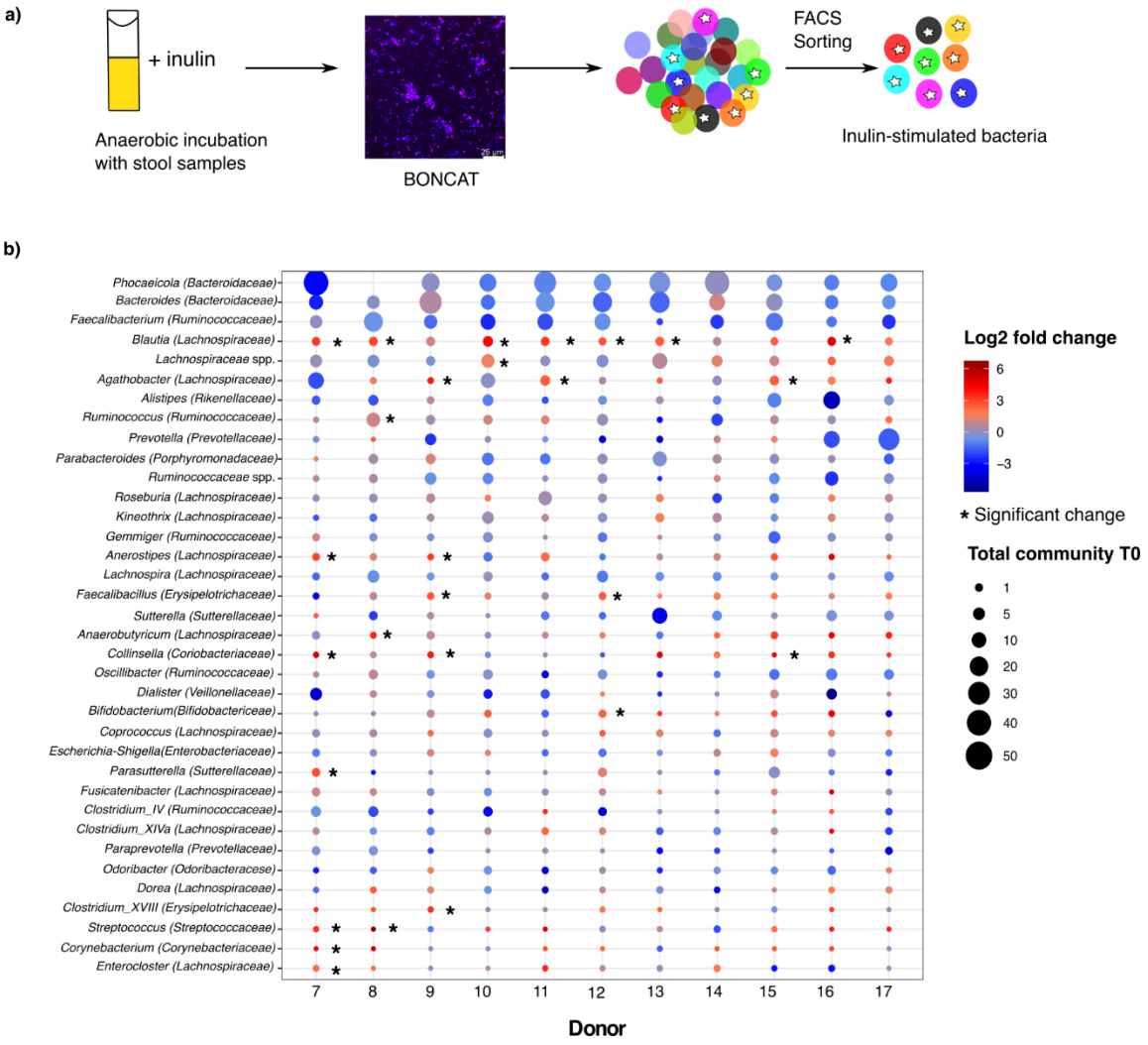

Figure 2. Translationally-active community after inulin supplementation. (a) Eleven fresh stool samples were incubated anaerobically in the presence of the prebiotic inulin. The 11 donors were different from the 6 donors enrolled for the MSN experiment. After 6 h, translationally-active cells were sorted with BONCAT-FACS based on Cy5 fluorescence signals (pink). Color code refers to different bacteria taxa and stars represent translationally active fraction sorted. **(b)** Log2 fold changes for each donor are shown at the genus-level. Bubble size indicates relative abundance in the starting sample. Asterisks indicate significantly enriched taxa after supplementation with inulin, as calculated with the Wald test ($p<0.05$, $n=33$). Genera with relative abundance > 0.5% were considered.

Targeted isolation of inulin-stimulated bacteria using Raman activated cell sorting

As a large diversity of microorganisms were found to be stimulated by inulin, we next evaluated their ability to degrade inulin using targeted isolation and pure culture physiological experiments (Figure 3a). For this purpose, 50% heavy water (D_2O)-containing medium was used for the incubations as a universal marker for cellular activity, as active cells incorporate deuterium (D) from heavy water into their biomass, resulting in carbon-deuterium (C-D) bonds that can be detected by Raman microspectroscopy[37]. Inulin supplementation of fecal samples resulted in metabolically-active cells incorporating D from D_2O above an established threshold level (measured as %CD) (Figure 3b). Control samples incubated with D_2O but not supplemented with inulin showed only negligible levels of D incorporation. Between 47 and 100% of cells from incubations were identified as D-labeled (Figure 3c), highlighting the ability of inulin to broadly stimulate the microbiota. We then sorted D-labeled cells from the incubations using Raman activated cell sorting (RACS)[38] (Supplementary Table 6, Supplementary Figure 9) and isolated pure cultures by plating the sorted fraction on YCFA-based plates to recover the greatest diversity of microbes possible[39] (Supplementary Table 7). In total we isolated 72 colonies from 9 of the 11 donors (4-19 colonies per sample; Supplementary Table 6) consisting of 10 bacterial genera and 18 species belonging to the phyla *Bacteroidetes* (*Bacteroides*, *Phocaeicola, Parabacteroide, Alistipes*), *Firmicutes* (*Ruminococcus, Weissella, Enterococcus*), and *Actinobacteria* (*Eggerthella, Gordonibacter, Bifidobacterium*) (Figure 3d, Supplementary Tables 7,8). *Bifidobacterium* spp. and *Eggerthella lenta* were the dominant isolates, with *Eggerthella lenta* being isolated from six different individuals (Figure 3d, Supplementary Tables 7,8). A phylogenetic tree of the 28 representative isolates is shown in Figure 3d. Most of the 28 representative strains were able to degrade inulin (Figure 3e) and inulin-supplemented media boosted the growth of almost all strains (Supplementary Table 7). Inulin degradation also led to the production of low DP oligosaccharides and monosaccharides (Supplementary Figure 10, Supplementary Table 7), which could potentially be used as a microbial “public good” by cross-feeding microbes in a complex community[40]. *Coriobacteriia* were among the most frequently recovered taxa from the RACS sorting and represented a significant proportion of D-labeled cells using Raman

microspectroscopy combined with fluorescence *in situ* hybridization (FISH; *Collinsella* and *Coriobacterium*: 62.2 ± 27.0% and *E. lenta*: 41.0 ± 17.0% of all D-labeled cells; Supplementary Figures 11,12). *E. lenta* and *Gordonibacter urolithinfaciens* isolates were also closely related to ASV sequences recovered from BONCAT-FACS (Supplementary Figure 13, Supplementary Table 9). Although genome analysis revealed the presence of putative glycoside hydrolases, no enzymes with high homology to characterized inulinases were detected (Supplementary Figures 14,15). Additionally, incubation of these strains with inulin did not increase their growth rate (Supplementary Figure 16), indicating that inulin and its component sugars are not utilized to an appreciable extent for growth.

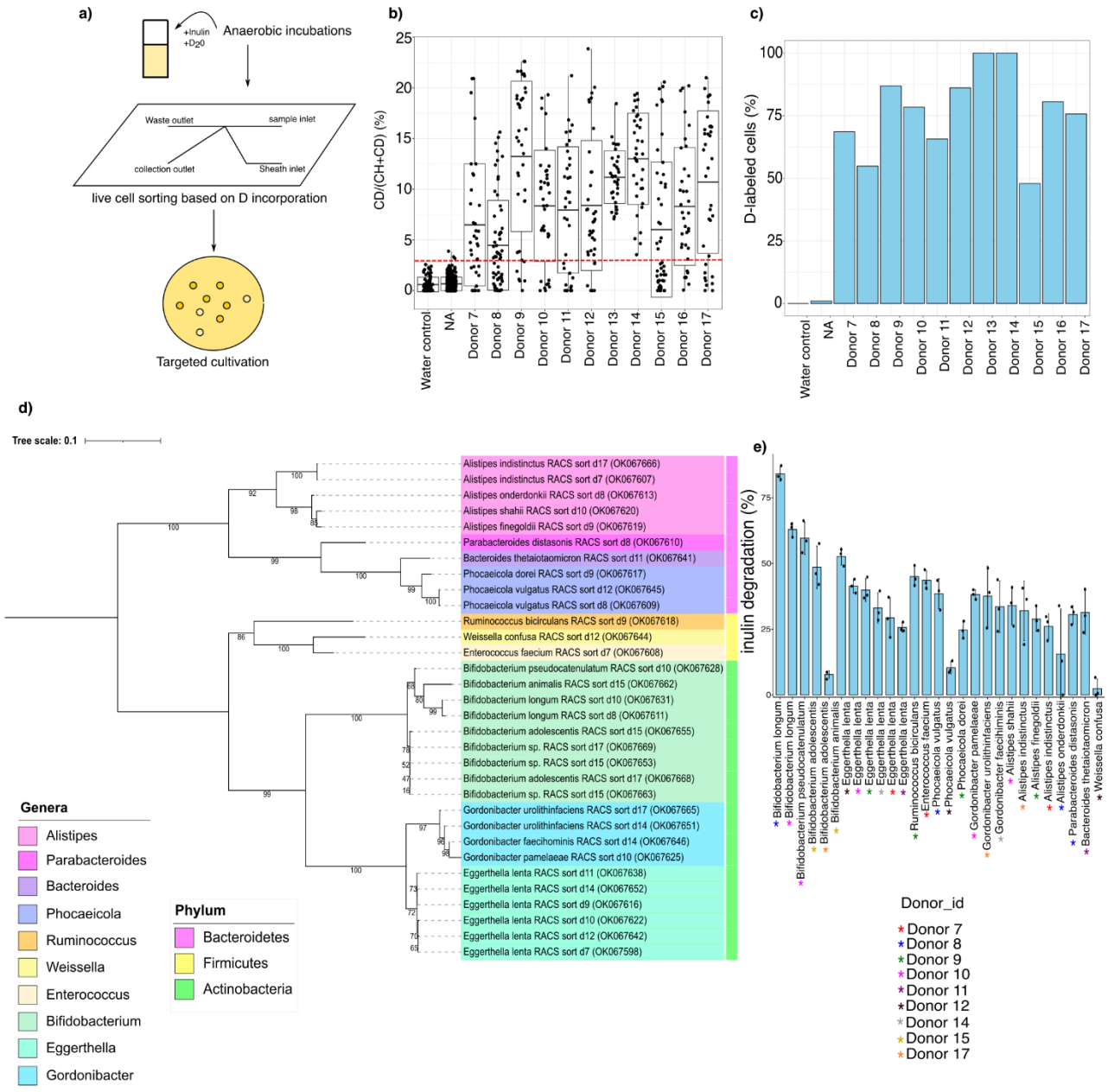

Figure 3. **RACS isolated strains are involved in inulin degradation. (a)** Experimental design. **(b)** Percentage of active cells measured by Raman microspectroscopy. The x-axis represents stool samples collected from 11 donors and incubated for 6 h in D_2O-containing media in the presence of inulin. The y-axis shows the level of D incorporation of randomly selected cells, as quantified by %CD. Each dot represents a random single cell measurement (water control: n=76, nothing added NA: n=313, donor 7: n=35, donor 8: n=62, donor 9: n=38, donor 10: n=37, donor 11: n=35, donor 12: n=36, donor 13: n=33, donor 14: n=35, donor 15: n=48, donor 16: n=36, donor 17: n=37). The red dashed line at 2.75% indicates the threshold for considering a cell labeled. It was determined by calculating the mean +3 sd of %CD in randomly selected

cells from a stool sample incubated without addition of D_2O (water control). Boxplot: boxplot medians (center lines), interquartile ranges (box ranges), whisker ranges. (**c**) Percentage of cells labeled (i.e., with %CD higher than threshold) per donor. (**d)** Phylogenetic analysis of representative strains isolated with RACS (OK067598-OK067669). Representative strains were selected as unique species isolated from each donor. The tree was generated with the maximum likelihood algorithm using IQtree, with the optimal model identified by modelFinder as K2P+I+G4 and rooted at mid-point. Each color in the tree denotes the different genera isolated and each color code represented as color strip show the different phyla (*Bacteroidetes*: pink, *Firmicutes*: yellow, *Actinobacteria*: green). (**e**) Inulin degradation of RACS isolates measured as percentage of inulin degraded by each strain after incubation in inulin supplemented media (YCFA-IN). Strains were sampled in the early stationary phase. Donors are underlined as colored asterisks in the figure. Triplicates measurements are shown. Error bars represent standard deviation of the mean.

Translationally-active microbiota and targeted isolation of XOS-stimulated bacteria

To compare the stimulation of the microbiota by inulin with another candidate prebiotic, we performed the same experimental approach using the prebiotic xylooligosaccharides (XOS). We incubated additional 6 samples in the presence of XOS, AHA and heavy water and sorted the XOS-active fractions by FACS and RACS. As reported for inulin and MSN-grafted inulin experiments, microbiome profiles had high technical reproducibility, with technical replicates only contributing to 1% of the variation in the dataset (PerMANOVA, p=0.671). The largest source of variability in the dataset was due to host inter-individual differences, which accounted for 51% of total variation (PerMANOVA, p=0.001, ANOSIM: p=0.001 and Bray-Curtis distances Supplementary Figure 17,a-d). Jackknife-based diversity estimates indicated that we had identified 80% of amplicon sequence variants (ASVs) and 93% of all genera that would be found if stool from additional donors were to be analyzed (Supplementary Figure 17,f). This suggests that XOS-active fraction of the microbiota is individualized similarly as in the inulin experiments. Part of this variation appears to be due to differences in frequency, as we also find that 35% of identified genera were detected in all six samples and 68% were present in at least half the samples (Supplementary Figure 17g).

After six hours incubation, XOS consistently stimulated the metabolic activity of *Bifidobacterium*, indicating a strong bifidogenic effect of XOS, as well as low-abundant *Alcaligenes* (Figure 4a-c; Supplementary Table 11). In agreement with this observation, the use of heavy water combined

with RACS allowed us to directly isolate members of the genera *Bifidobacterium* spp. (45 isolates) and *Collinsella aereofaciens* (4 isolated) as XOS utilizers (Figure 4 d,e; Supplementary Tables 12, 13). As for inulin, XOS-supplemented media boosted the growth of all the isolates (Supplementary Figure 18, Supplementary Table 14) and high-performance anion-exchange chromatography (HPAEC) showed a significant decreased level of xylobiose and xylotriose of the stool sample measured at 0 and 6 h (Student t-test; D-xylose $p=0.475$, xylobiose $p<0.0001$, xylotriose $p<0.0001$) (Supplementary Figure 19a) as well as a significant decrease of xylobiose and xylotriose for all the strains isolated with RACS (Student t-test or Wilcox test; D-xylose $p=0.876$, xylobiose $p<0.0001$, xylotriose $p<0.0001$) (Supplementary Figure 19b) indicating XOS degradation after 6 h incubation of the stool sample and after 24 h incubation with XOS-supplemented media for all the isolates.

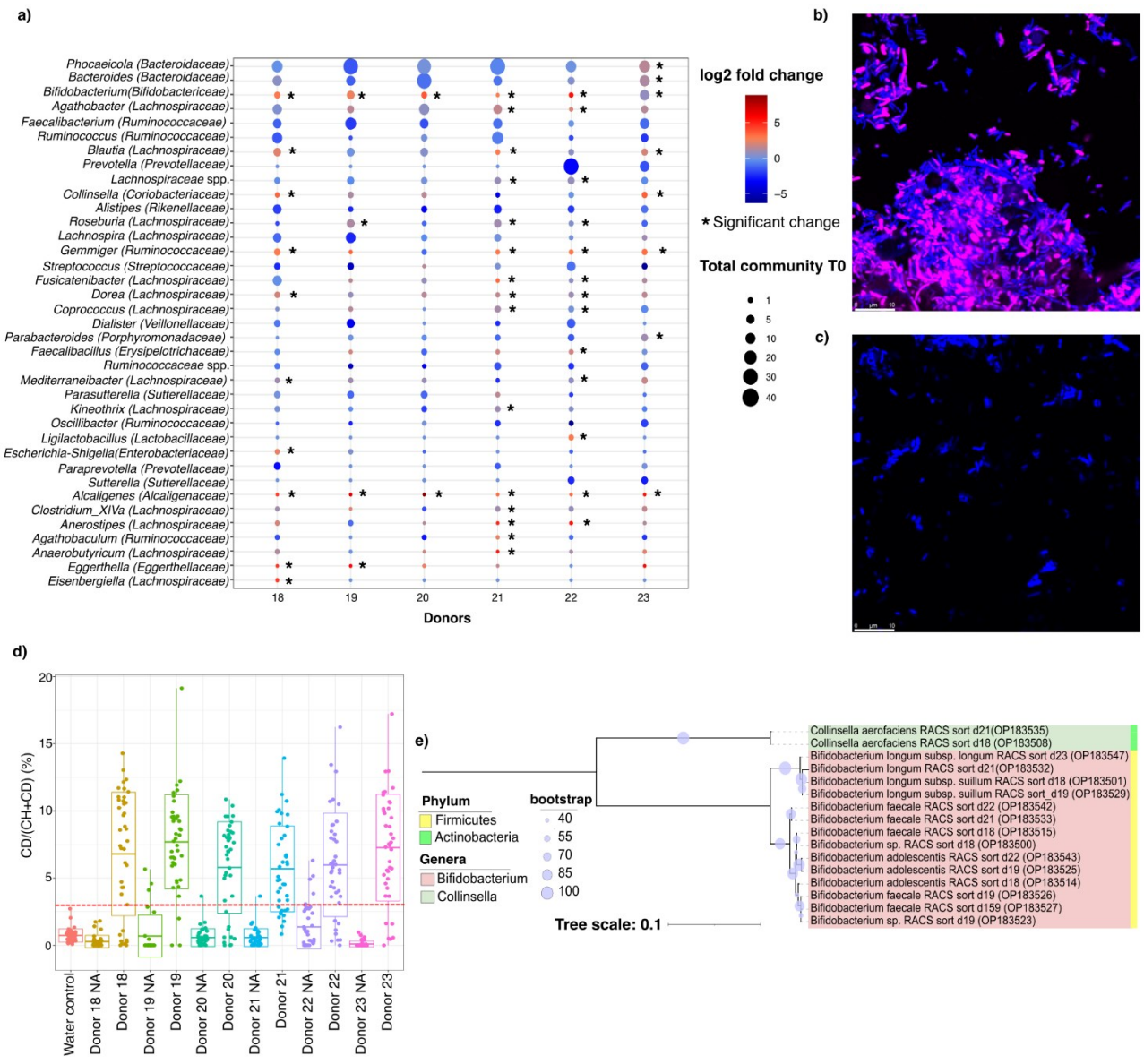

Figure 4. Translationally-active community and RACS isolated strains after XOS supplementation. (a) BONCAT-FACS: log2 fold changes for each donor are shown at the genus-level. Bubble size indicates relative abundance in the starting sample. Asterisks indicate significantly enriched taxa after supplementation with XOS, as calculated with the Wald test ($p<0.05$, n=36). Genera with relative abundance > 0.5% were considered. (**b**) Example of fluorescence microscopy images showing BONCAT-positive cells (pink, Cy5) after 6 h incubation with XOS. All cells are stained with DAPI (blue). (**c**) No amendment control shows no BONCAT signal. Both images were recorded using identical settings. (**d**) Percentage of active cells measured by Raman microspectroscopy. The x-axis represents 6 stool samples collected from 6 donors and incubated for 6 h in D_2O-containing media in the presence of XOS. The y-axis represents the level of D incorporation of randomly selected cells measured by %CD. Each dot represents a random single cell measurement (water control: n=40, donor 18 nothing added (NA): n=40, donor 18:

n=40, donor 19 NA: n=30, donor 19: n=40, donor 20 NA: n=40, donor 20: n=40, donor 21 NA: n=40, donor 21: n=40, donor 22 NA: n=40, donor 22: n=40, donor 23 NA: n=40, donor 23: n=40). The red dashed line at 2.55% indicates the threshold for considering a cell labeled. Boxplot: boxplot medians (center lines), interquartile ranges (box ranges), whisker ranges. (**e**) Phylogenetic analysis of representative strains isolated with RACS after XOS supplementation (OP183499-OP183547). The tree was generated with the maximum likelihood algorithm using IQtree, with the optimal model identified by modelFinder as TN+F+G4 and rooted at mid-point. Each color in the tree denotes the different genera isolated and each color code represented as color strip show the different phyla.

Discussion

Prebiotics are food constituents or dietary supplements reported to promote the growth of certain gut bacteria (mainly *Bifidobacterium*, and secondarily *Lactobacillus, Anaerostipes,* and *Faecalibacterium prausnitzii*)[41]. Generally, however, this capability is not systematically evaluated and molecular pathways sustaining the health-claims remain largely unexplored. In this study, we investigated the capability of the microbiota response to the widely used dietary supplement inulin combining multi-modal cell sorting methods (MSN-FACS, BONCAT-FACS, and RACS), physiological experiments, stable isotope probing (SIP), FISH, and genomic analyses. Polysaccharides are too large to be directly imported into the cell, so they must either first be partially hydrolyzed by secreted enzymes or captured by cell surface proteins with carbohydrate-binding modules[26-29]. At best of our knowledge, it has not yet known how inulin is imported in the cells, but it has only been proposed in *Bacteroides* spp. a mechanism of import across the outer membrane without surface pre-digestion[23].

Using inulin-grafted nanoparticles, we generated highly selective nanoprobes which enabled us to discover that many taxa are capable of binding inulin. We also found widespread translational activation of the microbiota due to inulin, with the most prominent inulin-responsive taxa being members of *Lachnospiraceae* including *Blautia*, as well as *Collinsella* (*Coriobacteriaceae*) and *Faecalibacillus* (*Erysipelotrichaceae*). BONCAT-FACS and MSN-FACS are powerful methods to target both inulin-binding and active fraction of the gut microbiota. There was some concordance between inulin-binding and translational activation assays, most notably for *Blautia*, *Ruminococcus*, and *Roseburia*, suggesting that inulin binding prior to hydrolysis is a common

strategy employed by gut bacteria. These observations are in accordance with previous work where strain-specific binding to glycans using glass beads was described[42]. However, the physiological effects and health benefit resulting from prebiotics utilization may be explained not only by changes in gut microbes abundance but also by changes in microbiota functionality or metabolism, which need to be taken into account for future studies[41].

Inulin response was individualized in both the translationally active and the inulin binding microbiota fraction. The existence of a substantial inter-individual variability in gut microbiome in response to dietary interventions is becoming increasingly evident[19,24]. In a previous study both the effect of resistant starch and its magnitude varied among individuals and indicated the need of personalized strategies in the modulation of gut microbiota[25]. Another human study highlighted a large inter-individual variation in the architecture of the gut microbiome in response to inulin supplementation[24] and in an animal study inulin did not alter overall microbiota composition but was able to induce donor-specific changes in the microbiota composition[43].

To gain insight into the physiology of inulin-responsive microbes, we performed targeted isolations with RACS (based on the deuterium signal) from stool samples from 11 donors. We recovered 72 colonies belonging to 18 different species, including *Eggerthella lenta*, *Bifidobacterium* spp. *Gordonibacter* spp., *Alistipes* spp., and *Phocaeicola*. Notably, *Bifidobacterium* spp. and *Ruminococcus* were also detected with BONCAT-MSN-FACS, *Eggerthellaceae* and *Bacteroidaceae* were enriched using both MSN-FACS and RACS. Dietary intervention studies, either performed in humans, laboratory animals, or *in vitro*, often report an increase in *Bifidobacterium* spp.[19] upon inulin supplementation, although increases in other taxa, such as *Anaerostipes, Lactobacillus, Parabacteroides*, *Blautia, and Collinsella* have also been reported[20,41,43-47]. Many of these studies include non-healthy participants and additionally are unable to distinguish effects of inulin on host gastrointestinal function from direct effects on the microbiome. Another factor to take into account is that fructan size (DP) that can impact incubation time and therefore site of fermentation in the gut, with FOS being more quickly fermented than inulin[48]. Long-chain fructans such as inulin may be fermented over a larger

portion of the colon[48] where the microbial community may slightly differ in composition[49,50]. It is important to acknowledge that our *ex-vivo* model reflects the colon community, and that different species in the small intestine may be the predominant inulin utilizers.

Our data suggest that a broader group of bacteria respond to inulin. Of note, most of the 18 isolated inulin-responsive species were able to degrade inulin in pure culture, suggesting that although monosaccharides are liberated during the hydrolysis of inulin, there may be limited cross-feeding of these sugars by non-inulin-utilizing species. The finding that members of the *Coriobacteriia* (*Eggerthella lenta* and *Gordonibacter* spp.) were among the most frequently detected bacteria in all of our inulin assays was particularly surprising, as they are more commonly associated with polyphenol and bile acid transformations and not with polysaccharides utilization[51]. Amongst the *Coriobacteriia*, the genera *Coriobacterium*, *Collinsella*, *Atopobium*, *Olsenella*, *Enorma, Arabiibacter massiliensis* are glucose-fermenting bacteria,[18,52,53] whereas *Eggerthella*, *Paraeggerthella*, *Adlercreutzia*, *Enterorhabdus*, *Asaccharobacter*, *Denitrobacterium*, *Cryptobacterium*, *Slackia*, and *Gordonibacter* have been considered to be asaccharolytic[52], although conflicting results with respect to sugar fermentation have been reported for *Eggerthella lenta*[52-54]. It has recently been shown that a key carbon source for *E. lenta* is acetate derived from arginine catabolism[55]. We found that neither inulin, glucose, nor fructose media supplemented with arginine boosted growth of *E.lenta* or *G. urolithinfaciens* in pure culture. It is therefore likely that these species were active in the original stool incubations due in part to metabolic interactions with other species and that they benefit indirectly from the inulin degradation process.

To complement our data, we compared our findings with inulin to another prebiotic, XOS, which is a polymer of xylose. Targeted isolations with RACS (based on the deuterium signal) identified *Bifidobacterium* spp. and *Collinsella aereofaciens* as XOS degraders. *Bifidobacterium* was enriched in all donors in both RACS and FACS, indicating the strong bifidogenic effect of XOS in accordance with other human and animal studies[56-58].

In summary, using multi-modal activity-based sorting combined with complementary techniques, we were able to identify a widespread inulin and XOS-responsive gut microbial community, including novel inulin-degrading species. This powerful approaches for detecting microbial guilds in the gut microbiota can be applied to a wide variety of research questions and is a framework that should facilitate the study of many activities of interest in the microbiome and future research on science-based dietary interventions.

Material and Methods

Samples collection

Fresh fecal samples were collected from 23 healthy subjects (13 females and 10 males, age mean ± sd :29.3 ± 5.6; BMI:mean ± sd: 23.2 ± 3.0). Donors that consumed antibiotic or food supplements containing probiotic/prebiotic in the previous six months as well as individuals suffering from chronic or acute intestinal disease were excluded from the study. All samples were self-collected using a fecal collection tube (Sarstedt, Germany). The study was approved by, and conducted in accordance, with the University of Vienna ethics committee (reference number 00161) and written informed consent was signed by all enrolled participants.

Synthesis of silica nanoparticles

Mobile composition of matter number forty-eight (MCM-48)-type mesoporous silica nanoparticles with a diameter of 150 nm were synthesized according to previous work[30,31]. After the synthesis, the material was calcinated at 550 °C for 5 h to remove the template. The silica nanoparticles were functionalized using a post-grafting procedure. The material was kept at 150 °C under vacuum to remove adsorbed water. After that the particles were suspended in toluene under argon at 110 °C. After stirring for 4 h, 4 mmol g-1 silica (3-aminopropyl)triethoxysilane (APTS) (Sigma-Aldrich, Austria) were added and left stirring overnight. Finally, the material was collected by centrifugation (after reaching room temperature) and washed with toluene followed

by three times washing with ethanol and dried at room temperature. Amino-functionalized MCM-48-type MSNs (0.11 g) were suspended in 15 ml dimethylformamide (DMF) (Alfa Aesar, Austria) in an ultrasonic bath. 0.0756 g of hydroxybenzotriazole (HOBt) (Sigma-Aldrich, Austria) and dissolved in 1 ml DMF, followed by the addition of 0.421 g of 2-(1H-benzotriazole-1-yl)-1,1,3,3-tetramethyluronium hexafluorophosphate (HBTU) (ACROS-Fisher, Austria). The obtained solution was added to COOH-Inulin (0.2 g, 1 eq) and the vial washed with 3 ml DMF. The mixture was stirred at room temperature for 10 min followed by the addition of 0.193 ml diisopropylethylamine (DIPEA) (Iris-Biothech; Germany). The particles were centrifuged for 20 min (7,000 x g) and mixed with the inulin solution, followed by stirring overnight. After that the solution was centrifuged, washed three times with DMF and three times with dichloromethane (DCM) (Sigma-Aldrich, Austria) and once with ethanol to remove unreacted substances, followed by drying in air until complete dryness. To anchor rhodamine B onto silica nanoparticles, 1 mg of Rhodamine B isothiocyanate (0.00186 mmol) (Sigma-Aldrich, Austria) was suspended in 4 ml toluene. At the same time 100 mg of the particles were stirred in 8 ml of toluene. The same equivalent of APTS (0.436 µl) was added to the rhodamine B solution resulting in a clear pink solution. Afterwards 1 ml of the obtained solution was added to the particle suspension and the reaction mixture was stirred overnight at room temperature. To collect the particles, the mixture was centrifuged (12,000 x g, 20 min) and washed with ethanol until the supernatant was of clear color (approx. 5-10 times). After that the material was left at room temperature for drying overnight.

Ex-vivo anaerobic incubations with mesoporous silica nanoparticles (MSNs)

Six fresh stool samples were immediately introduced into an anaerobic tent (85% N_2, 10% CO_2, 5% H_2). MSNs were freshly prepared for each experiment, resuspended in 1ml phosphate-buffered saline (PBS) and sonicated for at least 20 min until dissolution. Afterwards, the suspended nanoparticles were introduced into the anaerobic tent and were left for 30 min to allow oxygen reduction. Every reagent was introduced in the anaerobic tent the day before the experiment to ensure that they were anaerobic by the start of the experiment. 10 ml PBS was

added to 1 g of fecal sample. The samples were homogenized by vortexing and afterwards the homogenate filtered using a 40 μm size filter (Corning, Germany) to remove large particles. Samples were further diluted 1:10 in PBS to avoid background noise and autofluorescence in the rhodamine signal. Fecal samples were incubated in autoclaved Hungate tubes in the presence of MSNs at 37 °C for 1 h under anaerobic conditions. MSNs without inulin were used as negative controls for each experiment. Stool samples were diluted in total 1:200 and a final concentration of 2 mg/ml of MSNs were used for FACS experiments with 1:1 ratio between sample and MSNs. For confocal microscopy visualization 0.2 mg/ml of MSNs were used with 1:20 ratio between MSNs and sample. This proportion was optimal to display a homogenous distribution between bacteria and MSNs.

Part of the sample biomass were collected at 0 and 1 h incubation times and stored at -20 °C for additional DNA extractions. After the incubation time, samples were counter-stained with 4', 6-diamidino-2-phenylindole (DAPI) (Sigma-Aldrich, Austria) and used immediately for confocal microscopy visualization and FACS.

Confocal microscopy imaging

Bacterial cells and fluorescently labelled inulin-mesoporous silica nanoparticles were visualized with a Confocal LSM Zeiss 710 equipped with ELYRA PS. 1 system for super resolution. MSNs were chemically functionalized with rhodamine (depicted in light blue) and bacteria counterstained with DAPI (depicted in red) (Figure 1a). Structured illumination images (SIM) were acquired with a Plan Apochromat 100X/oil objective and grid 5 rotation. For spatial distribution, at least 40 images along the Z axes were imaged in randomly chosen optical fields and every experimental condition was imaged at least in triplicate. Image analysis applying deconvolution algorithms was performed on the central section of the image including consistently 13 acquisition layers.

Scanning electron microscopy (SEM)

SEM images were obtained using a FEI Verios 460 field emission scanning electron microscope at an accelerating voltage of 5 kV and a decelerating voltage of 4 kV. The landing voltage was 1 kV. The sample for SEM imaging was prepared by dispersing the powder sample on a carbon tape and keeping it under vacuum for 1 h before the imaging. The scale bars of the obtained micrographs were post-processed for better visualization (Figure 1a).

Fluorescence activated cell sorting (FACS)

Immediately before sorting, samples were filtered with a 35 mm nylon mesh using BD tubes 12 X 75 mm (BD, Germany) and analyzed using the cell sorter BD FACS Melody (BD, Germany) equipped with BD FACSChorus software (BD) as previously described[31,36]. By using FACS we aimed to select the bacteria population that bind the MSNs. Briefly, background noise of the machine and of PBS was detected using the parameters forward scatter (FSC) and side scatter (SSC). Bacteria were then displayed using the same settings in a scatter plot using the forward scatter (FSC) and side scatter (SSC) and pre-gated. Singlets discrimination was performed. MSNs resuspend in PBS and a sample incubated in the same conditions without MSNs but stained with DAPI, were used to set the gate for rhodamine positive signal. Rhodamine-DAPI double positive signal corresponding to the MSNs with bacteria attached, were then sorted into tubes. 500,000 events were sorted for each sample. Analysis of the samples showed a purity of >99%. FACS data were further analyzed with the R package flowCore[59].

DNA extraction, 16S rRNA gene-targeted amplicon sequencing and sequence pre-processing

DNA extraction was performed for both total microbial community (fecal samples incubated 1 h and 0 h with MSNs) and FACS-sorted fraction (fecal samples incubated 1 h with MSNs and sorted by FACS) using the QIAamp DNA mini kit (Qiagen, Germany) following the protocols for bacteria according to the manufacturer's instructions with an additional lysozyme step (Sigma-Aldrich, Austria)[36]. Sequencing was performed at the Joint Microbiome Facility of the Medical University of Vienna and the University of Vienna (project ID JMF-2009-4) and at Microsynth (Austria).16S

rRNA genes were amplified by two step PCR barcoding approach as previously described[60,61]. The V3-V4 regions of the 16S rRNA genes were amplified with the primers 341F (5'-CCT ACG GGN GGC WGC AG-3') and 785R (5'-GAC TAC HVG GGT ATC TAA TCC-3') containing 16 bp head adaptors (H1: 5'-GCTATGCGCGAGCTGC-3', H2: 5'-TAGCGCACACCTGGTA-3') and used in the first PCR step. Samples were then purified and normalized using a SequalPrep™ Normalization Plate Kit (Invitrogen). Afterwards a second barcoding PCR step was performed with unique dual barcodes (UDBs) as described in Pjevac et al., 2021. Samples were again purified and normalized using a SequalPrep™ Normalization Plate Kit and pooled and concentrated on columns (innuPREP PCRpure Kit, Analytik Jena). Next, sequence libraries were prepared with the Illumina TruSeq DNA Nano Kit and sequenced in paired-end mode (2×300 nt; v3 chemistry) on an Illumina MiSeq. After sequencing, amplicon pools were extracted from the raw sequencing data using the FASTQ workflow in BaseSpace (Illumina) with default parameters, and then sequences were demultiplexed with the python package demultiplex by permitting one mismatch each for barcodes, linkers, and primers[60,61]. 16S rRNA gene sequence data were processed into amplicon sequence variants (ASVs) using the Divisive Amplicon Denoising Algorithm (DADA2)[62] applying the recommended workflow[63]. FASTQ reads 1 and 2 were trimmed at 250 nt and 200 nt with allowed expected errors of 4 and 6, respectively. ASV sequences were subsequently classified using DADA2 and SILVA database SSU Ref NR 99 release 138 (https://doi.org/10.5281/zenodo.3986799).

Sequences from contaminants were removed using the R package decontam v1.6.0 using the default threshold value of 0.1 for the prevalence-based statistical test[64].

To avoid biases in downstream analysis related to uneven library depth, sequencing libraries were subsampled to a number of reads smaller than the smallest library (1000 reads). 1000 reads were sufficient to maintain a high coverage per library (mean: 98%). 16S rRNA gene sequence data has been deposited in the NCBI Short Read Archive under PRJNA718139.

Anaerobic incubations

Eleven fresh stool samples were introduced and process in an anaerobic tent (85% N_2, 10% CO_2, 5% H_2) immediately after collection. Inulin (2 mg/ml) (Sigma-Aldrich, Austria), fructose (2 mg/ml) (Carl Roth, Germany), FOS (2 mg/ml) (Sigma-Aldrich, Austria), XOS (2mg/ml) (Carl Roth, Germany) and no amendment control (nothing added) were used as amendments for the incubations. In this work, we did not compare different concentrations since 2 mg/ml is in line with nutritional recommendations[5,34]. 2X PBS was added to the fecal sample and the mixture was vigorously vortexed for 2-3 min until homogenized. Afterwards the samples were filtered using a 40 μm size filter (Corning, Germany) to remove large particles, then transferred to a new autoclaved tube and diluted 1:10 with 2X PBS. Subsequently, 2 ml of substrates in D_2O (heavy water) were transferred into autoclaved Hungate tubes, incubated with 2 ml of fecal sample and 5 mM non-canonical amino acid L-azidohomoalanine (AHA) (Baseclick, Germany). The samples were incubated at final volume of 4 ml in the presence of AHA (final concentration: 50 μM) and D_2O (final concentration: 50%). Samples were incubated in an anaerobic tent at 37 °C for 6 h. At the end of the incubation, the biomass was washed with PBS to remove traces of D_2O and AHA and subsamples of the biomass (1 ml) were washed twice in PBS, fixed in ethanol : PBS (1:1) and stored at -20 °C. Further sample aliquots of 1 ml each were collected for nucleic acid extraction, metabolite analysis, and stored at -80 °C until further use. Samples were further stored in 20% glycerol/PBS in crimp-sealed vials with rubber stoppers and stored at -80 °C for further RACS experiments.

Bioorthogonal non-canonical amino acid tagging (BONCAT), FACS, DNA extraction and 16S rRNA gene-targeted amplicon sequencing

Cu(I)-catalyzed click labelling of chemically fixed microbial cells was performed in solution according to Hatzenpichler et al.[35] right before sorting the cells with FACS[36]. The azide-alkyne click reaction was achieved via a Cu(I)-catalyzed reaction where a terminal alkyne coupled to the Cy5

alkyne fluorescence dye (Jena Bioscience, Germany) was linked to the azide group of AHA yielding a triazole[35].

A representation of BONCAT-inulin positive cells is shown in Supplementary Figure 5b. For flow cytometry sorting, bacteria were labeled in Cy5 dye and sorted as previously described[36] (Supplementary Figure 5e,f,g,h).

Absolute cell count was also performed with the cell sorter FACS Melody (BD, Germany) and BONCAT-positive cells were counted in triplicate for each sample (Supplementary Figure 5d). Absolute counting beads (CountBrightTM, Invitrogen, ThermoFisher Scientific, Austria) were used for cell counts according to the manufacturer's instructions.

Bacterial DNA from both total community (fecal samples incubated 0 h and 6 h with inulin, XOS FOS and fructose) and FACS sorted cells (fecal samples incubated 6 h with inulin, XOS, FOS and fructose and sorted by FACS) were extracted with a QIAamp DNA Mini Kit (Qiagen, Germany) following the manufacturer instruction with an additional lysozyme step (Sigma-Aldrich, Austria). PCR was performed with a two-step barcoding approach and sequence data were pre-processed as described above[60].16S rRNA gene sequence data has been deposited in the NCBI Short Read Archive under PRJNA718139.

Raman microspectroscopy

Single-cell Raman spectra were measured from all fecal samples amended with inulin and XOS and incubated for 6 h. To obtain Raman spectra of individual cells, 1.5 µl of each previously fixed sample (ethanol:PBS, 1:1) was directly spotted on an aluminum-coated slide (Al136; EMF Corporation, USA), washed by dipping into ice-cold Milli-Q (MQ) water (Millipore, Austria) to remove traces of buffer components, and air-dried. Single microbial cell spectra were acquired using a confocal Raman microspectroscope (LabRAM HR800, Horiba Scientific, France) equipped with a 532 nm neodymium-yttrium aluminum garnet (Nd:YAG) laser and 300 grooves/mm diffraction grating. Spectra were acquired with the software LabSpec 6 in the range of 400–3,200 cm^{-1} for 30 s and for each sample 35-40 individual cells were measured. For quantification of the

degree of D substitution in C-H bonds (%CD), the peaks assigned to the C-D (2,040–2,300 cm^{-1}) and C-H (2,800–3,100 cm^{-1}) bonds were calculated using integration of the specified region with the single cell analysis and testing tools for Raman microspectroscopy (Scattr) (http://shiny.csb.univie.ac.at:3838/scattr/)[37].

Raman activated cell sorting (RACS) and targeted isolation

RACS was performed following the design and working principle of the system as described by Lee et al[38,65]. Samples were incubated in D_2O-containing medium for 6 h in the presence of inulin and stored in 20% glycerol (balanced with PBS) at -80 °C. For sorting, the cells were thawed, pelleted by centrifugation (7 min, 7,000-9,000 x g), washed twice with 0.3 M glycerol (balanced with MQ water; to minimize the osmotic stress on the cells), and then resuspended in 500 µl of 0.3 M glycerol. Cells of interest were identified and sorted using a platform that combines the Raman microspectroscope (532 nm at 90 mW), optical tweezers (1,064 nm Nd:YAG laser at 500 mW), and a polydimethylsiloxane (PDMS) microfluidic device[38,65].

This microfluidic system has two outlets (each for a waste and a collection) and the sample stream is engineered to exit through the waste outlet by default. Individual cells are randomly captured within the sample stream using the optical tweezers and their Raman spectra are measured. Cells identified as D-labeled are translocated to a sample-free region (within the microfluidic device) and then released from the optical tweezers so that the flow carries them to the collection outlet for the collection, whereas cells identified as unlabeled are immediately released (without the translocation) to exit through the waste outlet and discarded. This process is fully automated using an in-house software written in MATLAB (version 4.2) and to this end the cell index P_C (which detects the capture of cells in the optical tweezers; $P_C = I_{1,620\text{-}1,670}/ I_{fluid,1,620\text{-}1,670}$, where I refers integrated intensity within the specific spectral window; $P_C>1$ upon the cell capture) and the labeling index P_L (which differentiates between D-labeled and unlabeled cells; $P_L = I_{2,040\text{-}2,300}/ I_{1,850\text{-}1,900}$) are employed. The threshold value for P_L=5.7 was chosen on the basis of mean + 2 sd of the control sample incubated with inulin in non-D_2O-containing medium (i.e., water control)[38,65].

After approximately 60-90 min, sorting was stopped and 50-60 µl liquid (containing the sorting cells) from the collection tube were collected in an Eppendorf tube, immediately introduced into an anaerobic tent and plated on rich media supplemented with 5 mg/ml glucose (YCFA-G, DSMZ 1611). Sorted samples were incubated at 37 °C until colony appearance on the plate. Single colonies were streaked on a new agar plate with YCFA-inulin (YCFA-IN) and incubated at 37 °C until new colonies were formed. For all sort experiments, the buffer 0.3 M glycerol/MQ water utilized was checked for purity and thus plated on YCFA-G overnight. No colonies growth was detected.

Colony PCR and Sanger sequencing

The 16S rRNA genes from resulting colonies YCFA-IN or YCFA-XOS selective agar plates were amplified by colony PCR using the primers 616V (5'- AGA GTT TGA TYM TGG CTC AG-3') and 1492R (5'-GGT TAC CTT GTT ACG ACT T-3'). Colonies from YCFA-G that were plated on YCFA-IN or XOS were also sequenced as quality control to assure that the isolates were pure cultures. A single colony was picked from the plate with the tip of the loop and dissolved in the PCR reaction mix. The PCR reaction mix (final concentrations; Green 1X Dream Taq Buffer, dNTPS 0.2 mM, BSA 0.2 mg/ml, Taq polymerase 0.05 U/µl, primers 1 µM) was prepared in a final volume of 50 µl per reaction. The amplification cycles were as follow: initial denaturation at 95 °C for 3 min, followed by 30 cycles at 95 °C for 30 s, 56 °C for 30 s, 72 °C for 1.5 min, and a final elongation at 72 °C for 10 min.

PCR products were visualized on 1.5% agarose gel electrophoresis and subsequently purified using QIAquick PCR Purification Kit (Qiagen, Germany) according to the manufacturer instruction. Concentrations were measured by Nanodrop, and samples were sent for Sanger sequencing at Microsynth AG (Vienna, Austria). Sorted bacterial strains were identified analyzing the obtained sequencing results in RDP seqmatch (https://rdp.cme.msu.edu). 16S rRNA gene sequence data of the strains isolated has been deposited in the GenBank with accession numbers OK067598-OK067669.

Cultivation in supplemented media: growth curves

All strains were grown in both solid and liquid YCFA medium until early stationary phase and growth data were recorded (Supplementary Table 7). To perform growth curves each individual strain identified by Sanger sequencing was grown in YCFA-G as starting broth at 37 °C in an anaerobic tent. When cultures reached their maximum OD_{600}, they were washed, diluted into the YCFA (DSMZ 1611) broth supplemented with inulin or XOS (YCFA-IN, YCFA-XOS) and in YCFA media without any amendment (YCFA-NA) which was used as a negative control, and dispensed into wells of a sterile 96-well flat- bottomed microtiter plate (Costar 3595, Corning, NY, USA). *E. lenta* and *G. urolithinfaciens* were also grown in modified YCFA DSMZ 1611 in the presence of 10 mg/ml arginine according to Noecker et al[55]. The starting OD_{600} was ~0.05. The prepared plates, which also included negative controls media (YCFA-IN, XOS and NA without addition of bacteria), were incubated for 120 h at 37°C in a microplate reader (MultiskanTM GO Microplate Spectrophotometer, Thermo Fisher Scientific) placed in an anaerobic tent using the SkanIt software (Thermo Fisher Scientific). The OD_{600} was recorded automatically every 30 min for a total of 120 h with a shaking of 5 s between readings. Each condition was tested in at least three technical replicates. Afterwards, growth curves were calculated using R statistical software (https://www.r-project.org/). In addition, cell supernatants were preserved at -80 °C for further thin layer chromatography (TLC) and fructan assay analysis.

Degree of polymerization evaluation by TLC (thin layer chromatography)

Supernatant from stool samples incubated for 6 h with inulin and RACS cultures were applied to 20 × 10 cm HPTLC silica gel 60 plates (Merck KGaA, Germany) using a Linomat 5 (Camag AG, Switzerland). 4 µl of sample (supernatant) or 2 µl of standard (fructose, glucose, sucrose, 1-kestose, and 1,1, kestotetraose at 2 mg/ml each) were applied per lane. The eluent was composed of 1-butanol:1-propanol:ethanol:water – 2:3:3:2; and the plate was developed three times. After developing, the carbohydrates were derivatized by spraying the plate with aniline-diphenylamine

reagent (diphenylamine 2%$_{w/v}$, aniline 2%$_{w/v}$ and phosphoric acid 15%$_{v/v}$ dissolved in acetone) and heating at 100 °C for 5 min[66,67]. The TLC plates were scanned and analyzed by densitometry with Gel Analyzer 19.1 1 (www.gelanalyzer.com). By using FOS and inulin as a standards, the maximum density was used as the retention factor (Rf) value utilized to create the degree of polymerization scale seen in Supplementary Figure 10. The presence of saccharide was deemed positive when the height of the density peak was 4x that of the baseline noise. *Phocaeicola vulgatus* (DSM1447) and *Bacteroides uniformis* (DSM6597), which encode inulinases, were used as positive controls[68].

Fructan assay

Inulinase activity was performed by measuring the remaining inulin after incubation by using the Fructan Assay kit (K-FRUC, Megazyme, Ireland) according to the manufacturer instructions. Briefly, to 200 μl of culture supernatant after 6 h treatment with inulin was added 200 μl of diluted enzyme solution (sucrase,β-amylase, pullulanase and maltase) and incubated at 30 °C for 30 min with the aim to hydrolyze sucrose, starch and other polysaccharides. Afterward, 200 μl of alkaline borohydride solution was added to the tube. The mixture was incubated at 40 °C for 30 min to effect complete reduction to sugar alcohols. Subsequently, 500 μl of 200 mM acetic acid was added to the tube with vigorous stirring on a vortex mixer. 200 μl aliquots of the previous solution were transferred in triplicate to new tubes and 100 μl of fructanase solution (containing a mixture of endo and exo-inulinases) were added to the samples (and 100 μl of 100 mM sodium acetate buffer as blanks). The tubes were incubated at 40 °C for 30 min to reach complete hydrolysis of inulin to D-fructose and D-glucose. Finally, 500 μl of 4-Hydroxybenzhydrazide (PAHBAH) reagent was added to all tubes [(samples, blanks, inulin control (2 and 5 mg/ml) and the fructose standard)] and incubated in a boiling water bath for 6 min. Afterward, the tubes were removed from the boiling water bath and immediately placed in cold water (18-20 °C) for 5 min. The absorbance was read at 410 nm against the reagent blank and each sample was measured in triplicates.

Fluorescence in situ hybridization (FISH)

Fecal samples were fixed in ethanol and stored in ethanol-PBS (1:1) at -20 °C. FISH was performed using a standard protocol[69] with the addition of two permeabilization steps[70]. Briefly, 5 μl of fixed sample was spotted on microscopy slides (Marienfeld, Germany) and dried in a humidified chamber at 46 °C for 5 min. The samples were then submitted to a dehydration step in an ethanol series (50-80-96%) for 3 min each. Samples were permeabilized in a humid chamber with lysozyme (10 mg/ml dissolved in 0.05 M EDTA pH:8.0 and 0.1 M Tris-HCl pH:7.4) and incubated for 60 min at 37 °C. Subsequently samples were treated with 60 U/ml achromopeptidase (Sigma-Aldrich, Austria) dissolved in 0.01 M NaCl and 0.01 M Tris-HCl, pH: 8.0 and incubated for 30 min at 37 °C. After permeabilization samples were washed in MQ water[70]. Afterward, 10 µl of hybridization buffer containing 10 or 5% formamide were applied with subsequent adding of 5 µM of specific probes [E.len194: 5'-CCTTGCCGTCTGGGCTTT-3 (Eggherthella lenta)[71], COR653: 5'-CCCTCCCMTACCGGACCC-3(Collinsella and Coriobacterium)[72], EUBmix338-I: 5'GCTGCCTCCCGTAGGAGT-3'(mostBacteria), EUBmix338-II:5'GCAGCCACCCGTAGGTGT-3'(*Planctomycetales*), and EUBmix338-III: 5'-GCTGCCACCCGTAGGTGT-3' (*Verrucomicrobiales*)][73,74]. Specifically, a 10% formamide hybridization buffer was used for E.len194[71] and 5% for COR653[72]. After 2 h of hybridization in a humidified chamber at 46°C, the slides were washed in the respective wash buffers and counter-stained with 4', 6 diamidino-2-phenylindole (DAPI). The NONEUB probe (5'ACTCCTACGGGAGGCAGC-3') was used as a negative control for Cy3 and FLUOS-dyes[75] and *Eggerthella lenta* pure culture isolated with RACS was used as positive control (Supplementary Figure 11,12). FISH images were taken with a confocal scanning laser microscope (Leica TCS SP8X, Mannheim, Germany) equipped with an Ar-laser (495 nm) for excitation of the FLUOS-dyes and He-Ne-lasers (550 nm) for excitation of Cy3. Pictures were acquired with a 63X or a 93X objectives, pinhole size of 1µm, resolution between 1024×1024 and 2396×2396 pixels and zoom factor of 1. Confocal microscopy images were collected and the biovolume fraction of Collinsella and Coriobacterium was calculated using the software daime[76].

Liquid-FISH combined with Raman microspectroscopy

Fecal samples fixed in ethanol : PBS (1:1) were used for liquid FISH analysis combined with Raman spectroscopy analysis. Liquid FISH was performed using a standard protocol[77] and with the same probes and procedures as describe above. Briefly, liquid *in situ* hybridization was performed resuspending the cell pellets in 10 µl hybridization buffer (HB). 1 µl of the respective probe (COR653 or E.len194) was added to the mixture and incubated at 46 °C for 2 h. Afterward, samples were washed by centrifugation at 40 °C (20,000 × g for 15 min), resuspended in 50 µl of pre-heated (48 °C) washing buffer (WB) and incubated at 46 °C for 15 min. Subsequently, the samples were centrifuged again at 40 °C (20,000 × g for 10 min) and resuspended in ice-cold 1X PBS. For Raman measurements, 1.5 µl of sample was applied on an aluminum slide and dried at 46 °C for 5 min as described above. Slide was placed under a 100X air objective and Raman spectra were recorded for randomly selected fluorescence positive cells were measured with an epifluorescence microscope combined with Raman microscope (LabRAM HR800, Horiba Scientific, France). 35-40 measurements were collected for each sample.

Isolation of genomic DNA and genomic sequencing

Isolation of genomic DNA of *Eggerthella lenta* 6.2 and *Gordonibacter urolithinfaciens* AL-11 was performed using the genomic DNA purification kit *according* to *manufacturer instruction (Promega, Germany).* Briefly, 1ml of culture was centrifuged at 13,000-16,000 x g for 2 min to pellet the cells. Cells were resuspended in 50 mM EDTA and 10 mg/ml lysozyme and incubated at 37 °C for 30-60 min. Afterwards, cells were centrifuged for 2 min at 13,000-16,000 x g, the supernatant was removed and cells were resuspended in lysis buffer and incubated at 80 °C for 5 min to further lyse the cells. 3 µl of RNase solution were added to the cell lysate and incubated at 37 °C for 15-60 min. 200 µl of protein precipitation solution was added to the RNase-treated cell lysate and incubated on ice for 5 min. Cells were centrifuged at 13,000-16,000 x g for 3 min and isopropanol was added to the cells supernatant. Tubes were mixed by inversion until the

thread-like strands of DNA was forming a visible mass. Subsequently, samples were centrifuged at 13,000-16,000 x g for 2 min and 70% ethanol was added to the samples. Tubes were gently inverted several times to wash the DNA pellet. The DNA was centrifuged at 13,000-16,000 x g for 2 min to remove the ethanol. Pellets were air-dried for 10-15 min at room temperature. Finally, 50 µl of DNA were eluted, DNA was rehydrated by incubating at 65 °C for 1 h and afterwards stored at -20 °C.

Sequencing libraries were prepared with the NEBNext® Ultra™ II FS DNA Library Prep Kit for Illumina® (NEB) and sequenced on the Illumina MiSeq platform (2x 300 bp v3 chemistry) following the manufacturer's instructions. Sequencing was performed at the Joint Microbiome Facility of the Medical University of Vienna and the University of Vienna (project ID JMF-19DM-2).

Sequencing data was extracted using the FASTQ workflow in BaseSpace (Illumina) with default parameters. Thereafter, adapter contaminations were removed and the data was quality filtered at a phred score of 15 using the bbduk function of BBMap (v36.20, https://github.com/BioInfoTools/BBMap). The quality trimmed sequence data was used as input for genome assembly with SPAdes[78], where kmers were iterated in steps of 10 between 11 and 121. Assembly quality was inspected with CheckM[79].

Annotation was performed with the RASTtk pipeline/annotation server using the default settings (https://rast.nmpdr.org/rast.cgi) and with EggNOG[80]. The whole genome project has been deposited at NCBI under the accession JAIPUQ000000000 for *Eggerthella lenta* 6.2 and JAIPUP000000000 for *Gordonibacter urolithinfaciens* AL-11 (PRJNA718139). Genomes were visualized with GCView Server[81]. Average nucleotide identity (ANI)[82] was calculated for *Eggerthella lenta* 6.2 and *Gordonibacter urolithinfaeciens* AL-11 genomes in comparison to publicly available reference genomes from the respective genera (Supplementary Table 10).

Phylogenetic tree reconstruction

Downloaded 16S rRNA sequences and RACS-derived 16S rRNA sequences were clustered at 100% identity using Usearch[83] into representative centroids. Representative centroids were first length filtered (>1200 bases) and then aligned using Mafft-linsi[84]. Trimal[85] was used to trim the ends of the alignment (-nogaps -terminalonly) and to remove poorly aligned internal sites (-gt 0.95). IQtree[86] was used for phylogenetic reconstruction of a reference tree under the GTR model with branch support evaluated with 1000 ultrafast bootstraps[87]. Blastn[88] was used to identify perfect matches between ASVs and sequences used for phylogenetic analysis. ASVs and short (<1200 nt) RACS/representative sequences were added to the alignment of trimmed sequences (>1200 nt) that was used for phylogenetic reconstruction using mafft (--addfragments, --keeplength) and placed into the reference tree using RAxML EPA[89]. An additional chimera check was performed using the online tool DECIPHER[90]. Finally, the phylogenetic trees were visualized and plotted using the R package ggtree[91] and iTOL[92].

High-performance anion-exchange chromatography (HPAEC)

XOS strains isolated with RACS were grown in XOS-supplemented media for 24 h. Sample supernatants were collected and analyzed by HPAEC (Dionex ICS 3000, ThermoFisher, Germany). The sugars were analyzed on a Dionex CarboPac PA20 (3 x 150 mm) column with an Dionex CarboPac PA20 (3 x 30 mm) guard column (solvent: 100 mM KOH, 35 min at 0.3 ml/min).

The standard carbohydrate waveform was used for detection, and the analyses were carried out in duplicate. The standards used for construction of the calibration curve were: D-xylose (Sigma Aldrich, St. Louis, MO, USA), xylobiose and xylotriose (Megazyme Ltd, Bray, Ireland). The XOS (Carl Roth) used for the experiments was composed of xylose (% w/w, 0.1%), xylobiose (38.9%), xylotriose (32.7%), xylotetraose (18.6%), xylopentaose (9.8%) as measured with HPAEC.

Statistical analysis

Statistical analysis was performed using R statistical software (https://www.r-project.org/) and GraphPad Prims version 7 (www.graphpad.com). Statistical analysis to compare samples groups was performed using ANOVA, Student's t-test, and the R package DESeq2 (v.1.30.1) that estimate variance-mean dependence in count data from high-throughput sequencing assays and test for differential expression based on a model using the negative binomial distribution[93,94]. The statistical significance of factors affecting microbiota composition and differences between time points was evaluated using non-parametric permutational multivariate analysis of variance (PerMANOVA), significant clustering of groups was evaluated with analysis of similarities (ANOSIM), ordination was performed using principal component analysis (PCoA) and non-metric multidimensional scaling (NMDS) in the vegan package (v.2.5-7) (https://cran.r-project.org/web/packages/vegan/vegan.pdf). Jackknife diversity index and Bray-Curtis distances were also calculated in the vegan package. Variables were expressed as mean (sd, standard deviation) and a probability value (p value) less than 0.05 was considered statistically significant and adjust p value with False Discovery Rate method (FDR) were used for multiple comparison.

Data availability

16S rRNA gene amplicon sequence data from FACS and RACS experiments has been deposited in the NCBI Short Read Archive under PRJNA718139. *Eggerthella lenta* 6.2 and *Gordonibacter urolithinfaeciens* AL-11 genomes were deposited at NCBI under accession JAIPUQ000000000 and JAIPUP000000000 respectively and under PRJNA718139. 16S rRNA gene sequences data of the strains isolated with RACS after inulin supplementation have been deposited in GenBank with accession numbers OK067598-OK067669 and RACS strains sequences isolated after XOS supplementation have been deposited in GenBank with accession numbers OP183499-OP183547.

We declare that the main data supporting the findings of this study are available within the paper and its Supplementary Information. The data that support the findings of this study are available from the corresponding author upon request.

Acknowledgements

This work was financially supported by the European Research Council (Starting Grant: FunKeyGut 741623), the Austrian Science Fund (P27831-B28) and the United States Department of Energy (DE- SC0019012). C.V.B and F.K. acknowledge the funding support of the University of Vienna (Austria).

We thank Jasmin Schwarz, and Gudrun Kohl from the Joint Microbiome Facility (University of Vienna, and Medical University of Vienna, Austria) for supporting in the genomic and 16S rRNA gene amplicon library preparation and the Core Facility MULTIMODAL IMAGING member of VLSI (Vienna Life Science Instruments) for supporting the recording of the confocal microscopy images of MSNs.

Authors contributions

A.R. and D.B. conceived, designed the study and the experiments. A.R. performed all the experiments, and the data analysis. A.R. and D.B. wrote the paper. J.M.C.R. and H.V. performed TLC and support in TLC data analysis and evaluation. H.R., D.I., N.H., J.W and C.K performed the experiments with the prebiotic XOS. S.L.S. and C.W.H. performed bioinformatic analysis and phylogeny. C.V.B. and F.K. prepared and provided mesoporous silica nanoparticles. G.D.F. performed structure illumination images (SIM). B.H. and P.P. performed genomic analysis and supported other bioinformatic analysis. M.P., K.S.L. M.Wag and R.S. supported the Raman microspetroscopy experiments. A.Sp. supported FACS analysis. A.Sc, M.Wag, M.Wat, N.J., M.V.B. and A.Ric. supported in data contribution and evaluation. G.N., S.K., and A.K. supported molecular biology experiments. All authors have approved the final version of the paper.

Competing interests

The authors declare no competing interests.

References

1 Porter, N. T. & Martens, E. C. The Critical Roles of Polysaccharides in Gut Microbial Ecology and Physiology. *Annu Rev Microbiol* **71**, 349-369, doi:10.1146/annurev-micro-102215-095316 (2017).

2 Holscher, H. D. Dietary fiber and prebiotics and the gastrointestinal microbiota. *Gut Microbes* **8**, 172-184, doi:10.1080/19490976.2017.1290756 (2017).

3 Gibson, G. R. & Roberfroid, M. B. Dietary modulation of the human colonic microbiota: introducing the concept of prebiotics. *J Nutr* **125**, 1401-1412, doi:10.1093/jn/125.6.1401 (1995).

4 Gibson, G. R. *et al.* Expert consensus document: The International Scientific Association for Probiotics and Prebiotics (ISAPP) consensus statement on the definition and scope of prebiotics. *Nat Rev Gastroenterol Hepatol* **14**, 491-502, doi:10.1038/nrgastro.2017.75 (2017).

5 Slavin, J. Fiber and prebiotics: mechanisms and health benefits. *Nutrients* **5**, 1417-1435, doi:10.3390/nu5041417 (2013).

6 Kolida, S., Tuohy, K. & Gibson, G. R. Prebiotic effects of inulin and oligofructose. *Br J Nutr* **87**, S193-197, doi:10.1079/BJNBJN/2002537 (2002).

7 Schaafsma, G. & Slavin, J. L. Significance of Inulin Fructans in the Human Diet. *Comprehensive Reviews in Food Science and Food Safety* **14**, 37-47, doi:10.1111/1541-4337.12119 (2015).

8 van Loo, J., Coussement, P., de Leenheer, L., Hoebregs, H. & Smits, G. On the presence of inulin and oligofructose as natural ingredients in the western diet. *Crit Rev Food Sci Nutr* **35**, 525-552, doi:10.1080/10408399509527714 (1995).

9 Moshfegh, A. J., Friday, J. E., Goldman, J. P. & Ahuja, J. K. Presence of inulin and oligofructose in the diets of Americans. *J Nutr* **129**, 1407S-1411S, doi:10.1093/jn/129.7.1407S (1999).

10 Guess, N. D., Dornhorst, A., Oliver, N. & Frost, G. S. A Randomised Crossover Trial: The Effect of Inulin on Glucose Homeostasis in Subtypes of Prediabetes. *Ann Nutr Metab* **68**, 26-34, doi:10.1159/000441626 (2016).

11 Zhang, Q. *et al.* Inulin-type fructan improves diabetic phenotype and gut microbiota profiles in rats. *PeerJ* **6**, e4446, doi:10.7717/peerj.4446 (2018).

12 Guo, X. *et al.* Rutin and Its Combination With Inulin Attenuate Gut Dysbiosis, the Inflammatory Status and Endoplasmic Reticulum Stress in Paneth Cells of Obese Mice Induced by High-Fat Diet. *Front Microbiol* **9**, 2651, doi:10.3389/fmicb.2018.02651 (2018).

13 Pool-Zobel, B. L. Inulin-type fructans and reduction in colon cancer risk: review of experimental and human data. *Br J Nutr* **93**, S73-90, doi:10.1079/bjn20041349 (2005).

14 Pandey, A. *et al.* Recent Developments in Microbial Inulinases: Its Production, Properties, and Industrial Applications. *Applied Biochemistry and Biotechnology* **81**, 35-52, doi:10.1385/abab:81:1:35 (1999).

15 Chijiiwa, R. *et al.* Single-cell genomics of uncultured bacteria reveals dietary fiber responders in the mouse gut microbiota. *Microbiome* **8**, 5, doi:10.1186/s40168-019-0779-2 (2020).
16 Boger, M. C. L., Lammerts van Bueren, A. & Dijkhuizen, L. Cross-Feeding among Probiotic Bacterial Strains on Prebiotic Inulin Involves the Extracellular exo-Inulinase of Lactobacillus paracasei Strain W20. *Appl Environ Microbiol* **84**, doi:10.1128/AEM.01539-18 (2018).
17 McKellar, R. C., Modler, H. W. & Mullin, J. Characterization of Growth and Inulinase Production by Bifidobacterium spp. on Fructooligosaccharides. *Bifidobacteria Microflora* **12**, 75-86, doi:10.12938/bifidus1982.12.2_75 (1993).
18 Lo, C. I. *et al.* Arabiibacter massiliensis gen. nov. sp. nov., New Anaerobic Bacterium Isolated from the Human Gut. *Curr Microbiol* **79**, 47, doi:10.1007/s00284-021-02739-8 (2022).
19 Le Bastard, Q. *et al.* The effects of inulin on gut microbial composition: a systematic review of evidence from human studies. *Eur J Clin Microbiol Infect Dis* **39**, 403-413, doi:10.1007/s10096-019-03721-w (2020).
20 Vandeputte, D. *et al.* Prebiotic inulin-type fructans induce specific changes in the human gut microbiota. *Gut* **66**, 1968-1974, doi:10.1136/gutjnl-2016-313271 (2017).
21 Holscher, H. D. *et al.* Agave Inulin Supplementation Affects the Fecal Microbiota of Healthy Adults Participating in a Randomized, Double-Blind, Placebo-Controlled, Crossover Trial. *J Nutr* **145**, 2025-2032, doi:10.3945/jn.115.217331 (2015).
22 Baxter, N. T. *et al.* Dynamics of Human Gut Microbiota and Short-Chain Fatty Acids in Response to Dietary Interventions with Three Fermentable Fibers. *mBio* **10**, doi:10.1128/mBio.02566-18 (2019).
23 Joglekar, P. *et al.* Genetic Variation of the SusC/SusD Homologs from a Polysaccharide Utilization Locus Underlies Divergent Fructan Specificities and Functional Adaptation in Bacteroides thetaiotaomicron Strains. *mSphere* **3**, doi:10.1128/mSphereDirect.00185-18 (2018).
24 Healey, G. *et al.* Habitual dietary fibre intake influences gut microbiota response to an inulin-type fructan prebiotic: a randomised, double-blind, placebo-controlled, cross-over, human intervention study. *Br J Nutr* **119**, 176-189, doi:10.1017/S0007114517003440 (2018).
25 Martinez, I., Kim, J., Duffy, P. R., Schlegel, V. L. & Walter, J. Resistant starches types 2 and 4 have differential effects on the composition of the fecal microbiota in human subjects. *PLoS One* **5**, e15046, doi:10.1371/journal.pone.0015046 (2010).
26 Ding, S. Y. *et al.* Cellulosomal scaffoldin-like proteins from Ruminococcus flavefaciens. *J Bacteriol* **183**, 1945-1953, doi:10.1128/JB.183.6.1945-1953.2001 (2001).
27 Mukhopadhya, I. *et al.* Sporulation capability and amylosome conservation among diverse human colonic and rumen isolates of the keystone starch-degrader Ruminococcus bromii. *Environ Microbiol* **20**, 324-336, doi:10.1111/1462-2920.14000 (2018).

28 Martens, E. C., Koropatkin, N. M., Smith, T. J. & Gordon, J. I. Complex glycan catabolism by the human gut microbiota: the Bacteroidetes Sus-like paradigm. *J Biol Chem* **284**, 24673-24677, doi:10.1074/jbc.R109.022848 (2009).
29 Boraston, A. B., Bolam, D. N., Gilbert, H. J. & Davies, G. J. Carbohydrate-binding modules: fine-tuning polysaccharide recognition. *Biochem J* **382**, 769-781, doi:10.1042/BJ20040892 (2004).
30 Florek, J., Caillard, R. & Kleitz, F. Evaluation of mesoporous silica nanoparticles for oral drug delivery - current status and perspective of MSNs drug carriers. *Nanoscale* **9**, 15252-15277, doi:10.1039/c7nr05762h (2017).
31 von Baeckmann, C. *et al.* Targeting Gut Bacteria Using Inulin-Conjugated Mesoporous Silica Nanoparticles. *Advanced Materials Interfaces*, doi:10.1002/admi.202102558 (2022).
32 Human Microbiome Project, C. Structure, function and diversity of the healthy human microbiome. *Nature* **486**, 207-214, doi:10.1038/nature11234 (2012).
33 Pereira, F. C. *et al.* Rational design of a microbial consortium of mucosal sugar utilizers reduces Clostridiodes difficile colonization. *Nat Commun* **11**, 5104, doi:10.1038/s41467-020-18928-1 (2020).
34 Lockyer, S. & Stanner, S. Prebiotics – an added benefit of some fibre types. *Nutrition Bulletin* **44**, 74-91, doi:10.1111/nbu.12366 (2019).
35 Hatzenpichler, R. *et al.* In situ visualization of newly synthesized proteins in environmental microbes using amino acid tagging and click chemistry. *Environ Microbiol* **16**, 2568-2590, doi:10.1111/1462-2920.12436 (2014).
36 Riva, A. *et al.* Conversion of Rutin, a Prevalent Dietary Flavonol, by the Human Gut Microbiota. *Front Microbiol* **11**, 585428, doi:10.3389/fmicb.2020.585428 (2020).
37 Berry, D. *et al.* Tracking heavy water (D2O) incorporation for identifying and sorting active microbial cells. *Proc Natl Acad Sci U S A* **112**, E194-203, doi:10.1073/pnas.1420406112 (2015).
38 Lee, K. S. *et al.* An automated Raman-based platform for the sorting of live cells by functional properties. *Nat Microbiol* **4**, 1035-1048, doi:10.1038/s41564-019-0394-9 (2019).
39 Browne, H. P. *et al.* Culturing of 'unculturable' human microbiota reveals novel taxa and extensive sporulation. *Nature* **533**, 543-546, doi:10.1038/nature17645 (2016).
40 Rakoff-Nahoum, S., Coyne, M. J. & Comstock, L. E. An ecological network of polysaccharide utilization among human intestinal symbionts. *Curr Biol* **24**, 40-49, doi:10.1016/j.cub.2013.10.077 (2014).
41 Hughes, R. L., Alvarado, D. A., Swanson, K. S. & Holscher, H. D. The Prebiotic Potential of Inulin-type Fructans: A Systematic Review. *Adv Nutr*, doi:10.1093/advances/nmab119 (2021).
42 Patnode, M. L. *et al.* Strain-level functional variation in the human gut microbiota based on bacterial binding to artificial food particles. *Cell Host Microbe* **29**, 664-673 e665, doi:10.1016/j.chom.2021.01.007 (2021).

43 Rodriguez, J. *et al.* Discovery of the gut microbial signature driving the efficacy of prebiotic intervention in obese patients. *Gut* **69**, 1975-1987, doi:10.1136/gutjnl-2019-319726 (2020).
44 Wang, X., Wang, T., Zhang, Q., Xu, L. & Xiao, X. Dietary Supplementation with Inulin Modulates the Gut Microbiota and Improves Insulin Sensitivity in Prediabetes. *Int J Endocrinol* **2021**, 5579369, doi:10.1155/2021/5579369 (2021).
45 Birkeland, E. *et al.* Prebiotic effect of inulin-type fructans on faecal microbiota and short-chain fatty acids in type 2 diabetes: a randomised controlled trial. *Eur J Nutr* **59**, 3325-3338, doi:10.1007/s00394-020-02282-5 (2020).
46 Dewulf, E. M. *et al.* Insight into the prebiotic concept: lessons from an exploratory, double blind intervention study with inulin-type fructans in obese women. *Gut* **62**, 1112-1121, doi:10.1136/gutjnl-2012-303304 (2013).
47 Carlson, J. L., Erickson, J. M., Hess, J. M., Gould, T. J. & Slavin, J. L. Prebiotic Dietary Fiber and Gut Health: Comparing the in Vitro Fermentations of Beta-Glucan, Inulin and Xylooligosaccharide. *Nutrients* **9**, doi:10.3390/nu9121361 (2017).
48 Stewart, M. L., Timm, D. A. & Slavin, J. L. Fructooligosaccharides exhibit more rapid fermentation than long-chain inulin in an in vitro fermentation system. *Nutr Res* **28**, 329-334, doi:10.1016/j.nutres.2008.02.014 (2008).
49 Riva, A. *et al.* A fiber-deprived diet disturbs the fine-scale spatial architecture of the murine colon microbiome. *Nat Commun* **10**, 4366, doi:10.1038/s41467-019-12413-0 (2019).
50 Zhang, Z. *et al.* Spatial heterogeneity and co-occurrence patterns of human mucosal-associated intestinal microbiota. *ISME J* **8**, 881-893, doi:10.1038/ismej.2013.185 (2014).
51 Rodriguez-Daza, M. C. *et al.* Polyphenol-Mediated Gut Microbiota Modulation: Toward Prebiotics and Further. *Front Nutr* **8**, 689456, doi:10.3389/fnut.2021.689456 (2021).
52 Gupta, R. S., Chen, W. J., Adeolu, M. & Chai, Y. Molecular signatures for the class Coriobacteriia and its different clades; proposal for division of the class Coriobacteriia into the emended order Coriobacteriales, containing the emended family Coriobacteriaceae and Atopobiaceae fam. nov., and Eggerthellales ord. nov., containing the family Eggerthellaceae fam. nov. *Int J Syst Evol Microbiol* **63**, 3379-3397, doi:10.1099/ijs.0.048371-0 (2013).
53 Thorasin, T., Hoyles, L. & McCartney, A. L. Dynamics and diversity of the 'Atopobium cluster' in the human faecal microbiota, and phenotypic characterization of 'Atopobium cluster' isolates. *Microbiology (Reading)* **161**, 565-579, doi:10.1099/mic.0.000016 (2015).
54 Eggerth, A. H. The Gram-positive Non-spore-bearing Anaerobic Bacilli of Human Feces. *J Bacteriol* **30**, 277-299, doi:10.1128/jb.30.3.277-299.1935 (1935).
55 Noecker, C. *et al.* Systems biology elucidates the distinctive metabolic niche filled by the human gut microbe Eggerthella lenta. *PLoS Biol* **21**, e3002125, doi:10.1371/journal.pbio.3002125 (2023).
56 Lin, S. H., Chou, L. M., Chien, Y. W., Chang, J. S. & Lin, C. I. Prebiotic Effects of Xylooligosaccharides on the Improvement of Microbiota Balance in Human Subjects. *Gastroenterol Res Pract* **2016**, 5789232, doi:10.1155/2016/5789232 (2016).

61

57 Finegold, S. M. *et al.* Xylooligosaccharide increases bifidobacteria but not lactobacilli in human gut microbiota. *Food Funct* **5**, 436-445, doi:10.1039/c3fo60348b (2014).
58 Christensen, E. G., Licht, T. R., Leser, T. D. & Bahl, M. I. Dietary xylo-oligosaccharide stimulates intestinal bifidobacteria and lactobacilli but has limited effect on intestinal integrity in rats. *BMC Res Notes* **7**, 660, doi:10.1186/1756-0500-7-660 (2014).
59 Hahne, F. *et al.* flowCore: a Bioconductor package for high throughput flow cytometry. *BMC Bioinformatics* **10**, 106, doi:10.1186/1471-2105-10-106 (2009).
60 Pjevac, P. *et al.* An Economical and Flexible Dual Barcoding, Two-Step PCR Approach for Highly Multiplexed Amplicon Sequencing. *Frontiers in Microbiology* **12**, doi:10.3389/fmicb.2021.669776 (2021).
61 Herbold, C. W. *et al.* A flexible and economical barcoding approach for highly multiplexed amplicon sequencing of diverse target genes. *Front Microbiol* **6**, 731, doi:10.3389/fmicb.2015.00731 (2015).
62 Callahan, B. J. *et al.* DADA2: High-resolution sample inference from Illumina amplicon data. *Nat Methods* **13**, 581-583, doi:10.1038/nmeth.3869 (2016).
63 Callahan, B. J., Sankaran, K., Fukuyama, J. A., McMurdie, P. J. & Holmes, S. P. Bioconductor Workflow for Microbiome Data Analysis: from raw reads to community analyses. *F1000Res* **5**, 1492, doi:10.12688/f1000research.8986.2 (2016).
64 Davis, N. M., Proctor, D. M., Holmes, S. P., Relman, D. A. & Callahan, B. J. Simple statistical identification and removal of contaminant sequences in marker-gene and metagenomics data. *Microbiome* **6**, 226, doi:10.1186/s40168-018-0605-2 (2018).
65 Lee, K. S. *et al.* Optofluidic Raman-activated cell sorting for targeted genome retrieval or cultivation of microbial cells with specific functions. *Nat Protoc* **16**, 634-676, doi:10.1038/s41596-020-00427-8 (2021).
66 Takagi, R., Tsujikawa, Y., Nomoto, R. & Osawa, R. Comparison of the Growth of Lactobacillus delbrueckii, L. paracasei and L. plantarum on Inulin in Co-culture Systems. *Biosci Microbiota Food Health* **33**, 139-146, doi:10.12938/bmfh.33.139 (2014).
67 Praznik, W., Loppert, R., Cruz Rubio, J. M., Zangger, K. & Huber, A. Structure of fructo-oligosaccharides from leaves and stem of Agave tequilana Weber, var. azul. *Carbohydr Res* **381**, 64-73, doi:10.1016/j.carres.2013.08.025 (2013).
68 Chung, W. S. *et al.* Modulation of the human gut microbiota by dietary fibres occurs at the species level. *BMC Biol* **14**, 3, doi:10.1186/s12915-015-0224-3 (2016).
69 Daims, H. Use of fluorescence in situ hybridization and the daime image analysis program for the cultivation-independent quantification of microorganisms in environmental and medical samples. *Cold Spring Harb Protoc* **2009**, pdb prot5253, doi:10.1101/pdb.prot5253 (2009).
70 Sekar, R. *et al.* An improved protocol for quantification of freshwater Actinobacteria by fluorescence in situ hybridization. *Appl Environ Microbiol* **69**, 2928-2935, doi:10.1128/AEM.69.5.2928-2935.2003 (2003).
71 Schwiertz, A., Le Blay, G. & Blaut, M. Quantification of different Eubacterium spp. in human fecal samples with species-specific 16S rRNA-targeted oligonucleotide probes. *Appl Environ Microbiol* **66**, 375-382, doi:10.1128/aem.66.1.375-382.2000 (2000).

72 Harmsen, H. J. *et al.* Development of 16S rRNA-based probes for the Coriobacterium group and the Atopobium cluster and their application for enumeration of Coriobacteriaceae in human feces from volunteers of different age groups. *Appl Environ Microbiol* **66**, 4523-4527, doi:10.1128/aem.66.10.4523-4527.2000 (2000).
73 Amann, R. I., Krumholz, L. & Stahl, D. A. Fluorescent-oligonucleotide probing of whole cells for determinative, phylogenetic, and environmental studies in microbiology. *J Bacteriol* **172**, 762-770, doi:10.1128/jb.172.2.762-770.1990 (1990).
74 Daims, H., Bruhl, A., Amann, R., Schleifer, K. H. & Wagner, M. The domain-specific probe EUB338 is insufficient for the detection of all Bacteria: development and evaluation of a more comprehensive probe set. *Syst Appl Microbiol* **22**, 434-444, doi:10.1016/S0723-2020(99)80053-8 (1999).
75 Wallner, G., Amann, R. & Beisker, W. Optimizing fluorescent in situ hybridization with rRNA-targeted oligonucleotide probes for flow cytometric identification of microorganisms. *Cytometry* **14**, 136-143, doi:10.1002/cyto.990140205 (1993).
76 Daims, H., Lucker, S. & Wagner, M. daime, a novel image analysis program for microbial ecology and biofilm research. *Environ Microbiol* **8**, 200-213, doi:10.1111/j.1462-2920.2005.00880.x (2006).
77 Huang, W. E. *et al.* Raman-FISH: combining stable-isotope Raman spectroscopy and fluorescence in situ hybridization for the single cell analysis of identity and function. *Environ Microbiol* **9**, 1878-1889, doi:10.1111/j.1462-2920.2007.01352.x (2007).
78 Bankevich, A. *et al.* SPAdes: a new genome assembly algorithm and its applications to single-cell sequencing. *J Comput Biol* **19**, 455-477, doi:10.1089/cmb.2012.0021 (2012).
79 Parks, D. H., Imelfort, M., Skennerton, C. T., Hugenholtz, P. & Tyson, G. W. CheckM: assessing the quality of microbial genomes recovered from isolates, single cells, and metagenomes. *Genome Res* **25**, 1043-1055, doi:10.1101/gr.186072.114 (2015).
80 Huerta-Cepas, J. *et al.* eggNOG 5.0: a hierarchical, functionally and phylogenetically annotated orthology resource based on 5090 organisms and 2502 viruses. *Nucleic Acids Res* **47**, D309-D314, doi:10.1093/nar/gky1085 (2019).
81 Grant, J. R. & Stothard, P. The CGView Server: a comparative genomics tool for circular genomes. *Nucleic Acids Res* **36**, W181-184, doi:10.1093/nar/gkn179 (2008).
82 Yoon, S. H., Ha, S. M., Lim, J., Kwon, S. & Chun, J. A large-scale evaluation of algorithms to calculate average nucleotide identity. *Antonie Van Leeuwenhoek* **110**, 1281-1286, doi:10.1007/s10482-017-0844-4 (2017).
83 Edgar, R. C. Search and clustering orders of magnitude faster than BLAST. *Bioinformatics* **26**, 2460-2461, doi:10.1093/bioinformatics/btq461 (2010).
84 Katoh, K., Kuma, K., Toh, H. & Miyata, T. MAFFT version 5: improvement in accuracy of multiple sequence alignment. *Nucleic Acids Res* **33**, 511-518, doi:10.1093/nar/gki198 (2005).
85 Capella-Gutierrez, S., Silla-Martinez, J. M. & Gabaldon, T. trimAl: a tool for automated alignment trimming in large-scale phylogenetic analyses. *Bioinformatics* **25**, 1972-1973, doi:10.1093/bioinformatics/btp348 (2009).

86 Nguyen, L. T., Schmidt, H. A., von Haeseler, A. & Minh, B. Q. IQ-TREE: a fast and effective stochastic algorithm for estimating maximum-likelihood phylogenies. *Mol Biol Evol* **32**, 268-274, doi:10.1093/molbev/msu300 (2015).
87 Minh, B. Q., Nguyen, M. A. & von Haeseler, A. Ultrafast approximation for phylogenetic bootstrap. *Mol Biol Evol* **30**, 1188-1195, doi:10.1093/molbev/mst024 (2013).
88 Altschul, S. F. *et al.* Gapped BLAST and PSI-BLAST: a new generation of protein database search programs. *Nucleic Acids Res* **25**, 3389-3402, doi:10.1093/nar/25.17.3389 (1997).
89 Stamatakis, A. RAxML version 8: a tool for phylogenetic analysis and post-analysis of large phylogenies. *Bioinformatics* **30**, 1312-1313, doi:10.1093/bioinformatics/btu033 (2014).
90 Wright, E. S., Yilmaz, L. S. & Noguera, D. R. DECIPHER, a search-based approach to chimera identification for 16S rRNA sequences. *Appl Environ Microbiol* **78**, 717-725, doi:10.1128/AEM.06516-11 (2012).
91 Yu, G. Using ggtree to Visualize Data on Tree-Like Structures. *Curr Protoc Bioinformatics* **69**, e96, doi:10.1002/cpbi.96 (2020).
92 Letunic, I. & Bork, P. Interactive Tree Of Life (iTOL) v5: an online tool for phylogenetic tree display and annotation. *Nucleic Acids Res* **49**, W293-W296, doi:10.1093/nar/gkab301 (2021).
93 Love, M. I., Huber, W. & Anders, S. Moderated estimation of fold change and dispersion for RNA-seq data with DESeq2. *Genome. Biol.* **15**, 550, doi:10.1186/s13059-014-0550-8 (2014).
94 Calgaro, M., Romualdi, C., Waldron, L., Risso, D. & Vitulo, N. Assessment of statistical methods from single cell, bulk RNA-seq, and metagenomics applied to microbiome data. *Genome Biol* **21**, 191, doi:10.1186/s13059-020-02104-1 (2020).

GUT MICROBES
2025, VOL. 17, NO. 1, 2525482
https://doi.org/10.1080/19490976.2025.2525482

Taylor & Francis
Taylor & Francis Group

RESEARCH PAPER

Lactulose selectively stimulates members of the gut microbiota, as determined by multi-modal activity-based sorting

Hamid Rasoulimehrabani[a,b], Alessandra Riva[a,c], Deniz Inan[a], Adnan Hodžić[a], Bela Hausmann[d,e], Georgi Nikolov[a], Sanaz Khadem[a], Norbert Hieger[a], Julia Wiesenbauer[a], Christina Kaiser[a], Verena Filz[f], Thomas Böttcher[f], and David Berry[a,d]

[a]Center for Microbiology and Environmental Systems Science, Department of Microbiology and Ecosystem Science, University of Vienna, Vienna, Austria; [b]Doctoral School in Microbiology and Environmental Science, University of Vienna, Vienna, Austria; [c]Chair of Nutrition and Immunology, TUM School of Life Sciences, Technical University of Munich, Freising, Germany; [d]Joint Microbiome Facility of the Medical University of Vienna and The University of Vienna, Vienna, Austria; [e]Department of Laboratory Medicine, Medical University of Vienna, Vienna, Austria; [f]Department of Biological Chemistry, University of Vienna, Vienna, Austria

ABSTRACT

There is much interest in the development of dietary supplements that selectively promote the growth of beneficial gut bacteria. The selectivity of many candidate prebiotics has, however, not been thoroughly investigated. Here, we evaluated stimulation of the human gut microbiota by the disaccharide lactulose using an *ex vivo* multimodal activity-based cell sorting approach. Incubation of human donor stool with lactulose resulted in growth or stimulation of a restricted diversity of bacterial genera, most prominently *Bifidobacterium*, *Collinsella*, and *Lactococcus*. Physiological analysis of lactulose-responsive strains isolated by Raman activated cell sorting revealed that most were capable of lactulose degradation. Among these isolates, *Lactococcus lactis* could not degrade lactulose, but its growth was boosted by co-cultivation with lactulose degraders. This suggests that inter-species facilitation contributes to the lactulose degradation niche. Moreover, we observed that lactulose selectively activates metabolically important taxa, including health-associated genera such as *Faecalibacterium* and *Gemmiger*[1,2,3], potentially indicating broader functional effects beyond compositional changes. These results provide novel insights into the physiology and ecology of lactulose utilization by the human gut microbiota and underscore the potential of lactulose as a prebiotic dietary supplement.

ARTICLE HISTORY
Received 14 March 2025
Revised 13 June 2025
Accepted 20 June 2025

KEYWORDS
Raman microspectroscopy; prebiotics; BONCAT; RACS; keystone species

Chapter 2

Lactulose selectively stimulates members of the gut microbiota, as determined by multi-modal activity-based sorting

Hamid Rasoulimehrabani[1,2], Alessandra Riva[1,3], Deniz Inan[1], Adnan Hodžić[1], Bela Hausmann[4,5], Georgi Nikolov[1], Sanaz Khadem[1], Norbert Hieger[1], Julia Wiesenbauer[1], Christina Kaiser[1], Verena Filz[6], Thomas Böttcher[6], David Berry[1,4*]

[1]Center for Microbiology and Environmental Systems Science, Department of Microbiology and ecosystem Science, University of Vienna, Austria

[2]Doctoral School in Microbiology and Environmental Science, University of Vienna, Vienna, Austria

[3]Chair of Nutrition and Immunology, TUM School of Life Sciences, Technical University of Munich, 85354 Freising, Germany

[4]Joint Microbiome Facility of the Medical University of Vienna and the University of Vienna, Austria

[5]Department of Laboratory Medicine, Medical University of Vienna, Austria

[6] Department of Biological Chemistry, University of Vienna, Austria

* Address correspondence to David Berry: david.berry@univie.ac.at

Abstract

There is much interest in the development of dietary supplements that selectively promote the growth of beneficial gut bacteria. The selectivity of many candidate prebiotics has, however, not been thoroughly investigated. Here, we evaluated stimulation of the human gut microbiota by the disaccharide lactulose using an *ex vivo* multimodal activity-based cell sorting approach. Incubation of human donor stool with lactulose resulted in growth or stimulation of a restricted diversity of bacterial genera, most prominently *Bifidobacterium*, *Collinsella*, and *Lactococcus*. Physiological analysis of lactulose-responsive strains isolated by Raman activated cell sorting revealed that most were capable of lactulose degradation. Among these isolates, *Lactococcus lactis* could not degrade lactulose, but its growth was boosted by co-cultivation with lactulose degraders. This suggests that inter-species facilitation contributes to the lactulose degradation niche. Moreover, we observed that lactulose selectively activates metabolically important taxa, including health-associated genera such as *Faecalibacterium* and *Gemmiger*[1–3], supporting broader functional effects beyond compositional changes. These results provide novel insights into the physiology and ecology of lactulose utilization by the human gut microbiota and underscore the potential of lactulose as a prebiotic dietary supplement.

Introduction

The human gastrointestinal tract hosts a diverse community of microorganisms known as the gut microbiota that plays important roles in multiple aspects of human physiology, including digestion and nutrition, metabolism, and immune and neurological function[4,5]. The microbiota is particularly dense and diverse in the large intestine, where it is dominated by the bacterial phyla *Bacillota, Bacteroidota, Actinomycetota,* and *Pseudomonadota*[6]. The composition of the gut microbiota is influenced by several factors, with diet being an important determinant[7,8]. Diets rich in non-digestible polysaccharides have been shown to increase the abundance of beneficial gut microbes, particularly members of *Bacillota* and *Actinomycetota*[9]. Additionally, supplementation of diet with non-digestible dietary polysaccharides such as inulin,

fructooligosaccharides (FOS), and galactooligosaccharides has been reported to support the growth of taxa such as *Bifidobacterium* and *Lactobacillus*[10,11]. This has led to the concept of prebiotics, which are specific dietary supplements that selectively promote the growth of certain gut microorganisms, modulate microbiota function, and confer a health benefit to the host[12–12]. However, for many candidate prebiotics, it remains unclear which specific taxa are stimulated and how their metabolic interactions influence gut microbiome dynamics[6].

Among candidate prebiotics, lactulose has emerged as a promising yet underexplored synthetic disaccharide, composed of fructose and galactose linked by a β-1,4-glycosidic bond[16,17]. It is primarily used in medicine for treating constipation, hepatic encephalopathy, and diabetes[16, 18, 19]. Recent *in vitro* and *in vivo* studies have indicated that lactulose at low doses may also have prebiotic effects[20] and can increase the intestinal levels of *Bifidobacterium* and *Lactobacillus*[21], which may help in maintaining gut health by boosting production of short-chain fatty acids (SCFAs) and inhibiting enteric pathogens[16, 17]. In both human and mouse models, oral intake of lactulose increased intestinal *Bifidobacterium* and acetate production, resulting in gut lumen acidification that inhibited antibiotic-resistant bacteria and was associated with reduced infection rates and improved liver disease outcomes[22]. In the present study, we examined the stimulatory effect of lactulose on the gut microbiota of healthy human adults in *ex vivo* incubations. We employed a multi-modal activity-based sorting approach to identify which microbial cells were metabolically active under the applied incubation conditions. Our findings were further validated through physiological analysis and co-cultivation assays, which revealed that lactulose not only promoted the growth and metabolic activity of a subset of gut bacteria, but also enabled ecological facilitation within the microbiota. These results highlight lactulose's role in shaping community structure by selectively stimulating primary degraders such as *Bifidobacterium adolescentis* and *Collinsella aerofaciens*, which in turn facilitated the growth of non-degraders like *Lactococcus lactis*.

Results

Lactulose is rapidly degraded by the gut microbiota

We employed a multi-modal activity-based sorting approach to identify gut microbes that are stimulated by lactulose[23]. Freshly collected fecal samples from six healthy adults were incubated anaerobically for 6 h with lactulose or its component monosaccharides, galactose and fructose, in the presence of the cellular activity markers D_2O and L-azidohomoalanine (AHA; Supplementary Figure 1). 6 h incubations were previously determined to be suitable for detecting gut microbiota response to carbohydrates using these activity markers[23]. Lactulose degradation by the gut microbiota was detected in all donor samples (Figure 1a). 29-58% of added lactulose was degraded by 6 h, indicating that, despite some interindividual variability in degradation kinetics, the gut microbiota from all donors demonstrated a considerable capacity to degrade lactulose.

Lactulose drives both conserved and individualized microbial population dynamics

The gut microbiota of all donors was dominated on average by the phyla *Bacillota* (46.6%) and *Bacteroidota* (44.9%), with contributions from *Pseudomonadota* (4.6%) and *Actinomycetota* (3.8%; Figure 1b). Analysis of genus-level microbiome profiles of all samples revealed that most of the variation in the dataset was attributable to inter-individual differences, with donor-specific effects accounting for 78.6% of the total variation ($R^2 = 0.786$, $p = 0.001$, $n = 36$ samples). This was also the primary driver of clustering observed in the principal coordinates analysis (PerMANOVA, $p = 0.125$; Figure 1c), reflecting considerable baseline differences in microbial composition across donors.

We next evaluated which bacterial genera grew upon lactulose amendment, as inferred by a significant increase in relative abundance, either in individual donor microbiomes or across the donor cohort. *Bifidobacterium* was the only genus that consistently increased in relative abundance across all six donors by 6 h in lactulose supplemented samples, but not in no

amendment samples (DESeq2, Wald Test p.adj<0.05; Figure 1d, Supplementary Figure 2). This observation aligns with prior studies reporting lactulose-induced bifidogenic effects in both in vitro and clinical settings[22,24]. In addition, the relative abundances of *Collinsella, Gemmiger, Ruminococcus, Oscillibacter, Agathobacter, Anaerobutyrium*, *Escherichia*, and *Blautia* were significantly increased by 6 h in one or more donors, potentially reflecting a donor-specific response to lactulose supplementation (Supplementary Data 1). Incubations were also conducted with the two constituent monosaccharides of lactulose, galactose and fructose, to assess any differences in microbial responses and community shifts. *Bifidobacterium* was the most abundant genus that consistently increased in relative abundance in the presence of either sugar, though several other taxa were increased in one or both sugar in samples from one or more donors (Supplementary Figure 3, Supplementary Data 2 - 3).

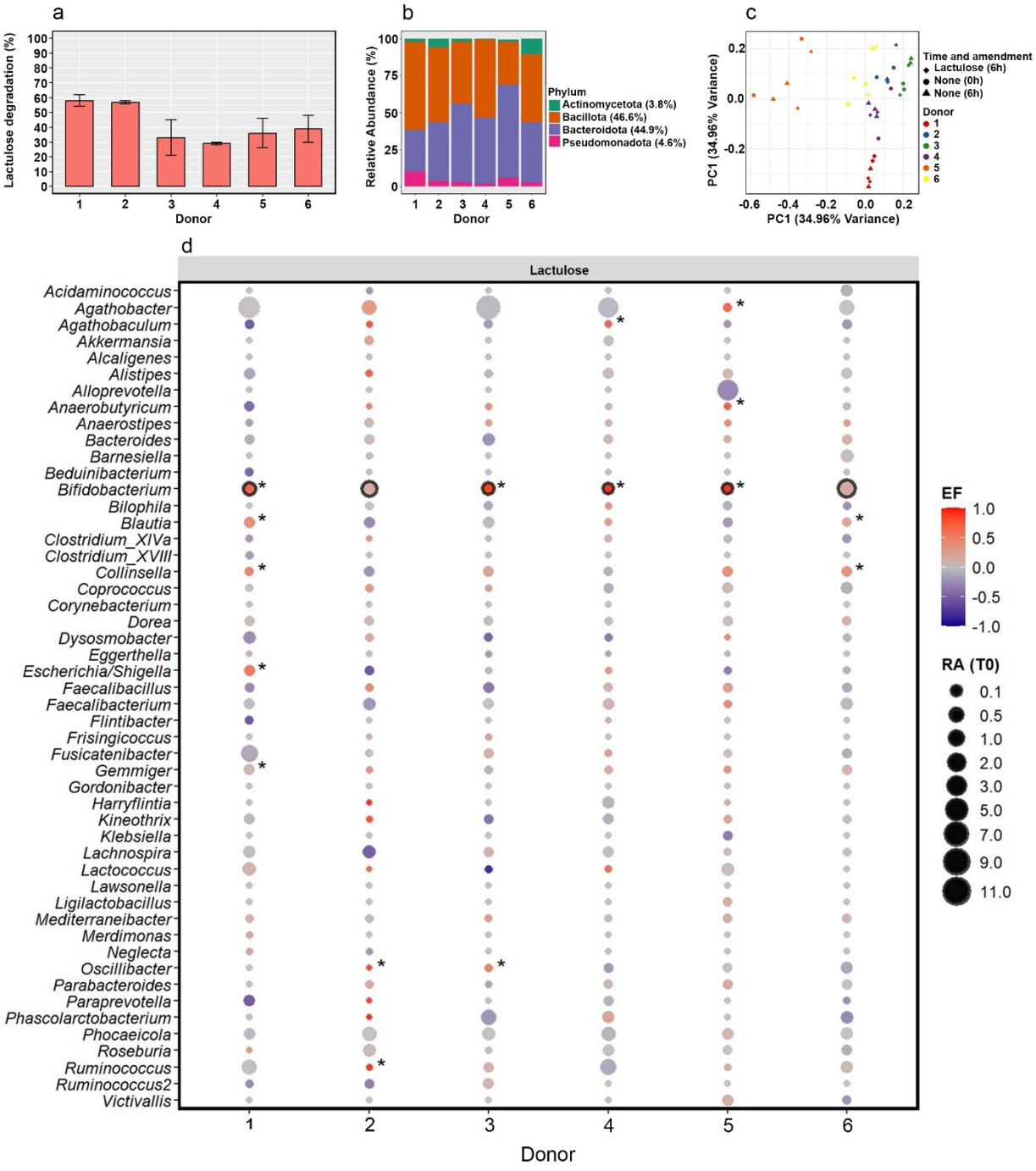

Figure 1. Lactulose degradation and gut microbiome composition. (a) Lactulose degradation (%) after 6h of anaerobic incubation with fresh fecal samples from 6 donors (mean ± SD: 41.5% ± 12.5, n = 12) measured with HPAEC. The bar represents the mean of two technical replicates and error bars indicate the standard deviation. (b) Phylum-level composition (relative abundance, as %) of fecal samples prior to incubation (t = 0 h). The mean of technical replicates is shown. The mean of relative abundances across the sample set are listed in the legend. (c) Principal coordinate analysis (PCoA) ordination of genus-level

microbiome profiles for lactulose-amended samples at 6 hours and no amendment samples at 0 and 6 hours. Technical replicates are shown. (d) Change in relative abundance of abundant bacterial genera after 6 h incubation of lactulose-amended samples. Bubble size indicates relative abundance (RA) at 0h. The change in relative abundance during incubation, calculated as a normalized and scaled enrichment factor (EF; see Materials and Methods), is indicated by bubble color. Genera significantly enriched in individual donors are marked with an asterisk and those significantly enriched across all six donors (as determined by DESeq2, Wald Test, $p<0.05$, n = 36 samples) are outlined in black.

Lactulose induces translational activity in a subset of the microbiota

As increases in relative abundance may not necessarily be a sensitive indicator of cellular response to lactulose, we next evaluated microbial stimulation by lactulose using L-azidohomoalanine (AHA) labeling as a marker of cellular translational activity, followed by bioorthogonal non-canonical amino acid tagging (BONCAT) with fluorescence-activated cell sorting (FACS)[23,25]. This approach allows for sorting and sequencing of translationally active as well as non-active cells (Figure 2a). Translationally active cells were detected by fluorescence microscopy in all lactulose-amended samples but not in no amendment samples after 6 hours of incubation, and therefore BONCAT-positive cells from 6 h lactulose incubations as well as BONCAT-negative cells from 6 h no amendment samples were sorted with FACS and subjected to 16S rRNA gene amplicon sequencing. Principal coordinates analysis (PCoA) of the genus-level microbiome profiles revealed donor-driven clustering (Figure 2b; $R^2 = 0.5069$, $p = 0.001$, n=36 samples). However, BONCAT-positive cells from lactulose-amended samples clustered separately from non-active cells of no amendment samples from each donor ($R^2 = 0.1003$, $p = 0.001$, n=24 samples).

The genera that were most consistently stimulated by lactulose amendment across the donor cohort were *Bifidobacterium, Collinsella, Gemmiger, and Phocaeicola* (Figure 2c, Supplementary Data 4). Multiple taxa were significantly stimulated in individual donors, including *Blautia, Clostridium, Eggerthella, Bacteroides, Faecalibacterium, Anaerostipes,* and *Escherichia/Shigella*. *Collinsella*, *Eggerthella, Faecalibacterium* and *Gemmiger* were also stimulated across all donors for both fructose and galactose incubations, potentially indicating their ability to metabolize

these substrates (Supplementary Data 5-6). *Bacteroides* was stimulated across all donors in fructose incubations and *Bifidobacterium* was stimulated across all donors in galactose incubations (Supplementary Figure 4).

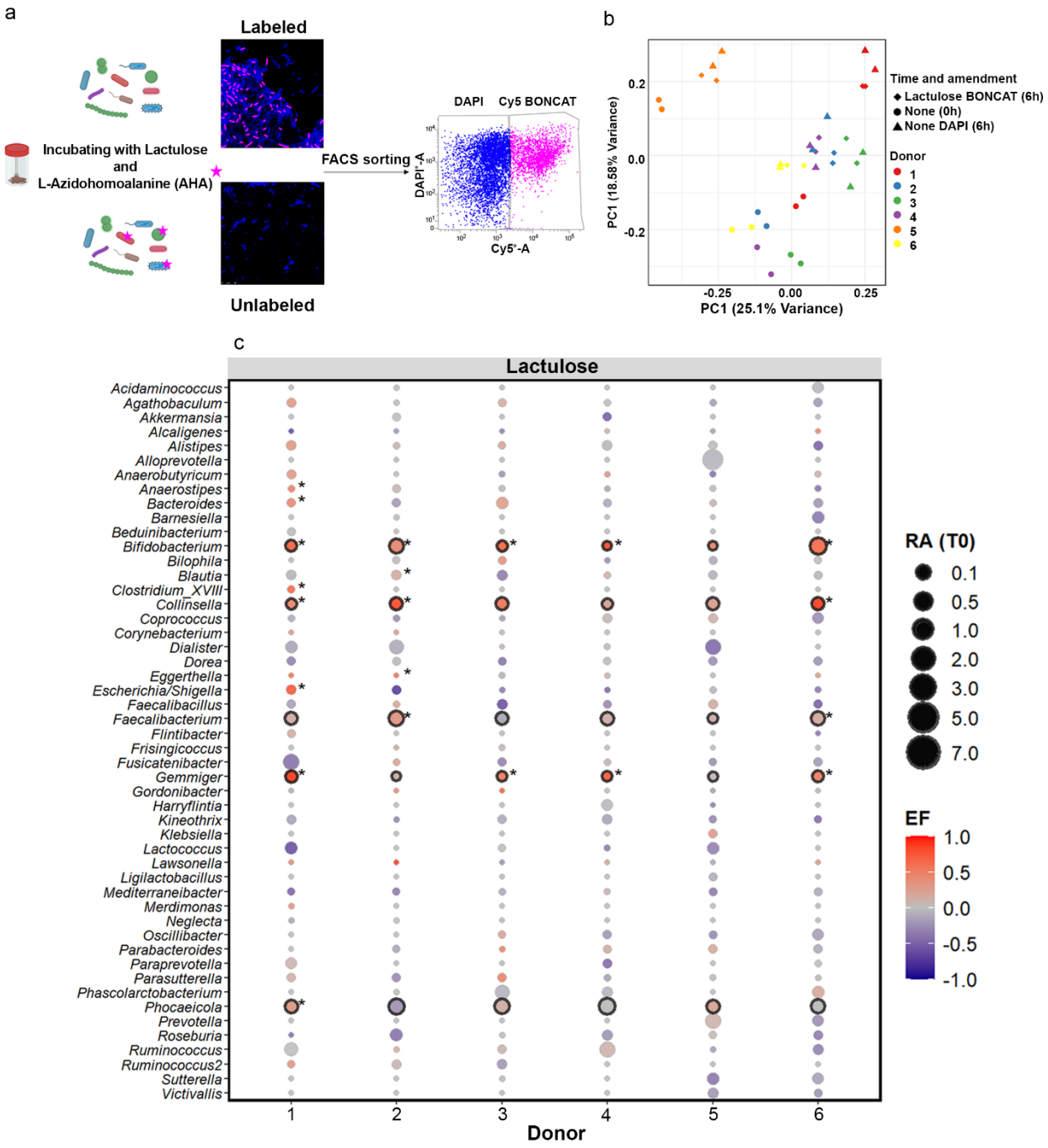

Figure 2. Identification of translationally-active cells. (a) Schematic representation of the workflow for sorting of translationally active cells using L-azidohomoalanine (AHA) labeling as a marker of cellular translational activity and bioorthogonal non-canonical amino acid tagging (BONCAT) with fluorescence-activated cell sorting (FACS)[23,26]. Translationally active cells were visualized through Cy5 fluorescence (pink) in microscopy images, while total bacterial cells were stained with DAPI (blue). BONCAT-positive cells were then sorted using fluorescence-activated cell sorting (FACS) based on Cy5 fluorescence intensity (BONCAT, pink) and DAPI signals (blue). Sorted translationally active fractions represent metabolically active bacteria responding to lactulose, enabling downstream taxonomic identification via 16S rRNA gene sequencing. (b) Principal coordinate analysis (PCoA) ordination of genus-level microbiome profiles. "None (0h)" represents baseline (pre-incubation) microbiomes. "None DAPI (6h)" represents BONCAT-negative FACS-sorted cells after 6 h incubation of no amendment samples. "Lactulose BONCAT (6h)" represents BONCAT-positive FACS-sorted cells after 6 h incubation of lactulose-amended samples. Technical replicates were performed. (c) Change in relative abundance of abundant bacterial genera after 6 h incubation of lactulose-amended samples. Bubble size indicates relative abundance (RA) at 0h. The difference in relative abundance of each genus between BONCAT-positive FACS-sorted cells (lactulose BONCAT 6h) of lactulose-amended samples and BONCAT-negative FACS-sorted cells of no amendment samples after 6 h incubation (None DAPI 6h) was calculated as a normalized and scaled enrichment factor (EF; see Materials and Methods) and is indicated by bubble color. Genera significantly enriched in individual donors are marked with an asterisk and those significantly enriched across all six donors (as determined with DESeq2) are outlined in black.

Targeted cultivation of lactulose-stimulated bacteria by Raman activated cell sorting

We next employed heavy water (D_2O) activity labeling combined with Raman activated cell sorting (RACS)[23,27] to isolate and physiologically characterize cells stimulated by lactulose amendment. The metabolic activity of individual microbial cells from incubations was assessed using Raman microspectroscopy, which measures the incorporation of deuterium (D) from D_2O into cellular structures, resulting in the formation of detectable C-D bonds (quantified as %CD; Figure 3a). Across all donors, %CD values were significantly higher in cells from lactulose-amended samples compared to no amendment samples, indicating stimulation of metabolic activity by lactulose (ANOVA, $p<0.001$; Figure 3b).

Deuterium-labeled cells were then sorted from lactulose-amended samples using RACS and isolated by plating. Sorting and cultivation resulted in the recovery of 30 bacterial colonies, which were classified via near-full-length 16S rRNA gene sequencing. The isolates included *Collinsella*

(n=17), *Lactococcus* (n=3), and *Bifidobacterium* (n=10). This included several well-defined species such as *Bifidobacterium adolescentis, Bifidobacterium longum, Collinsella aerofaciens* and *Lactococcus lactis*, as well as strains with sequences that matched multiple closely related species within the same genus, reflecting a conservative genus-level classification where precise species identification was not possible (Figure 3c, Supplementary Data 7). For comparison, direct isolation of bacteria on the same cultivation medium led to the isolation of species of *Bifidobacterium, Collinsella,* and *Phoecaicola* but not *Lactococcus* (Supplementary Figure 5), indicating a partial but incomplete overlap in recovered taxa with the two approaches.

One isolate of each species from each donor was then selected as a representative for physiological analysis. The addition of lactulose to cultivation medium stimulated the growth of all tested strains except *L. lactis* (Figure 3c). Likewise, significant lactulose degradation was observed by cultures of all tested *Bifidobacterium* spp. and some *C. aerofaciens* but not by *L. lactis*. For comparison, we conducted a random sorting experiment with RACS, in which cells were collected regardless of their metabolic activity, and isolated 20 strains. Only 7 of these strains were able to grow on a medium where lactulose was the main carbon source, underscoring the selectivity of the RACS approach (Supplementary Figure 6).

To gain insights into the enzymes responsible for lactulose degradation, we performed RNAseq on *B. adolescentis* grown in a medium containing either lactulose, lactose, or glucose. Among the six annotated β-galactosidase genes in its genome, one gene, CCMPN/A_D1907, was highly expressed in the presence of lactulose (Supplementary Figure 7). Interestingly, it was also highly expressed in the presence of lactose and has 83% sequence identity to the well-characterized *Escherichia coli* β-galactosidase responsible for lactose cleavage (LacZ, UniProt accession P00722). To confirm that a bacterial β-galactosidase can cleave both lactose and lactulose, we evaluated the enzymatic activity of *E. coli* β-galactosidase. Degradation of both lactulose and lactose, as well as release of their constituent monosaccharides, was observed under incubation conditions, albeit with slightly reduced activity in cleaving lactulose (Supplementary Figure 8).

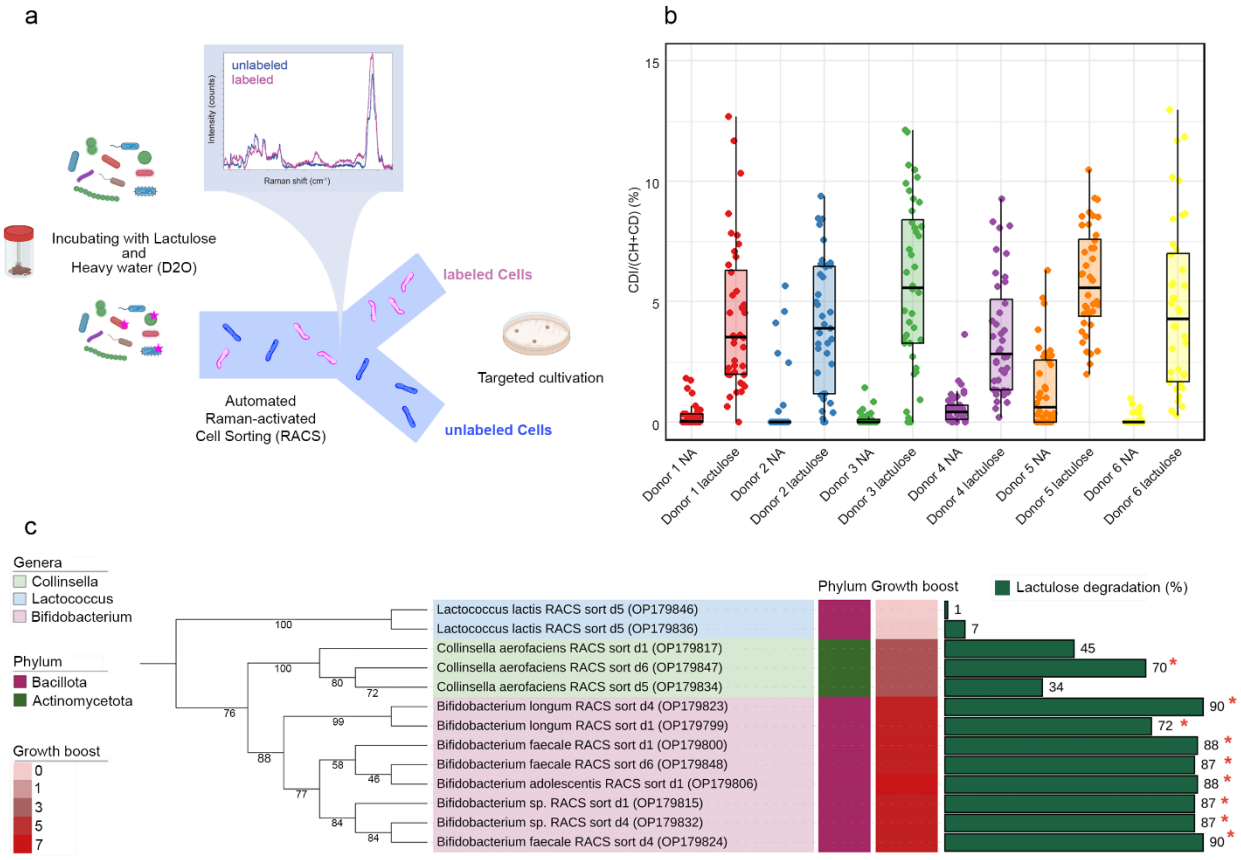

Figure 3. Sorting and physiological analysis of active cells. (a) Schematic of the detection and sorting of metabolically active cells via and D_2O labeling and Raman-activated cell sorting. Labeled cells (pink) exhibit a C-D peak at 2040–2300 cm^{-1}, indicating deuterium incorporation and metabolic activity, while unlabeled cells (blue) lack this signal. Targeted cultivation is performed after sorting the labeled cells. (b) Single-cell metabolic activity of cells. Dot plot showing the percentage of deuterium incorporation (%CD) into single microbial cells from fecal samples of 6 donors (D1–D6). Cells were incubated for 6 hours in D_2O-containing media with lactulose or without (No Amendment, NA). Each dot represents a single-cell measurement, and boxplots summarize the distribution of %CD values. Statistical analysis across all donors confirmed a significant effect of lactulose treatment on microbial metabolic activity (ANOVA, $p<0.001$, $n=471$). (c) Identification and physiological characterization of lactulose stimulated cells. Phylogenetic tree of bacteria isolated using Raman-activated cell sorting. The phylogenetic tree was constructed using the maximum likelihood algorithm in IQ-TREE and rooted at the mid-point, with branch support evaluated using 1000 ultrafast bootstrap replicates. The aligned sequences were used to generate the tree, which was then visualized and annotated in iTOL. Several strains, including *Bifidobacterium sp., Bifidobacterium longum subsp. suillum,* and *Bifidobacterium faecale* showed ambiguous species-level assignments based on BLAST analysis. These strains matched multiple closely related species at ≥97% similarity, with some aligning to different species within the same genus. To maintain consistency in taxonomic classification, these isolates were assigned species names based on their highest-confidence BLAST match, acknowledging the limitations of 16S rRNA gene sequencing for precise species differentiation. This approach aligns with the

conservative cut-off threshold described in the Methods section, which included a 97% similarity threshold and the exclusion of uncultured sequences. Growth boost indicates the area under the growth curve in YCFA-lactulose relative to the no-amendment control. Lactulose degradation (%) shows the percentage of lactulose degraded after 24 hours of incubation. Asterisks (*) indicate strains with significant lactulose degradation (mean ± SD: 67.7% ± 31.8, n = 28) measured with HPAEC.

Lactulose degraders support the growth of *L. lactis*

As *L. lactis* was labeled with heavy water but was unable to utilize lactulose, this raised the question as to whether growth of *L. lactis* was supported indirectly by lactulose degraders. To test this hypothesis, co-cultivation of *L. lactis* with lactulose degraders (either *C. aerofaciens* or *B. adolescentis*) was performed to evaluate whether inter-species interactions could enhance the growth of *L. lactis* in the presence of lactulose. As expected, *L. lactis* was unable to grow alone in a lactulose-supplemented medium while both *B. adolescentis* and *C. aerofaciens* grew well, reaching stationary phase in approximately 15 h and 48 h, respectively (Figure 4a). In co-culture in lactulose-supplemented medium, both *B. adolescentis* and *C. aerofaciens* facilitated the growth of *L. lactis,* as quantified by qPCR (Figure 4b). Notably, the abundances of *B. adolescentis* and *C. aerofaciens* were not significantly affected, positively or negatively, by the presence of *L. lactis*.

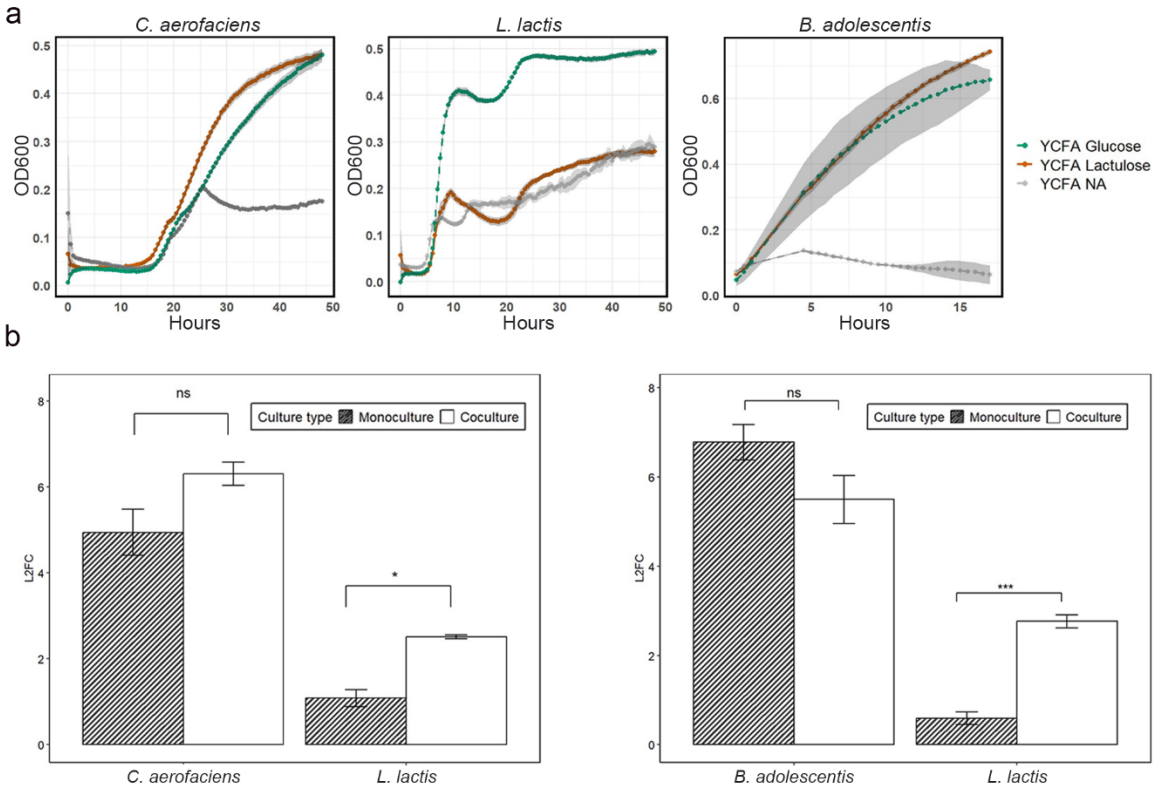

Figure 4. Pure and co-culture of strains in lactulose-containing medium. (a) Growth curves (OD600) for *L. lactis*, *C. aerofaciens*, and *B. adolescentis* were monitored in YCFA Glucose, YCFA Lactulose, and YCFA No Amendment (NA) media. The growth curves of *L. lactis* and *C. aerofaciens* were measured over 48 hours, while *B. adolescentis* was measured over 15 hours reaching log phase. (b) Log2 fold change in growth of *L. lactis* in lactulose-supplemented media was compared between monoculture and coculture conditions with *C. aerofaciens* and *B. adolescentis*. Significant growth enhancement of *L. lactis* (Student's t-test, $p < 0.05$, $n = 6$) in coculture with *C. aerofaciens* and (Student's t-test, $p < 0.001$, $n = 6$) in coculture with *B. adolescentis* is indicated with asterisks (*).

Discussion

There is considerable interest in evaluating the potential for dietary supplements to promote a gut microbiota that supports health by, for example, enhancing digestion, training the immune system, protecting against the invasion of enteric pathogens, or producing desirable bioactive compounds such as SCFAs[28–30]. One of the targets of prebiotics has been to promote the abundance of *Bifidobacteria*, which can provide numerous services in the gut[31]. Previous studies

have indicated that non-digestible polysaccharides such as inulin, FOS, and GOS may be promising bifidogenic dietary supplements that promote the growth of *Bifidobacterium* species in the gut, although not all studies are in agreement[32–35]. Lactulose, a synthetic disaccharide composed of galactose and fructose, has been traditionally used as a laxative and in the treatment of hepatic encephalopathy, but it also exhibits prebiotic effects at low doses[18]. This makes it a particularly valuable compound for investigating mechanisms of gut microbiota modulation in both healthy and disease contexts[22]. Indeed, previous studies have reported increased *Bifidobacterium* abundance following lactulose supplementation not only in healthy adults but also in patients with liver disease, supporting its broader relevance as a microbiota-directed intervention[22]. Although lactulose is currently used primarily for clinical purposes, it is not commonly consumed as a dietary supplement. However, our findings suggest that lactulose can selectively modulate gut microbes and promote cooperative interactions within the microbiota. These results underscore the need for further human studies to evaluate its potential as a microbiome-supporting and health-promoting dietary component. In this study, we employed multimodal cell sorting approaches to identify and characterize bacteria in the gut microbiota responsive to lactulose supplementation. Our findings demonstrate that *Bifidobacterium* spp., along with a few other taxa such as *Collinsella* and *Lactococcus*, are stimulated by the presence of lactulose. This is in line with the results of studies in humans that have evaluated lactulose's bifidogenic effects[22,24]. While previous studies have primarily linked lactulose fermentation to the growth of *Bifidobacterium* and *Lactobacillus* species[16], our findings reveal that lactulose also promotes *Collinsella* and *Lactococcus*, highlighting its broader but still targeted impact on gut microbiota composition. In addition, we observed translational activity in several other taxa, including *Gemmiger*, *Phocaeicola* and *Faecalibacterium*, suggesting that lactulose activates more microbial groups than previously recognized. This wider pattern of activation indicates that lactulose can enhance the metabolic activity of gut bacteria in ways that may not be visible through methods focused only on changes in abundance. Notably, taxa such as *Faecalibacterium* and *Gemmiger* which are generally considered beneficial for host health[1–3], showed metabolic activity in response to lactulose, highlighting its ability to selectively stimulate functionally important

members of the gut microbiota. Lactulose is produced industrially by the isomerization of lactose[36,37]. Although the biochemistry of bacterial lactose degradation is well characterized, bacterial lactulose degradation is less well studied. We identified a β-galactosidase gene (CCMPN/A_D1907) that *B. adolescentis* highly upregulates when grown on both lactose and lactulose. This enzyme shares homology with LacZ in *E. coli*, which cleaves lactose[38]. We determined that the *E. coli* LacZ is also capable of cleaving lactulose, suggesting that LacZ homologs in other species may also have this dual activity. Future work should explore to what extent lactulose affinities of β-galactosidase variants encoded by differing members of the gut microbiota determine competitiveness in the lactulose utilization niche.

In addition to direct lactulose degradation, our study highlights the importance of cross-feeding interactions within the gut microbiota. The gut microbiota is an interconnected community in which microbes exchange metabolic products such as SCFAs and amino acids[39,40]. We found that lactulose not only stimulates lactulose-degrading bacteria such as *B. adolescentis* and *C. aerofaciens* but also facilitates the growth of other species that do not directly degrade lactulose. This study adds new evidence showing that *L. lactis*, a bacterium typically known for breaking down lactose in dairy products[41], becomes metabolically active in response to lactulose. We demonstrated that *L. lactis* is indirectly stimulated through cross-fed metabolites provided by primary degraders, despite its inability to directly cleave lactulose. Co-culture experiments confirmed that *B.adolescentis* and *C.aerofaciens* support the growth of *L. lactis* via metabolite exchange. This finding reveals that *L. lactis* can benefit from a cooperative interaction with lactulose-degrading bacteria, highlighting how lactulose can shape microbial communities through indirect metabolic support. Similar cross-feeding mechanisms have been described for other prebiotics such as inulin and FOS [23,42], where primary degraders release metabolites that benefit non-degraders, suggesting that lactulose may drive comparable ecological interactions. Our integrative approach of combining BONCAT-FACS, Raman-activated cell sorting (RACS), and transcriptomics allows for the identification of both primary degraders and metabolically stimulated non-degraders. This single-cell framework provides a mechanistic view of how prebiotics reshape community function, offering a platform for the functional evaluation of other

microbiota targeted interventions. Our approach represents an expansion of previous single-cell methodologies, as we not only identified primary lactulose degraders, but also evaluated downstream ecological interactions through co-culture experiments. This integrative strategy allowed us to identify specific ecological interactions, including metabolic cross-feeding, that may otherwise remain undetected through compositional or activity-based analyses alone. This approach is broadly adaptable and could be extended to study other candidate prebiotics, ultimately contributing to a deeper understanding of microbial ecology and community level responses to dietary interventions. One limitation of our study is that fecal samples were vortexed for 2–3 minutes during homogenization, which may have introduced mild mechanical stress. While this approach is consistent with widely used protocols in microbiome research and microbial activity was confirmed via BONCAT, Raman, and cultivation assays, we cannot fully exclude the possibility that this may bias recovery of fragile cell types. Future studies should consider testing alternative homogenization strategies to further minimize this potential bias. Further work is needed to determine whether monosaccharides produced from lactulose cleavage or other metabolic products are responsible for the facilitation of *L. lactis* growth, but these findings underscore the importance of microbial interactions and metabolic exchanges in shaping gut microbiota composition and function.

Conclusions

This study provides new insights into the prebiotic potential of lactulose, highlighting its bifidogenic effects and broader impact on gut microbiota. By employing the advanced single cell techniques BONCAT-FACS and RACS, we identified lactulose-responsive bacteria in the gut microbiota. Our findings demonstrate that lactulose not only promotes the growth of *Bifidobacterium* but also enhances the translational activity of multiple other taxa such as *Collinsella*, *Gemmiger*, *Faecalibacterium* and *Phocaeicola*. Our study also highlights the importance of cross-feeding interactions between primary degraders and other species. These results highlight lactulose's ability to modulate microbial activity and inter-species interactions, offering a mechanistic understanding of how gut communities respond to specific substrates.

Unlike previous prebiotic studies that mainly rely on taxonomic shifts to infer microbial function, our approach demonstrates that lactulose directly activates metabolically important taxa and promotes cooperative interactions that enhance nutrient utilization. Future work should further elucidate the inter-species interactions and ecological dependencies through which primary degraders of prebiotics support the growth of other community members and assess whether these microbial responses translate into health-related outcomes or justify the use of lactulose in prebiotic therapy.

Materials and methods

Fecal sample collection and anaerobic incubations

Fresh fecal samples were collected from 6 healthy participants (3 females and 3 males; BMI average: 23.3 ± 5.0). Participants who had taken antibiotics or consumed probiotic/prebiotic supplements within the past six months, or those with any chronic or acute intestinal conditions, were excluded from the study[43,44]. Each participant collected their own sample using a sterile faeces tube with a spoon and screw cap (Sarstedt, Germany). Health status was further assessed using a standardized questionnaire addressing diet, medication use, gastrointestinal history, and lifestyle factors. For the purposes of this study, participants were considered healthy if they reported no chronic or acute intestinal conditions and had not recently used antibiotics, probiotics, or prebiotics. The protocol was approved by the ethics committee of the University of Vienna, with all participating subjects signing written informed consent (reference number 00161).

Immediately after collection, fresh fecal samples were transferred into an anaerobic tent containing a gas mixture of 85% N_2, 10% CO_2, and 5% H_2[45,46]. All subsequent handling steps, including mixing, vortexing, and filtration, were performed entirely within the anaerobic chamber to ensure that the microbial cells remained viable under oxygen-free conditions. To investigate microbial responses, lactulose, fructose, and galactose (2 mg/ml each, Carl Roth and Sigma-

Aldrich)[47] were used as substrates. A control set without any amendments was used to determine the baseline microbial activity in the absence of the added sugars. Approximately 1 g of fecal material was mixed with 10 ml of 2× PBS and vortexed vigorously for 2–3 minutes until homogenized, and then filtered through a 40 µm mesh (Corning, Germany) to eliminate large particulates. The filtrate was diluted 1:10 with 2x PBS in sterile tubes. 2 ml of each substrate was dissolved in D_2O to autoclaved Hungate tubes containing 2 ml of the homogenized fecal material and 5mM L-azidohomoalanine (AHA; Baseclick, Germany)[23]. The total volume was adjusted to 4 ml with final concentrations of 50 µM AHA and 50% D_2O. Incubation was performed at 37 °C for 6 hours under anaerobic conditions. After incubation, the samples were washed with PBS to extract any remaining D_2O and AHA. For preservation, 1 ml of each sample was fixed with 50% ethanol/PBS mixture and stored at -20 °C, and 1 ml was stored at -80 °C. for nucleic acids and metabolites analysis. For subsequent RACS experiments, samples were maintained in 20% glycerol/PBS and kept at -80 °C in crimp-sealed vials.

BONCAT labeling and microscopy

In this experiment, lactulose was provided as a substrate to stimulate microbial activity, and AHA incorporation into newly synthesized proteins was used to directly identify translationally active cells[25]. To visualize metabolically active microbial cells, fixed samples were prepared for fluorescence labeling on glass slides. Each fixed sample was pipetted 10 µl onto a microscopy slide (Marienfeld, Germany) and incubated at 46°C for 10 minutes to promote cell adhesion to the surface. The slides were then dehydrated by placing them for 3 minutes each in three ethanol solutions with increasing concentrations (50%, 80%, and 96%), and then allowed to air dry. For the labeling reaction, a dye premix was prepared by mixing 1.25 µl of 20 mM $CuSO_4$, 2.50 µl of 50 mM THPTA (tris(3-hydroxypropyltriazolylmethyl) amine), and 0.30 µl of Cy5 alkyne dye (Jena Bioscience, Germany). This mixture was kept in the dark at room temperature for 3 minutes to allow it to activate[25]. In the next step, the dye premix was added to 221 µl of 1x PBS containing 12.5 µl of freshly prepared 100 mM sodium ascorbate and 12.5 µl of freshly prepared 100 mM

aminoguanidine hydrochloride. The final mix was gently inverted once (without vortexing) to ensure proper mixing. From this final mixture, 30 µl were added to each well of the slide to cover the sample. The slides were then incubated in a humid chamber at room temperature for 30 minutes in the dark. During this time, the fluorescent dye reacted with the azide group of AHA (L-azidohomoalanine) in the cells, labeling metabolically active cells with a Cy5 signal. After the reaction, the slides were washed three times with 1x PBS for 3 minutes each. The dehydration step was repeated by placing the slides again into 50%, 80%, and 96% ethanol for 3 minutes each, followed by air drying. For DNA staining, 10 µl of DAPI (4',6-diamidino-2-phenylindole) (Sigma-Aldrich, Austria) was added to each well, and the slides were incubated in the dark at room temperature for 10 minutes. Slides were briefly dipped in cold Milli-Q water, air-dried again, and mounted with glycerol. Finally, the slides were imaged using confocal laser scanning microscopy (CLSM). In the overlay images, DAPI-stained cells appeared blue, while metabolically active cells labeled with Cy5 appeared pink[26].

Liquid BONCAT and fluorescence-activated cell sorting

To identify metabolically active microbial cells, a BONCAT approach was employed in conjunction with FACS[48,49]. The cells were labelled with a Cy5 alkyne dye via Cu(I)-catalysed click chemistry, as previously described[26]. In summary, the chemically fixed microbial cells were suspended in a click reaction mixture containing $CuSO_4$, THPTA, sodium ascorbate, aminoguanidine hydrochloride, and Cy5 alkyne dye[25]. Approximately 300–500 µL of fixed sample was used per labeling reaction. Subsequently, the cells were washed and resuspended in PBS containing DAPI for the purpose of assessing total cell numbers[50]. After labeling, Cells were gated based on DAPI fluorescence to detect DNA-containing cells and Cy5 fluorescence to identify BONCAT-positive cells. The full gating strategy, including controls and threshold definitions, is provided in the supplementary information (Supplementary Figure 9). The labelled cells were sorted according to their Cy5 fluorescence intensity using the cell sorter FACS Melody (BD, Germany). A total of 500,000 events were collected per sample at a flow rate of 10 µL/min[51].

16S rRNA gene amplicon sequencing

To characterize the microbial community composition, DNA was extracted from both the entire faecal sample (0 and 6 hours incubation), the entire sorted microbial community stained with DAPI and the subpopulation of metabolically active cells (FACS-sorted cells) after 6 hours of incubation with lactulose, fructose, galactose, or no amendment. The QIAamp DNA Mini Kit (Qiagen, Germany) was utilized for DNA extraction, incorporating an additional lysozyme step to enhance recovery[52,53]. The 16S rRNA gene was subsequently amplified using a dual-barcoding, two-step PCR two-step approach[54], to determine the microbial community structure. The V3–V4 hypervariable region was targeted using primers 341F (5'-CCT ACG GGN GGC WGC AG-3') and 785R (5'-GAC TAC HVG GGT ATC TAA TCC-3'), with 16-bp head adapters (H1: 5'-GCT ATG CGC GAG CTG C-3'; at the 5' end of both the forward and reverse primer) added during the first PCR step[55]. PCR products were purified and normalized using SequalPrep™ Normalization Plate Kit (Invitrogen), which also removes primer dimers and normalizes DNA yield followed by a second PCR step with unique dual barcodes[54]. Samples were pooled and concentrated using the innuPREP PCRpure Kit (Analytik Jena) and sequencing libraries were prepared using the Illumina TruSeq Nano DNA Library Prep Kit. Libraries were sequenced in paired-end mode (2 × 300 bp, v3 chemistry) on an Illumina MiSeq platform at the Joint Microbiome Facility of the Medical University of Vienna and the University of Vienna (Project ID JMF-2102-07). Demultiplexed reads were processed using the DADA2 pipeline (v1.18.0) to infer amplicon sequence variants (ASVs)[56]. The pipeline included primer trimming, quality filtering, error modeling, dereplication, sample inference, merging of paired-end reads, chimera removal, and ASV table construction. Taxonomic assignment was performed using the SILVA SSU Ref NR 99 database (release 138.1)[57]. Contaminant sequences were filtered using the prevalence-based method from the decontam R package (v1.6.0)[58]. The resulting sequence data have been deposited in the NCBI Short Read Archive under accession number PRJNA718139.

Raman microspectroscopy on slides

Fecal samples were amended with lactulose and incubated for 6 hours. An unamended control sample was included for comparison[59]. Both lactulose-amended and control samples were fixed with ethanol:PBS (1:1) to preserve cellular integrity. For analysis, 1.5 µL of each fixed sample was spotted onto an aluminum-coated slide (Al136; EMF Corporation, USA) and air-dried at 30°C [59]. Subsequently, the slides were dipped in ice-cold Milli-Q water (Millipore, Austria) twice to remove residual buffer components and air-dried again[60].

Raman spectra of individual microbial cells were acquired using a confocal Raman microspectroscope (LabRAM HR800, Horiba Scientific, France) equipped with a 532 nm neodymium-yttrium aluminum garnet (Nd:YAG) laser and a 300 grooves/mm diffraction grating[61]. Spectra were collected in the wavenumber range of 400–3200 cm^{-1} using LabSpec 6 software (Horiba Scientific, France) with an acquisition time of 10 seconds and 5 accumulations per measurement. For each sample, 30–40 individual cells were analyzed.

The degree of deuterium substitution (%CD) in C-H bonds was quantified by integrating the peak areas of the C-D (2040–2300 cm^{-1}) and C-H (2800–3100 cm^{-1}) stretching vibrations using the single-cell analysis and testing tools for Raman microspectroscopy (Scattr) (https://shiny.lisc.univie.ac.at/scattr/)[62] .The threshold for %CD was determined by calculating the mean + 3 times the standard deviation (SD) of %CD values obtained from randomly selected cells in a control sample incubated without lactulose or D_2O addition[62]. Raman data has been deposited in MicrobioRaman platform within the BioStudies database[63] with accession numbers S-MBRS12.

Raman-activated cell sorting

Raman-activated cell sorting (RACS) was performed on cells incubated for 6 hours in a medium containing D_2O and lactulose. After incubation, the cells were preserved in 20% glycerol balanced with PBS and stored at -80°C. Before sorting, the frozen cells were thawed, pelleted by

centrifugation at approximately 9000×g for 7 minutes, washed twice with 0.3M glycerol/MQ water buffer to minimize osmotic stress, and finally resuspended in 500 µl of the same solution.

The RACS platform combined a Raman microspectroscope operating at 532 nm and 90mW, optical tweezers employing a 1064 nm Nd:YAG laser at 500mW, and a polydimethylsiloxane (PDMS) microfluidic device[27,64]. The microfluidic system was fabricated using a base and curing agent mixed at a 10:1 ratio, polymerized at 75°C, and mounted on a glass coverslip[64]. This system featured two outlets designed to default the sample stream through the waste outlet unless redirected by optical tweezers[64].

During sorting, cells were identified based on their Raman spectra, with deuterium-labeled cells being translocated to a collection outlet, while unlabeled cells were discarded through the waste outlet[64]. The sorting process was automated using in-house MATLAB software (version 4.2), employing two indices: the cell index (Pc), indicating cell capture, and the labeling index (PL), differentiating labeled from unlabeled cells. Pc measured spectrum of Raman signal in the region between 1620-1670 cm^{-1} and the integrated intensity I (Pc = $\frac{\mathrm{I}\ 1620-1670}{\mathrm{I\ fluid}\ 1620-1670}$)[27]. This specific region was chosen as it is largely unaffected by the Raman spectrum of used materials polydimethylsiloxane (PDMS) and glass. On the other hand, the 'labelling index' PL is determined by the comparison of the region of the deuterium peak in the Raman spectrum 2,040-2,300 cm^{-1} (integrated intensity: I2,040-2,300) to the region between 1,850-1,900 cm-1 (integrated intensity: I1,850-1,900) ($P_L = \frac{\mathrm{I2040-2300}}{\mathrm{I1850-1900}}$) [27]. The threshold for PL was set at 5.7 (n=110 cells) based on random cell sorting amended with glucose and incubated without deuterated water(D2O).

After sorting, 50µl of the sorted cells were collected, immediately transferred to an anaerobic tent, and cultured on YCFA. The cells were incubated at 37°C until colonies appeared, then streaked on new plates with YCFA-lactulose medium and cultured again to ensure colony formation. To verify the purity of the 0.3 M glycerol/MQ water buffer used during sorting, an aliquot of the buffer was cultured overnight under the same conditions. No microbial growth was observed, confirming it as a sterile negative control[23,59].

Taxonomic identification of bacterial isolates

For the molecular characterization of isolated bacterial colonies, colony PCR was performed to amplify the 16S rRNA gene. The PCR master mix was prepared under sterile conditions in the PCR hood and included 5 µL of 10x Green Dream Taq Buffer including 20 mM MgCl2 (Thermo Fisher Scientific, Waltham, MA, USA),5 µL of dNTPs 2 mM (Thermo Fisher Scientific),1 µL of each primer (forward: 616V, 5'-AGA GTT TGA TYM TGG CTC AG-3'; reverse: 1492R, 5'-GGT TAC CTT GTT ACG ACT T-3') at a final concentration of 50 µM (Thermo Fisher Scientific),0.5 µL of BSA 20 mg/mL (Thermo Fisher Scientific), 0.5 µL of Dream Taq DNA Polymerase 5 U/µL (Thermo Fisher Scientific) and 37 µL of nuclease-free water (Thermo Fisher Scientific) in a final volume of 50 µl per reaction. The amplification protocol followed an initial denaturation at 95 °C for 3 minutes, then 30 cycles at 95°C for 30 seconds, 56°C for 30 seconds, 72°C for 1.5 minutes, and a final elongation at 72 °C for 10 minutes[65]. Amplified PCR products were visualized via 1% agarose gels electrophoresis and purified using the InnuPREP PCRpure Kit (Analytik Jena, Germany) according to the manufacturer's instructions[66]. The concentration of each purified product was quantified using a Nanodrop device (Thermo Fisher Scientific, MA, USA)[67]. Subsequently, samples were sent to Microsynth AG (Vienna, Austria) for Sanger sequencing. Sequencing results were analyzed using a combination of 4Peaks 1.8 (Nucleobytes, Amsterdam, Netherlands) and Serial Cloner 2.6 for alignment, and the online tool DECIPHER to check for chimeras.[68] To identify the bacterial taxa, the NCBI nucleotide collection database (https://blast.ncbi.nlm.nih.gov/) was employed. All sequences were compared to the NCBI database using a minimum threshold of 96% sequence similarity. Most isolates showed ≥98% identity to known reference strains, supporting reliable species-level assignments. However, for sequences with 96-97% similarity that matched multiple closely related species, a conservative genus-level classification was adopted to account for the limitations of 16S rRNA gene sequencing for precise species differentiation. This approach included the use of a 97% similarity cut-off for genus-level classification, as sequences within this range often align to multiple closely related species. Uncultured sequences were excluded to improve taxonomic accuracy and focus on well-characterized type strains, reducing the risk of

misclassification. The sequences were then deposited in GenBank, with accession numbers OP179799-OP179820, OP179823, OP179824, OP179826-OP179849.

Growth characterization of isolates

Strains were cultured in both solid and liquid YCFA medium until reaching the early stationary phase. Each strain, identified via Sanger sequencing, was grown in YCFA-glucose (YCFA-G) broth at 37°C in an anaerobic environment. Upon reaching maximum OD600, cultures were washed and diluted into YCFA broth supplemented with lactulose (YCFA-Lact) and YCFA media without any amendment (YCFA-NA), serving as a negative control. These cultures were dispensed into wells of a sterile 96-well microtiter plate (Costar 3595, Corning, NY, USA) in three technical replicates. The plate was incubated for 120 hours at 37°C in an anaerobic microplate reader (MultiskanTM GO, ThermoFisher Scientific) using SkanIt Software RE for Microplate Readers RE, ver. 6.1.0.51 (ThermoFisher Scientific) for shaking (5 seconds) and OD600 measurement every 30 minutes[23]. Growth curves were subsequently calculated using R statistical software (https://www.r-project.org/). Supernatants from these cultures were collected and stored at -80°C for further HPAEC analysis.

Lactulose degradation analysis by high-performance anion-exchange chromatography with pulsed amperometric detection (HPAEC-PAD)

Bacterial strains isolated RACS and fecal samples were analyzed for lactulose degradation by high performance anion exchange chromatography (HPAEC) utilizing a Dionex ICS 3000 system (ThermoFisher, Germany)[69]. Supernatants were centrifuged at 24,000 × g, and clear supernatants (20 µl) were diluted with 480 µl of 20% v/v methanol and filtered into injection vials using a syringe filter (0.22 µm, polyethersulfone membrane). The samples were injected into an ICS-3000 system (Thermo Fisher Scientific Inc., Sunnyvale CA, USA), and oligosaccharides were separated using a Carbopac PA1 precolumn (4 × 50 mm) followed by an analytical PA1 column (4 × 250 mm). Elution was performed with 16 mM NaOH + 6 mM NaOAc at 1 ml/min. The sugars were separated

on a Dionex CarboPac PA20 column (3 × 150mm) with a Dionex CarboPac PA20 guard column (3 × 30mm), using a solvent of 100mM KOH, at a flow rate of 0.3 ml/min, over 35 minutes[70]. Duplicate analyses were performed employing the standard carbohydrate waveform for detection. Calibration curves were established utilizing standards of fructose and galactose (Sigma-Aldrich, St. Louis, MO, USA), with lactulose (Carl Roth) employed for experimentation and measurement via HPAEC.

Coculture experiments

To determine the optimal time points for late log-phase growth, growth curves were first established for *L. lactis, C. aerofaciens*, and *B. adolescentis* in YCFA medium supplemented with Lactulose, Glucose, or left without amendment (NA)[23]. Following this, each bacterial strain was grown as both monocultures and cocultures to assess their interactions. For coculture experiments, equal volumes (50 µL each) of log-phase cultures were mixed. Samples were collected at 0 hours, 15 hours, and 48 hours to monitor growth patterns and capture the late log-phase activity in both pure and mixed cultures.

Primer design was performed using Primer3Plus to generate strain-specific primers for *L. lactis, C. aerofaciens*, and *B. adolescentis*[71,72]. The primers used were Coll16S-F (5´-TGCTACAATGGCCGGTACAG-3´) and Coll16S-R (5´-AGCAACTCCGACTTCATGGG-3´) for *C. aerofaciens* (product length: 114 bp, Tm: 68°C), Lact16S-F1 (5´-CTCTAACGAGACTGCCGGTG-3´) and Lact16S-R1 (5´-GCGACTCGTTGTACCATCCA-3´) for *L. lactis* (product length: 113 bp, Tm: 68°C), and Bifido16S-F (5´-TCCGGTGTGAAAGTCCATCG-3´) and Bifido16S-R (5´-CCGTTACACCGGGAATTCCA-3´) for *B. adolescentis* (product length: 94 bp, Tm: 68°C). Primer specificity was validated by performing PCR with each strain using its specific primer and primers designed for the other strains, followed by gel electrophoresis to verify the absence of nonspecific amplification products[73]. Gradient PCR was utilized to optimize primer annealing temperatures for precise binding[74]. DNA standards were prepared by culturing each strain to an optical density (OD) of 0.1 at 600 nm, followed by DNA extraction[75–77]. To optimize qPCR reproducibility and allow reliable comparisons of DNA concentrations across samples, we established a calibration curve

using 10-fold serial dilutions of DNA extracted from pure cultures. Subsequently, qPCR was performed using these strain-specific primers to quantify the abundance of *L. lactis, C. aerofaciens* and *B. adolescentis* in both pure cultures and cocultures at various time points. Each sample was tested in triplicate.

RNAseq of *Bifidobacterium adolescentis*

B. adolescentis was revived from glycerol stocks by inoculating 50 µl of the pure culture into 5 mL YCFA-Glucose broth and incubated overnight at 37°C under anaerobic conditions. Cells were harvested by centrifugation at 13,000 rpm for 1 minute, washed twice with 500 µl 1× PBS, and resuspended in 1 mL 1× PBS. For the experimental setup, 50 µl of the washed cell suspension was inoculated into 10 mL of MRS medium containing one of the three substrates: glucose, lactose, or lactulose. Cultures were grown in four biological replicates under anaerobic conditions at 37°C until the late log growth phase. At the late log phase, cultures were centrifuged at maximum speed for 10 minutes at 4°C in 15 mL Falcon tubes. Supernatants were carefully removed, and the cell pellets were stored at -80°C for subsequent RNA extraction. Sequencing libraries were prepared from DNA-clean RNA extracted using the NEBNext Ultra II FS Directional Library Preparation Kit, after rRNA depletion with the RiboZero Plus Kit (Illumina)**,** following the manufacturer's instructions. Libraries were pooled equimolarly and sequenced on a NovaSeq6000 (Illumina) in paired-end mode (2 × 100 bp, 200 cycles) at the Joint Microbiome Facility (JMF) of the University of Vienna and Medical University of Vienna (Project ID: JMF-2212-19). Gene expression levels were quantified in fragments per kilobase of transcript per million mapped reads (FPKM)[78]. Differentially expressed genes were identified using DESeq2 with statistical significance determined at an adjusted p-value cutoff of 0.05[79]. Heatmaps displaying log2 fold change (L2FC) in gene expression across substrate conditions were generated using the pheatmap package in Rstudio. The RNA sequencing data generated from this study are available in the NCBI Sequence Read Archive (SRA) under accession number [PRJNA1208440].

Statistical analysis

Statistical analyses were performed using R statistical software (https://www.r-project.org/, v4.2.1)[80]. Data visualization was conducted using the ggplot2 package (v3.5.1)[81]. To analyze the Enrichment Factor (EF) between samples, the relative abundance (RA) of bacterial genera was calculated for lactulose-amended samples by comparing the differences between BONCAT-positive FACS-sorted cells and BONCAT-negative FACS-sorted cells. The EF was computed using the relative abundance of each genus at 6 hours in the lactulose-amended samples compared to its relative abundance at 0 hours. A positive EF (> 0) indicates that a genus was enriched in the lactulose-amended samples, while a negative EF (< 0) indicates that a genus was depleted relative to its baseline abundance at 0 hours.

For the differential abundance testing, the DESeq2 (v1.38.3)[82] package was used to analyze the variation between groups (lactulose-amended vs. control). All tests were performed at a significance threshold of p-value < 0.05, and multiple comparisons were corrected using the Benjamini-Hochberg method to control the false discovery rate (FDR)[83]. This correction method ensures that the risk of false positives is minimized when testing many hypotheses simultaneously. The resulting dataset contains the log2 fold changes (LFC) for each genus, along with the associated p-values and adjusted p-values (FDR). Genera with an adjusted p-value < 0.05 were considered statistically significant and included in the final analysis. Bubble plots were used to visualize the results, where the bubble size represents the relative abundance at baseline (0 h), the color indicates whether the genus was significantly enriched or depleted in the lactulose-amended samples. and statistical significance was determined for each genus.

Additionally, PERMANOVA (Permutational Multivariate Analysis of Variance) was employed to evaluate community-wide differences in the microbiota profiles of lactulose-amended versus control samples. This was carried out using the vegan(v2.6.4) package, which is designed for multivariate statistical analysis[84]. The adonis function from the vegan package was used for calculating significance of differences between groups, based on Bray-Curtis dissimilarity

distances calculated from genus-level abundance data[85]. This allowed for the testing of whether differences between sample groups were statistically significant in a multivariate context.

Funding

This work was financially supported by the European Research Council (FunKeyGut 741623), the United States Department of Energy (DE- SC0019012) and Austrian Science Fund (FW912002 – MAINTAIN and doi.org/10.55776/COE7). The work of A.H. was supported by the Austrian Science Fund (FWF P36130).

Author contributions

H.R., A.R., and D.B. conceived and designed the study. H.R. performed all the experiments and data analysis. D.I. performed the Raman and RACS experiments. G.N., N.H., and S.K. contributed to FACS and molecular biology experiments. A.H. designed and supported the coculture experiments. J.W. conducted HPAEC and supported data analysis and evaluation. B.H. contributed to bioinformatic analyses. V.F. supported the enzyme experiments. H.R. and D.B. wrote the manuscript. All authors revised and approved the manuscript, and all have approved the final version of the paper.

Data Availability

The 16S rRNA gene amplicon sequence data generated in this study from FACS have been deposited in the NCBI Short Read Archive under accession number PRJNA718139. The sequences of RACS strains isolated following lactulose supplementation have been deposited in GenBank, with accession numbers OP179799–OP179820, OP179823, OP179824, and OP179826–OP179849. Sequences from random sorting by RACS and isolation via direct sample plating on YCFA-Lactulose agar Plates are also available in GenBank, with accession numbers PQ722470–

PQ722509. Raman data have been deposited in the MicrobioRaman platform within the BioStudies database under accession number S-MBRS12. RNA sequencing data generated from this study are available in the NCBI Sequence Read Archive (SRA) under accession number PRJNA1208440.

Acknowledgements

We thank all members of the Joint Microbiome Facility (JMF) for sequencing our samples. We also thank Ludwig Seidel from the Division of Terrestrial Ecosystem Research for running and analyzing the HPAEC samples included in this study. Additionally, we thank Marie Rutsch and Forough Soltanieh for their assistance in creating the illustrations and figure design for this paper.

References

1. Martín, R. *et al.* Faecalibacterium: a bacterial genus with promising human health applications. *FEMS Microbiol. Rev.* 47, 1–18 (2023).
2. Jan, T. *et al.* Next generation probiotics for human health: An emerging perspective. *Heliyon* 10, e35980 (2024).
3. Deng, D. *et al.* Microbiome analysis of gut microbiota in patients with colorectal polyps and healthy individuals. *Sci. Rep.* 15, 1–9 (2025).
4. Merlo, G., Bachtel, G. & Sugden, S. G. Gut microbiota, nutrition, and mental health. *Front. Nutr.* 11, 1–11 (2024).
5. Liu, Y. Y. Controlling the human microbiome. *Cell Syst.* 14, 135–159 (2023).
6. Zmora, N., Suez, J. & Elinav, E. You are what you eat: diet, health and the gut microbiota. *Nat. Rev. Gastroenterol. Hepatol.* 16, 35–56 (2019).
7. Nova, E., Gómez-Martinez, S. & González-Soltero, R. The Influence of Dietary Factors on the Gut Microbiota. *Microorganisms* 10, (2022).
8. Castonguay-Paradis, S. *et al.* Dietary food patterns as determinants of the gut microbiome–endocannabinoidome axis in humans. *Sci. Rep.* 13, 1–10 (2023).
9. Hou, K. *et al.* Microbiota in health and diseases. *Signal Transduct. Target. Ther.* 7, (2022).
10. Gibson, G. R. *et al.* Expert consensus document: The International Scientific Association for Probiotics and Prebiotics (ISAPP) consensus statement on the definition and scope of prebiotics. *Nat. Rev. Gastroenterol. Hepatol.* 14, 491–502 (2017).
11. Holscher, H. D. Dietary fiber and prebiotics and the gastrointestinal microbiota. *Gut Microbes* 8, 172–184 (2017).
12. Cunningham, M. *et al.* Shaping the Future of Probiotics and Prebiotics. *Trends Microbiol.* 29, 667–685 (2021).
13. Louis, P., Hold, G. L. & Flint, H. J. The gut microbiota, bacterial metabolites and colorectal cancer. *Nat. Rev. Microbiol.* 12, 661–672 (2014).
14. Deehan, E. C. *et al.* Revisiting the Concepts of Prebiotic and Prebiotic Effect in Light of Scientific and Regulatory Progress—A Consensus Paper From the Global Prebiotic Association. *Adv. Nutr.* 15, 100329 (2024).
15. Ríos-Covián, D. *et al.* Intestinal short chain fatty acids and their link with diet and human health. *Front. Microbiol.* 7, 1–9 (2016).
16. Karakan, T., Tuohy, K. M. & Janssen-van Solingen, G. Low-Dose Lactulose as a Prebiotic for Improved Gut Health and Enhanced Mineral Absorption. *Front. Nutr.* 8, 1–15 (2021).

17. Lu, E., Yeung, M. & Yeung, C. K. Comparative Analysis of Lactulose and Fructooligosaccharide on Growth Kinetics, Fermentation, and Antioxidant Activity of Common Probiotics. *Food Nutr. Sci.* 09, 161–178 (2018).

18. Chu, N., Ling, J., Jie, H., Leung, K. & Poon, E. The potential role of lactulose pharmacotherapy in the treatment and prevention of diabetes. *Front. Endocrinol. (Lausanne).* 13, 1–10 (2022).

19. Yoo, S., Jung, S. C., Kwak, K. & Kim, J. S. The Role of Prebiotics in Modulating Gut Microbiota: Implications for Human Health. *Int. J. Mol. Sci.* 25, (2024).

20. Ruszkowski, J. & Witkowski, J. M. Lactulose: Patient- and dose-dependent prebiotic properties in humans. *Anaerobe* 59, 100–106 (2019).

21. Bai, J., Wang, B., Tan, X., Huang, L. & Xiong, S. Regulatory effect of lactulose on intestinal flora and serum metabolites in colitis mice: In vitro and in vivo evaluation. *Food Chem. X* 19, 100821 (2023).

22. Odenwald, M. A. *et al.* Bifidobacteria metabolize lactulose to optimize gut metabolites and prevent systemic infection in patients with liver disease. *Nat. Microbiol.* 8, 2033–2049 (2023).

23. Riva, A. *et al.* Identification of inulin-responsive bacteria in the gut microbiota via multi-modal activity-based sorting. *Nat. Commun.* 14, (2023).

24. Bouhnik, Y. *et al.* Lactulose ingestion increases faecal bifidobacterial counts: A randomised double-blind study in healthy humans. *Eur. J. Clin. Nutr.* 58, 462–466 (2004).

25. Hatzenpichler, R. *et al.* In situ visualization of newly synthesized proteins in environmental microbes using amino acid tagging and click chemistry. *Environ. Microbiol.* 16, 2568–2590 (2014).

26. Hatzenpichler, R. *et al.* Visualizing in situ translational activity for identifying and sorting slow-growing archaeal - bacterial consortia. *Proc. Natl. Acad. Sci. U. S. A.* 113, E4069–E4078 (2016).

27. Lee, K. S. *et al.* An automated Raman-based platform for the sorting of live cells by functional properties. *Nat. Microbiol.* 4, 1035–1048 (2019).

28. Swanson, K. S. *et al.* The International Scientific Association for Probiotics and Prebiotics (ISAPP) consensus statement on the definition and scope of synbiotics. *Nat. Rev. Gastroenterol. Hepatol.* 17, 687–701 (2020).

29. Cheng, W. *et al.* Effect of functional oligosaccharides and ordinary dietary fiber on intestinal microbiota diversity. *Front. Microbiol.* 8, 1–11 (2017).

30. Collins, S. M. *et al.* Development of a prebiotic blend to influence in vitro fermentation effects, with a focus on propionate, in the gut. *FEMS Microbiol. Ecol.* 97, (2021).

31. You, S. *et al.* The promotion mechanism of prebiotics for probiotics: A review. *Front. Nutr.* 9, (2022).

32. Lessard-Lord, J. *et al.* Short term supplementation with cranberry extract modulates gut microbiota in human and displays a bifidogenic effect. *npj Biofilms Microbiomes* 10, (2024).

33. Davis, L. M. G., Martínez, I., Walter, J., Goin, C. & Hutkins, R. W. Barcoded pyrosequencing reveals that consumption of galactooligosaccharides results in a highly specific bifidogenic response in humans. *PLoS One* 6, 1–10 (2011).

34. Tandon, D. *et al.* A prospective randomized, double-blind, placebo-controlled, dose-response relationship study to investigate efficacy of fructo-oligosaccharides (FOS) on human gut microflora. *Sci. Rep.* 9, 1–15 (2019).

35. Kebbe, M. *et al.* Effects of Infant Formula Supplemented With Prebiotics on the Gut Microbiome , Gut Environment , Growth Parameters , and Safety and Tolerance : A Systematic Review and Meta-Analysis. 00, 1–26 (2025).

36. Ubilla, C. *et al.* Synthesis of Lactulose in Continuous Stirred Tank Reactor With β-Galactosidase of Apergillus oryzae Immobilized in Monofunctional Glyoxyl Agarose Support. *Front. Bioeng. Biotechnol.* 8, 1–14 (2020).

37. Wang, H., Yang, R., Hua, X., Zhao, W. & Zhang, W. Enzymatic production of lactulose and 1-lactulose: Current state and perspectives. *Appl. Microbiol. Biotechnol.* 97, 6167–6180 (2013).

38. LacZ β-galactosidase: Structure and function of an enzyme of historical and molecular biological importance - Juers - 2012 - Protein Science - Wiley Online Library.

39. Culp, E. J. & Goodman, A. L. Cross-feeding in the gut microbiome: Ecology and mechanisms. *Cell Host Microbe* 31, 485–499 (2023).

40. Koh, A., De Vadder, F., Kovatcheva-Datchary, P. & Bäckhed, F. From dietary fiber to host physiology: Short-chain fatty acids as key bacterial metabolites. *Cell* 165, 1332–1345 (2016).

41. Kondrotiene, K., Zavistanaviciute, P., Aksomaitiene, J., Novoslavskij, A. & Malakauskas, M. Lactococcus lactis in Dairy Fermentation—Health-Promoting and Probiotic Properties. *Fermentation* 10, 1–39 (2024).

42. Xiao, M. *et al.* Cross-feeding of bifidobacteria promotes intestinal homeostasis: a lifelong perspective on the host health. *npj Biofilms Microbiomes* 10, (2024).

43. Holmes, Z. C. *et al.* Microbiota responses to different prebiotics are conserved within individuals and associated with habitual fiber intake. *Microbiome* 10, 1–16 (2022).

44. Suez, J. *et al.* Post-Antibiotic Gut Mucosal Microbiome Reconstitution Is Impaired by

Probiotics and Improved by Autologous FMT. *Cell* 174, 1406-1423.e16 (2018).

45. Wang, Q., Spenkelink, B., Boonpawa, R., Rietjens, I. M. C. M. & Beekmann, K. Use of Physiologically Based Kinetic Modeling to Predict Rat Gut Microbial Metabolism of the Isoflavone Daidzein to S-Equol and Its Consequences for ERα Activation. *Mol. Nutr. Food Res.* 64, 1–13 (2020).

46. Shen, J. *et al.* Large-scale phage cultivation for commensal human gut bacteria. *Cell Host Microbe* 31, 665-677.e7 (2023).

47. Slavin, J. Fiber and prebiotics: Mechanisms and health benefits. *Nutrients* 5, 1417–1435 (2013).

48. Riva, A. *et al.* Conversion of Rutin, a Prevalent Dietary Flavonol, by the Human Gut Microbiota. *Front. Microbiol.* 11, 1–11 (2020).

49. Couradeau, E. *et al.* Probing the active fraction of soil microbiomes using BONCAT-FACS. *Nat. Commun.* 10, (2019).

50. Reichart, N. J. *et al.* Activity-based cell sorting reveals responses of uncultured archaea and bacteria to substrate amendment. *ISME J.* 14, 2851–2861 (2020).

51. Mestrum, S. G. C. *et al.* Optimized gating strategy and supporting flow cytometry data for the determination of the Ki-67 proliferation index in the diagnosis of myelodysplastic syndrome. *Data Br.* 41, 107976 (2022).

52. Vural, H. C. & Ozgun, D. An improving DNA isolation method for identification of anaerobic bacteria in human colostrum and faeces samples. 3, 95–100 (2011).

53. Ketchum, R. N. *et al.* DNA Extraction Method Plays a Significant Role When Defining Bacterial Community Composition in the Marine Invertebrate Echinometra mathaei. *Front. Mar. Sci.* 5, 1–13 (2018).

54. Pjevac, P. *et al.* An Economical and Flexible Dual Barcoding, Two-Step PCR Approach for Highly Multiplexed Amplicon Sequencing. *Front. Microbiol.* 12, (2021).

55. Herbold, C. W. *et al.* A flexible and economical barcoding approach for highly multiplexed amplicon sequencing of diverse target genes. *Front. Microbiol.* 6, 1–8 (2015).

56. Jeske, J. T. & Gallert, C. Microbiome Analysis via OTU and ASV-Based Pipelines—A Comparative Interpretation of Ecological Data in WWTP Systems. *Bioengineering* 9, (2022).

57. Quast, C. *et al.* The SILVA ribosomal RNA gene database project: Improved data processing and web-based tools. *Nucleic Acids Res.* 41, 590–596 (2013).

58. Davis, N. M., Proctor, Di. M., Holmes, S. P., Relman, D. A. & Callahan, B. J. Simple statistical identification and removal of contaminant sequences in marker-gene and metagenomics data. *Microbiome* 6, 1–15 (2018).

59. Pereira, F. C. *et al.* Rational design of a microbial consortium of mucosal sugar utilizers reduces Clostridiodes difficile colonization. *Nat. Commun.* 11, (2020).

60. Cui, D., Kong, L., Wang, Y., Zhu, Y. & Zhang, C. In situ identification of environmental microorganisms with Raman spectroscopy. *Environ. Sci. Ecotechnology* 11, 100187 (2022).

61. Eichorst, S. A. *et al.* Advancements in the application of NanoSIMS and Raman microspectroscopy to investigate the activity of microbial cells in soils. *FEMS Microbiol. Ecol.* 91, 1–14 (2015).

62. Berry, D. *et al.* Tracking heavy water (D2O) incorporation for identifying and sorting active microbial cells. *Proc. Natl. Acad. Sci. U. S. A.* 112, E194–E203 (2015).

63. Lee, K. S. *et al.* MicrobioRaman: an open-access web repository for microbiological Raman spectroscopy data. *Nat. Microbiol.* 9, 1152–1156 (2024).

64. Lee, K. S. *et al.* Optofluidic Raman-activated cell sorting for targeted genome retrieval or cultivation of microbial cells with specific functions. *Nat. Protoc.* 16, 634–676 (2021).

65. Lorenz, T. C. Polymerase chain reaction: Basic protocol plus troubleshooting and optimization strategies. *J. Vis. Exp.* 1–15 (2012) doi:10.3791/3998.

66. Brinkmann, N. *et al.* Intensive tropical land use massively shifts soil fungal communities. *Sci. Rep.* 9, 1–11 (2019).

67. Desjardins, P. & Conklin, D. NanoDrop microvolume quantitation of nucleic acids. *J. Vis. Exp.* 1–4 (2010) doi:10.3791/2565.

68. Wright, E. S. Using DECIPHER v2.0 to analyze big biological sequence data in R. *R J.* 8, 352–359 (2016).

69. Cataldi, T. R. I., Campa, C. & De Benedetto, G. E. Carbohydrate analysis by high-performance anion-exchange chromatography with pulsed amperometric detection: The potential is still growing. *Fresenius. J. Anal. Chem.* 368, 739–758 (2000).

70. Henshall, A. High Performance Anion Exchange Chromatography with Pulsed Amperometric Detection (HPAE- PAD). (1999) doi:10.1201/9780203909577.ch20.

71. Untergasser, A. *et al.* Primer3Plus, an enhanced web interface to Primer3. *Nucleic Acids Res.* 35, (2007).

72. Hernández, I., Sant, C., Martínez, R. & Fernández, C. Design of Bacterial Strain-Specific qPCR Assays Using NGS Data and Publicly Available Resources and Its Application to Track Biocontrol Strains. *Front. Microbiol.* 11, 1–11 (2020).

73. Hung, J. H. & Weng, Z. Designing polymerase chain reaction primers using Primer3Plus. *Cold Spring Harb. Protoc.* 2016, 821–826 (2016).

74. Bustin, S. & Huggett, J. qPCR primer design revisited. *Biomol. Detect. Quantif.* 14, 19–28

(2017).

75. Gravel, J., Paradis-bleau, C. & Schmitzer, A. R. This journal is © The Royal Society of Chemistry 2017 Electronic Supporting Information Adaptation of a bacterial membrane permeabilization assay for quantitative evaluation of benzalkonium chloride as membrane disrupting agent Table of contents Influence. 1–16 (2017).

76. Ahmed, R. *et al.* Graphene-Based Bacterial Filtration via Electrostatic Adsorption. *Adv. Mater. Interfaces* 9, (2022).

77. Paladines, L. *et al.* Investigation of Conditions for Capture of Live Legionella pneumophila with Polyclonal and Recombinant Antibodies. *Biosensors* 12, (2022).

78. Trapnell, C. *et al.* Differential gene and transcript expression analysis of RNA-seq experiments with TopHat and Cufflinks. *Nat. Protoc.* 7, 562–578 (2012).

79. Rosati, D. *et al.* Differential gene expression analysis pipelines and bioinformatic tools for the identification of specific biomarkers: A review. *Comput. Struct. Biotechnol. J.* 23, 1154–1168 (2024).

80. Team., R. C. *R: A Language and Environment for Statistical Computing (Version 4.2.0) [Computer Software]*. (2022).

81. Wickham, H. *Ggplot2: Elegant Graphics for Data Analysis*. (Springer International Publishing, 2016).

82. Love, M. I., Huber, W. & Anders, S. Moderated estimation of fold change and dispersion for RNA-seq data with DESeq2. *Genome Biol.* 15, 1–21 (2014).

83. Benjamini, Y. & Hochberg, Y. Controlling the False Discovery Rate: A Practical and Powerful Approach to Multiple Testing. *J. R. Stat. Soc. Ser. B* 57, 289–300 (1995).

84. Oksanen, J. & Simpson, G. L. Package ‘ vegan ’. (2022).

85. Anderson, M. J. Non-Parametric MANOVA. *Austral Ecol.* 32–46 (2001).

Rasoulimehrabani *et al. Microbiome Res Rep.* 2025;4:30
DOI: 10.20517/mrr.2025.29

Microbiome Research Reports

Original Article

Open Access

Check for updates

Evaluating the prebiotic activity of arabinogalactan on the human gut microbiota using 16S rRNA gene sequencing and Raman-activated cell sorting

Hamid Rasoulimehrabani[1,2], Sanaz Khadem[1], Adnan Hodžić[1], Miriam Philipp[1], Rebecca Gallo[1,2], Georgi Nikolov[1], Joana Séneca[3], Julia Ramesmayer[3], Patrik Sivulič[4], David Berry[1,3]

[1]Center for Microbiology and Environmental Systems Science, Department of Microbiology and Ecosystem Science, University of Vienna, Vienna 1030, Austria.
[2]Doctoral School in Microbiology and Environmental Science, University of Vienna, Vienna 1030, Austria.
[3]Joint Microbiome Facility of the Medical University of Vienna and the University of Vienna, Vienna 1030, Austria.
[4]Department of Natural Drugs, Faculty of Pharmacy, Masaryk University in Brno, Brno 612 00, Czech Republic.

Correspondence to: Prof. David Berry, Centre for Microbiology and Environmental Systems Science, Department of Microbiology and Ecosystem Science, University of Vienna, University Biology Building (UBB), Djerassiplatz 1, Vienna 1030, Austria. E-mail: david.berry@univie.ac.at

How to cite this article: Rasoulimehrabani H, Khadem S, Hodžić A, Philipp M, Gallo R, Nikolov G, Séneca J, Ramesmayer J, Sivulič P, Berry D. Evaluating the prebiotic activity of arabinogalactan on the human gut microbiota using 16S rRNA gene sequencing and Raman-activated cell sorting. *Microbiome Res Rep.* 2025;4:30. https://dx.doi.org/10.20517/mrr.2025.29

Received: 28 Apr 2025 **First Decision:** 6 Jun 2025 **Revised:** 11 Jul 2025 **Accepted:** 31 Jul 2025 **Published:** 14 Aug 2025

Academic Editor: Miguel Gueimonde **Copy Editor:** Pei-Yun Wang **Production Editor:** Pei-Yun Wang

Chapter 3

Evaluating the prebiotic activity of arabinogalactan on the human gut microbiota using 16S rRNA gene sequencing and Raman-activated cell sorting

Hamid Rasoulimehrabani[1,2], Sanaz Khadem[1], Adnan Hodžić[1], Miriam Philipp[1], Rebecca Gallo[1,2], Georgi Nikolov[1], Joana Séneca[3], Julia Ramesmayer[3], Patrik Sivulič[4], David Berry[1,3*]

[1]Center for Microbiology and Environmental Systems Science, Department of Microbiology and ecosystem Science, University of Vienna, 1030 Vienna, Austria

[2]Doctoral School in Microbiology and Environmental Science, University of Vienna, 1030 Vienna, Austria

[3]Joint Microbiome Facility of the Medical University of Vienna and the University of Vienna, 1030 Vienna, Austria

[4]Department of Natural Drugs, Faculty of Pharmacy, Masaryk University in Brno, 612 00 Brno, Czech Republic

* Address correspondence to Prof. Dr. David Berry, Centre for Microbiology and Environmental Systems Science, Department of Microbiology and ecosystem Science, University of Vienna, University Biology Building (UBB), Djerassiplatz 1, 1030 Vienna, Austria. david.berry@univie.ac.at

Abstract

Background: Arabinogalactan is a complex plant-derived polysaccharide proposed to function as a selective prebiotic, yet the microbial taxa directly involved in its metabolism and the cooperative dynamics within the gut microbiota remain incompletely defined.

Methods: Here, we combined community level sequencing with targeted single-cell activity profiling to investigate how arabinogalactan shapes gut microbial composition and function. Fecal samples from ten healthy individuals were incubated *ex vivo* with arabinogalactan, and microbial responses were assessed using 16S rRNA gene amplicon sequencing alongside Raman-activated cell sorting (RACS) and coculture experiments.

Results: Arabinogalactan consistently enriched *Bifidobacterium* and *Gemmiger* across donors, with *Bifidobacterium* also responding to galactose and *Gemmiger* and *Blautia* stimulated by arabinose, the two monosaccharide components of arabinogalactan. RACS enabled the selective isolation of metabolically active arabinogalactan responders, including *Bifidobacterium longum* and *Faecalibacterium prausnitzii*, along with other strains from the phyla *Actinomycetota*, *Bacteroidota*, and *Bacillota*. Notably, coculture experiments revealed that *B. longum* not only degraded arabinogalactan efficiently but also supported the growth of non-degrading species via metabolic cross-feeding. These cooperative interactions highlight *B. longum* as a keystone species in arabinogalactan utilization and suggest broader community-level benefits from its activity.

Conclusion: Together, our findings demonstrate arabinogalactan's bifidogenic effect and its potential to promote functionally important microbes within the gut ecosystem. This study also highlights the utility of RACS for linking microbial identity to function, enabling the targeted recovery of active strains from complex communities.

Keywords: Arabinogalactan, *Bifidobacterium longum*, gut microbiota, prebiotics, Raman-activated cell sorting, microbial cross-feeding

Introduction

The human gut microbiota is essential for maintaining host health through its roles in nutrient metabolism, immune regulation, and protection against pathogens [1]. Microbial community composition in the gut is influenced by various factors, with diet recognized as a major determinant [2]. At baseline, the adult gut microbiota predominantly consists of bacteria belonging to the phyla *Bacillota*, *Bacteroidota*, *Actinomycetota*, *Verrucomicrobiota*, and *Pseudomonadota [3–5]*. However, the relative abundance of these phyla exhibits considerable variability among individuals, underscoring substantial inter-individual differences in microbiota structure and functionality [6]. Non-digestible dietary fibers are increasingly recognized for their ability to selectively modulate the composition and function of the gut microbiota [7]. These fibers, often termed prebiotics, resist digestion by human enzymes, reaching the large intestine intact, where they are selectively fermented by certain gut microbes, thereby conferring health benefits to the host [8]. Well-studied prebiotics include oligosaccharides such as fructooligosaccharides (FOS) and galactooligosaccharides (GOS), as well as polysaccharides like inulin, resistant starch, and beta-glucans, which have been shown to selectively stimulate the growth of beneficial gut microbes such as *Bifidobacterium* and *Lactobacillus [8–10]*.

Arabinogalactan is a plant-derived polysaccharide that has recently been proposed as a potential prebiotic [11,12]. Prebiotics are defined as substrates selectively utilized by host microorganisms that confer a health benefit [13]. This definition emphasizes both microbial selectivity and demonstrable benefit to the host. In this context, arabinogalactan fulfills key prebiotic criteria by reaching the colon undigested, being selectively fermented by beneficial gut bacteria such as *Bifidobacterium*, and contributing to the production of health-promoting short-chain fatty acids (SCFAs) [14]. It is naturally abundant in certain dietary sources, notably larch wood and legumes [11,15]. Arabinogalactan is a structurally complex, branched polysaccharide typically composed of a galactan backbone with β-1,3- and/or β-1,6-glycosidic linkages, and contains side chains made of arabinose and galactose residues [16]. Fermentation of arabinogalactan by the gut

microbiota results in the production of SCFAs, particularly propionate and butyrate, along with other organic acids [17,18]. These metabolites can contribute to lowering intestinal pH and promoting a gut environment associated with improved host health [19]. Arabinogalactan supplementation has been shown to selectively increase the abundance of *Bifidobacterium* species, indicating its potential bifidogenic effect [14,20,21]. However, the specific microbial taxa directly involved in arabinogalactan metabolism, as well as the dynamics of their metabolic interactions within the broader microbial ecosystem, remain incompletely characterized [22–25]. Efficient utilization of complex polysaccharides like arabinogalactan can involve cooperative interactions among multiple microbial species [26,27]. Primary degraders can break down complex polysaccharides via CAZymes, releasing metabolites that support secondary consumers [28]. Identifying these microbial interactions is key to understanding how polysaccharides such as arabinogalactan selectively modulates gut microbiota and promotes host health [14,28]. These microbial shifts can benefit the host by enhancing SCFA production, supporting gut barrier integrity, and modulating immune responses [29].

To investigate the microbial response to arabinogalactan at both community and single-cell resolution, we employed an integrated *ex vivo* approach using fecal samples from ten healthy donors. First, we characterized community-level shifts through 16S rRNA gene amplicon sequencing, assessing compositional changes driven by arabinogalactan supplementation. Next, we utilized single-cell Raman microspectroscopy combined with deuterium (D_2O) labeling to identify individual microbial cells actively metabolizing arabinogalactan. Metabolically active bacteria were selectively isolated via Raman-activated cell sorting (RACS) and subsequently characterized to confirm their physiological capacity to degrade arabinogalactan. Finally, coculture experiments between a primary arabinogalactan degrader - *Bifidobacterium longum* - and metabolically active, non-degrading isolates provided insights into potential cooperative interactions, illustrating how *B. longum* facilitates secondary growth via metabolic cross-feeding. Together, our results provide mechanistic insight into how arabinogalactan selectively enriches

specific gut microbes and promotes cooperative interactions, supporting its role as a functionally selective prebiotic.

Materials and methods

Sample Collection and Incubation

Stool samples were collected from 10 healthy adults (five males and five females; mean BMI: 24.43 ± 3.69). Participants were excluded if they had taken antibiotics, consumed prebiotic or probiotic products in the past six months, or had a known history of gastrointestinal disorders or recent digestive illness [30,31]. Participants collected their own stool samples using sterile screw-cap containers equipped with built-in collection spoons (Sarstedt, Germany). The study was approved by the Ethics Committee of the University of Vienna, and all individuals provided written informed consent (reference number: 00161).

Immediately following collection, fecal material was transferred into an anaerobic chamber (gas mixture: 85% N_2, 10% CO_2, 5% H_2) to maintain strict anaerobic conditions [32,33]. To assess microbiota responses, fecal homogenates were incubated with arabinogalactan, arabinose, and galactose (2 mg/ml final concentration, Carl Roth and Sigma-Aldrich) [7], while unamended samples were used as negative controls. Samples were homogenized in 2x PBS by vigorous vortexing (2–3 minutes), passed through a 40 µm mesh filter (Corning, Germany) to remove large debris, and diluted 1:10 with 2x PBS.

Each sugar was dissolved in D_2O and added to sterile Hungate tubes containing 2 ml of the fecal homogenate. The final volume was adjusted to 4 ml, yielding a 50% D_2O concentration. Incubations were carried out anaerobically at 37 °C for 6 and 24 h. Following incubation, cells were rinsed with PBS to eliminate residual D_2O. For downstream processing, 1 ml of each sample was fixed in 50% ethanol/PBS and stored at −20 °C, while an additional 1 ml aliquot was frozen at −80 °C for subsequent nucleic acid and metabolite analysis. For RACS, aliquots were preserved in 20% glycerol/PBS and stored at −80 °C in crimp-sealed vials.

The entire preparation process, including sample homogenization, filtration, and substrate addition, took approximately 30 minutes. This point was considered as the initial time point (0 h) in the dataset and used as the reference for all downstream analyses.

DNA Extraction and 16S rRNA Amplicon Sequencing

To assess shifts in microbial composition, DNA was isolated from stool samples harvested at 0, 6, and 24 hours after treatment with arabinogalactan, arabinose, galactose, or without any amendment. DNA was extracted using the QIAamp DNA Mini Kit (Qiagen, Germany), incorporating a lysozyme pre-treatment step to enhance cell lysis and optimize DNA recovery [34]. The 16S rRNA gene was amplified using a two-step PCR approach with dual barcoding, allowing for high-resolution profiling of microbial community composition [35]. Sequencing was performed at the Joint Microbiome Facility (JMF) of the Medical University of Vienna and the University of Vienna (Project ID: JMF-2307-05). The resulting sequence datasets have been deposited in the NCBI Short Read Archive under the BioProject accession number PRJNA1244259.

Single-Cell Raman Analysis of Arabinogalactan-Stimulated Gut Microbiota

To assess microbial responses, fecal samples were exposed to arabinogalactan for 6 and 24 h, while parallel incubations without amendment were used as controls. To maintain cellular integrity, samples were fixed in a 1:1 mixture of ethanol and PBS. For Raman measurements, 1 µL of each fixed sample was applied to an aluminum-coated slide (Al136; EMF Corporation, USA) and allowed to air-dry at 30 °C [36,37]. Residual buffer components were removed by dipping the slides twice in ice-cold Milli-Q water (Millipore, Austria), followed by air drying [38]. Spectral acquisition was performed using a confocal Raman microspectroscope (LabRAM HR800, Horiba Scientific, France) equipped with a 532 nm Nd:YAG laser and a diffraction grating of 300 grooves/mm [39]. Prior to measurement, the laser was calibrated using a silicon crystal standard, and the sample slide was brought into focus using a 100× objective [40]. Cell clusters were visually selected, and a mapping grid was applied to the designated area for targeted measurement. An

acquisition time of 0.3 seconds was chosen to match the conditions used in RACS, allowing direct comparison between the two approaches. Preliminary tests indicated that using 4 accumulations provided the clearest spectra while minimizing laser exposure and preserving cell integrity. A delay time of 0 s was used, and binning was set to 1 to achieve the highest spectral resolution.

A total of 30 to 40 single microbial cells were analyzed per sample. Spectra were considered valid if they showed a clear C–H stretch (2800–3100 cm^{-1}) and a phenylalanine peak (~1000 cm^{-1}), confirming signal origin from cellular material [41,42]. Deuterium incorporation was identified via the C–D stretch (2040–2300 cm^{-1}), reflecting active metabolism [36]. The percentage of deuterium-labeled bonds (%CD) was calculated as the ratio of C–D to total C–H and C–D signals using the Scattr analysis tool (https://shiny.lisc.univie.ac.at/scattr/). The threshold for metabolic activity was determined based on %CD values from cells incubated without the addition of D_2O (water control), calculating the mean plus 3 times the standard deviation (SD) [39].

Targeted Isolation of Arabinogalactan-Responsive Cells via RACS

RACS was performed on fecal samples incubated for 6 h with D_2O and arabinogalactan to isolate metabolically active cells. After incubation, cells were preserved in 20% glycerol/PBS and stored at −80 °C. For sorting, frozen samples were thawed, pelleted at 9000 × g for 7 minutes, and washed twice with 0.3 M PBS/glycerol solution to minimize osmotic stress [43]. The final cell pellet was resuspended in 500 µL of the same buffer and loaded into a 500 µL Hamilton syringe under anaerobic conditions. The RACS platform was consisted of a confocal Raman microscope (532 nm, 90 mW), optical tweezers using a 1064 nm Nd:YAG laser (500 mW), and a polydimethylsiloxane (PDMS)-based microfluidic sorting device [43]. The PDMS chips were fabricated by mixing base elastomer (Sylgard 184TM, Dow corning, Michigan, USA) and curing agent mixed at a 10:1 ratio, polymerized at 75°C, and mounted on a glass coverslip [43]. During the sorting process, cells were sorted by their Raman spectral profiles, allowing deuterium-labeled cells to be directed to the collection outlet, whereas unlabeled cells were guided toward the waste outlet [44]. Cells were identified and sorted based on Raman spectra using automated MATLAB software (version 4.2) based on two indices. The cell index (Pc), indicating cell capture

and defined as the integrated Raman signal between 1620–1670 cm^{-1} relative to the surrounding medium and the labeling index (PL) was calculated as the ratio of C–D stretch (2040–2300 cm^{-1}) to a reference region (1850–1900 cm^{-1}) [43]. Thresholds for Pc and PL were set based on glucose-incubated controls without D_2O (Pc = 1.1; PL = 6.0). Labeled cells were directed into a collection outlet using optical tweezers, while unlabeled cells were routed to waste.

The sorting process for each sample lasted approximately 60 to 90 minutes. After sorting, 50 µL of the collected cell suspension was immediately plated on YCFA agar plate and incubated anaerobically at 37 °C. A 50 µL aliquot of the sheath buffer was also plated as a negative control. Colonies recovered after initial plating were subsequently transferred onto YCFA-arabinogalactan plates for confirmation of growth, and successfully grown isolates were preserved as glycerol stocks at -80 °C. The RACS platform has an average throughput of up to 500 cells per hour and a sorting accuracy of 98.3 ± 1.7% [44]. For each donor, the total number of D_2O-labeled cells analyzed, sorted, and successfully cultivated was recorded. The post sorting cultivation success rate defined as the percentage of colonies recovered relative to the number of labeled cells sorted ranged from 0.6 % to 32.96 % across donors (Supplementary table 1).

16S rRNA Gene Sequencing of RACS Isolated Bacteria

To genetically characterize the bacterial isolates obtained from RACS, colony PCR targeting the 16S rRNA gene was conducted. All PCR mixtures were assembled in a sterile PCR hood to prevent contamination. The reaction mix (50 µL total volume) contained the following components: 5 µL of 10× Green Dream Taq Buffer with 20 mM $MgCl_2$ (Thermo Fisher Scientific, USA), 5 µL of 2 mM dNTP mix (Thermo Fisher Scientific), 1 µL of each primer, 616V (5'-AGA GTT TGA TYM TGG CTC AG-3') and 1492R (5'-GGT TAC CTT GTT ACG ACT T-3') with the final concentration of 50 µM (Thermo Fisher Scientific), 0.5 µL of 20 mg/mL BSA (Thermo Fisher Scientific), 0.5 µL of DreamTaq DNA Polymerase (5 U/µL) (Thermo Fisher Scientific), and 37 µL of nuclease-free water (Thermo Fisher Scientific). PCR amplification conditions were as follows: initial denaturation at 95 °C for 3 min; 30 cycles of 95 °C for 30 s, 56 °C for 30 s, and 72 °C for 90 s; followed by a final extension at 72 °C for 10 min. Amplified fragments were checked by electrophoresis on 1% agarose gels and

purified using the InnuPREP PCRpure Kit (Analytik Jena, Germany) as per the manufacturer's instructions. DNA concentrations were quantified using a Nanodrop spectrophotometer (Thermo Fisher Scientific, USA). The purified PCR products were submitted to Microsynth Austria GmbH (Vienna, Austria) for Sanger sequencing. Resulting chromatograms were processed and evaluated using 4Peaks (version 1.8, Nucleobytes, Amsterdam) and aligned in Serial Cloner (version 2.6). Potential chimeric sequences were identified using the online DECIPHER tool [45]. Taxonomic assignments were made by comparing the sequences against the NCBI nucleotide collection database (https://blast.ncbi.nlm.nih.gov/) with a minimum similarity threshold of 96%. Verified sequences were subsequently uploaded to GenBank under accession numbers PQ407681 - PQ407778.

Growth Curve Analysis

Bacterial strains identified by Sanger sequencing were grown anaerobically at 37°C in both solid and liquid YCFA-glucose (YCFA-G) medium. Once cultures reached early stationary phase, as determined by OD600, cells were harvested, washed, and resuspended in fresh YCFA medium containing either arabinogalactan (YCFA-AG) or no supplement (YCFA-NA) as a control. Each culture was distributed into a sterile 96-well microplate (Costar 3595, Corning, NY, USA) in triplicate. The plate was incubated for 48 h at 37°C using an anaerobic microplate reader (Multiskan™ GO, Thermo Fisher Scientific), with optical density at 600 nm measured every 30 minutes and continuous shaking (5 seconds before each readout) controlled by SkanIt Software RE (v6.1.0.51). Growth kinetics were analyzed using R (https://www.r-project.org/), and the resulting culture supernatants were harvested and stored at −80°C.

Coculture Evaluation

To investigate potential metabolic interactions, coculture experiments were performed using *B. longum* and eight non-degrading strains previously identified via RACS as unable to utilize arabinogalactan independently. These strains included *E. lenta*, *C. aerofaciens*, *P. coprocola*, *D. welbionis*, *R. bicirculans*, *P. faecium*, *P. merdae*, and *A. shahii*. Each strain was incubated

anaerobically at 37 °C in YCFA medium supplemented with arabinogalactan (YCFA-AG), both as a monoculture and in coculture with *B. longum*. For coculture setups, equal volumes (50 µL) of log-phase cultures of *B. longum* and the respective non-degrader were mixed. Samples were collected at 0 h and 24 h to monitor growth progression and capture late log-phase activity.

Strain-specific primers were designed using Primer3Plus to enable quantitative PCR (qPCR) analysis of strain abundance in both monocultures and cocultures [46]. The primers used for each strain were as follows: BifL-F (GAGATACGGCTTCCCTTCGG) and BifL-R (CATAATCCGCTGGCAACACG) for *B. longum* (Product length: 126 bp, Tm: 60°C), Egg-F (CGCGGCCCATTAGGTAGTAG) and Egg-R (AGTCTGGGCCGTATCTCAGT) for *E. lenta* (Product length: 106 bp, Tm: 60°C), Coll-F (TGCTACAATGGCCGGTACAG) and Coll-R (AGCAACTCCGACTTCATGGG) for *C. aerofaciens* (Product length: 114 bp, Tm: 60°C), Phoc-F (CGTGAGGTGTCGGCTTAAGT) and Phoc-R (TCCTCGCATCTTACGATGGC) for *P. coprocola* (Product length: 105 bp, Tm: 60°C), Dyso-F (GAGCTCGCGTCTGATTAGCT) and Dyso-R (TGTCTCAGTCCCAATGTGGC) for *D. welbionis* (Product length: 100 bp, Tm: 60°C), Rumino-F (GAGCTCGCGTCTGATTAGCT) and Rumino-R (TGTCTCAGTCCCAATGTGGC) for *R. bicirculans* (Product length: 100 bp, Tm: 60°C), Phas-F (AGTAAACGAGGAAGCCACGG) and Phas-R (AAGCCGCCTACATGCTCTTT) for *P. faecium* (Product length: 105 bp, Tm: 60°C), Para-F (GTGTGTTTGAGGTAGGCGGA) and Para-R (GTAAGCTGCCTTCGCAATCG) for *P. merdae* (Product length: 84 bp, Tm: 60°C), Alis-F (AGCTGGTTGGTGAGGTAACG) and Alis-R (TGGTCCGTGTCTCAGTACCA) for *A. shahii* (Product length: 89 bp, Tm: 60°C). Primer specificity was validated using PCR with both specific and non-specific templates and optimized using gradient PCR to determine optimal annealing temperatures. For qPCR quantification, DNA standards were prepared by growing each strain to OD_{600} = 0.1, followed by DNA extraction. The 10-fold serial dilutions of the extracted DNA were used to establish standard curves for absolute quantification. The qPCR reactions were run in triplicate for each sample, enabling accurate quantification of bacterial abundance in both monocultures and cocultures across the selected time points. This setup allowed us to evaluate strain-specific growth responses and potential cross-feeding interactions mediated by *B. longum* during arabinogalactan degradation.

Statistical Analysis and Reproducibility

All analyses were conducted in R statistical software (v4.2.1; https://www.r-project.org/) [47]. Data preprocessing and transformation were performed using the data.table, dplyr, and tidyr packages, and visualizations were generated with ggplot2 (v3.5.1) [48]. Microbial community-level differences were assessed using the vegan package (v2.6.4) [49], applying Bray–Curtis dissimilarity and PERMANOVA[49]. To evaluate taxon-level responses to dietary amendments, enrichment factors (EF) were calculated by comparing genus-level relative abundances at 6 and 24 hours to their corresponding baseline (no amendment) at the same time points. The EF was computed using the formula $EF = 2A / (A + B) - 1$, where A and B represent the relative abundances in treated and control conditions, respectively. This approach enabled genus-level comparisons across donors while keeping the output values within a defined and symmetric range between -1 and 1. Because we did not include external spike-ins or perform absolute quantification, enrichment factors (EF) were calculated based on relative changes within each individual donor, comparing treated and control conditions separately for each donor. Genera with $EF > 0$ were considered enriched, and those with $EF < 0$ depleted. Statistical significance was assessed using z-scores derived from RA comparisons, with p-values adjusted using the Benjamini-Hochberg false discovery rate (FDR) method [50]. Genera with $EF > 0$ and FDR-adjusted $p < 0.05$ were considered significantly enriched. Bubble plots were used to visualize results, where bubble size reflected relative abundance of baseline at initial time point (0 h), bubble color encoded EF, and statistically significant genera were annotated with asterisks. DESeq2 (v1.38.3) was also used for differential abundance testing, modeling genus-level count data with a negative binomial distribution [51]. Donor identity and time point were included as variables in the model design. We selected DESeq2 for this analysis because it supports modeling donor identity as well as treatment effects, which was essential for accounting for the high inter-individual variability observed across donors. Genera with FDR-adjusted $p < 0.05$ were considered significantly differentially abundant. The combination of EF and DESeq2 provided complementary insights into both donor-specific and consistent taxon-level responses to arabinogalactan supplementation. To

assess shifts in microbial community structure between arabinogalactan-amended and control samples, permutational multivariate analysis of variance (PERMANOVA) was performed using the vegan package (v2.6.4) in R. The adonis function was applied to test for differences in community composition based on Bray–Curtis dissimilarity metrics computed from genus-level relative abundance profiles [49]. This multivariate approach allowed us to evaluate whether overall microbial community structures varied significantly between treatments, beyond changes at the individual taxon level.

Results

Selective Enrichment of Gut Microbes in Response to Arabinogalactan Supplementation

To characterize the baseline microbial community structure prior to incubation, we performed 16S rRNA gene amplicon sequencing on fecal samples collected from all ten donors at the initial time point (0 h). Across the donors, the gut microbiota was predominantly composed of members of the phyla *Bacillota* (50.8%) and *Bacteroidota* (40.3%), with lower contributions from *Verrucomicrobiota* (4.1%), *Pseudomonadota* (2.9%), and *Actinomycetota* (1.9%) (Figure 1a).

Analysis of genus-level microbiome profiles revealed that most of the variation in microbial composition was explained by donor-specific differences, with inter-individual effects accounting for 71.3% of the total variation (R^2 = 0.713, p = 0.001; n = 20 samples). This donor effect was also the main factor driving the clustering pattern observed in the principal coordinates analysis, indicating pronounced baseline differences in gut microbiota across individuals (Figure 1b). Despite this variation, microbial communities incubated with arabinogalactan for 6 h showed a consistent shift relative to 0 h and 6 h no amendment (NA) samples. A significant effect of arabinogalactan treatment on microbial community composition was detected (R^2 = 0.121, p = 0.004), indicating that the induced shifts were consistently reproducible across distinct microbiota backgrounds.

To assess the extended short-term effects of supplementation, we incubated samples for 24 h. Similar to the 6 h time point, community composition remained strongly donor-driven (R^2 = 0.703, p = 0.001), yet arabinogalactan treatment still explained a significant portion of the variation

between groups (R^2 = 0.123, p = 0.004). These results confirm that the observed community shifts are sustained over time and continue to reflect a robust and reproducible response to arabinogalactan across different individuals (Supplementary Figure 1).

We next identified bacterial genera that were selectively enriched in response to arabinogalactan after 6 h of incubation. Genus-level differential abundance analysis revealed that *Bifidobacterium* and *Gemmiger* showed a consistent and significant increase across the donors, but not in the no amendment samples (DESeq2, Wald Test $p.adj < 0.05$; Figure 1c, Supplementary Figure 2). This highlights a conserved response to arabinogalactan supplementation, suggesting these genera may play a central role in its metabolism. The enrichment of *Bifidobacterium* across the donor samples reflects a robust bifidogenic response to arabinogalactan treatment. This effect was not observed in unamended controls, highlighting that the enrichment was specifically induced by arabinogalactan. In addition, other taxa — including *Alistipes*, *Bacteroides*, *Blautia*, *Catenibacterium*, *Collinsella*, *Faecalibacterium*, *Oscillibacter*, *Parabacteroides*, *Phascolarctobacterium*, *Phocaeicola*, and *Ruminococcus* — showed significant enrichment in one or more donors, reflecting donor-specific shifts in microbial composition (Supplementary Data 1). To assess whether these effects were maintained or intensified over time, we performed an additional incubation with arabinogalactan for 24 h. The enrichment patterns observed at 6 h were largely preserved, with *Bifidobacterium* and *Gemmiger* continuing to show significant increases across the donors (Supplementary Figure 3, Supplementary Data 2). In contrast, incubations without any amendment (NA) for 6 or 24 h did not result in any consistent or significant enrichment at the genus level across donors (Supplementary Figure 2), supporting that the observed microbial changes were specifically driven by arabinogalactan treatment.

To further distinguish the effects of arabinogalactan from those of its constituent monosaccharides, we incubated the same donor samples with either galactose or arabinose for 6 and 24 h. Galactose consistently stimulated a significant enrichment of *Bifidobacterium* across the donors at both time points (Supplementary Data 3-4). In contrast, arabinose triggered significant enrichment of *Blautia* at both time points, while *Gemmiger* was enriched at 6 h but

not at 24 h. Notably, *Anaerostipes* showed significant enrichment across the donors specifically at 24 h (Supplementary Figures 4–5, Supplementary Data 5-6).

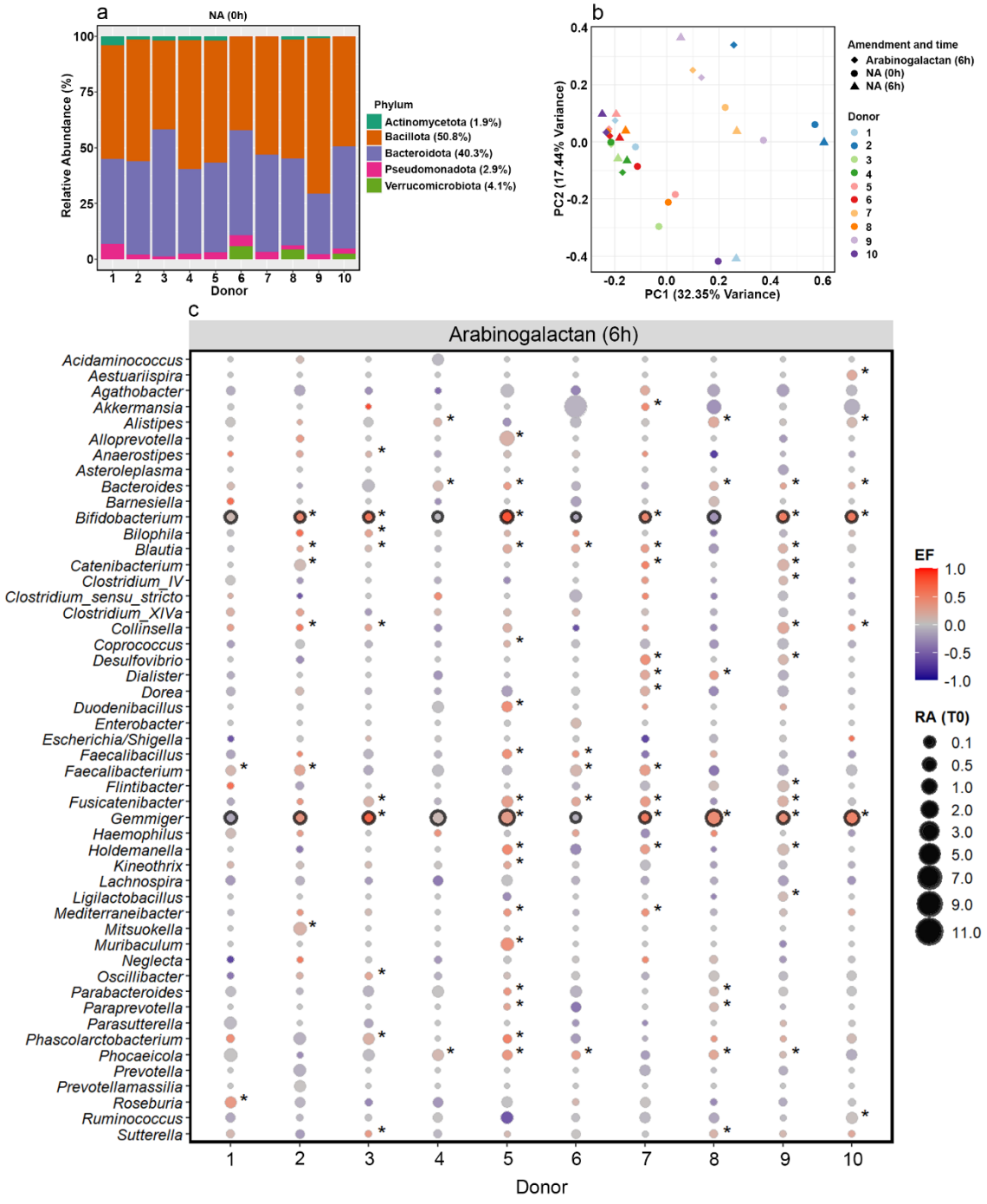

Figure 1. Baseline gut microbiota composition and response to arabinogalactan. (a) Relative abundances (%) of fecal microbiota at the phylum level across ten donors at the baseline (0 h). Average values for each phylum across all donors are provided in the legend. **(b)** Principal coordinate analysis (PCoA) of genus-level microbial communities, illustrating the clustering pattern of samples after 6-hour incubation with arabinogalactan, compared to no amendment (NA) samples at 0 and 6 h. Color and shape indicate donor identity and treatment condition, highlighting both individual and treatment-related differences. **(c)** Enrichment patterns of dominant bacterial genera after 6 h incubation with arabinogalactan. Bubble size indicates the relative abundance at 0 h, and color indicates the scaled enrichment factor (EF), as described in the Materials and Methods section. Genera with significant enrichment in individual donors are indicated by an asterisk, while those consistently enriched across all donors are highlighted with a black outline (DESeq2, Wald Test p.adj < 0.05, n = 30 samples).

Targeted cultivation of arabinogalactan-responsive bacteria using Raman-based activity profiling

To identify metabolically active gut microbes responding to arabinogalactan, we performed D_2O labeling followed by single-cell Raman microspectroscopy. Deuterium incorporation, quantified as the percentage of C–D bonds relative to total C–H and C–D (%CD), was used to assess microbial metabolic activity [36]. After 6 h of incubation, cells from arabinogalactan-supplemented microcosms showed significantly higher %CD values compared to their matched no-amendment (NA) controls, indicating that arabinogalactan stimulated microbial metabolism across nearly all donors (Figure 2a). A similar pattern of increased metabolic activity was also observed after 24 h of incubation (Supplementary Figure 6), confirming that the effect of arabinogalactan was consistent over time.

To isolate metabolically active taxa responsive to arabinogalactan, we next employed RACS following 6 h incubations with D_2O and arabinogalactan. A total of 98 strains were recovered from RACS-enriched fractions across all donors and classified via near-full-length 16S rRNA gene sequencing as *Bifidobacterium longum* (n = 45), *Collinsella aerofaciens* (n = 26), *Alistipes shahii* (n = 5), *Alistipes senegalensis* (n = 1), *Alistipes putredinis* (n = 2), *Alistipes onderdonkii* (n = 3), *Bacteroides uniformis* (n = 2), *Bacteroides stercoris* (n = 1), *Catenibacterium mitsuokai* (n = 6), *Dysosmobacter welbionis* (n = 1), *Eggerthella lenta* (n = 1), *Faecalibacterium prausnitzii* (n = 1), *Parabacteroides merdae* (n = 1), *Phascolarctobacterium faecium* (n = 1), *Phocaeicola coprocola* (n

= 1), and *Ruminococcus bicirculans* (n = 1). These strains belonged to three different phyla: *Actinomycetota* (72 strains), *Bacteroidota* (16 strains), and *Bacillota* (10 strains) (Supplementary Figure 7, Supplementary Data 7).

A total of 16 strains were selected as representative isolates for downstream analysis (Figure 2b). One representative per species was chosen to assess its physiological response to arabinogalactan. To functionally characterize arabinogalactan responders, we selected 16 representative isolates from the 98 strains recovered by RACS, ensuring broad phylogenetic coverage while minimizing redundancy among closely related strains. A single *B. longum* strain was chosen for coculture assays based on its high recovery frequency (n = 45) and robust growth on arabinogalactan. Growth assays and coculture experiments were conducted in triplicate. Quantitative growth boosts were calculated as area under the curve (AUC) in arabinogalactan-supplemented versus no-amendment media, with statistical significance determined by Student's t-test ($p < 0.05$). The $\log_2$ fold changes in coculture abundance, quantified by qPCR, represent mean ± standard deviation from three replicates. Error bars and individual data points are included to illustrate replicate variation. The addition of arabinogalactan to the cultivation medium stimulated the growth of *B. longum*, *F. prausnitzii*, *C. mitsuokai*, *B. uniformis*, and *B. stercoris*.

Since the remaining strains had incorporated deuterium from D_2O (indicating metabolic activity) but were unable to utilize arabinogalactan as a sole carbon source, we hypothesized that their growth might be indirectly supported by primary arabinogalactan degraders. *B. longum* was selected as the focal degrader as it was the most frequently isolated species and due to its robust growth on arabinogalactan. To test this hypothesis, we performed coculture experiments in which incubating each non-arabinogalactan utilizing isolate together with *B. longum* for 24 h in the presence of arabinogalactan. As expected, none of these strains grew in monoculture, but all displayed significant growth when cocultured with *B. longum*, suggesting that *B. longum* facilitated their proliferation through metabolic cross-feeding. Notably, the growth of *B. longum* itself was significantly reduced in cocultures with *Eggerthella lenta*, *Dysosmobacter welbionis*, *Ruminococcus bicirculans*, *Phascolarctobacterium faecium*, and *Phocaeicola coprocola*.

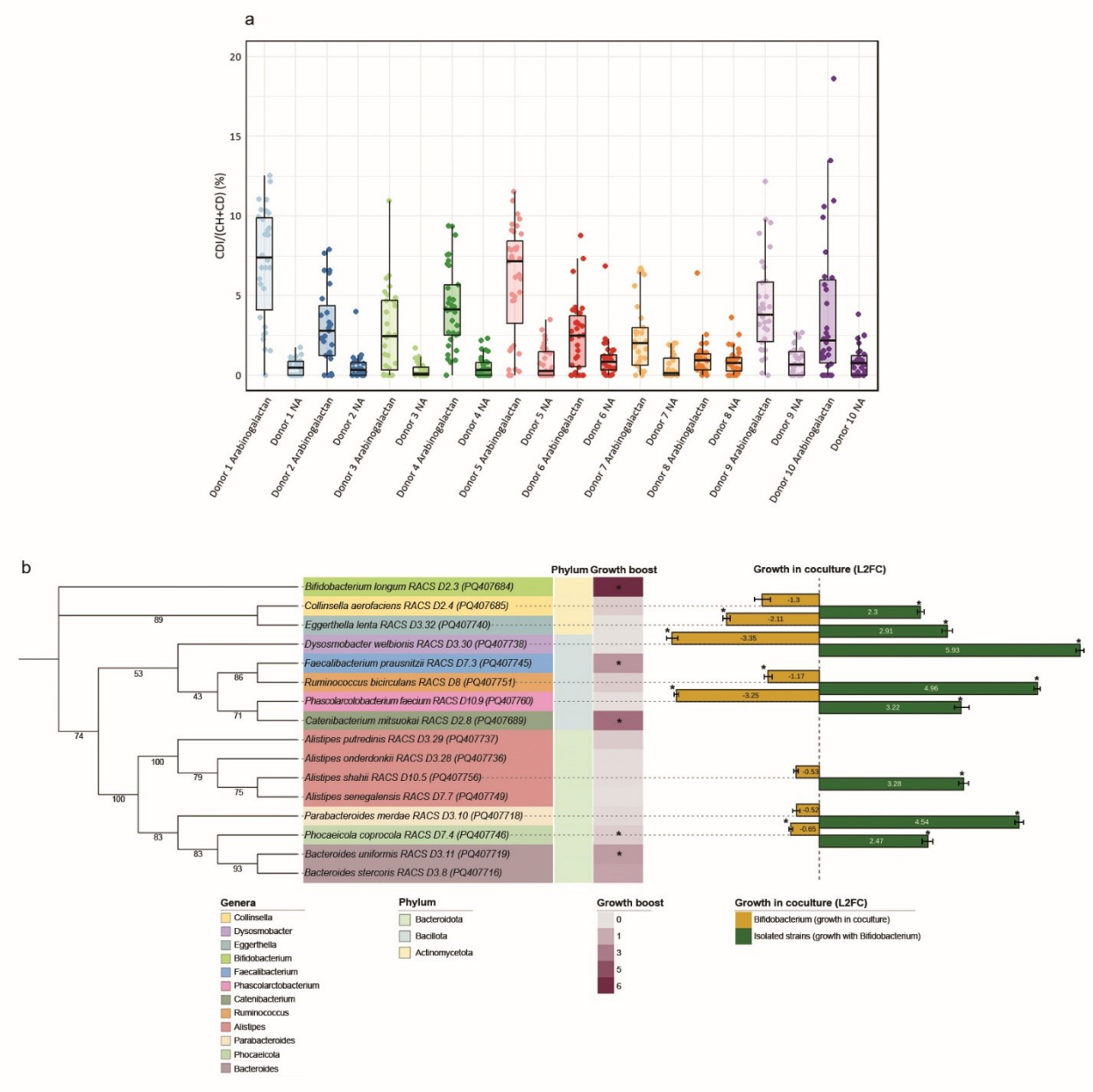

Figure 2. Raman-based detection and physiological analysis of arabinogalactan-responsive gut microbes. (a) Single-cell analysis of microbial metabolic activity in response to arabinogalactan. The percentage of deuterium incorporation (%CD) was measured in individual cells following 6 h incubation with D_2O, with or without arabinogalactan. The dots indicate single-cell measurements collected from each ten donors, while boxplots illustrate the spread of %CD values across conditions. Statistical testing across all donors revealed a significant increase in microbial metabolic activity following arabinogalactan treatment (ANOVA, $p < 0.001$, $n = 607$). **(b)** Phylogenetic and physiological profiling of representative arabinogalactan-responsive isolates. A mid-point rooted maximum likelihood phylogenetic tree was

generated from near full-length 16S rRNA gene sequences of 16 representative strains isolated via RACS. Branch support values are based on 1000 ultrafast bootstrap replicates. The tree generation was performed using the aligned sequences, with subsequent visualization annotated in iTOL [52]. The heatmap displays growth boost, calculated as the area under the growth curve in arabinogalactan-supplemented media relative to no-amendment control, based on three technical replicates per condition. Asterisks indicate statistically significant differences in AUC between the two conditions (Student's t-test, $p < 0.05$, $n = 6$). Color. Bar plots show log2 fold change (L2FC) in abundance of each strain after 24 h coculture with *Bifidobacterium longum*, as quantified by qPCR based on the average of three technical replicates. Asterisks (*) indicate significant differences in growth (Student's t-test, $p < 0.05$, $n = 6$).

Discussion

Dietary fibers that selectively stimulate specific gut microbes are increasingly recognized for their potential to promote host health by modulating immunity, improving gut function, and contributing to the production of bioactive metabolites such as SCFAs [7,13,53,54]. Prebiotics such as inulin, FOS, and GOS have been explored for their capacity to selectively enrich microbial groups involved in carbohydrate fermentation and short-chain fatty acid production [8,39]. These include *Bifidobacterium*, *Lactobacillus*, and *Faecalibacterium*, which are frequently associated with gut health and beneficial physiological functions [39,55–58]. However, their effects are not always consistent across studies, and the underlying microbial mechanisms are still not fully understood [59,60]. *Bifidobacterium*, in particular, is widely recognized as a keystone member of the gut microbiota with a central role in fiber degradation and ecosystem function [61].

In this study, we evaluated the selective effects of arabinogalactan, a complex polysaccharide composed of the monosaccharides galactose and arabinose. Arabinogalactan consistently enriched both *Bifidobacterium* and *Gemmiger* across the donors at both the 6 h and 24 h incubation time points. However, this pattern was not observed in unamended controls. Interestingly, galactose alone led to a consistent enrichment of *Bifidobacterium*, while arabinose selectively enriched *Gemmiger* at 6 h and *Blautia* and *Anaerostipes* at 24 h. These findings show that while each monosaccharide selectively stimulated specific taxa, the intact polysaccharide elicited a more coordinated response simultaneously promoting both *Bifidobacterium* and *Gemmiger* in a way that was not observed with the individual sugars. Notably, similar enrichment patterns in response to galactose, arabinose, and arabinogalactan have been reported in previous

studies and are consistent with our findings [61–66]. For instance, the enrichment of *Bifidobacterium* in response to galactose has been reported in transcriptomic studies examining growth on GOS and galactose rich substrates [62]. In another study, *Blautia* proliferation increased via cross-feeding, following the release of arabinose from arabinoglycan containing diets in the gut of malnourished mice [61]. Additionally, *B. longum* was found to be stimulated during the *in vitro* fermentation of arabinogalactan using a dynamic colon model [66]. These overlaps highlight the consistency of certain microbial responses, while our use of RACS based isolation and strain-level functional validation provides new insights into active degraders and cooperative interactions, distinguishing our study from previous work.

B. longum was identified as a key species in arabinogalactan degradation, both in terms of abundance and metabolic function. It was the most frequently recovered taxon using RACS and demonstrated the ability to degrade arabinogalactan as a sole carbon source. Additional strains such as *F. prausnitzii*, *C. mitsuokai*, *B. uniformis*, and *B. stercoris* also showed the capacity to utilize arabinogalactan in monoculture. Among the additional responders, *F. prausnitzii* is notable for its well-known butyrate production, anti-inflammatory properties, and role in strengthening gut barrier function and modulating host immunity [67]. In contrast, several other isolates including *E. lenta, C. aerofaciens, P. coprocola*, and *R. bicirculans* were metabolically active but unable to grow on arabinogalactan alone, suggesting a dependence on external metabolic support. While previous studies have suggested that certain taxa such as *Bifidobacterium*, *Faecalibacterium*, and *Phascolarctobacterium* may contribute to arabinogalactan degradation [18,68], our application of RACS enabled the targeted recovery of a wider set of responsive strains, expanding the current understanding of bacteria capable of utilizing arabinogalactan. Several strains that failed to grow on arabinogalactan in monoculture showed increased growth when cocultured with *B. longum*. These coculture dynamics point to *B. longum* acting as a keystone degrader that enables the growth of other taxa, potentially through metabolic byproducts or cross-feeding interactions [69,70]. In addition to its ecological role as a keystone degrader, *B. longum* is widely recognized for its beneficial impact on host health [71]. Numerous studies have shown that it contributes to intestinal barrier integrity, modulates immune responses, and inhibits pathogen colonization

through the production of organic acids and competitive exclusion mechanisms [72]. The stimulation of *B. longum* suggests that arabinogalactan may offer reproducible bifidogenic benefits, reinforcing its potential as a functionally selective prebiotic.

Similar to *Bifidobacterium, Gemmiger* displayed a robust increase across the donor samples following arabinogalactan supplementation. However, despite its consistent enrichment, *Gemmiger* was not among the metabolically active strains isolated using RACS. This may be due to cultivation challenges or limitations in cell sorting, possibly related to its strict growth requirements [73–75]. While RACS is highly effective for detecting and isolating metabolically active cells, the technique has certain limitations. The laser used for Raman spectroscopy can transfer energy that may damage fragile cells and reduce their viability. Additionally, post-sorting recovery can be challenging for strictly anaerobic taxa that are highly sensitive to oxygen or require very specific growth conditions, which can limit successful cultivation after sorting. Interestingly, we successfully isolated *F. prausnitzii*, an oxygen sensitive butyrate producer closely related to *Gemmiger [76]*. A 16S rRNA sequence comparison revealed that the dominant *Gemmiger* ASV shares 92.79% identity with *Faecalibacterium*, suggesting phylogenetic proximity and possibly overlapping ecological roles [77,78]. This suggests that both taxa may participate in functions such as arabinogalactan fermentation and butyrate production under anaerobic conditions. However, individual strains can differ in which sugars they break down, which enzymes they produce, and how well they grow under gut conditions. Therefore, detailed genome sequencing and experimental validation of substrate utilization and enzyme expression will be important to determine whether *Gemmiger* functionally overlaps with *F. prausnitzii* or contributes unique metabolic activities within the gut community.

Our findings highlight arabinogalactan as a functionally selective prebiotic that enriches specific gut microbes, most notably *B. longum*. Unlike other confirmed prebiotics such as inulin or GOS, which stimulate multiple primary degraders [8,39,79], arabinogalactan targets a narrower group of responsive taxa. *B. longum* not only degrades the polysaccharide but also facilitates the growth of non-degraders, likely through cooperative metabolic interactions. These findings support the use of arabinogalactan as a candidate for targeted modulation of the gut microbiota. Unlike

broad-spectrum prebiotics such as inulin, which are utilized by a wide range of gut microbes, arabinogalactan shows a narrower specificity, primarily stimulating *B. longum* and a few other taxa. This targeted effect may enable more precise modulation of microbiota composition. *Bifidobacterium* species are well known for efficiently fermenting short-chain oligosaccharides such as fructooligosaccharides (FOS) and galactooligosaccharides (GOS) using specialized glycoside hydrolases [14]. Enzymes belonging to the families GH32, GH43 and GH68 cleave β-fructosidic linkages in FOS, while GH2, GH42 and GH43 families target galactosidic bonds in GOS [80,81]. β-Galactanases, including enzymes from the GH30, GH40, and GH43 families, are key for degrading the galactan backbone of arabinogalactan (AG), releasing galactose and short-chain galactooligosaccharides [14]. Although we did not directly investigate the genetic mechanisms underlying *B. longum*'s polysaccharide utilization, prior studies have reported multiple glycoside hydrolases (GHs) in *B. longum* species, including GH30, GH40, GH43, GH51, GH121, GH146 and GH127 families, which are implicated in hydrolyzing arabinogalactan linkages [68,82–84]. Future work should include genome mining and transcriptomic profiling of *B. longum* grown on arabinogalactan to identify upregulated hydrolases and transport systems involved in its metabolism. Additionally, confirming whether similar GHs occur in other relevant taxa, including *Gemmiger* and the representative isolates identified in this study, will help clarify whether these organisms contribute to direct polysaccharide breakdown or rely primarily on cross-fed metabolites. Notably, publicly available genomes from *Gemmiger* spp. encode various GHs that are crucial for carbohydrate metabolism. Among these, the GH101 and GH112 families are of particular interest for their roles in the degradation of complex carbohydrates [85]. Likewise, *F. prausnitzii* genomes contain many different CAZymes, including GH43, GH33, GH78, GH4, and GH170. *F. prausnitzii* has also been reported to degrade rhamnose, which can be found as a side chain in plant polysaccharides such as arabinogalactan [68,86]. These findings support the hypothesis that taxa beyond *Bifidobacterium* may play a direct role in arabinogalactan breakdown. Future genome-resolved and transcriptomic analyses will be essential to validate the functional roles of these organisms and deepen our understanding of community level carbohydrate utilization dynamics.

While 16S rRNA gene sequencing provided valuable insights into community-level shifts in response to arabinogalactan, it has notable limitations in taxonomic resolution, functional interpretation, and differential abundance testing. For instance, the 16S rRNA gene cannot reliably distinguish closely related species or infer the enzymatic capabilities responsible for fiber degradation. To address these challenges, we used RACS to isolate and validate metabolically active taxa at the strain level. This dual approach helped bridge the gap between community profiling and functional activity. However, future studies could benefit from incorporating multi-omics strategies such as shotgun metagenomics, metatranscriptomics, or metabolomics to resolve microbial interaction networks, uncover the genetic basis of arabinogalactan metabolism, and characterize host-relevant metabolic outputs with greater phylogenetic and functional resolution. In future studies, using absolute microbiome quantification approaches such as those based on internal standards or spike-ins could provide more accurate estimates of microbial abundance. Future work should clarify the metabolic pathways involved in arabinogalactan degradation, including the identity of breakdown products and their role in supporting non-degraders. Metabolite profiling of *B. longum* could reveal key compounds responsible for these effects. Additionally, profiling the metabolites produced by *B. longum* during this process may reveal key compounds that facilitate the proliferation of otherwise inactive taxa. Additionally, it will be important to investigate why the presence of certain strains in coculture reduces *B. longum* growth and how this influences overall carbon utilization dynamics. Quantifying how much arabinogalactan and its component sugars are consumed by both individual isolates and mixed microbial communities will provide clearer insights into their degradation capabilities and metabolic contributions. Finally, improving cultivation protocols and post sorting recovery conditions may enhance the isolation of sensitive or slow-growing taxa, providing a more comprehensive view of the microbial networks shaped by selective prebiotics such as arabinogalactan.

There are several limitations to this study that should be acknowledged. Firstly, our reliance on 16S rRNA gene sequencing restricts taxonomic resolution and does not provide direct information

on the functional activities, metabolic pathways, or specific enzymes involved in arabinogalactan metabolism. However, this approach still allowed us to robustly identify key taxa that responded to arabinogalactan, providing valuable ecological insights. This limits our ability to draw conclusions about the metabolic mechanisms driving the observed microbial changes. In addition, we did not perform direct enzymatic assays, which would have helped confirm the involvement of particular enzymes in arabinogalactan degradation. All data are reported as relative abundances rather than absolute quantities. Implementing absolute quantification methods, such as digital PCR (dPCR) or spike-in standards, in future studies could enable more robust and quantitative assessments of microbial dynamics [87]. Despite this, the changes in relative abundance provided consistent and interpretable patterns across donors. The RACS technique, while powerful for isolating metabolically active cells, also presents challenges. Some taxa, such as *Gemmiger*, were not recovered, likely due to cultivation difficulties, sensitivity to laser exposure, or because strictly anaerobic organisms are more difficult to isolate with this method. As a result, some metabolically active and enriched taxa may have been missed among the isolates. Improved cultivation protocols and alternative single-cell approaches could help address this limitation. Furthermore, while coculture experiments indicated cross-feeding interactions, the precise metabolic intermediates exchanged between strains were not identified. Targeted metabolomics and comprehensive analysis of arabinogalactan utilization would be valuable for elucidating the nature of these metabolic exchanges and utilization patterns. Nonetheless, our experiments demonstrated clear ecological relationships and potential for cooperative interactions within the microbial community. Our study was conducted *in vitro* using fecal samples from healthy donors but the effects of arabinogalactan on microbiota from individuals with dysbiosis or gut disease remain unexplored. Another limitation is the limited number of human donors included in this study. A larger number of donors and samples would make the results more reliable and improve our findings across more diverse populations. Future research involving clinical studies or animal models will be important to assess the impact of arabinogalactan supplementation under more physiologically relevant and disease-specific conditions. Finally, the absence of complementary multi-omics approaches, such as shotgun

metagenomics, transcriptomics, or genome sequencing, limits the functional interpretation of our findings. Integrating these techniques in future research will be essential for a more comprehensive understanding of arabinogalactan's impact on the gut microbiome. Despite these limitations, the integrative methods used in this study provide a strong foundation for future investigations.

In conclusion, this study demonstrates that arabinogalactan acts as a functionally selective dietary fiber that consistently enriches beneficial members of the gut microbiota, most notably *B. longum*. Using an integrated *ex vivo* framework combining 16S rRNA gene sequencing with RACS, we identified key taxa actively responding to arabinogalactan supplementation across microbiota from multiple human donors. Among the 98 metabolically active strains isolated, *B. longum* accounted for approximately 46% and was selected for detailed physiological characterization based on its high recovery rate and known role in fiber degradation. *B. longum* emerged as a central degrader, directly utilizing arabinogalactan and facilitating the growth of non-degrading strains through metabolic cross-feeding. While isolates from *Bacteroidota* and *Bacillota* were also recovered, this study focused on *Actinomycetota* due to the dominance of *Bifidobacterium* in the RACS-sorted fraction. The targeted recovery and physiological assessment of isolates from three dominant gut phyla **Actinomycetota**, **Bacteroidota**, and **Bacillota** revealed that most metabolically active strains belonged to **Actinomycetota**, primarily due to the high prevalence of *Bifidobacterium*. These results underscore arabinogalactan's selective influence on gut microbial community composition and highlight the potential of single-cell techniques like RACS to uncover functionally important microbial interactions within complex ecosystems.

Author contributions

H.R., and D.B. planned and designed the study. H.R. conducted all the experiments and performed the data analyses. S.K. performed the RACS experiments and contributed data and bioinformatic analysis. M.P. conducted the Raman microspectroscopy measurements. G.N., contributed to molecular biology experiments. A.H. designed and supported the coculture experiments. S.K., and R.G. carried out sample collection and incubation. J.S. contributed to bioinformatic

processing. J.R. extracted DNA from all samples. P.S. contributed to the growth curve and coculture experiments. H.R. and D.B. wrote the manuscript with input from all co-authors. All authors approved the final version of the manuscript.

Financial support and sponsorship

This study received financial support from the European Research Council (FunKeyGut 741623) and the Austrian Science Fund (10.55776/DOC69; 10.55776/COE7).

Conflicts of interest

The authors declare that they have no conflicts of interest related to this work.

Ethical Approval and Consent to Participate

All experimental procedures involving human fecal samples were conducted in accordance with the approval of the Ethics Committee of the University of Vienna, and all participants provided written informed consent (reference number: 00161).

Consent for publication

Not applicable.

Data Availability

All 16S rRNA gene amplicon sequencing data generated during this study are available in the NCBI Short Read Archive under the accession number PRJNA1244259. The Sequences of RACS-isolated strains following arabinogalactan supplementation have been submitted to GenBank under accession numbers PQ407681 to PQ407778. The Raman spectroscopy dataset has been submitted to the BioStudies database and is accessible through the MicrobioRaman platform under the accession number S-MBRS14.

References

1. Belkaid Y, Hand TW. Role of the microbiota in immunity and inflammation. Cell [Internet]. 2014;157(1):121–41. Available from: http://dx.doi.org/10.1016/j.cell.2014.03.011
2. David LA, Maurice CF, Carmody RN, Gootenberg DB, Button JE, Wolfe BE, Ling A V., Devlin AS, Varma Y, Fischbach MA, Biddinger SB, Dutton RJ, Turnbaugh PJ. Diet rapidly and reproducibly alters the human gut microbiome. Nature [Internet]. 2014;505(7484):559–63. Available from: http://dx.doi.org/10.1038/nature12820
3. Turnbaugh PJ, Hamady M, Yatsunenko T, Cantarel BL, Duncan A, Ley RE, Sogin ML, Jones WJ, Roe BA, Affourtit JP, Egholm M, Henrissat B, Heath AC, Knight R, Gordon JI. A core gut microbiome in obese and lean twins. Nature. 2009;457(7228):480–4.
4. Qin J, Li R, Raes J, Arumugam M, Burgdorf KS, Manichanh C, Nielsen T, Pons N, Levenez F, Yamada T, Mende DR, Li J, Xu J, Li S, Li D, Cao J, Wang B, Liang H, Zheng H, Xie Y, Tap J, Lepage P, Bertalan M, Batto JM, Hansen T, Le Paslier D, Linneberg A, Nielsen HB, Pelletier E, Renault P, Sicheritz-Ponten T, Turner K, Zhu H, Yu C, Li S, Jian M, Zhou Y, Li Y, Zhang X, Li S, Qin N, Yang H, Wang J, Brunak S, Doré J, Guarner F, Kristiansen K, Pedersen O, Parkhill J, Weissenbach J, Bork P, Ehrlich SD, Wang J, Antolin M, Artiguenave F, Blottiere H, Borruel N, Bruls T, Casellas F, Chervaux C, Cultrone A, Delorme C, Denariaz G, Dervyn R, Forte M, Friss C, Van De Guchte M, Guedon E, Haimet F, Jamet A, Juste C, Kaci G, Kleerebezem M, Knol J, Kristensen M, Layec S, Le Roux K, Leclerc M, Maguin E, Melo Minardi R, Oozeer R, Rescigno M, Sanchez N, Tims S, Torrejon T, Varela E, De Vos W, Winogradsky Y, Zoetendal E. A human gut microbial gene catalogue established by metagenomic sequencing. Nature. 2010;464(7285):59–65.
5. Eckburg PB, Bik EM, Bernstein CN, Purdom E, Dethlefsen L, Sargent M, Gill SR, Nelson KE, Relman DA. Microbiology: Diversity of the human intestinal microbial flora. Science (80-). 2005;308(5728):1635–8.
6. Huttenhower C, Gevers D, Knight R, Abubucker S, Badger JH, Chinwalla AT, Creasy HH, Earl AM, Fitzgerald MG, Fulton RS, Giglio MG, Hallsworth-Pepin K, Lobos EA, Madupu R, Magrini V, Martin JC, Mitreva M, Muzny DM, Sodergren EJ, Versalovic J, Wollam AM,

Worley KC, Wortman JR, Young SK, Zeng Q, Aagaard KM, Abolude OO, Allen-Vercoe E, Alm EJ, Alvarado L, Andersen GL, Anderson S, Appelbaum E, Arachchi HM, Armitage G, Arze CA, Ayvaz T, Baker CC, Begg L, Belachew T, Bhonagiri V, Bihan M, Blaser MJ, Bloom T, Bonazzi V, Paul Brooks J, Buck GA, Buhay CJ, Busam DA, Campbell JL, Canon SR, Cantarel BL, Chain PSG, Chen IMA, Chen L, Chhibba S, Chu K, Ciulla DM, Clemente JC, Clifton SW, Conlan S, Crabtree J, Cutting MA, Davidovics NJ, Davis CC, Desantis TZ, Deal C, Delehaunty KD, Dewhirst FE, Deych E, Ding Y, Dooling DJ, Dugan SP, Michael Dunne W, Scott Durkin A, Edgar RC, Erlich RL, Farmer CN, Farrell RM, Faust K, Feldgarden M, Felix VM, Fisher S, Fodor AA, Forney LJ, Foster L, Di Francesco V, Friedman J, Friedrich DC, Fronick CC, Fulton LL, Gao H, Garcia N, Giannoukos G, Giblin C, Giovanni MY, Goldberg JM, Goll J, Gonzalez A, Griggs A, Gujja S, Kinder Haake S, Haas BJ, Hamilton HA, Harris EL, Hepburn TA, Herter B, Hoffmann DE, Holder ME, Howarth C, Huang KH, Huse SM, Izard J, Jansson JK, Jiang H, Jordan C, Joshi V, Katancik JA, Keitel WA, Kelley ST, Kells C, King NB, Knights D, Kong HH, Koren O, Koren S, Kota KC, Kovar CL, Kyrpides NC, La Rosa PS, Lee SL, Lemon KP, Lennon N, Lewis CM, Lewis L, Ley RE, Li K, Liolios K, Liu B, Liu Y, Lo CC, Lozupone CA, Dwayne Lunsford R, Madden T, Mahurkar AA, Mannon PJ, Mardis ER, Markowitz VM, Mavromatis K, McCorrison JM, McDonald D, McEwen J, McGuire AL, McInnes P, Mehta T, Mihindukulasuriya KA, Miller JR, Minx PJ, Newsham I, Nusbaum C, Oglaughlin M, Orvis J, Pagani I, Palaniappan K, Patel SM, Pearson M, Peterson J, Podar M, Pohl C, Pollard KS, Pop M, Priest ME, Proctor LM, Qin X, Raes J, Ravel J, Reid JG, Rho M, Rhodes R, Riehle KP, Rivera MC, Rodriguez-Mueller B, Rogers YH, Ross MC, Russ C, Sanka RK, Sankar P, Fah Sathirapongsasuti J, Schloss JA, Schloss PD, Schmidt TM, Scholz M, Schriml L, Schubert AM, Segata N, Segre JA, Shannon WD, Sharp RR, Sharpton TJ, Shenoy N, Sheth NU, Simone GA, Singh I, Smillie CS, Sobel JD, Sommer DD, Spicer P, Sutton GG, Sykes SM, Tabbaa DG, Thiagarajan M, Tomlinson CM, Torralba M, Treangen TJ, Truty RM, Vishnivetskaya TA, Walker J, Wang L, Wang Z, Ward D V., Warren W, Watson MA, Wellington C, Wetterstrand KA, White JR, Wilczek-Boney K, Wu Y, Wylie KM, Wylie T, Yandava C, Ye L, Ye Y, Yooseph S, Youmans BP, Zhang L, Zhou Y, Zhu Y, Zoloth L, Zucker JD,

Birren BW, Gibbs RA, Highlander SK, Methé BA, Nelson KE, Petrosino JF, Weinstock GM, Wilson RK, White O. Structure, function and diversity of the healthy human microbiome. Nature [Internet]. 2012;486(7402):207–14. Available from: http://dx.doi.org/10.1038/nature11234

7. Slavin J. Fiber and Prebiotics: Mechanisms and Health Benefits. Nutrients [Internet]. 2013 Apr 22;5(4):1417–35. Available from: https://www.mdpi.com/2072-6643/5/4/1417
8. Gibson GR, Hutkins R, Sanders ME, Prescott SL, Reimer RA, Salminen SJ, Scott K, Stanton C, Swanson KS, Cani PD, Verbeke K, Reid G. Expert consensus document: The International Scientific Association for Probiotics and Prebiotics (ISAPP) consensus statement on the definition and scope of prebiotics. Nat Rev Gastroenterol Hepatol [Internet]. 2017;14(8):491–502. Available from: http://dx.doi.org/10.1038/nrgastro.2017.75
9. Davani-Davari D, Negahdaripour M, Karimzadeh I, Seifan M, Mohkam M, Masoumi SJ, Berenjian A, Ghasemi Y. Prebiotics: Definition, types, sources, mechanisms, and clinical applications. Foods. 2019;8(3):1–27.
10. Holscher HD. Dietary fiber and prebiotics and the gastrointestinal microbiota. Gut Microbes. 2017;8(2):172–84.
11. Dion C, Chappuis E, Ripoll C. Does larch arabinogalactan enhance immune function? A review of mechanistic and clinical trials. Nutr Metab [Internet]. 2016;13(1). Available from: http://dx.doi.org/10.1186/s12986-016-0086-x
12. Uauy R. Foreword. Br J Nutr [Internet]. 2009 Jul 1;101(S2):S1–S1. Available from: https://www.cambridge.org/core/product/identifier/S0007114509990511/type/journal_article
13. Gibson GR, Roberfroid MB. Dietary Modulation of the Human Colonic Microbiota: Introducing the Concept of Prebiotics. J Nutr [Internet]. 1995 Jun;125(6):1401–12. Available from: https://linkinghub.elsevier.com/retrieve/pii/S0022316623035514
14. Wang Y, LaPointe G. Arabinogalactan Utilization by Bifidobacterium longum subsp. longum NCC 2705 and Bacteroides caccae ATCC 43185 in Monoculture and Coculture.

Microorganisms [Internet]. 2020 Oct 31;8(11):1703. Available from: https://www.mdpi.com/2076-2607/8/11/1703

15. Kim K, Kim CY. Rheological properties of arabinogalactan solutions related to the carbohydrate composition of different legumes. Korean J Food Preserv [Internet]. 2023 Oct;30(5):785–96. Available from: http://www.ekosfop.or.kr/archive/view_article?doi=10.11002/kjfp.2023.30.5.785
16. Rakhmanberdyeva RK, Zhauynbayeva KS, Senchenkova SN, Shashkov AS, Bobakulov KM. Structure of arabinogalactan and pectin from the Silybum marianum. Carbohydr Res [Internet]. 2019;485(May):107797. Available from: https://doi.org/10.1016/j.carres.2019.107797
17. Wang M, Wichienchot S, He X, Fu X, Huang Q, Zhang B. In vitro colonic fermentation of dietary fibers: Fermentation rate, short-chain fatty acid production and changes in microbiota. Trends Food Sci Technol [Internet]. 2019;88(November 2018):1–9. Available from: https://doi.org/10.1016/j.tifs.2019.03.005
18. Sun Y, Hu J, Zhang S, He H, Nie Q, Zhang Y, Chen C, Geng F, Nie S. Prebiotic characteristics of arabinogalactans during in vitro fermentation through multi-omics analysis. Food Chem Toxicol [Internet]. 2021;156(August):112522. Available from: https://doi.org/10.1016/j.fct.2021.112522
19. Victoria Obayomi O, Folakemi Olaniran A, Olugbemiga Owa S. Unveiling the role of functional foods with emphasis on prebiotics and probiotics in human health: A review. J Funct Foods [Internet]. 2024;119(March):106337. Available from: https://doi.org/10.1016/j.jff.2024.106337
20. Wang Y, Liu Y, Ivusic Polic I, Chandran Matheyambath A, LaPointe G. Modulation of human gut microbiota composition and metabolites by arabinogalactan and Bifidobacterium longum subsp. longum BB536 in the Simulator of the Human Intestinal Microbial Ecosystem (SHIME®). J Funct Foods [Internet]. 2021 Dec;87:104820. Available from: https://linkinghub.elsevier.com/retrieve/pii/S1756464621004692
21. Sasaki Y, Horigome A, Odamaki T, Xiao J zhong, Ishiwata A, Ito Y, Kitahara K, Fujita K. Novel

3- O -α- d -Galactosyl-α- l -Arabinofuranosidase for the Assimilation of Gum Arabic Arabinogalactan Protein in Bifidobacterium longum subsp. longum. Atomi H, editor. Appl Environ Microbiol [Internet]. 2021 Apr 27;87(10):1–20. Available from: https://journals.asm.org/doi/10.1128/AEM.02690-20

22. Onumpai C, Kolida S, Bonnin E, Rastall RA. Microbial Utilization and Selectivity of Pectin Fractions with Various Structures. Appl Environ Microbiol [Internet]. 2011 Aug 15;77(16):5747–54. Available from: https://journals.asm.org/doi/10.1128/AEM.00179-11

23. Lindstad LJ, Lo G, Leivers S, Lu Z, Michalak L, Pereira G V., Røhr ÅK, Martens EC, McKee LS, Louis P, Duncan SH, Westereng B, Pope PB, La Rosa SL. Human gut faecalibacterium prausnitzii deploys a highly efficient conserved system to cross-feed on b-mannanderived oligosaccharides. MBio. 2021;12(3).

24. Culp EJ, Goodman AL. Cross-feeding in the gut microbiome: Ecology and mechanisms. Cell Host Microbe [Internet]. 2023 Apr 12;31(4):485–99. Available from: https://doi.org/10.1016/j.chom.2023.03.016

25. Cartmell A, Muñoz-Muñoz J, Briggs JA, Ndeh DA, Lowe EC, Baslé A, Terrapon N, Stott K, Heunis T, Gray J, Yu L, Dupree P, Fernandes PZ, Shah S, Williams SJ, Labourel A, Trost M, Henrissat B, Gilbert HJ. A surface endogalactanase in Bacteroides thetaiotaomicron confers keystone status for arabinogalactan degradation. Nat Microbiol [Internet]. 2018 Oct 22;3(11):1314–26. Available from: https://www.nature.com/articles/s41564-018-0258-8

26. Culp EJ, Goodman AL. Cross-feeding in the gut microbiome: Ecology and mechanisms. Cell Host Microbe. 2023;31(4):485–99.

27. Wang S, Mu L, Yu C, He Y, Hu X, Jiao Y, Xu Z, You S, Liu SL, Bao H. Microbial collaborations and conflicts: unraveling interactions in the gut ecosystem. Gut Microbes [Internet]. 2024;16(1):1–18. Available from: https://doi.org/10.1080/19490976.2023.2296603

28. Lombard V, Golaconda Ramulu H, Drula E, Coutinho PM, Henrissat B. The carbohydrate-active enzymes database (CAZy) in 2013. Nucleic Acids Res [Internet]. 2014 Jan;42(D1):D490–5. Available from: https://academic.oup.com/nar/article-

lookup/doi/10.1093/nar/gkt1178

29. Shi E, Nie M, Wang X, Jing H, Feng L, Xu Y, Zhang Z, Zhang G, Li D, Dai Z. Polysaccharides affect the utilization of β-carotene through gut microbiota investigated by in vitro and in vivo experiments. Food Res Int [Internet]. 2023 Dec;174:113592. Available from: https://linkinghub.elsevier.com/retrieve/pii/S0963996923011407

30. Holmes ZC, Villa MM, Durand HK, Jiang S, Dallow EP, Petrone BL, Silverman JD, Lin PH, David LA. Microbiota responses to different prebiotics are conserved within individuals and associated with habitual fiber intake. Microbiome [Internet]. 2022;10(1):1–16. Available from: https://doi.org/10.1186/s40168-022-01307-x

31. Falony G, Joossens M, Vieira-Silva S, Wang J, Darzi Y, Faust K, Kurilshikov A, Bonder MJ, Valles-Colomer M, Vandeputte D, Tito RY, Chaffron S, Rymenans L, Verspecht C, De Sutter L, Lima-Mendez G, D'hoe K, Jonckheere K, Homola D, Garcia R, Tigchelaar EF, Eeckhaudt L, Fu J, Henckaerts L, Zhernakova A, Wijmenga C, Raes J. Population-level analysis of gut microbiome variation. Science (80-) [Internet]. 2016 Apr 29;352(6285):560–4. Available from: https://www.science.org/doi/10.1126/science.aad3503

32. Wang Q, Spenkelink B, Boonpawa R, Rietjens IMCM, Beekmann K. Use of Physiologically Based Kinetic Modeling to Predict Rat Gut Microbial Metabolism of the Isoflavone Daidzein to S -Equol and Its Consequences for ERα Activation. Mol Nutr Food Res [Internet]. 2020 Mar 25;64(6):1–13. Available from: https://onlinelibrary.wiley.com/doi/10.1002/mnfr.201900912

33. Bénard M V., Arretxe I, Wortelboer K, Harmsen HJM, Davids M, de Bruijn CMA, Benninga MA, Hugenholtz F, Herrema H, Ponsioen CY. Anaerobic Feces Processing for Fecal Microbiota Transplantation Improves Viability of Obligate Anaerobes. Microorganisms [Internet]. 2023 Sep 5;11(9):2238. Available from: https://www.mdpi.com/2076-2607/11/9/2238

34. Salonen A, Nikkilä J, Jalanka-Tuovinen J, Immonen O, Rajilić-Stojanović M, Kekkonen RA, Palva A, de Vos WM. Comparative analysis of fecal DNA extraction methods with phylogenetic microarray: Effective recovery of bacterial and archaeal DNA using

mechanical cell lysis. J Microbiol Methods [Internet]. 2010 May;81(2):127–34. Available from: https://linkinghub.elsevier.com/retrieve/pii/S0167701210000667

35. Pjevac P, Hausmann B, Schwarz J, Kohl G, Herbold CW, Loy A, Berry D. An Economical and Flexible Dual Barcoding, Two-Step PCR Approach for Highly Multiplexed Amplicon Sequencing. Front Microbiol [Internet]. 2021 May 20;12(May). Available from: https://www.frontiersin.org/articles/10.3389/fmicb.2021.669776/full

36. Berry D, Mader E, Lee TK, Woebken D, Wang Y, Zhu D, Palatinszky M, Schintlmeister A, Schmid MC, Hanson BT, Shterzer N, Mizrahi I, Rauch I, Decker T, Bocklitz T, Popp J, Gibson CM, Fowler PW, Huang WE, Wagner M. Tracking heavy water (D 2 O) incorporation for identifying and sorting active microbial cells. Proc Natl Acad Sci [Internet]. 2015 Jan 13;112(2):E194–203. Available from: https://pnas.org/doi/full/10.1073/pnas.1420406112

37. Eichorst SA, Strasser F, Woyke T, Schintlmeister A, Wagner M, Woebken D. Advancements in the application of NanoSIMS and Raman microspectroscopy to investigate the activity of microbial cells in soils. Häggblom M, editor. FEMS Microbiol Ecol [Internet]. 2015 Oct;91(10):fiv106. Available from: https://academic.oup.com/femsec/article-lookup/doi/10.1093/femsec/fiv106

38. Cui D, Kong L, Wang Y, Zhu Y, Zhang C. In situ identification of environmental microorganisms with Raman spectroscopy. Environ Sci Ecotechnology [Internet]. 2022;11:100187. Available from: https://doi.org/10.1016/j.ese.2022.100187

39. Riva A, Rasoulimehrabani H, Cruz-Rubio JM, Schnorr SL, von Baeckmann C, Inan D, Nikolov G, Herbold CW, Hausmann B, Pjevac P, Schintlmeister A, Spittler A, Palatinszky M, Kadunic A, Hieger N, Del Favero G, von Bergen M, Jehmlich N, Watzka M, Lee KS, Wiesenbauer J, Khadem S, Viernstein H, Stocker R, Wagner M, Kaiser C, Richter A, Kleitz F, Berry D. Identification of inulin-responsive bacteria in the gut microbiota via multi-modal activity-based sorting. Nat Commun [Internet]. 2023 Dec 14;14(1):8210. Available from: https://www.nature.com/articles/s41467-023-43448-z

40. Henry DG, Jarvis I, Gillmore G, Stephenson M, Emmings JF. Assessing low-maturity

organic matter in shales using Raman spectroscopy: Effects of sample preparation and operating procedure. Int J Coal Geol [Internet]. 2018;191(February):135–51. Available from: https://doi.org/10.1016/j.coal.2018.03.005

41. Caro TA, Kashyap S, Brown G, Chen C, Kopf SH, Templeton AS. Single-cell measurement of microbial growth rate with Raman microspectroscopy. FEMS Microbiol Ecol [Internet]. 2024 Aug 13;100(9). Available from: https://academic.oup.com/femsec/article/doi/10.1093/femsec/fiae110/7729285
42. Stöckel S, Kirchhoff J, Neugebauer U, Rösch P, Popp J. The application of Raman spectroscopy for the detection and identification of microorganisms. J Raman Spectrosc [Internet]. 2016 Jan 7;47(1):89–109. Available from: https://analyticalsciencejournals.onlinelibrary.wiley.com/doi/10.1002/jrs.4844
43. Lee KS, Pereira FC, Palatinszky M, Behrendt L, Alcolombri U, Berry D, Wagner M, Stocker R. Optofluidic Raman-activated cell sorting for targeted genome retrieval or cultivation of microbial cells with specific functions. Nat Protoc [Internet]. 2021;16(2):634–76. Available from: http://dx.doi.org/10.1038/s41596-020-00427-8
44. Lee KS, Palatinszky M, Pereira FC, Nguyen J, Fernandez VI, Mueller AJ, Menolascina F, Daims H, Berry D, Wagner M, Stocker R. An automated Raman-based platform for the sorting of live cells by functional properties. Nat Microbiol [Internet]. 2019;4(6):1035–48. Available from: http://dx.doi.org/10.1038/s41564-019-0394-9
45. Wright ES, Yilmaz LS, Noguera DR. DECIPHER, a Search-Based Approach to Chimera Identification for 16S rRNA Sequences. Appl Environ Microbiol [Internet]. 2012 Feb;78(3):717–25. Available from: https://journals.asm.org/doi/10.1128/AEM.06516-11
46. Untergasser A, Nijveen H, Rao X, Bisseling T, Geurts R, Leunissen JAM. Primer3Plus, an enhanced web interface to Primer3. Nucleic Acids Res [Internet]. 2007 May 8;35(Web Server):W71–4. Available from: https://academic.oup.com/nar/article-lookup/doi/10.1093/nar/gkm306
47. R Studio Team. A language and environment for statistical computing [Internet]. Vol. 3, R Foundation for Statistical Computing. 2021. https://www.R-project.org. Available from:

http://www.r-project.org

48. Valero-Mora PM. ggplot2: Elegant Graphics for Data Analysis [Internet]. Journal of Statistical Software. Springer International Publishing; 2010. (Use R!; vol. 35). Available from: https://books.google.at/books?id=RTMFswEACAAJ
49. Oksanen J, Simpson GL. Package ‘ vegan .’ 2022;(March).
50. Benjamini Y, Hochberg Y. Controlling the False Discovery Rate: A Practical and Powerful Approach to Multiple Testing. J R Stat Soc Ser B Stat Methodol [Internet]. 1995 Jan 1;57(1):289–300. Available from: https://doi.org/10.1111/j.2517-6161.1995.tb02031.x
51. Love MI, Huber W, Anders S. Moderated estimation of fold change and dispersion for RNA-seq data with DESeq2. Genome Biol [Internet]. 2014 Dec 5;15(12):550. Available from: https://genomebiology.biomedcentral.com/articles/10.1186/s13059-014-0550-8
52. Letunic I, Bork P. Interactive Tree of Life (iTOL) v6: recent updates to the phylogenetic tree display and annotation tool. Nucleic Acids Res [Internet]. 2024 Jul 5;52(W1):W78–82. Available from: https://academic.oup.com/nar/article/52/W1/W78/7645242
53. Kau AL, Ahern PP, Griffin NW, Goodman AL, Gordon JI. Human nutrition, the gut microbiome and the immune system. Nature [Internet]. 2011 Jun 16;474(7351):327–36. Available from: https://www.nature.com/articles/nature10213
54. Valdes AM, Walter J, Segal E, Spector TD. Role of the gut microbiota in nutrition and health. BMJ [Internet]. 2018 Jun 13;361:k2179. Available from: https://www.bmj.com/lookup/doi/10.1136/bmj.k2179
55. O’Callaghan A, van Sinderen D. Bifidobacteria and Their Role as Members of the Human Gut Microbiota. Front Microbiol [Internet]. 2016 Jun 15;7(JUN). Available from: http://journal.frontiersin.org/Article/10.3389/fmicb.2016.00925/abstract
56. Rinninella E, Raoul P, Cintoni M, Franceschi F, Miggiano GAD, Gasbarrini A, Mele MC. What is the Healthy Gut Microbiota Composition? A Changing Ecosystem across Age, Environment, Diet, and Diseases. Microorganisms [Internet]. 2019 Jan 10;7(1):14. Available from: https://www.mdpi.com/2076-2607/7/1/14
57. Hill C, Guarner F, Reid G, Gibson GR, Merenstein DJ, Pot B, Morelli L, Canani RB, Flint HJ,

Salminen S, Calder PC, Sanders ME. The International Scientific Association for Probiotics and Prebiotics consensus statement on the scope and appropriate use of the term probiotic. Nat Rev Gastroenterol Hepatol [Internet]. 2014 Aug 10;11(8):506–14. Available from: https://www.nature.com/articles/nrgastro.2014.66

58. Hughes RL, Alvarado DA, Swanson KS, Holscher HD. The Prebiotic Potential of Inulin-Type Fructans: A Systematic Review. Adv Nutr [Internet]. 2022 Mar;13(2):492–529. Available from: https://linkinghub.elsevier.com/retrieve/pii/S2161831322000746

59. Scott KP, Gratz SW, Sheridan PO, Flint HJ, Duncan SH. The influence of diet on the gut microbiota. Pharmacol Res [Internet]. 2013;69(1):52–60. Available from: http://dx.doi.org/10.1016/j.phrs.2012.10.020

60. Bindels LB, Delzenne NM, Cani PD, Walter J. Towards a more comprehensive concept for prebiotics. Nat Rev Gastroenterol Hepatol [Internet]. 2015 May 31;12(5):303–10. Available from: https://www.nature.com/articles/nrgastro.2015.47

61. Xiao M, Zhang C, Duan H, Narbad A, Zhao J, Chen W, Zhai Q, Yu L, Tian F. Cross-feeding of bifidobacteria promotes intestinal homeostasis: a lifelong perspective on the host health. npj Biofilms Microbiomes [Internet]. 2024 Jun 19;10(1):47. Available from: https://www.nature.com/articles/s41522-024-00524-6

62. González R, Klaassens ES, Malinen E, de Vos WM, Vaughan EE. Differential Transcriptional Response of Bifidobacterium longum to Human Milk, Formula Milk, and Galactooligosaccharide. Appl Environ Microbiol [Internet]. 2008 Aug;74(15):4686–94. Available from: https://journals.asm.org/doi/10.1128/AEM.00122-08

63. Liu M, Liu Z, Zhang N, Cao Z, Fu J, Yuan W, Wu H, Shang H. Preparation of polysaccharides from Crepis tectorum Linn. and the regulation effects on intestinal microbiota. Process Biochem [Internet]. 2023;130(2888):50–66. Available from: https://doi.org/10.1016/j.procbio.2023.04.004

64. Gao X, Xu FS, Li T, Huang P, Yu L, Tian F, Zhao J, Chen W, Zhai Q. CAZymes-associated method to explore glycans that mitigate DSS-induced colitis via targeting Bacteroides cellulosilyticus. Int J Biol Macromol [Internet]. 2024;258(P1):128694. Available from:

https://doi.org/10.1016/j.ijbiomac.2023.128694

65. Peterson CT, Sharma V, Iablokov SN, Albayrak L, Khanipov K, Uchitel S, Chopra D, Mills PJ, Fofanov Y, Rodionov DA, Peterson SN. 16S rRNA gene profiling and genome reconstruction reveal community metabolic interactions and prebiotic potential of medicinal herbs used in neurodegenerative disease and as nootropics. Loor JJ, editor. PLoS One [Internet]. 2019 Mar 19;14(3):e0213869. Available from: https://dx.plos.org/10.1371/journal.pone.0213869

66. Aguirre M, Bussolo de Souza C, Venema K. The Gut Microbiota from Lean and Obese Subjects Contribute Differently to the Fermentation of Arabinogalactan and Inulin. Loh G, editor. PLoS One [Internet]. 2016 Jul 13;11(7):e0159236. Available from: https://dx.plos.org/10.1371/journal.pone.0159236

67. He X, Zhao S, Li Y. Faecalibacterium prausnitzii: A Next-Generation Probiotic in Gut Disease Improvement. Chen T, editor. Can J Infect Dis Med Microbiol [Internet]. 2021 Mar 5;2021:1–10. Available from: https://www.hindawi.com/journals/cjidmm/2021/6666114/

68. Fujita K, Sasaki Y, Kitahara K. Degradation of plant arabinogalactan proteins by intestinal bacteria: characteristics and functions of the enzymes involved. Appl Microbiol Biotechnol [Internet]. 2019 Sep 5;103(18):7451–7. Available from: http://link.springer.com/10.1007/s00253-019-10049-0

69. Hirmas B, Gasaly N, Orellana G, Vega-Sagardía M, Saa P, Gotteland M, Garrido D. Metabolic Modeling and Bidirectional Culturing of Two Gut Microbes Reveal Cross-Feeding Interactions and Protective Effects on Intestinal Cells. Baranzini S, editor. mSystems [Internet]. 2022 Oct 26;7(5):1–20. Available from: https://journals.asm.org/doi/10.1128/msystems.00646-22

70. Steinert RE, Rehman A, Sadabad MS, Milanese A, Wittwer-Schegg J, Burton JP, Spooren A. Microbial micronutrient sharing, gut redox balance and keystone taxa as a basis for a new perspective to solutions targeting health from the gut. Gut Microbes [Internet]. 2025;17(1). Available from: https://doi.org/10.1080/19490976.2025.2477816

71. Ku S, Haque MA, Jang MJ, Ahn J, Choe D, Jeon JI, Park MS. The role of Bifidobacterium in longevity and the future of probiotics. Food Sci Biotechnol [Internet]. 2024;33(9):2097–110. Available from: https://doi.org/10.1007/s10068-024-01631-y
72. Wong CB, Odamaki T, Xiao J zhong. Beneficial effects of Bifidobacterium longum subsp. longum BB536 on human health: Modulation of gut microbiome as the principal action. J Funct Foods [Internet]. 2019;54(January):506–19. Available from: https://doi.org/10.1016/j.jff.2019.02.002
73. GOSSLING J, MOORE WEC. Gemmiger formicilis, n.gen., n.sp., an Anaerobic Budding Bacterium from Intestines. Int J Syst Bacteriol [Internet]. 1975 Apr 1;25(2):202–7. Available from: https://www.microbiologyresearch.org/content/journal/ijsem/10.1099/00207713-25-2-202
74. Salanitro JP, Muirhead PA, Goodman JR. Morphological and physiological characteristics of Gemmiger formicilis isolated from chicken ceca. Appl Environ Microbiol [Internet]. 1976 Oct;32(4):623–32. Available from: https://journals.asm.org/doi/10.1128/aem.32.4.623-632.1976
75. Zenner C, Hitch TCA, Riedel T, Wortmann E, Tiede S, Buhl EM, Abt B, Neuhaus K, Velge P, Overmann J, Kaspers B, Clavel T. Early-Life Immune System Maturation in Chickens Using a Synthetic Community of Cultured Gut Bacteria. Metcalf JL, editor. mSystems [Internet]. 2021 Jun 29;6(3):e01300-20. Available from: https://journals.asm.org/doi/10.1128/mSystems.01300-20
76. Fitzgerald CB, Shkoporov AN, Sutton TDS, Chaplin A V., Velayudhan V, Ross RP, Hill C. Comparative analysis of Faecalibacterium prausnitzii genomes shows a high level of genome plasticity and warrants separation into new species-level taxa. BMC Genomics [Internet]. 2018 Dec 14;19(1):931. Available from: https://bmcgenomics.biomedcentral.com/articles/10.1186/s12864-018-5313-6
77. Guo W, Sun L, Yue H, Guo X, Chen L, Zhang J, Chen Z, Wang Y, Wang J, Lei W. Associations of Intermittent Hypoxia Burden with Gut Microbiota Dysbiosis in Adult Patients with

Obstructive Sleep Apnea. Nat Sci Sleep [Internet]. 2024 Sep;Volume 16(September):1483–95. Available from: https://www.dovepress.com/associations-of-intermittent-hypoxia-burden-with-gut-microbiota-dysbio-peer-reviewed-fulltext-article-NSS

78. Qian L, Huang J, Qin H. Probiotics and dietary intervention modulate the colonic mucosa-associated microbiota in high-fat diet populations. Turkish J Gastroenterol [Internet]. 2020 May 12;31(4):295–304. Available from: https://turkjgastroenterol.org/en/probiotics-and-dietary-intervention-modulate-the-colonic-mucosa-associated-microbiota-in-high-fat-diet-populations-136660

79. Arnold JW, Roach J, Fabela S, Moorfield E, Ding S, Blue E, Dagher S, Magness S, Tamayo R, Bruno-Barcena JM, Azcarate-Peril MA. The pleiotropic effects of prebiotic galacto-oligosaccharides on the aging gut. Microbiome [Internet]. 2021 Dec 28;9(1):31. Available from: https://microbiomejournal.biomedcentral.com/articles/10.1186/s40168-020-00980-0

80. Alberto F, Bignon C, Sulzenbacher G, Henrissat B, Czjzek M. The Three-dimensional Structure of Invertase (β-Fructosidase) from Thermotoga maritima Reveals a Bimodular Arrangement and an Evolutionary Relationship between Retaining and Inverting Glycosidases. J Biol Chem [Internet]. 2004 Apr;279(18):18903–10. Available from: https://linkinghub.elsevier.com/retrieve/pii/S0021925819754507

81. Andersen JM, Barrangou R, Hachem MA, Lahtinen SJ, Goh YJ, Svensson B, Klaenhammer TR. Transcriptional analysis of oligosaccharide utilization by Bifidobacterium lactisBl-04. BMC Genomics [Internet]. 2013 Dec 10;14(1):312. Available from: https://bmcgenomics.biomedcentral.com/articles/10.1186/1471-2164-14-312

82. Fujita K, Tsunomachi H, Lixia P, Maruyama S, Miyake M, Dakeshita A, Kitahara K, Tanaka K, Ito Y, Ishiwata A, Fushinobu S. Bifidobacterial GH146 β-l-arabinofuranosidase for the removal of β1,3-l-arabinofuranosides on plant glycans. Appl Microbiol Biotechnol [Internet]. 2024 Dec 7;108(1):199. Available from: https://link.springer.com/10.1007/s00253-024-13014-8

83. Fujita K, Sakamoto A, Kaneko S, Kotake T, Tsumuraya Y, Kitahara K. Degradative enzymes for type II arabinogalactan side chains in Bifidobacterium longum subsp. longum. Appl Microbiol Biotechnol [Internet]. 2019 Feb 18;103(3):1299–310. Available from: http://link.springer.com/10.1007/s00253-018-9566-4

84. Fujita K, Takashi Y, Obuchi E, Kitahara K, Suganuma T. Characterization of a novel β-l-arabinofuranosidase in bifidobacterium longum: Functional elucidation of a duf1680 protein family member. J Biol Chem [Internet]. 2014;289(8):5240–9. Available from: http://dx.doi.org/10.1074/jbc.M113.528711

85. Xu J, Xu R, Jia M, Su Y, Zhu W. Metatranscriptomic analysis of colonic microbiota's functional response to different dietary fibers in growing pigs. Anim Microbiome [Internet]. 2021 Dec 3;3(1):45. Available from: https://animalmicrobiome.biomedcentral.com/articles/10.1186/s42523-021-00108-1

86. Li W, Lin X, Liang H, Wu Z, Wang M, Sun J, Li X, He W, Gao X, Hu T, Xiao L, Zou Y. Genomic and functional diversity of the human-derived isolates of Faecalibacterium. Front Microbiol [Internet]. 2024 May 30;15(May). Available from: https://www.frontiersin.org/articles/10.3389/fmicb.2024.1379500/full

87. Barlow JT, Bogatyrev SR, Ismagilov RF. A quantitative sequencing framework for absolute abundance measurements of mucosal and lumenal microbial communities. Nat Commun [Internet]. 2020;11(1):1–13. Available from: http://dx.doi.org/10.1038/s41467-020-16224-6

Discussion

The modulation of the human gut microbiota by dietary fibers and prebiotics has been widely studied over the past decades. Established prebiotics such as inulin, fructooligosaccharides (FOS) and galactooligosaccharides (GOS) have consistently been shown to support the growth of beneficial genera, particularly *Bifidobacterium* and *Lactobacillus*, in several studies including in vitro experiments, animal models and human clinical trials (Christensen et al., 2022; Parhi et al., 2024). For example, human studies Involving supplementation with inulin or FOS have shown increased abundance of *Bifidobacterium* and *Faecalibacterium prausnitzii*, along with higher production of short-chain fatty acids (SCFAs) such as butyrate and acetate, which are associated with improved gut barrier integrity, immune modulation and overall metabolic health (Sheng et al., 2023; Tandon et al., 2019). These compositional and functional changes have been correlated with various health benefits, including reduced inflammation, better digestive health, and protection against pathogens (O'Riordan et al., 2022; L. Y. Wang et al., 2024).

Despite these advances, it has become clear that different prebiotics show varying degrees of selectivity, and their effects on the gut microbiota depend on several factors. These include the chemical structure of the prebiotic, the baseline composition of the host microbiota, and the specific mode of administration (Cunningham et al., 2021). While early research focused on plant-derived dietary fibers, recent studies, including those in this thesis, have expanded to encompass a broader spectrum of prebiotics, such as the synthetic compound lactulose. The main aim of this work was to determine whether the prebiotics investigated could stimulate a wider range of beneficial gut bacteria than previously reported. By directly comparing the effects of these prebiotics, this research provides new insights into how targeted dietary interventions can modulate gut microbiota composition and support overall health.

In Chapter 1 of my thesis, I investigated the effects of Xylooligosaccharide (XOS) supplementation on the human gut microbiota. XOS is considered a promising prebiotic because of its ability to selectively stimulate beneficial gut microbes. In vitro studies have shown that supplementation

increases the abundance of *Bifidobacterium*, enhances short-chain fatty acid production, and supports gut health (Kaur et al., 2021). While previous studies have examined the impact of XOS supplementation on gut microbiota composition, the present work aimed to show which bacteria were metabolically active in XOS utilization by applying single-cell level analyses.

To address this gap, I employed a multi-modal approach including 16S rRNA gene sequencing, BONCAT-FACS, Raman-activated cell sorting (RACS), high-performance anion-exchange chromatography (HPAEC), and targeted cultivation. These methods allowed me to directly identify and characterize metabolically active XOS responders at both the community and strain level. I also evaluated the growth of isolated strains in pure culture with XOS as the sole carbon source. This strategy allowed the direct linking of metabolic activity to specific taxa, clarifying which bacteria within the gut microbiota were actively responding to XOS.

Consistent with previous reports, this study observed a strong bifidogenic effect of XOS, with *Bifidobacterium* consistently identified as the dominant translationally active genus across all tested donors. This was further supported by the successful isolation of 45 *Bifidobacterium* strains using heavy water combined with RACS (Riva et al., 2023). Notably, this study identified *Collinsella aerofaciens* as a consistent XOS responder, showing both metabolic activation and successful isolation from donor samples. While earlier reports suggested that *Collinsella* can utilize XOS, this work provides the first direct functional evidence that *C. aerofaciens* is metabolically active in response to XOS supplementation across multiple human donors. We isolated *Collinsella* strains through RACS that were actively utilizing XOS, confirming their role as primary degraders alongside *Bifidobacterium*.

High-performance anion-exchange chromatography (HPAEC) showed that both *Bifidobacterium* and *Collinsella* strains isolated using RACS significantly degraded the main short-chain XOS components, xylobiose and xylotriose. This degradation was also observed at the community level, where stool samples collected at 0 and 6 hours after supplementation showed marked reductions in xylobiose and xylotriose concentrations, and at the single-strain level, where all tested *Bifidobacterium* and *Collinsella* isolates displayed the same activity after 24 hours

incubation (Riva et al., 2023). Together, these results provide clear evidence linking substrate utilization with specific taxonomic responders, offering insight into how prebiotics reshape microbial communities under ex vivo conditions. The combination of heavy water labeling and RACS provided direct evidence that XOS supplementation increases translational activity, indicating active microbial growth and metabolism rather than concluding functionality from changes in relative abundance, as often done in previous prebiotic studies. In summary, this study shows that single-cell activity-based techniques, such as BONCAT-FACS and RACS, are effective in identifying the specific microbes in the human gut that respond to changes in diet. Additionally, these methods offer a robust approach for investigating how these microbes utilize different nutrients and interact within the gut ecosystem.

In Chapter 2, I focused on lactulose, a synthetic disaccharide composed of galactose and fructose, which has long been used in clinical medicine as a laxative and in the management of hepatic encephalopathy (Chu et al., 2022). Its primary clinical effect is to increase osmotic pressure in the colon, resulting in water retention and softer stool (Gunn et al., 2024). Lactulose fermentation by gut microbes produces short-chain fatty acids, which lower colonic pH and create conditions that limit bacterial ammonia production. This acidification can also shift ammonia flux from the blood into the gut lumen, where it is excreted. Additional mechanisms for ammonia reduction include microbial utilization of ammonia during amino acid synthesis and the trapping of ammonium in the colon, contributing to lower systemic ammonia levels in patients with liver disease (Bloom & Tapper, 2023). In recent years, lactulose has gained attention as a potential prebiotic because it resists digestion in the upper gastrointestinal tract, reaching the colon where it serves as a fermentable substrate for beneficial gut microbes (Karakan et al., 2021). Many studies have found that low-dose lactulose supplementation increases the abundance of *Bifidobacterium* and *Lactobacillus*, genera that are associated with immune modulation, short-chain fatty acid production, lowered colonic pH, and inhibition of potential pathogens (Chu et al., 2022). Most previous studies relied on in vivo interventions and community profiling techniques such as 16S rRNA gene sequencing, which reveal broad changes in microbial composition or relative

abundance. However, these approaches cannot identify which strains are metabolically active or elucidate the microbial interactions, such as cross-feeding, that drive these effects.

To address these limitations, my study employed ex vivo incubations of fresh human fecal samples and high-resolution single-cell approaches to precisely characterize the gut microbiota's response to lactulose. In addition to BONCAT-FACS (which labels translationally active cells) and Raman-activated cell sorting (RACS, which sorts cells based on single-cell metabolic activity), I used high-performance anion-exchange chromatography (HPAEC) to quantify lactulose degradation both by the whole microbial community and by isolated strains in pure culture. Using a plate reader, I screened the growth of each isolated strain in lactulose as the sole carbon source, providing a functional assessment of their utilization capacity. Furthermore, cross-feeding experiments were conducted to investigate cooperative interactions between primary lactulose degraders and secondary strains that could not grow on lactulose alone, revealing the ecological relationships underlying substrate utilization.

BONCAT-FACS allowed me to detect which cells were actively synthesizing proteins after lactulose supplementation, while RACS enabled the isolation and characterization of these metabolically active strains, providing functional validation of their ecological roles. These integrated approaches revealed that lactulose selectively stimulates *Bifidobacterium*, as seen in previous studies, and directly promotes *Collinsella*, a genus with emerging health relevance (Wolf et al., 2019). Importantly, my research showed that *Lactococcus lactis*, which is a species typically associated with dairy fermentation becomes metabolically active in response to lactulose via cross-feeding from primary degraders like *Bifidobacterium adolescentis* and *Collinsella aerofaciens* (Rasoulimehrabani, Riva, et al., 2025). HPAEC analysis quantified how much lactulose could be utilized by both isolated strains and the total microcosm community, while plate reader growth curves confirmed the ability of specific taxa to use lactulose in monoculture. Finally, transcriptomic RNA sequencing identified a β-galactosidase gene that was strongly upregulated in *B. adolescentis* during growth on lactulose, clarifying the enzymatic mechanism enabling lactulose utilization.

In summary, while previous studies established lactulose as a prebiotic capable of enriching beneficial gut bacteria, they often did not address which strains were metabolically active or clarify how microbial interactions shape these responses. My work builds on this foundation by providing new evidence for the cooperative interactions supported by lactulose, demonstrating the value of single-cell and activity-based techniques, and revealing previously unrecognized responsive taxa within the gut microbiota. These advances contribute to a clearer and more mechanistic understanding of how lactulose shapes microbial communities and highlight new opportunities for developing more targeted microbiome based dietary interventions.

The third chapter of my thesis investigated the plant-derived polysaccharide arabinogalactan (AG), composed of galactose and arabinose (Barclay et al., 2019), which has gained considerable attention in recent years as a candidate prebiotic. Previous studies have demonstrated that dietary supplementation with arabinogalactan can selectively promote the growth of beneficial gut bacteria, with a consistent increase in *Bifidobacterium* and, in some cases, positive effects on *Bacteroides* and *Faecalibacterium* (Sun et al., 2021). These microbial shifts are linked to increased short-chain fatty acid (SCFA) production, enhanced gut barrier integrity, and modulation of immune responses (Y. Wang et al., 2021). However, most prior research has relied on community-level compositional profiling, which does not clarify which strains are metabolically active or how interactions among microbes drive these changes. To address these gaps, my research combined high-resolution 16S rRNA gene sequencing, single-cell Raman-activated cell sorting (RACS), and targeted coculture experiments. Using ex vivo incubations of fresh fecal samples from healthy donors, I examined the effects of arabinogalactan supplementation on gut microbiota.

Consistent with earlier reports, arabinogalactan supplementation reproducibly enriched *Bifidobacterium* across all donor samples. Importantly, I also observed robust enrichment of *Gemmiger*, a taxon whose response to arabinogalactan had not previously been characterized. When the monosaccharides of arabinogalactan were tested individually, galactose consistently enriched *Bifidobacterium* and arabinose promoted *Gemmiger* and some other genera. In contrast, the intact arabinogalactan polysaccharide led to a simultaneous enrichment of both *Bifidobacterium* and *Gemmiger* in all donors, a combined response not observed with either

sugar alone. These finding underscores that complex polysaccharides can drive community shifts not achievable with simple sugars, highlighting the importance of studying intact polymers for the design of targeted prebiotic interventions.

Through RACS, I isolated a broad range of bacterial strains, revealing a distinct pattern of arabinogalactan utilization. *Bifidobacterium longum* was the most frequently recovered and demonstrated a strong ability to degrade arabinogalactan as a sole carbon source. Other primary degraders included *Faecalibacterium prausnitzii, Catenibacterium mitsuokai, Bacteroides uniformis*, and *Bacteroides stercoris* (Rasoulimehrabani et al., 2025). These species are well known for their roles in fiber fermentation, SCFA production, gut barrier maintenance, and immune modulation (Ferreira-Halder et al., 2017; Huang et al., 2023; Zafar & Saier, 2021). Among them, *F. prausnitzii* is particularly notable for its substantial butyrate production and well-documented anti-inflammatory effects (Lenoir et al., 2020).

In contrast, *Eggerthella lenta, Collinsella aerofaciens, Phocaeicola coprocola,* and *Ruminococcus bicirculans* were metabolically active but could not grow on arabinogalactan alone. These secondary degraders required a primary degrader like *B. longum* for growth, as shown in coculture experiments, and may participate in further breakdown of metabolites and SCFA production via metabolic cooperation (Rasoulimehrabani et al., 2025). These findings underscore the importance of cross-feeding and cooperative networks in shaping community-level responses to arabinogalactan.

Interestingly, although *Gemmiger* was reproducibly enriched, it was not recovered as a metabolically active isolate via RACS, likely due to strict anaerobic requirements or sorting sensitivity (Zenner et al., 2021). In contrast to *Gemmiger*, which was not recovered as a metabolically active isolate, *F. prausnitzii*, which is phylogenetically related to *Gemmiger* (Fitzgerald et al., 2018), was successfully isolated. The dominant *Gemmiger* ASV showed 92.79% 16S rRNA gene identity with *F. prausnitzii*, suggesting overlapping ecological roles such as arabinogalactan fermentation and butyrate production, though their metabolic capacities may differ.

Overall, my findings demonstrate that *B. longum* consistently emerges as a metabolically active and enriched responder, functioning as a keystone species that supports the growth of other, non-degrading taxa. This research reveals how arabinogalactan shapes gut microbial communities, providing a basis for selecting prebiotics, probiotics, or dietary fibers that match an individual's gut microbiota profile, and for developing customized synbiotic formulations. Demonstrating that selective fibers can enrich keystone degraders and establish cooperative networks emphasizes the value of targeting both primary degraders and their associated taxa to achieve desired outcomes. Future research should include larger and more diverse groups of participants and use whole-genome sequencing together with functional omics approaches to identify the genes and metabolic pathways that allow gut bacteria to break down arabinogalactan. These findings can then be applied to develop scientifically validated microbiome-based dietary strategies and interventions.

Conclusion

This thesis advances our understanding of how specific prebiotics, including xylooligosaccharides (XOS), lactulose, and arabinogalactan, selectively modulate the human gut microbiota. By integrating single-cell activity-based methods with ex vivo incubations and targeted cultivation, I was able to directly identify metabolically active responders and clarify the functional impact of each prebiotic. Across all projects, *Bifidobacterium* consistently appeared as a key responder, emphasizing its central role in gut health. The XOS project further revealed *Collinsella aerofaciens* as a frequent, metabolically active XOS utilizer. In the lactulose study, single-cell analyses revealed that *Collinsella* and *Lactococcus lactis* were also stimulated, with *L. lactis* benefiting from cross-feeding provided by primary degraders. The arabinogalactan project identified *Bifidobacterium longum* as a keystone degrader that supports the growth of secondary taxa such as *Eggerthella lenta, Collinsella aerofaciens, Phocaeicola coprocola,* and *Ruminococcus bicirculans*, highlighting the importance of metabolic cooperation within the gut microbiota. Together, these findings show that specific prebiotics can shape the gut microbiota in distinct and targeted ways, often by

promoting interactions in which primary degraders break down complex substrates that support the growth of other beneficial bacteria. This work provides a mechanistic basis for future dietary interventions and highlights the potential of next-generation prebiotics to enhance gut and overall host health through targeted modulation of the microbiome.

References

Barclay, T. G., Day, C. M., Petrovsky, N., & Garg, S. (2019). Review of polysaccharide particle-based functional drug delivery. *Carbohydrate Polymers*, *221*(January), 94–112. https://doi.org/10.1016/j.carbpol.2019.05.067

Bloom, P. P., & Tapper, E. B. (2023). Lactulose in cirrhosis: Current understanding of efficacy, mechanism, and practical considerations. *Hepatology Communications*, *7*(11), 1–9. https://doi.org/10.1097/HC9.0000000000000295

Christensen, C. M., Kok, C. R., Auchtung, J. M., & Hutkins, R. (2022). Prebiotics enhance persistence of fermented-food associated bacteria in in vitro cultivated fecal microbial communities. *Frontiers in Microbiology*, *13*(September), 1–18. https://doi.org/10.3389/fmicb.2022.908506

Chu, N., Ling, J., Jie, H., Leung, K., & Poon, E. (2022). The potential role of lactulose pharmacotherapy in the treatment and prevention of diabetes. *Frontiers in Endocrinology*, *13*(September), 1–10. https://doi.org/10.3389/fendo.2022.956203

Cunningham, M., Azcarate-Peril, M. A., Barnard, A., Benoit, V., Grimaldi, R., Guyonnet, D., Holscher, H. D., Hunter, K., Manurung, S., Obis, D., Petrova, M. I., Steinert, R. E., Swanson, K. S., van Sinderen, D., Vulevic, J., & Gibson, G. R. (2021). Shaping the Future of Probiotics and Prebiotics. *Trends in Microbiology*, *29*(8), 667–685. https://doi.org/10.1016/j.tim.2021.01.003

Ferreira-Halder, C. V., Faria, A. V. de S., & Andrade, S. S. (2017). Action and function of Faecalibacterium prausnitzii in health and disease. *Best Practice and Research: Clinical Gastroenterology*, *31*(6), 643–648. https://doi.org/10.1016/j.bpg.2017.09.011

Fitzgerald, C. B., Shkoporov, A. N., Sutton, T. D. S., Chaplin, A. V., Velayudhan, V., Ross, R. P., & Hill, C. (2018). Comparative analysis of Faecalibacterium prausnitzii genomes shows a high level of genome plasticity and warrants separation into new species-level taxa. *BMC Genomics*, *19*(1), 931. https://doi.org/10.1186/s12864-018-5313-6

Gunn, D., Yeldho, C., Hoad, C., Menys, A., Gowland, P., Marciani, L., & Spiller, R. (2024).

Mechanisms underlying the laxative effect of lactulose: A randomized placebo-controlled trial showing increased small bowel water and motility unaltered by the 5-HT3 receptor antagonist, ondansetron. *Neurogastroenterology and Motility*, *36*(4), 1–10. https://doi.org/10.1111/nmo.14754

Huang, P., Zhang, P., Du, J., Gao, C., Liu, J., Tan, Y., & Chen, S. (2023). Association of fecal short-chain fatty acids with clinical severity and gut microbiota in essential tremor and its difference from Parkinson's disease. *Npj Parkinson's Disease*, *9*(1), 1–8. https://doi.org/10.1038/s41531-023-00554-5

Karakan, T., Tuohy, K. M., & Janssen-van Solingen, G. (2021). Low-Dose Lactulose as a Prebiotic for Improved Gut Health and Enhanced Mineral Absorption. *Frontiers in Nutrition*, *8*(July), 1–15. https://doi.org/10.3389/fnut.2021.672925

Kaur, A. P., Bhardwaj, S., Dhanjal, D. S., Nepovimova, E., Cruz-martins, N., Kuča, K., Chopra, C., Singh, R., Kumar, H., Şen, F., Kumar, V., Verma, R., & Kumar, D. (2021). Plant prebiotics and their role in the amelioration of diseases. *Biomolecules*, *11*(3), 1–28. https://doi.org/10.3390/biom11030440

Lenoir, M., Martín, R., Torres-Maravilla, E., Chadi, S., González-Dávila, P., Sokol, H., Langella, P., Chain, F., & Bermúdez-Humarán, L. G. (2020). Butyrate mediates anti-inflammatory effects of Faecalibacterium prausnitzii in intestinal epithelial cells through Dact3. *Gut Microbes*, *12*(1), 1–16. https://doi.org/10.1080/19490976.2020.1826748

O'Riordan, K. J., Collins, M. K., Moloney, G. M., Knox, E. G., Aburto, M. R., Fülling, C., Morley, S. J., Clarke, G., Schellekens, H., & Cryan, J. F. (2022). Short chain fatty acids: Microbial metabolites for gut-brain axis signalling. *Molecular and Cellular Endocrinology*, *546*(January). https://doi.org/10.1016/j.mce.2022.111572

Parhi, P., Liu, S. Q., & Choo, W. S. (2024). Synbiotics: Effects of prebiotics on the growth and viability of probiotics in food matrices. *Bioactive Carbohydrates and Dietary Fibre*, *32*(September), 100462. https://doi.org/10.1016/j.bcdf.2024.100462

Rasoulimehrabani, H., Khadem, S., Hodži, A., Philipp, M., Gallo, R., Joana, S., Ramesmayer, J., Sivuli, P., & Berry, D. (2025). Evaluating the prebiotic activity of arabinogalactan on the human gut microbiota using 16S rRNA gene sequencing and Raman-activated cell sorting. https://doi.org/10.20517/mrr.2025.29

Rasoulimehrabani, H., Riva, A., Inan, D., Hodžić, A., Hausmann, B., Nikolov, G., Khadem, S., Hieger, N., Wiesenbauer, J., Kaiser, C., Filz, V., Böttcher, T., & Berry, D. (2025). Lactulose selectively stimulates members of the gut microbiota, as determined by multi-modal activity-based sorting. *Gut Microbes*, *17*(1). https://doi.org/10.1080/19490976.2025.2525482

Riva, A., Rasoulimehrabani, H., Cruz-Rubio, J. M., Schnorr, S. L., von Baeckmann, C., Inan, D., Nikolov, G., Herbold, C. W., Hausmann, B., Pjevac, P., Schintlmeister, A., Spittler, A., Palatinszky, M., Kadunic, A., Hieger, N., Del Favero, G., von Bergen, M., Jehmlich, N., Watzka, M., … Berry, D. (2023). Identification of inulin-responsive bacteria in the gut microbiota via multi-modal activity-based sorting. *Nature Communications*, *14*(1), 8210. https://doi.org/10.1038/s41467-023-43448-z

Sheng, W., Ji, G., & Zhang, L. (2023). Immunomodulatory effects of inulin and its intestinal metabolites. *Frontiers in Immunology*, *14*(August), 1–16. https://doi.org/10.3389/fimmu.2023.1224092

Sun, Y., Hu, J., Zhang, S., He, H., Nie, Q., Zhang, Y., Chen, C., Geng, F., & Nie, S. (2021). Prebiotic characteristics of arabinogalactans during in vitro fermentation through multi-omics analysis. *Food and Chemical Toxicology*, *156*(August), 112522. https://doi.org/10.1016/j.fct.2021.112522

Tandon, D., Haque, M. M., Gote, M., Jain, M., Bhaduri, A., Dubey, A. K., & Mande, S. S. (2019). A prospective randomized, double-blind, placebo-controlled, dose-response relationship study to investigate efficacy of fructo-oligosaccharides (FOS) on human gut microflora. *Scientific Reports*, *9*(1), 1–15. https://doi.org/10.1038/s41598-019-41837-3

Wang, L. Y., He, L. H., Xu, L. J., & Li, S. B. (2024). Short-chain fatty acids: bridges between diet, gut microbiota, and health. *Journal of Gastroenterology and Hepatology (Australia)*, *39*(9), 1728–1736. https://doi.org/10.1111/jgh.16619

Wang, Y., Liu, Y., Ivusic Polic, I., Chandran Matheyambath, A., & LaPointe, G. (2021). Modulation of human gut microbiota composition and metabolites by arabinogalactan and Bifidobacterium longum subsp. longum BB536 in the Simulator of the Human Intestinal Microbial Ecosystem (SHIME®). *Journal of Functional Foods*, *87*, 104820. https://doi.org/10.1016/j.jff.2021.104820

Wolf, A. R., Wesener, D. A., Cheng, J., Houston-Ludlam, A. N., Beller, Z. W., Hibberd, M. C., Giannone, R. J., Peters, S. L., Hettich, R. L., Leyn, S. A., Rodionov, D. A., Osterman, A. L., & Gordon, J. I. (2019). Bioremediation of a Common Product of Food Processing by a Human Gut Bacterium. *Cell Host and Microbe*, *26*(4), 463-477.e8. https://doi.org/10.1016/j.chom.2019.09.001

Zafar, H., & Saier, M. H. (2021). Gut Bacteroides species in health and disease. *Gut Microbes*, *13*(1), 1–20. https://doi.org/10.1080/19490976.2020.1848158

Zenner, C., Hitch, T. C. A., Riedel, T., Wortmann, E., Tiede, S., Buhl, E. M., & Abt, B. (2021). Early-Life Immune System Maturation in Chickens Using a. *MSystems*, *6*(3), e01300-20.

Supplementary material chapter 1

Supplementary figures 1 – 19

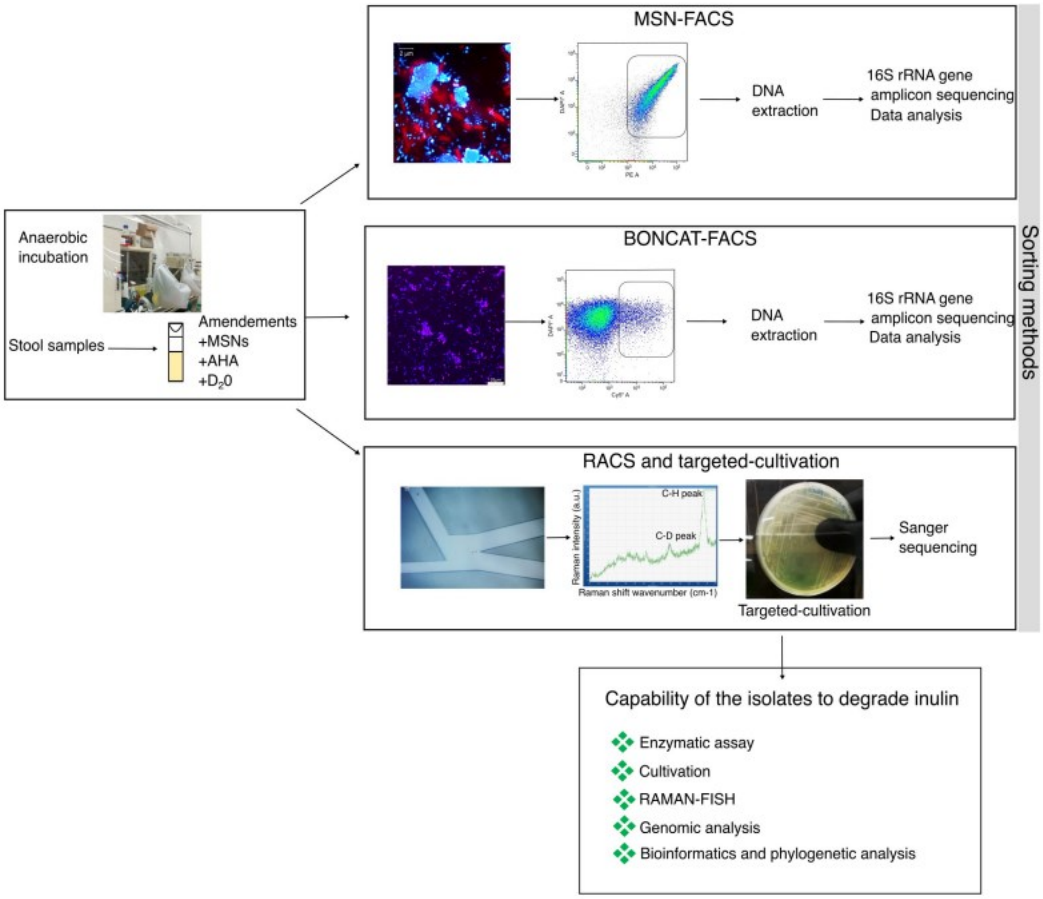

Supplementary Figure 1. Experimental design of the study. Fresh stool samples were incubated under anaerobic conditions and in the presence of the mesoporous silica nanoparticles (MSNs) functionalized with inulin and labeled with the fluorescence dye rhodamine to evaluate the spatial interaction between gut bacteria and MSNs grafted with inulin. The MSNs together with the bacteria were sorted by FACS and their 16S rRNA genes were amplified and sequenced to detect bacterial taxa able to interact with MSNs. Subsequently fresh stool samples were incubated under anaerobic condition and in the presence of the activity markers [(L-Azidohomoalanine [AHA] and heavy water [D2O]). Active cells were sorted with BONCAT-FACS and their 16S rRNA genes were amplified and sequenced. Responder strains were directly

isolated and cultivated with RACS and subsequently identified by Sanger sequencing. Further experiments were carried out to study the capability of the isolates to degrade inulin. Fructan assay and cultivation were performed in inulin supplemented medium. RAMAN-FISH was carried out to verify the deuterium incorporation for some *Coriobacteriia* members. Whole genome sequencing, bioinformatics, and phylogenetic analysis were performed for *Coriobacteriia* members *Eggerthella lenta* and *Gordonibacter urolithinfaciens*.

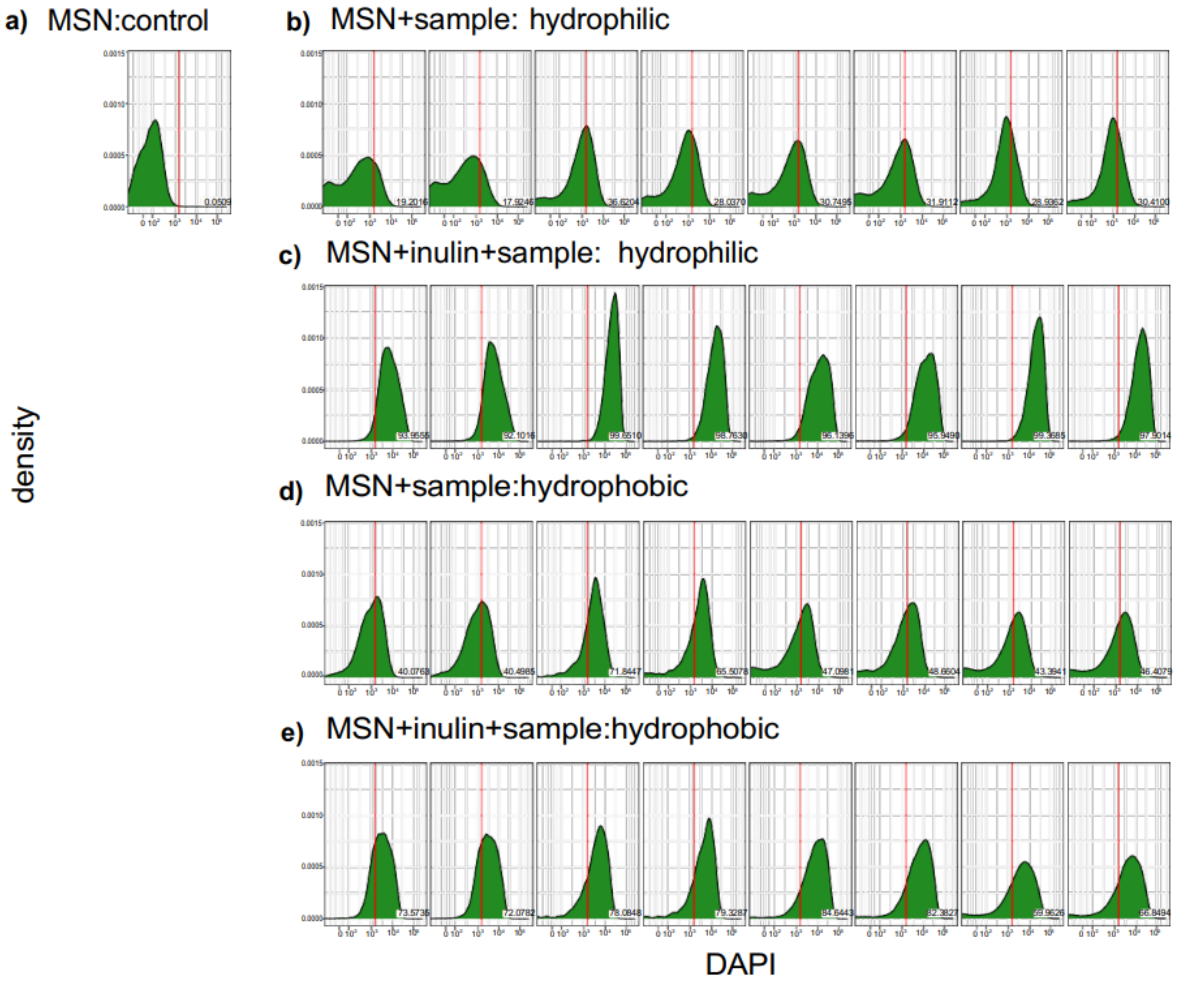

Supplementary Figure 2. Detection of binding bacteria to MSNs after anaerobic incubation via FACS analyses. Density plots show the intensity of the DAPI signal in the gate encompassing the rhodamine labeled MSNs [DAPI signal (x-axis), density (y-axis)]. MSN without inulin or stool sample is represented as control (a) and shows no DAPI signal. An example of 4 samples in duplicates is displayed. DAPI fluorescence intensity percentages for each MSNs type are shown. Higher DAPI signal (bacteria signal) in the gate encompassing the rhodamine labeled MSNs was detected in the inulin-coupled hydrophilic

MSNs (c) and inulin-coupled hydrophobic MSNs (e) with respect to the corresponding starting material (b, d).

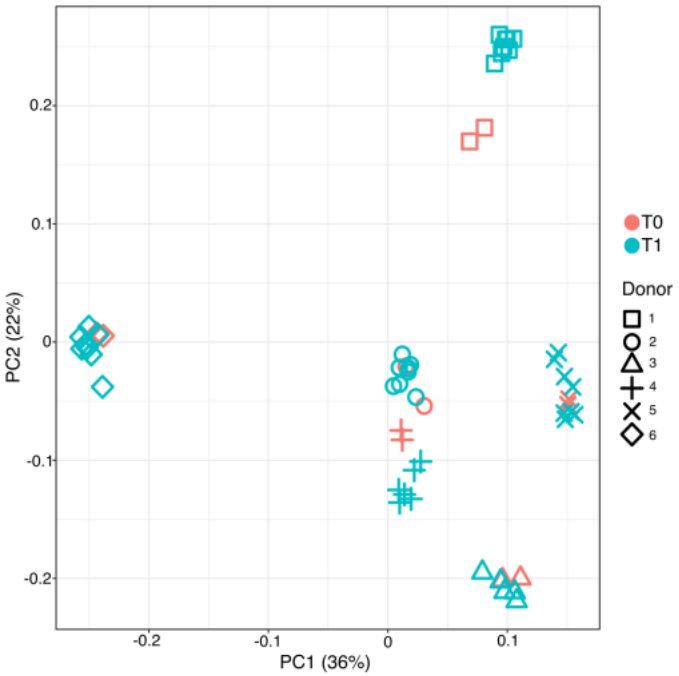

Supplementary Figure 3. Principal coordinates analysis ordination of 16S rRNA gene amplicon profiles from mesoporous silica nanoparticle (MSN) at 0 and 1 h in incubations. Samples from total community at 0 (red) and 1 h (blue) are shown. Ordination shows significant grouping by donors, depicted with different symbols (PerMANOVA: p=0.001, n=60 samples).

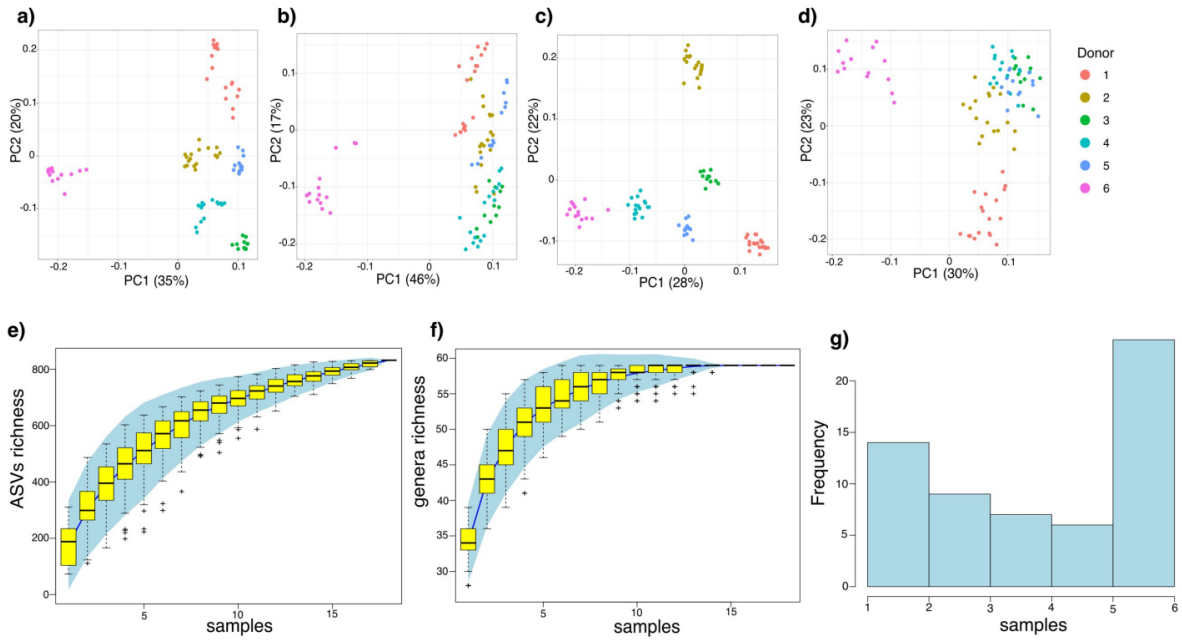

Supplementary Figure 4. Principal coordinates analysis ordination of 16S rRNA gene amplicon profiles from mesoporous silica nanoparticle (MSN) incubation experiments. (a, b) Samples from total community, as well as from sorted inulin-grafted and ungrafted hydrophobic and hydrophilic MSNs, are shown in technical duplicate. Samples are colored by donor stool and show a clear clustering by donor. Principal coordinates analysis based on Bray-Curtis distances performed at (a) ASV and (b) genus levels (PerMANOVA: p=0.001; ANOSIM: p=0.001 for both ASV and genera comparisons, n=108 samples) and based on Bray-Curtis distances on binary (presence/absence) data performed at (c) ASV and (d) genus levels (PerMANOVA: p=0.001; ANOSIM: p=0.001 for both ASV and genus comparisons, n=108 samples) are shown. (e, f) Species accumulation curves at ASVs and genera level for the inulin-binding fraction of the microbiota of each MSNs type. (g) Histogram shows the prevalence of the most abundant genera (>1%) in the six samples.

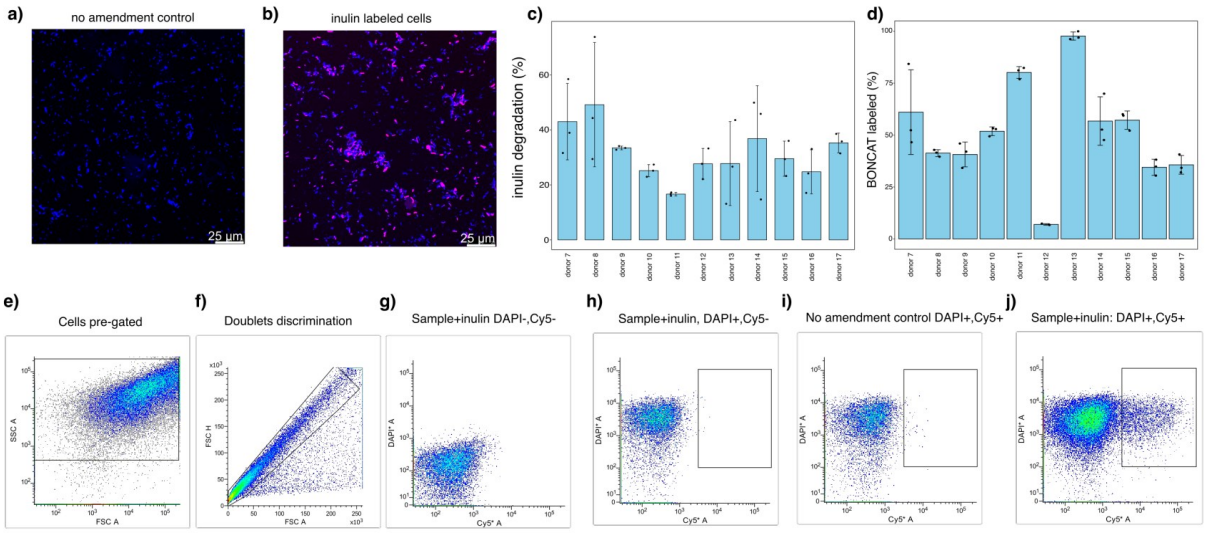

Supplementary Figure 5. FACS-sorting gating strategy for BONCAT labelled cells. (a) No amendment control shows no BONCAT signal. (b) Active cells show a positive BONCAT signal (pink, Cy5) after 6 h incubation with inulin. All cells are stained with DAPI (blue). Both microscopy images were recorded using identical settings. (c) Results from the fructan assay shows inulin degradation by the total community (mean ± sd: 31.7 ± 13%, n=11 samples). Triplicates measurements are shown. (d) Percentage of positive BONCAT cells by donor (mean ± sd: 51.3 ± 24.3%, n=11 samples). Triplicates measurements are shown. Error bars represent standard deviation of the mean. (e-h) Bacteria were sorted with a FACS Melody cell sorter. The sorting gate was chosen to select the active fraction upon incubation with inulin. e) Bacteria were visualized using the forward scatter (FSC) and side scatter (SSC) and pre-gated, f) Doublets discrimination was performed to ensure that they were excluded from analysis to avoid false positive in the sorting experiments. Cy5 negative cells were used to select the gate: (g) unstained cells, (h) DAPI-stained cells, (i), no amendment control, (j), DAPI- and Cy5-labeled cells.

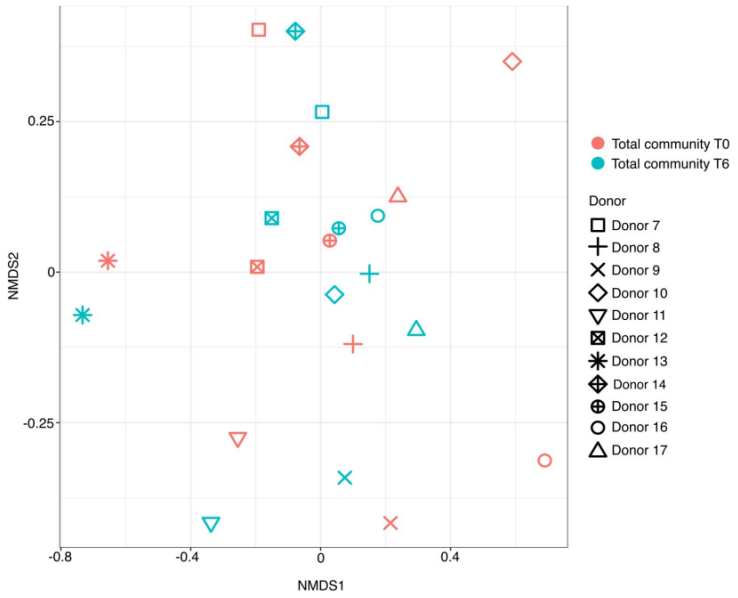

Supplementary Figure 6. Total community after inulin supplementation of 16S rRNA gene amplicon profiles. No significant difference was detected in the total community comparing 0 h (red dots) and 6 h (blue dots) (PerMANOVA, p=0.591, n=22 samples). Ordination shows significant grouping by donors, depicted with different symbols (PerMANOVA: p=0.001, n=22 samples).

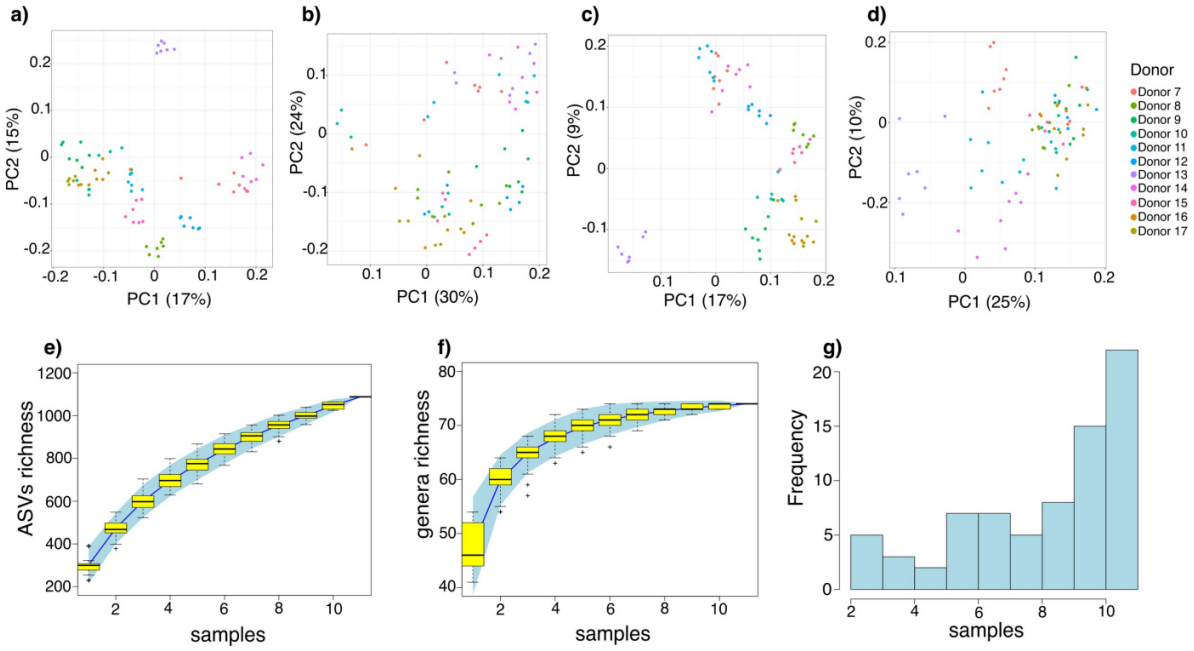

Supplementary Figure 7. Principal coordinates analysis ordination of 16S rRNA gene amplicon profiles from BONCAT incubation experiments after inulin supplementation. (a,b) Samples from total community

incubations, as well as from active fraction are shown. Samples are colored by donor and show a clear clustering by donor. Principal coordinates analysis based on Bray-Curtis distances performed at (a) ASV and (b) genus levels (PerMANOVA: p=0.001; ANOSIM: p=0.001 for both ASV and genus comparisons, n=77 samples) and based on Bray-Curtis distances on binary (presence/absence) data performed at (c) ASV and (d) genus levels (PerMANOVA: p=0.001; ANOSIM: p=0.001 for both ASV and genus comparisons, n=77 samples) are shown. (e, f) Species accumulation curves at ASV and genus level for the inulin-active fraction of the microbiota. (g) Histogram of the prevalence of the most abundant genera (>1%) in the eleven samples.

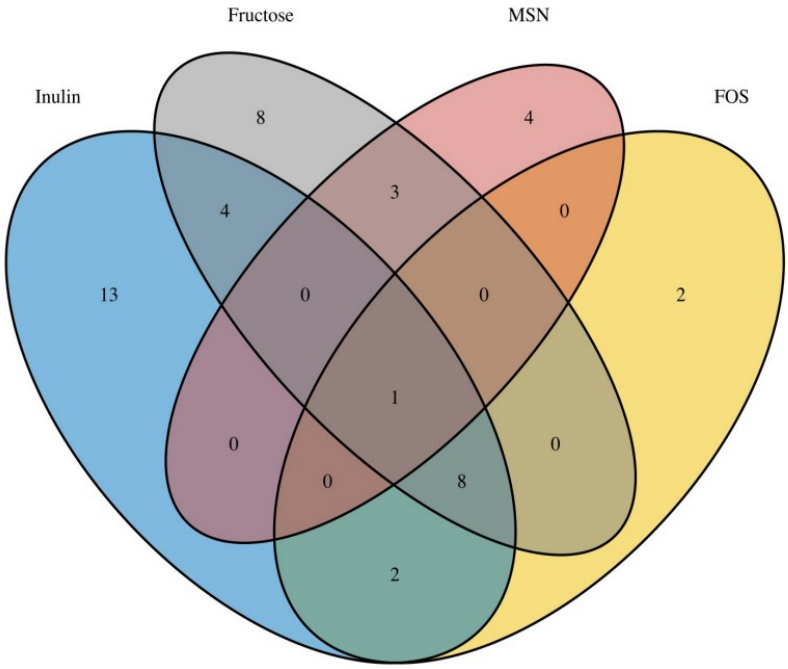

Supplementary Figure 8. Venn diagram of enriched ASVs after incubation with different substrates and BONCAT-based sorting of translationally active microbial community members. Venn diagram shows shared and unique ASVs after inulin, FOS, fructose amendments that were enriched in the sorted fraction as well as the enrichments of MSN-FACS sorted cells. Venn diagram shows 13, 8, 4, and 2 unique ASVs for inulin, fructose, MSN, and FOS enrichments respectively. 11 ASVs were shared between inulin and FOS enrichments, 13 between inulin and fructose enrichments and 9 between FOS and fructose enrichments. 3 enriched ASVs from the binding experiments were shared with ASVs enriched after fructose amendment (ASV_2st_345: *Lachnospiraceae Blautia*, ASV_2ua_io6: *Bacteroidaceae Phocaeicola*, ASV_s62_9ct: *Lachnospiraceae Blautia*, ASV_sj9_cdm: *Ruminococcaceae Ruminococcus*) and 1 between binding experiments, inulin and FOS supplementation (ASV_2st_345= *Lachnospiraceae Blautia*). Details of unique and shared ASVs between the groups are shown in Supplementary Table 5.

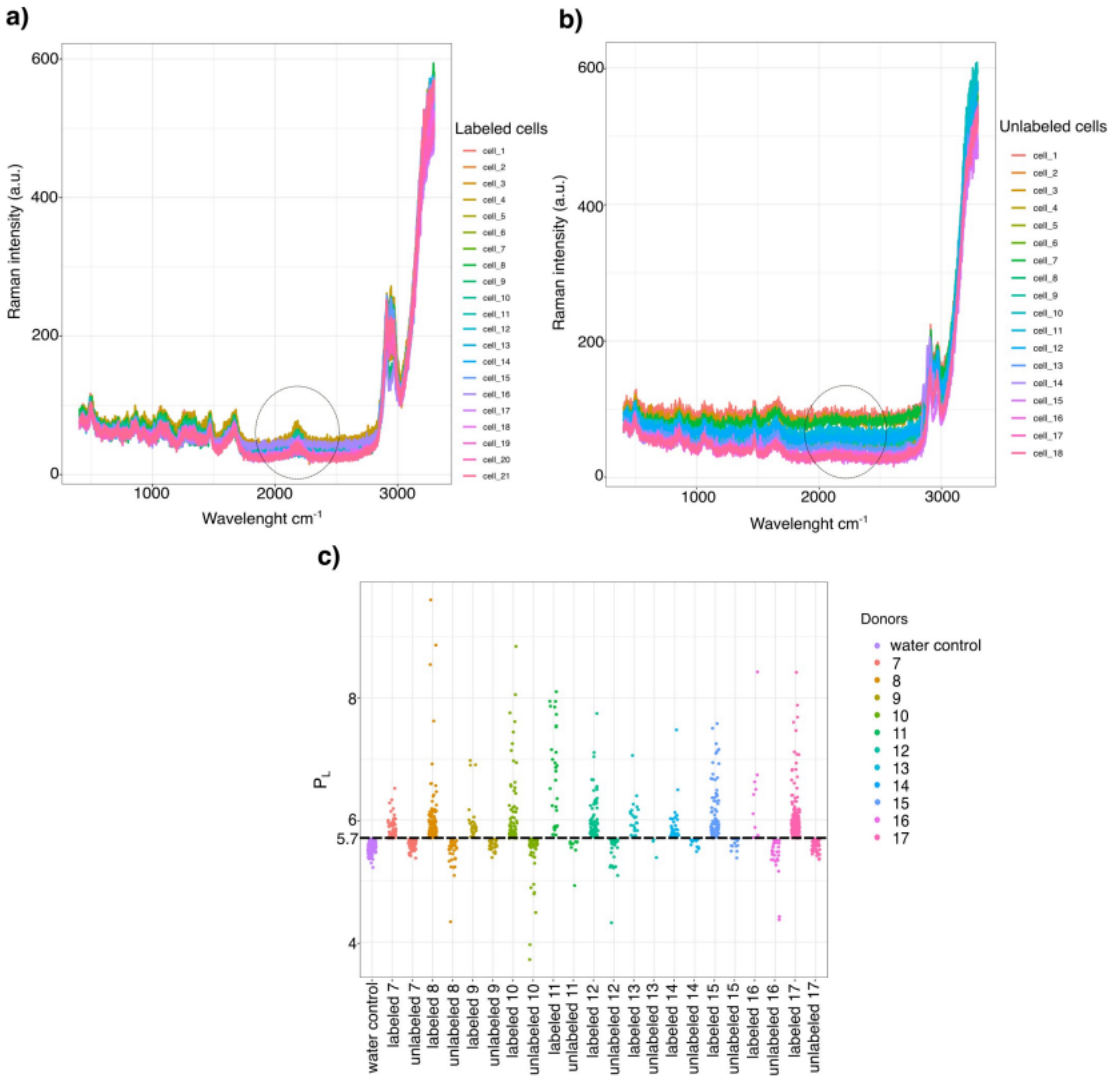

Supplementary Figure 9. Raman spectra of D-labeled and unlabeled cells in RACS. (a) Example of Raman spectra of D-labeled and sorted cells. (b) Example of Raman spectra of unlabeled and rejected cells. The C-D peak region of the Raman spectrum (2,040-2,300 cm-1) representing D incorporation is depicted by a circle. (c) PL threshold was calculated as mean+2 sd of the water control (inulin in H2O, n=116). The dashed line denotes the threshold PL value adopted based on these controls (PL = 5.7). Cells with a PL > 5.7 were considered labeled and thus sorted, while cells with a PLS 5.7 were considered unlabeled and thus rejected. Dots depicted with different colors represent all cells analyzed for each donor. Numbers of labeled and unlabeled cells for each donor are shown in Supplementary Table 6.

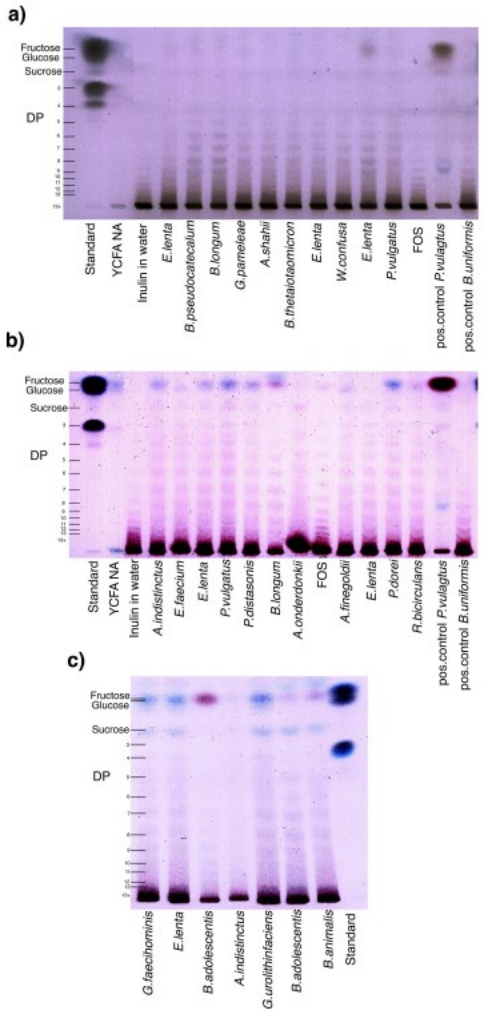

Supplementary Figure 10. Thin layer chromatography of RACS strains. (a-c) Degree of polymerization (DP) distribution evaluation. Standard: fructose, glucose (DP 1), sucrose (DP 2), 1,1 kestotriose (DP 3) and 1,1,1 kestotetraose (DP 4). Inulin in water and YFCA were used as controls. Neither of these show the presence of monosaccharides or saccharides with a DP 14 less than 9. *Phocaeicola vulgatus* (DSM1447) and *Bacteroides uniformis* (DSM6597) were used as positive control strains. All strains tested show the capability of inulin degradation at different levels. Strains were sampled in their early stationary phase. (a) *Eggertella lenta* (donor 10), *Bifidobacterium pseudocatenulatum* (donor 10), *Bifidobacterium longum* (donor 10) *Gordonibacter pamelaeae* (donor 10), *Alistipes shahii* (donor 10), *Bacteroides thetaiotaomicron* (donor 11), *Eggerthella lenta* (donor 11), *Weissella confusa* (donor 12), *Eggertella lenta* (donor 12), *Phocaeicola vulgatus* (donor 12). (b) *Alistipes indistinctus* (donor 7), *Enterococcus faecium* (donor 7), *Eggertella lenta* (donor 7), *Phocaeicola vulgatus* (donor 8), *Parabacteroides distasonis* (donor 8), *Bifidobacterium longum* (donor 8), *Alistipes onderdonkii* (donor 8), *Alistipes finegoldii* (donor 9), *Eggertella lenta* (donor 9), *Phocaeicola dorei* (donor 9), *Ruminococcus bicirculans* (donor 9). (c) *Gordonibacter* faecihominis (donor 14), *Eggerthella lenta* (donor 14), *Bifidobacterium adolescentis* (donor 17), *Alistipes*

indistinctus (donor 17), *Gordonibacter urolithinfaciens* (donor 17), *Bifidobacterium adolescentis* (donor 15), *Bifidobacterium animalis* (donor 15).

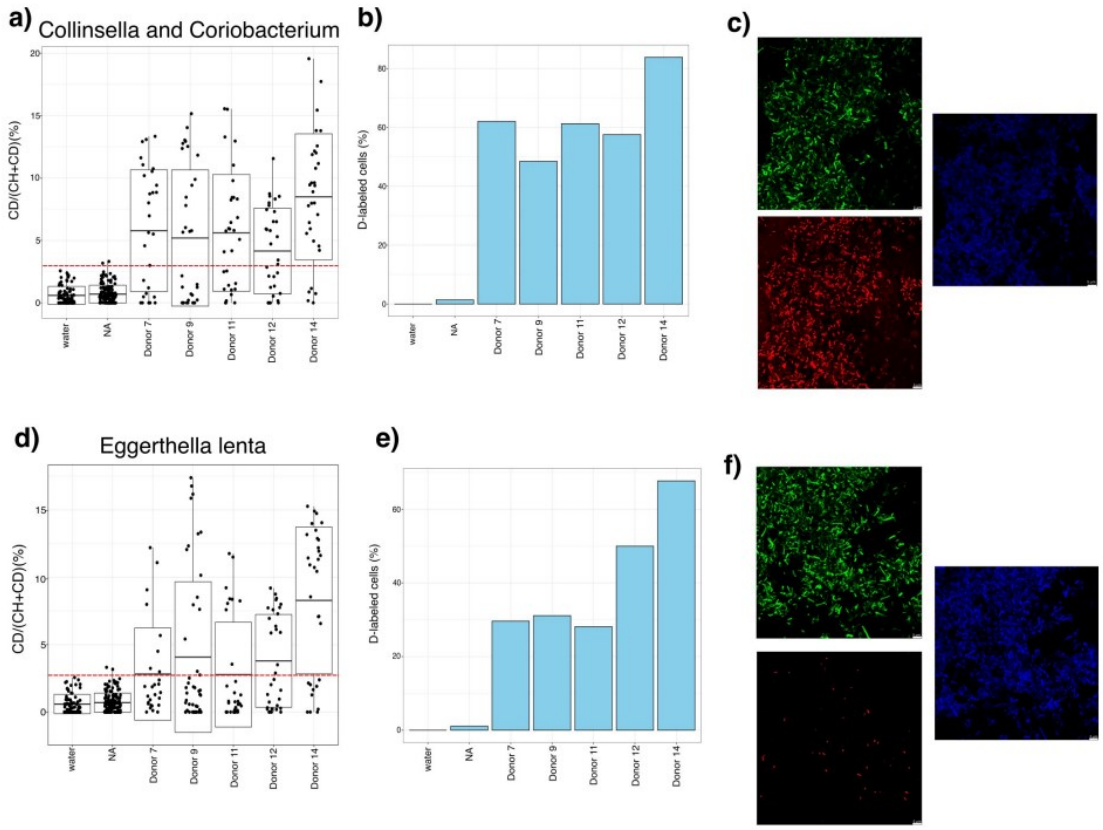

Supplementary Figure 11. *Coriobacteriia* show high metabolic activity after inulin supplementation: Raman-FISH experiments on stool samples amended with inulin revealed deuterium incorporation for both *Collinsella, Coriobacterium* and *Eggerthella lenta*. (a) Raman measurements of FISH-identified *Collinsella, Coriobacterium* cells in stool samples from donors 7, 9, 11, 12, and 14 after 6 h incubation with inulin. The y-axis represents the percentage of active cells (%CD) based on deuterium incorporation. Each dot represents a random single cell measurement (water control: n=76 cells, nothing added NA n=142 cells, donor 7 n=29 cells, donor 9 n=33 cells, donor 11 n=31 cells, donor 12 n=33 cells, donor 14 n=31 cells). The red dashed line at 2.75% indicates the threshold for considering a cell labelled as previously explained. Boxplot: boxplot medians (center lines), interquartile ranges (box ranges), whisker ranges, scale bar 5 µm. (b) Percentage of deuterium-labeled *Collinsella, Coriobacterium* cells per donor. (c) Representative FISH image of a stool sample. The pictures show *Collinsella, Coriobacterium* stained with the specific probes COR653 (red), all bacteria stained with EUB 338 I-III (green), and DAPI staining (blue). (d) Raman measurements of positive *Eggerthella lenta* cells in stool samples from donors 7, 9, 11, 12, and 14 after 6 h incubation with inulin (water control: n=76 cells, nothing added NA n=142 cells, donor 7 n=27 cells, donor 9 n=45 cells, donor 11 n=32 cells, donor 12 n=32 cells, donor 14 n=31 cells). (e) Percentage of deuterium-labeled *Eggerthella lenta* cells per donor. (f) Representative FISH image of a stool sample. The

pictures show *Eggerthella lenta* stained with the specific probes *E.lenta* 194 (red), all bacteria stained with EUB 338 I-III (green), and DAPI staining (blue).

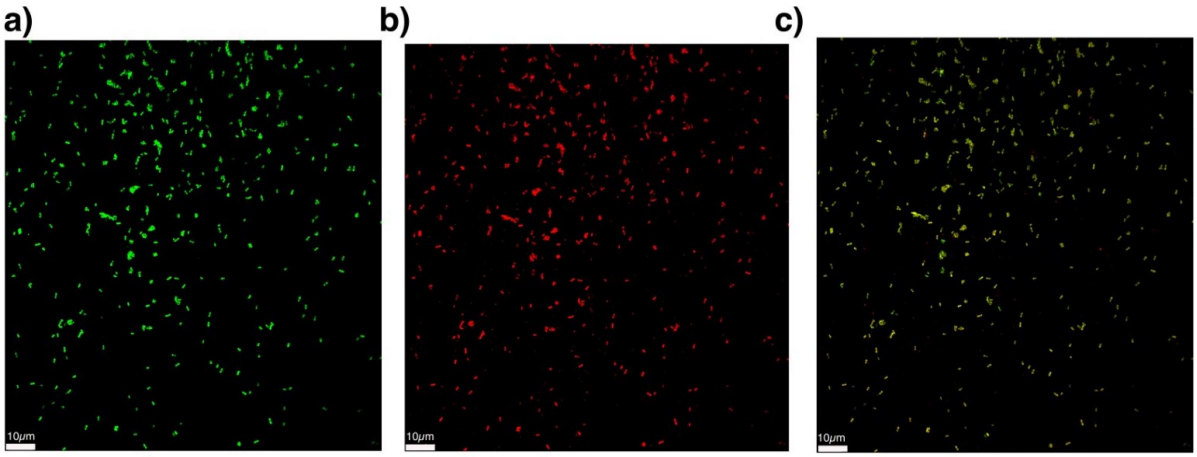

Supplementary Figure 12. FISH of *Eggerthella lenta* isolated with RACS. (a) *Eggerthella lenta* isolated with RACS stained with probes for all bacteria (EUB 338 I-III; green) and (b) the specific probe *E.len*194 (red). (c) overlay of signals.

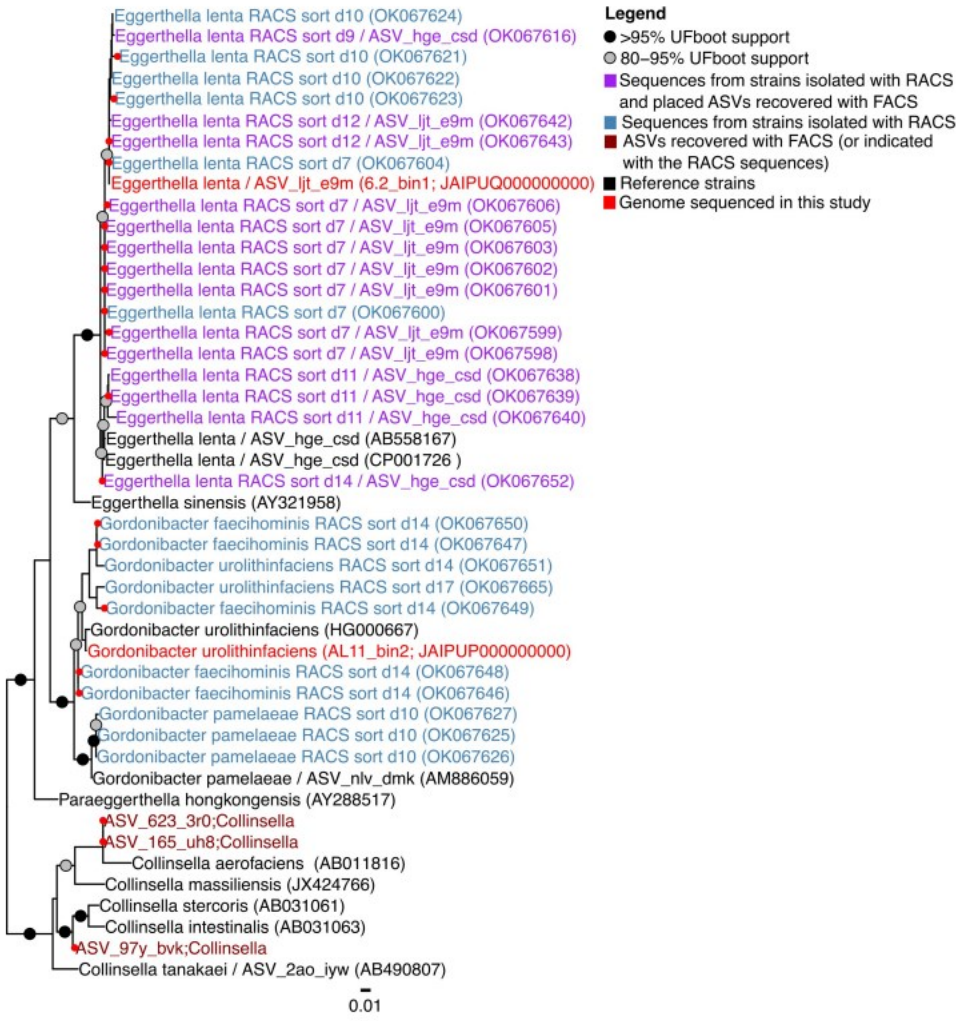

Supplementary Figure 13. Phylogenetic tree of the class *Coriobacteriia* members build with 16S rRNA gene amplicon ASV sequences from FACS-sorted cells and sequences from the strains isolated with RACS. Black dots indicate support values > 95% and grey dot between 80 and 95%, red dots indicate the sequences shorter than 1200 nucleotides placed in the tree. Sequences from the strains isolated with RACS are indicate in blue, ASVs recovered with FACS from both BONCAT and MSN sort experiments are indicated in purple or indicated with the RACS sequences, black labels indicate the type strains used as reference sequences and in red are indicated the 16S rRNA sequences recovered from genomes of *Gordonibacter urolithinfaciens AL*-11 and *Eggerthella lenta 6.2* sequenced in this study. Accession numbers are indicated in parenthesis.

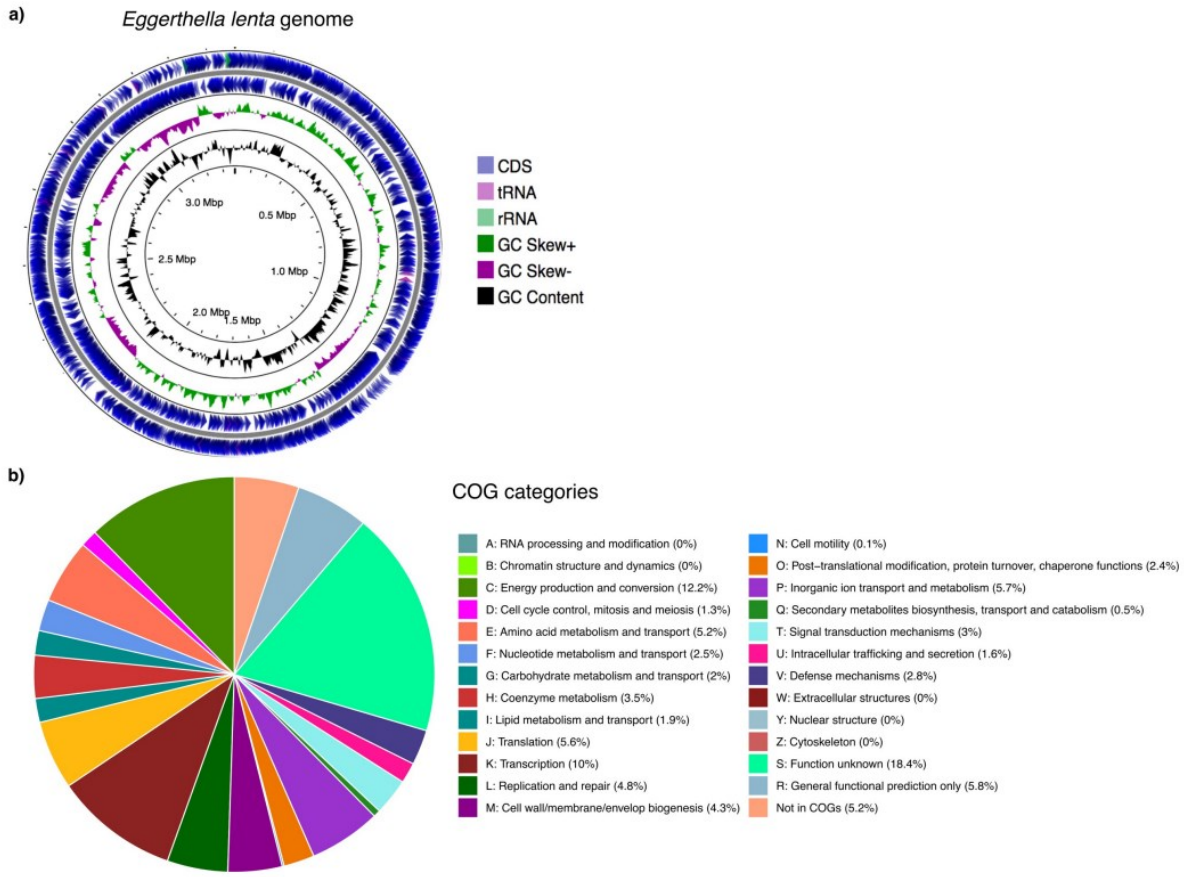

Supplementary Figure 14. Genome representation of *Eggerthella lenta 6.2*. (a) Circular map of the *Eggerthella lenta* genome. Circles from the outside to the inside show the positions of protein-coding genes (blue), tRNA genes (violet) and rRNA genes (light green) on the positive (circle 1), and negative (circle 2) strands. Circles 3 and 4 show plots of GC content and GC skew plotted as the deviation from the average for the entire sequence. The genome was visualized with GCView Server. (b) Percentage of genes associated with the respective COG functional category. Genome annotations revealed a predicted 2.0% of genes involved in carbohydrate metabolism and transport for *E. lenta 6.2*, including several different glycoside hydrolases, ABC transporters, permeases and sugar phosphotransferase systems (PTS).

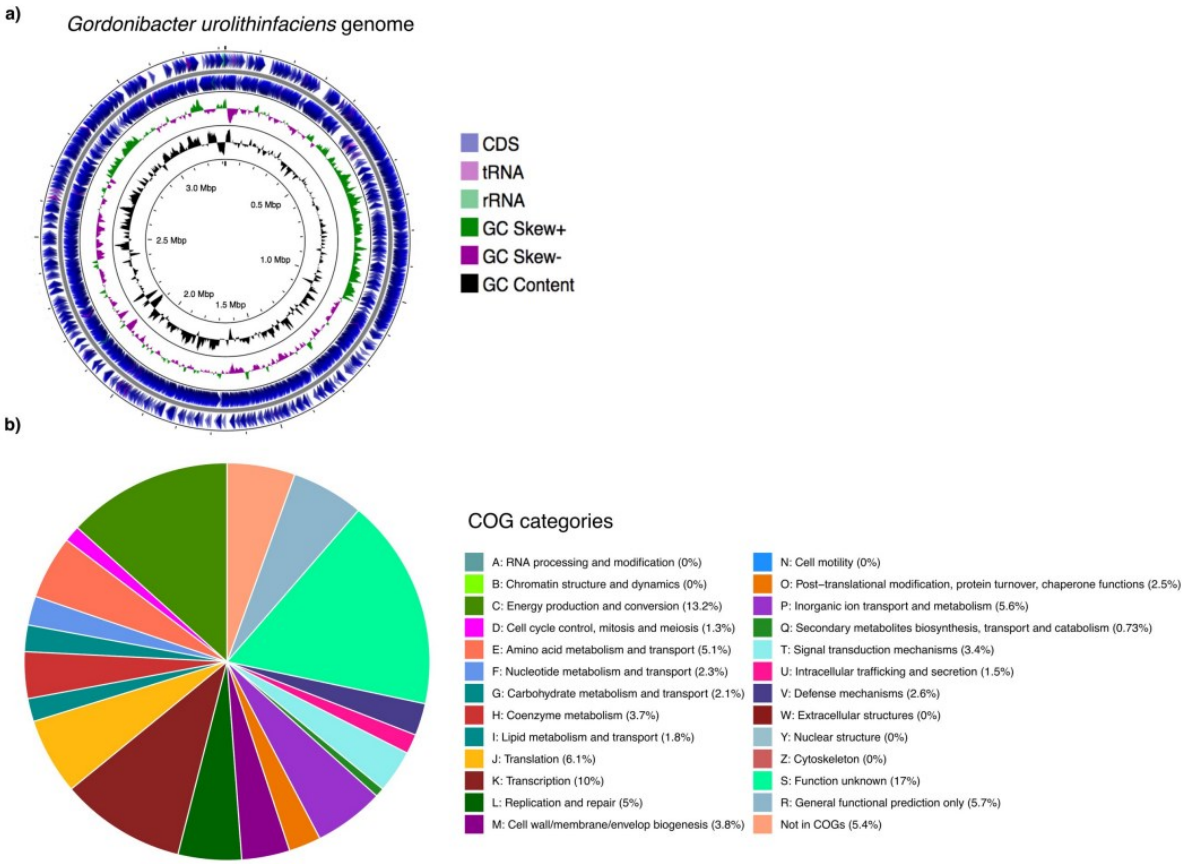

Supplementary Figure 15. Genome representation of *Gordonibacter urolithinfaciens AL-11*. (a) Circular map of the *Gordonibacter urolithinfaciens* genome. Circles from the outside to the inside show the positions of protein-coding genes (blue), tRNA genes (violet) and rRNA genes (light green) on the positive (circle 1), and negative (circle 2) strands. Circles 3 and 4 show plots of GC content and GC skew plotted as the deviation from the average for the entire sequence. The genome was visualized with GCView Server. (b) Percentage of genes associated with the respective COG functional categories. Genome annotations revealed a predicted and 2.1% of genes involved in carbohydrate metabolism and transport for *G. urolithinfaciens AL-11*, including several different glycoside hydrolases, ABC transporters, permeases and sugar phosphotransferase systems (PTS).

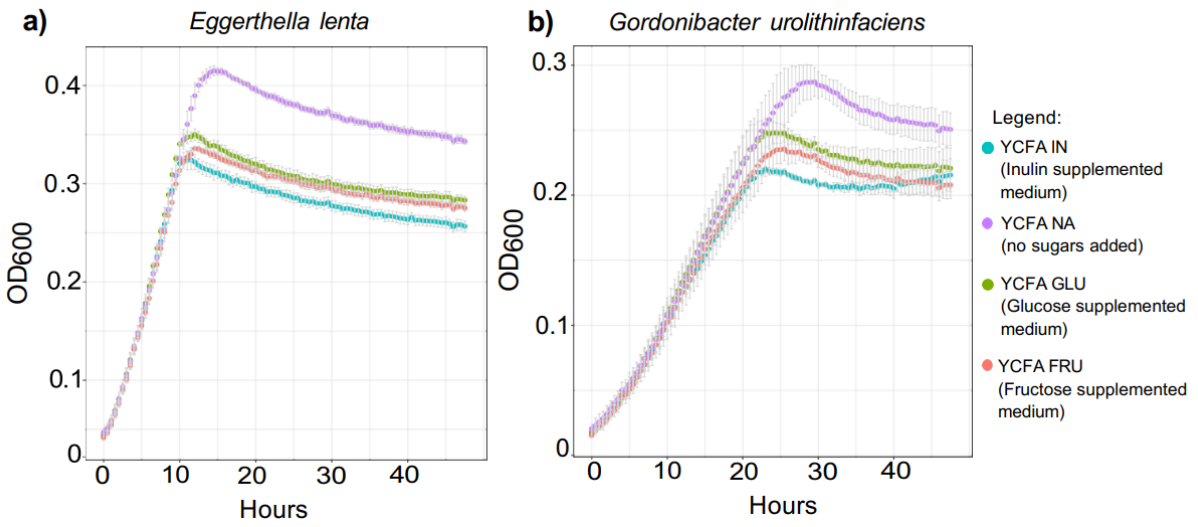

Supplementary Figure 16. Growth curves of *Eggerthella lenta* and *Gordonibacter urolithinfaciens* isolated with RACS after inulin, glucose, or fructose supplementation. (a) *Eggerthella lenta* and (b) *Gordonibacter urolithinfaciens* were grown in inulin (light blue), glucose (green) and fructose (red) supplemented YCFA-medium and in YCFA-medium without any other sugar added (NA, violet) that was used as control. The medium was prepared using the recipe from DSMZ 1611 modified with the addition of 10 mg/ml arginine. The growth curves are expressed as mean values (three replicates) ± sd of optical densities measured at 600 nm.

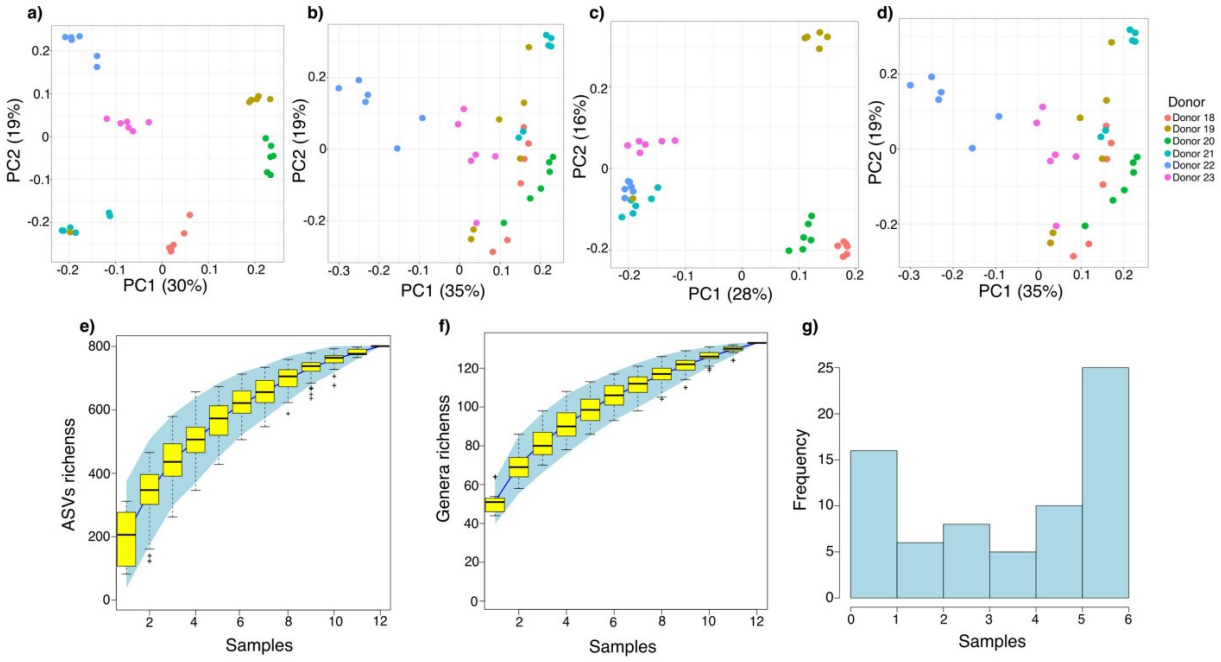

Supplementary Figure 17. Principal coordinates analysis ordination of 16S rRNA gene amplicon profiles from BONCAT incubation experiments after XOS supplementation. (a,b) Samples from total community

incubations, as well as from active fraction are shown. Samples are colored by donor and show a clear clustering by donor. Principal coordinates analysis based on Bray-Curtis distances performed at (a) ASV and (b) genus levels (PerMANOVA: p=0.001; ANOSIM: p=0.001 for both ASV and genus comparisons, n=36 sample) and based on Bray-Curtis distances on binary (presence/absence) data performed at (c) ASV and (d) genus levels (PerMANOVA: p=0.001; ANOSIM: p=0.001 for both ASV and genus comparisons, n=36 sample) are shown. (e, f) Species accumulation curves at ASV and genus level for the XOS-active fraction of the microbiota. (g) Histogram of the prevalence of the most abundant genera (>1%) in the six samples.

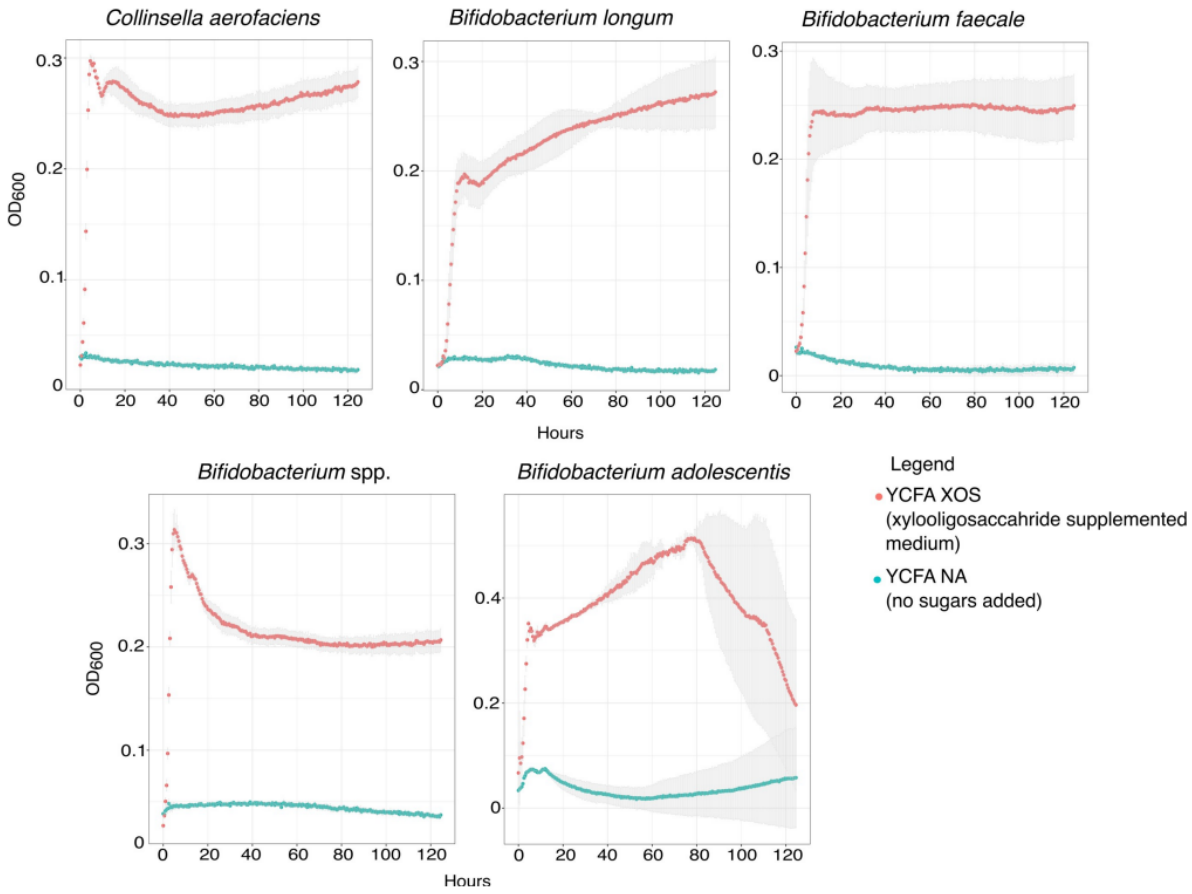

Supplementary Figure 18. Growth curves of representative strains isolated with RACS after XOS supplementation. Growth curves of the most representative strains isolated with RACS. Representative strains were selected choosing all the different species isolated. All strains were grown in XOS supplemented YCFA-medium (red) and in YCFA-medium without XOS and any other sugar added (NA, blue) that was used as control. The medium was prepared using the recipe from DSMZ 1611. The growth curves are expressed as mean values (three replicates) ± sd of optical densities measured at 600 nm.

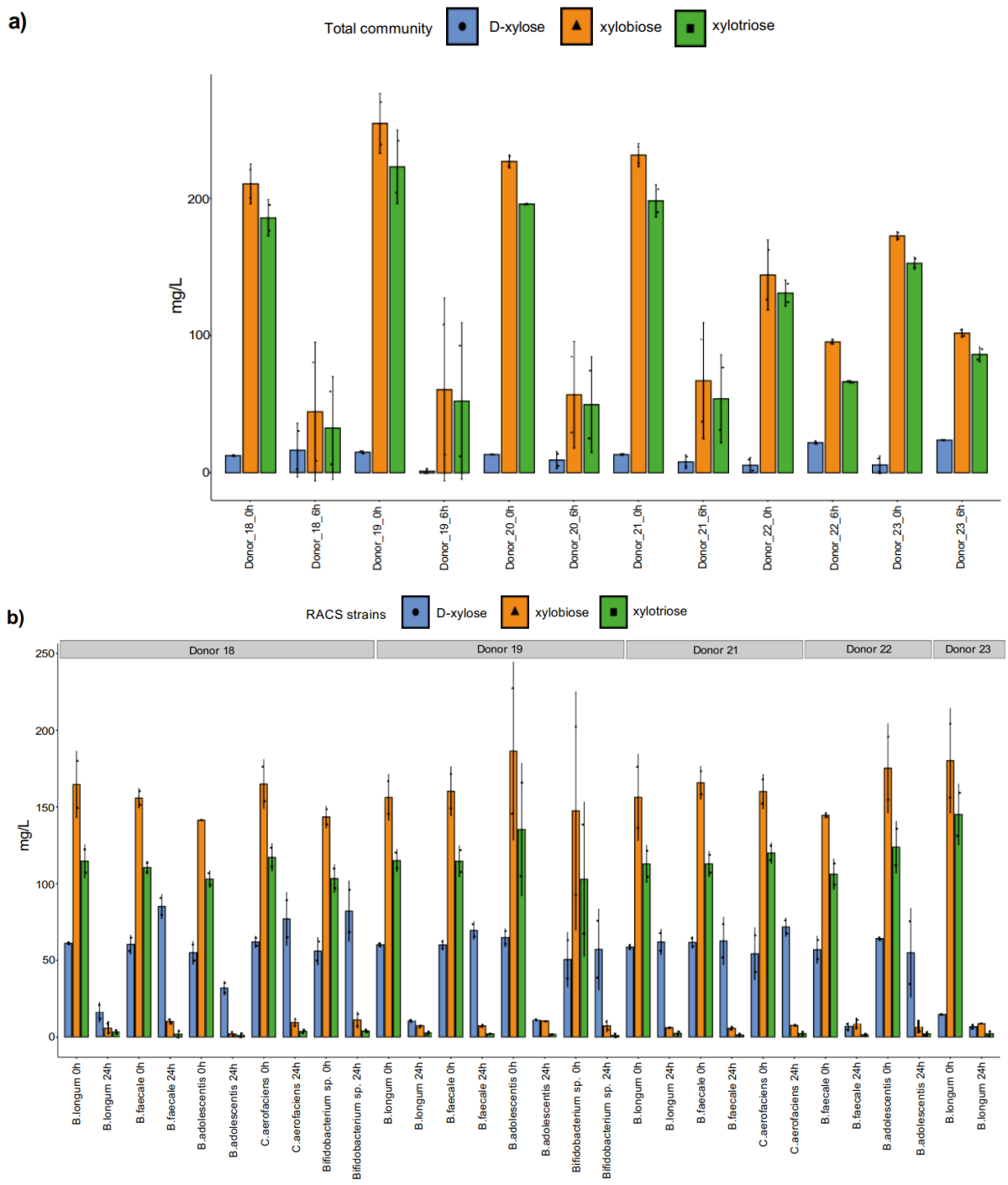

Supplementary Figure 19. HPAEC measurements of D-xylose, xylobiose and xylotriose for the total community and each RACS isolates for each donor. (a) HPAEC measurement of the stoolsample at 0 and 6 h (total community). A statistical significance decrease was observed after 6 h for xylobiose (0 h: 206.7 ± 40.7, 6 h: 70.9 ± 37.4, n=12 samples, Student t-test). (b) RACS-sorted strains were grown at 24 h in XOS-supplemented media and compare to 0 h time point. Student t-test or Wilcox test comparing 0h with 24h;

D-xylose (0 h: 56.14 ± 13.11, 24 h: 47.15 ±30.74, p=0.876, n=60 samples), xylobiose (0 h: 160.21 ± 25.32, 24 h: 7.69 ± 2.95, p<0.0001,n=60 samples), xylotriose (0 h: 115.88 ± 18.35, 24 h: 2.32± 1.41, p<0.0001, n=60 samples). Student t-test comparing each bacteria isolated: *Bifidobacterium longum*, D-xylose (0 h: 48.78 ± 7.42, 24 h: 24.02 ± 11.3, p= 0.724, n=8 samples), xylobiose (0 h: 164.4 ± 7.78, 24 h: 7 ± 0.71, p<0.0001, n=8 samples), xylotriose, (0 h: 122 ± 6.18, 24 h: 2.76 ± 0.47, p<0.0001, n=8 samples); *Bifobacterium faecale*, D-xylose (0 h: 59.87 ± 1.69, 24 h: 56.07 ± 11.59, p<0.0001, n=8 samples), xylobiose (0 h: 156.6 ± 3.98, 24 h: 8 ± 0.83, p= 0.0005, n=8 samples), xylotriose (0 h: 111.1 ± 2.54, 24 h: 71.77± 0.43, p= 0.0001, n=8 samples), *Bifobacterium adolescentis*, D-xylose (0 h: 61.41 ± 2.64, 24 h: 32.58 i± 9.96, p= 0.013, n=8 samples), xylobiose (0 h: 167.7 ± 14.58, 24 h: 6.36 ± 1.7, p= 0.0002, n=8 samples), xylotriose (0 h: 120.7 ± 10.39, 24 h: 1.72 ± 0.46, p<0.0001, n=8 samples), *Bifobacterium sp*., D-xylose (0 h: 53.75 ± 11.87, 24 h: 69.36 ± 13.26, p= 0.281, n=8 samples), xylobiose (0 h: 145.5 ± 22.49, 24 h: 9.32 ± 2.17, p= 0.003, n=8 samples), xylotriose (0 h: 103.2 ± 14.72, 24 h: 2.61 ± 1.03, p= 0.001, n=8 samples), *Collinsella aerofaciens*, D-xylose (0 h: 58.26 ± 5.44, 24 h: 74.48 ± 7.7, p=0.999, n=8 samples), xylobiose (0 h: 162.5 ± 5.77, 24 h: 8.68 ± 1, p= 0.016, n=8 samples), xylotriose (0 h: 118.6 ± 3.26, 24 h: 3.11 ± 0.73, p= 0.035, n=8 samples). Error bars represent standard deviation of the mean. Each dot represents a single measurement (samples were measured in duplicates, n=60 for RACS strains and n=24 for total community). D-xylose (blue), xylobiose (orange) and xylotriose (green).

Supplementary tables 1-6

Supplementary Table 1. List of unique and shared ASVs of enrichments detected after inulin, FOS, fructose, and MSN amendments.

	Unique ASVs	Taxa
Inulin	ASV_27v_mrq	Unclassified *Lachnospiraceae*
	ASV_29g_ajq	*Lachnospiraceae Anaerostipes*
	ASV_29p_drg	Unclassified *Lachnospiraceae*
	ASV_5z7_fi0	*Lachnospiraceae Anaerostipes*
	ASV_64u_lsr	*Lachnospiraceae Roseburia*
	ASV_6fr_khd	*Sutterellaceae Parasutterella*
	ASV_9eq_kr6	*Streptococcaceae Streptococcus*
	ASV_fcp_dbf	*Corynebacteriaceae Corynebacterium*
	ASV_fqm_8pm	*Streptococcaceae Streptococcus*
	ASV_jvz_svl	Unclassified *Lachnospiraceae*
	ASV_nw9_e4l	*Lachnospiraceae Anaerostipes*
	ASV_p02_b8f	*Lachnospiraceae Blautia*
	ASV_pxk_1ex	*Lachnospiraceae Anaerostipes*
MSN	ASV_t5i_a3k	*Veillonellaceae Dialister*
	ASV_ter_b2k	*Eggerthellaceae Raoultibacter*
	ASV_tg8_il9	*Lachnospiraceae Roseburia*
	ASV_kp7_w4p	*Selenomonadaceae Mitsuokella*
Fructose	ASV_76c_zrb	*Clostridiales*
	ASV_avd_9fb	*Desulfovibrionaceae Desulfovibrio*
	ASV_cns_p1y	*Ruminococcaceae Gemmiger*
	ASV_dqn_jls	*Bifidobacteriaceae Bifidobacterium*
	ASV_ic9_xvj	*Bifidobacteriaceae Bifidobacterium*
	ASV_ram_s25	*Bacteroidaceae Phocaeicola*
	ASV_sy7_30v	*Lachnospiraceae Kineothrix*
	ASV_t9m_xq7	*Bacteroidaceae Phocaeicola*
FOS	ASV_6ea_nz7	*Lachnospiraceae Blautia*
	ASV_a7l_qve	Unclassified *Lachnospiraceae*
	Shared ASVs	**Taxa**
Inulin-FOS	ASV_165_uh8	*Coriobacteriaceae Collinsella*
	ASV_2st_345	*Lachnospiraceae Blautia*
	ASV_4ma_8bd	*Lachnospiraceae Agathobacter*
	ASV_82p_r33	*Bifidobacteriaceae Bifidobacterium*
	ASV_ap2_sf2	*Erysipelotrichaceae Clostridium_XVIII*
	ASV_dx5_pax	*Erysipelotrichaceae Faecalibacillus*
	ASV_e9p_tub	*Lachnospiraceae Blautia*
	ASV_hcf_4f5	*Lachnospiraceae Blautia*
	ASV_hwd_896	*Lachnospiraceae Anaerobutyricum*
	ASV_jbt_n3b	Unclassified *Lachnospiraceae*
	ASV_ski_ka3	*Lachnospiraceae Blautia*
Inulin-Fructose	ASV_165_uh8	*Coriobacteriaceae Collinsella*
	ASV_2st_345	*Lachnospiraceae Blautia*
	ASV_623_3r0	*Coriobacteriaceae Collinsella*
	ASV_7s4_sc0	*Sutterellaceae Parasutterella*
	ASV_82p_r33	*Bifidobacteriaceae Bifidobacterium*
	ASV_dx5_pax	*Erysipelotrichaceae Faecalibacillus*
	ASV_e21_cmv	*Erysipelotrichaceae Amedibactrium*
	ASV_e9p_tub	*Lachnospiraceae Blautia*
	ASV_hcf_4f5	*Lachnospiraceae Blautia*
	ASV_hwd_896	*Lachnospiraceae Anaerobutyricum*
	ASV_jbt_n3b	Unclassified *Lachnospiraceae*
	ASV_kaw_sk8	*Ruminococcaceae Ruminococcus*
	ASV_ski_ka3	*Lachnospiraceae Blautia*
Inulin-MSN	ASV_2st_345	*Lachnospiraceae Blautia*
FOS-Fructose	ASV_165_uh8	*Coriobacteriaceae Collinsella*
	ASV_2st_345	*Lachnospiraceae Blautia*
	ASV_82p_r33	*Bifidobacteriaceae Bifidobacterium*
	ASV_dx5_pax	*Erysipelotrichaceae Faecalibacillus*
	ASV_e9p_tub	*Lachnospiraceae Blautia*
	ASV_hcf_4f5	*Lachnospiraceae Blautia*
	ASV_hwd_896	*Lachnospiraceae Anaerobutyricum*
	ASV_jbt_n3b	Unclassified *Lachnospiraceae*
	ASV_ski_ka3	*Lachnospiraceae Blautia*
FOS-MSN	ASV_2st_345	*Lachnospiraceae Blautia*
Fructose-MSN	ASV_2st_345	*Lachnospiraceae Blautia*
	ASV_2ua_io6	*Bacteroidaceae Phocaeicola*

ASV_s62_9ct	*Lachnospiraceae Blautia*
ASV_sj9_cdm	*Ruminococcaceae Ruminococcus*

Supplementary Table 2. D-labeled and unlabeled cells measured during RACS for each donor after inulin supplementation. Total number of cells sorted and colonies recovered are shown. Recovery represents the percentage of colonies recovered from the labeled cells.

	Donors										
	7	**8**	**9**	**10**	**11**	**12**	**13**	**14**	**15**	**16**	**17**
D-labeled	76	91	28	81	30	77	24	33	74	11	182
Unlabeled	56	37	31	53	9	29	3	13	14	27	45
Total	132	128	59	134	39	106	27	46	88	38	227
Labeled (%)	57%	71%	47%	60%	76%	72%	88%	71%	84%	29%	80%
Colonies recovered (n)	11	6	4	19	4	4	0	7	12	0	5
Recovery (%)	14.4%	6.6%	14.3%	23.4%	13.3%	5.2%	0%	21.2%	16.2%	0%	2.7%

Supplementary Table 3. Characteristics of isolates for each donor after inulin supplementation. Percentage of inulin used (detected concentration/starting concentration × 100) as determined by the fructan assay, and the degree of polymerization evaluation performed with thin layer chromatography (TLC) is shown. 13+ indicates that the TLC resolving limit is degree of polymerization (DP) 13. Monosaccharide concentration was measured with the fructan assay, and the type of monosaccharide released was determined by TLC. Growth capability on rich media YCFA supplemented with glucose, inulin or no addition of sugars is shown. Maximum OD600 detected in liquid culture during growth in inulin media is shown.

Strains	Donor	Inulin used (%)	DP range	Monosaccharide detected by fructan assay mg/ml	Monosaccharides detected by TLC	Growth on YCFA+ G[£]	Growth on YCFA+ IN[$]	Growth on YCFA NA*	Max OD_{600} YCFA IN	Max OD_{600} YCFA NA
Alistipes indistinctus	7	26.05	4-13+	0.2	glucose	+	+	+/-	0.2	0.05
Enterococcus faecium	7	43.5	4-13+	0.2	glucose	+	+	+/-	0.15	0.1
Eggerthella lenta	7	29.3	4-13+	0.2	glucose	+	+	+	0.1	0.04
Phocaeicola vulgatus	8	38.4	3-13+	0.3	glucose	+	+	-	0.3	0.08
Parabacteroides distasonis	8	30.5	4-13+	0.2	glucose	+	+	-	0.6	0.17
Bifidobacterium longum	8	84	5-13+	0.3	glucose, fructose	+	+	+	0.17	0.13
Alistipes onderdonkii	8	5.3	6-13+	0.5	-	+	+	+	0.18	0.24
Alistipes finegoldii	9	28.8	5-13+	0.4	glucose	+	+	+/-	0.1	0.08
Eggerthella lenta	9	39.8	5-13+	0.5	-	+	+	+/-	0.09	0.05
Phocaeicola dorei	9	24.7	4-13+	0.14	glucose	+	+	+	0.1	0.02
Ruminococcus bicirculans	9	45	4-13+	0.05	fructose	+	+	+/-	0.15	0.005
Bifidobacterium pseudocatenulatum	10	59.6	4-13+	0	fructose	+	+	-	0.06	0.03
Eggerthella lenta	10	41.3	5-13+	0	fructose	+	+	+/-	0.09	0.05
Bifidobacterium longum	10	65.9	4-13+	0.07	-	+	+	+/-	0.08	0.05
Gordonibacter pameleae	10	38.1	4-13+	0.16	glucose	+	+	+/-	0.05	0.04
Alistipes shahii	10	32.4	4-13+	0.01	-	+	+	+/-	0.13	0.09
Bacteroides thetaiotaomicron	11	30.4	5-13+	0	-	+	+	-	0.06	0.005
Eggerthella lenta	11	24.8	5-13+	0	-	+	+	+/-	0.05	0.03
Weisella confusa	12	0.1	5-13+	0.08	-	+	+	-	0.09	0.03
Eggerthella lenta	12	51.8	4-13+	0.08	fructose	+	+	-	0.07	0.05
Phocaeicola vulgatus	12	9.4	5-13+	0.47	-	+	+	+/-	0.05	0.01
Gordonibacter faecihominis	14	33.5	4-13+	0.007	glucose	+	+	+/-	0.08	0.03
Eggerthella lenta	14	33	4-13+	0	glucose	+	+	+/-	0.07	0.03
Bifidobacterium adolescentis	15	59.3	4-13+	0.93	fructose	+	+	+	0.4	0.15
Bifidobacterium animalis	15	7.8	4-13+	0	fructose	+	+	+	0.02	0.02
Bifidobacterium adolescentis	17	48.5	6-13+	0	fructose	+	+	+/-	0.2	0.1
Alistipes indistinctus	17	32	6-13+	0	-	+	+	+/-	0.07	0.005
Gordonibacter urolithinfaeciens	17	37.8	4-13+	0	glucose	+	+	+/-	0.07	0.02

Legend: [£] YCFA-glucose, [$]YCFA-inulin,[*]YCFA-no amendment, + positive growth, - negative growth

Supplementary Table 4. ANI genome comparisons. Average Nucleotide Identity (ANI) comparisons were calculated between *E. lenta 6.2, G. urolithinfaciens AL-11* and reference genomes deposited in NCBI. Average nucleotide identity (ANI) comparison of isolates 6.2 and AL-11 confirmed their assignment to strains of *E. lenta* (98.34% ANI to the type strain *E.lenta 1899 B*/DSM 2243) within the genus Eggerthella, and *G. urolithinfaciens* (98.69% ANI to the type strain *G. urolithinfaciens* DSM 27213) within the genus *Gordonibacter*, respectively.

Comparison for *E.lenta* 6.2	**OrthoANI u-value (%)**
Eggerthella lenta GCA_000024265.1	98.34
Eggerthella sinensis CGA_003339815.1	84.24
Eggerthella guodeyninii GCA_009834925.2	88.26
Eggerthella timoniensis GCA_900184265.1	87.07
Comparison for *Gordonibacter* AL-11	
Gordonibacter pameleae GCA_000210055.1	92.95
Candidatus Gordonibacter avicola GCA_019113915.1	79.75
Gordonibacter urolithinfaciens GCA_902386185.1	98.69
Gordonibacter massiliensis GCA_902386835.1	85.23

Supplementary Table 5. D-labeled and unlabeled cells measured during RACS for each donor after XOS supplementation. Total number of cells sorted and colonies recovered are shown. Recovery represents the percentage of colonies recovered from the labeled cells.

	Donors					
	18	**19**	**20**	**21**	**22**	**23**
D-labeled	26	8	4	8	14	1
Unlabeled	360	29	154	91	102	118
Total	386	37	158	99	116	119
Labeled (%)	6.7%	21.6%	2.5%	8%	12%	0.84%
Colonies recovered (n)	25	8	1	8	11	1
Recovery (%)	96.1%	100%	25%	100%	78.5%	100%

Supplementary Table 6. Isolate characteristics for each donor after XOS supplementation. Maximum OD600 detected in liquid culture during growth in XOS compared to the medium without addition of sugars is shown.

Strains	**Donor**	**Max OD_{600} YCFA XOS**	**Max OD_{600} YCFA NA**
Bifidobacterium longum	18	0.45	0.02
Bifobacterium faecale	18	0.41	0.04
Bifidobacterium adolescentis	18	0.51	0.07
Collinsella aerofaciens	18	0.32	0.06
Bifidobacterium spp.	18	0.31	0.05
Bifidobacterium longum	19	0.27	0.03
Bifobacterium faecale	19	0.29	0.15
Bifidobacterium adolescentis	19	0.33	0.04
Bifidobacterium longum	21	0.30	0.23
Bifobacterium faecale	21	0.29	0.04
Collinsella aerofaciens	21	0.29	0.03
Bifobacterium faecale	22	0.25	0.02
Bifidobacterium adolescentis	22	0.38	0.28
Bifidobacterium longum	23	0.40	0.10

Supplementary material chapter 2

Supplementary figures 1 – 9

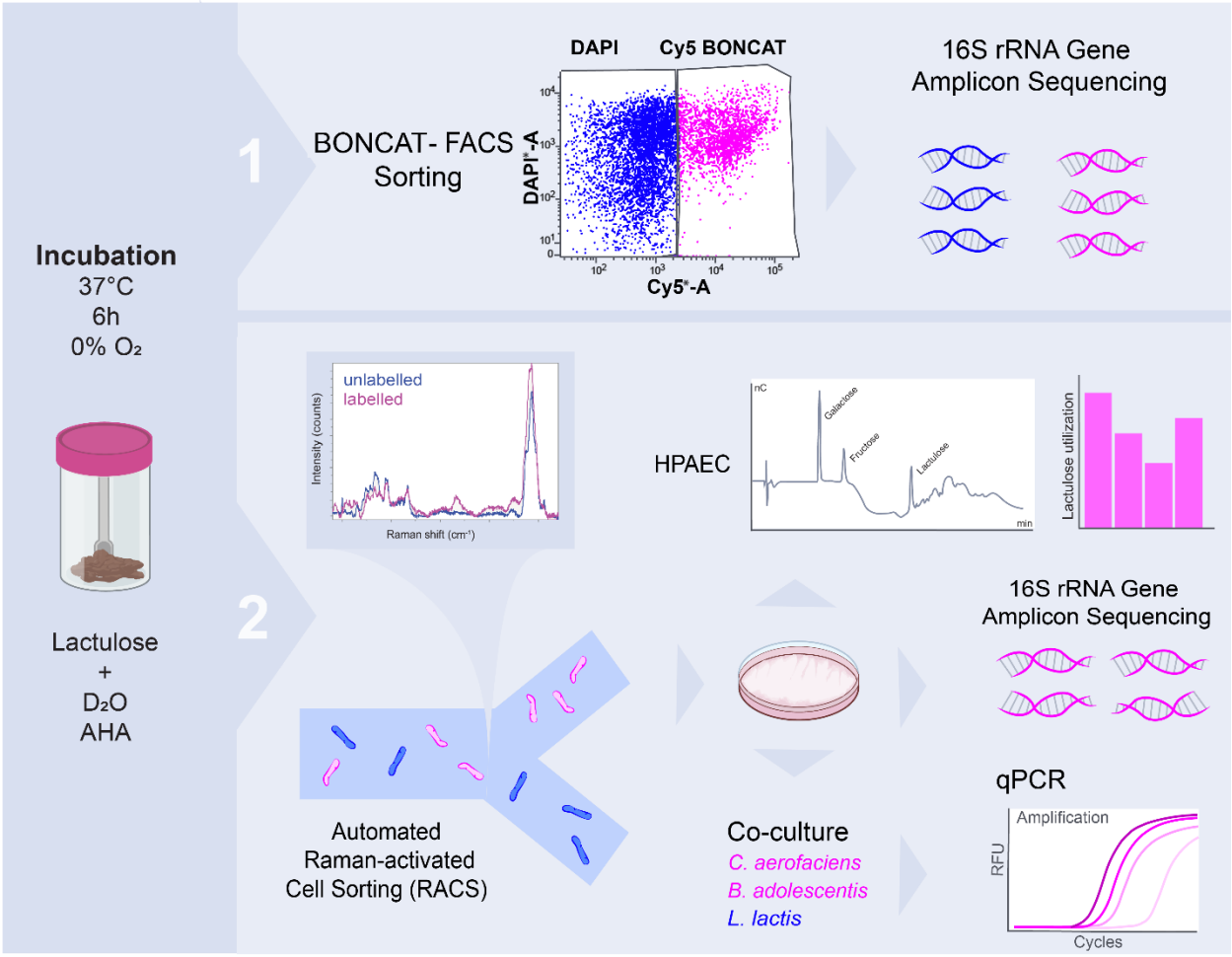

Supplementary Figure 1. Outline of experiments and analyses. Fresh fecal samples were anaerobically incubated with lactulose of its component monosaccharides as well as the cellular activity markers D_2O and L-azidohomoalanine (AHA). Bioorthogonal non-canonical amino acid tagging coupled with fluorescence-activated cell sorting (BONCAT-FACS) was used to detect metabolically active and inactive cells by 16S rRNA gene amplicon sequencing. Raman-activated cell sorting (RACS) was then employed for targeted isolation of active cells, which were subsequently identified by 16S rRNA gene amplicon sequencing and whose lactulose degradation capability was determined by high-performance anion-

exchange chromatography (HPAEC). Coculture experiments with *Collinsella aerofaciens*, *Bifidobacterium adolescentis*, and *Lactococcus lactis* were conducted, and qPCR was used to monitor growth.

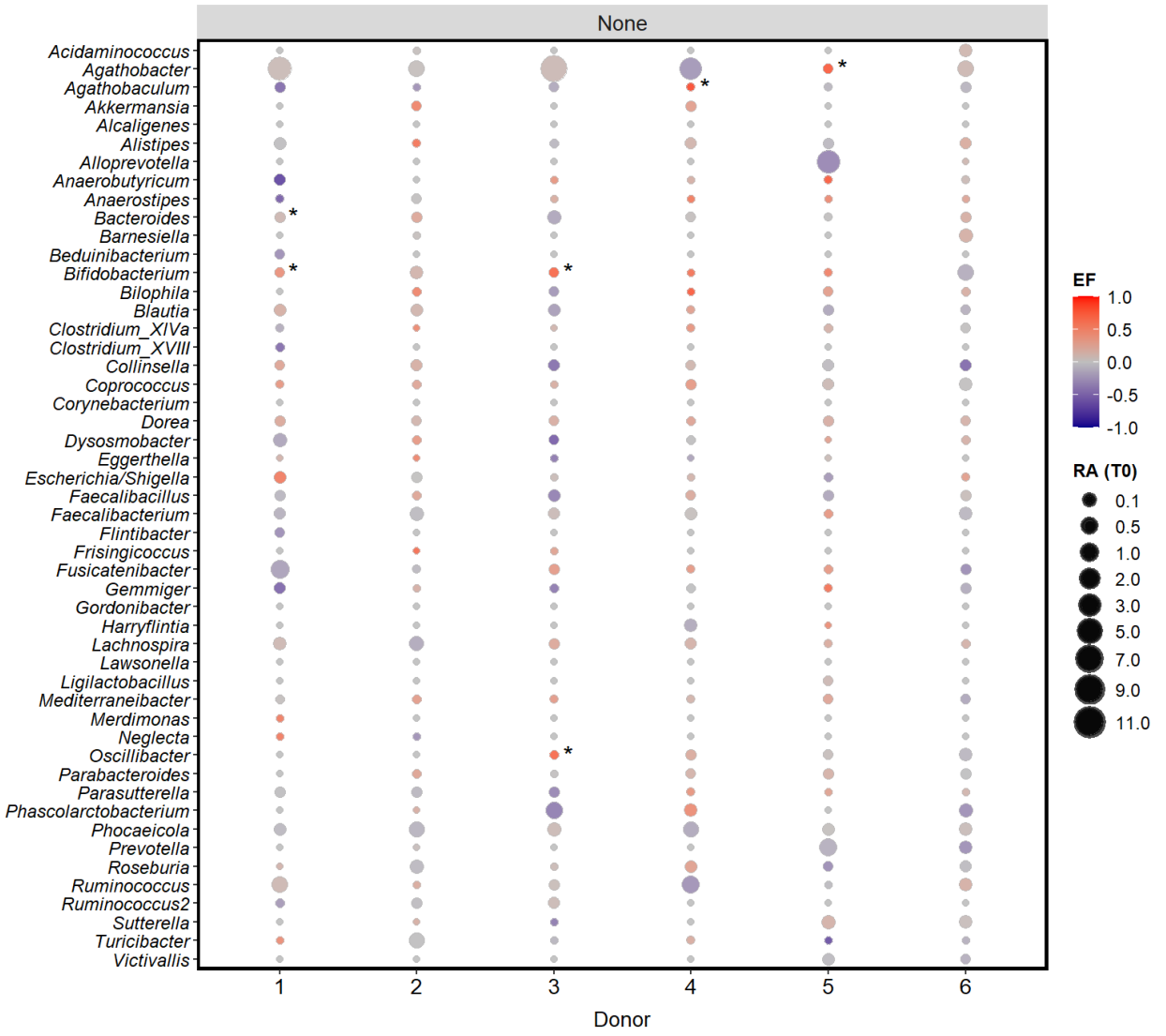

Supplementary Figure 2. No amendment control. Change in relative abundance of abundant bacterial genera after 6 h incubation in no amendment samples. Bubble size indicates relative abundance (RA) at 0h. The change in relative abundance during incubation, calculated as a normalized and scaled enrichment factor (EF), is indicated by bubble color. Genera significantly enriched in individual donors are marked with an asterisk and those significantly enriched across all six donors (as determined with DESeq2) are outlined in black.

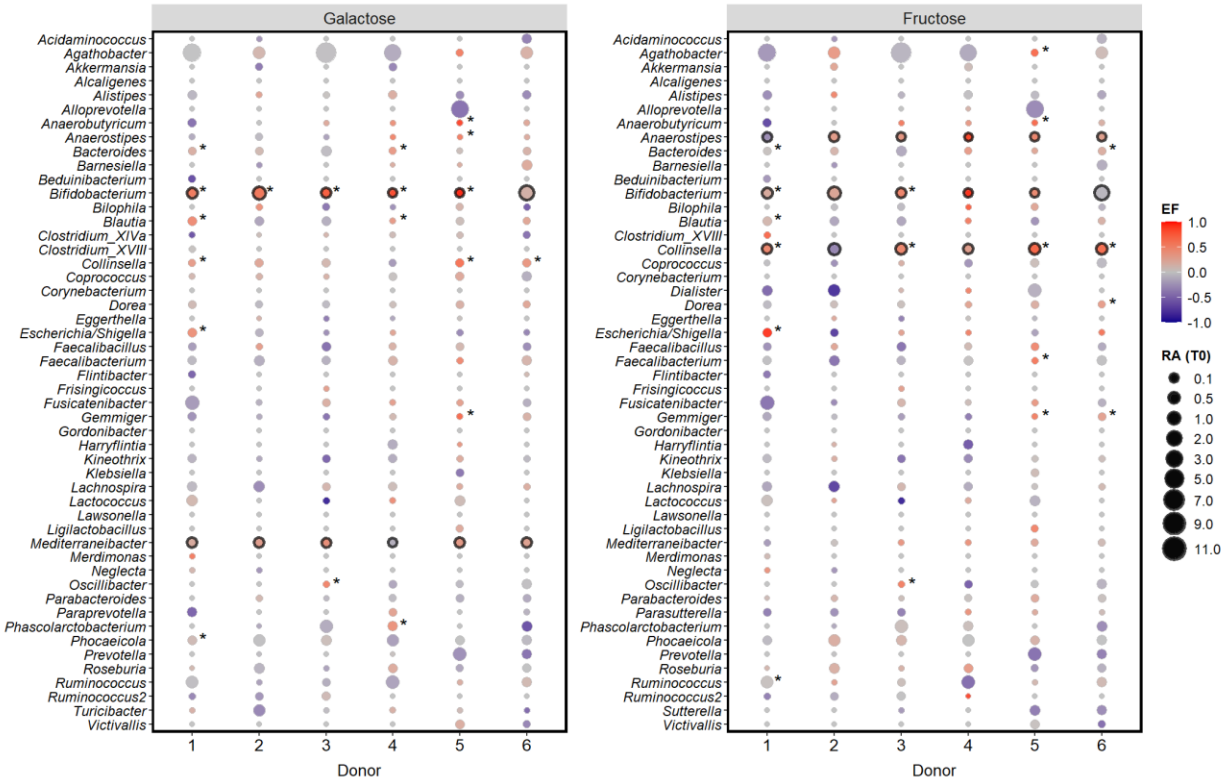

Supplementary Figure 3. Incubation with galactose and fructose. Change in relative abundance of abundant bacterial genera after 6 h incubation in galactose- and fructose-amended samples. Bubble size indicates relative abundance (RA) at 0h. The change in relative abundance during incubation, calculated as a normalized and scaled enrichment factor (EF), is indicated by bubble color. Genera significantly enriched in individual donors are marked with an asterisk and those significantly enriched across all six donors (as determined with DESeq2) are outlined in black.

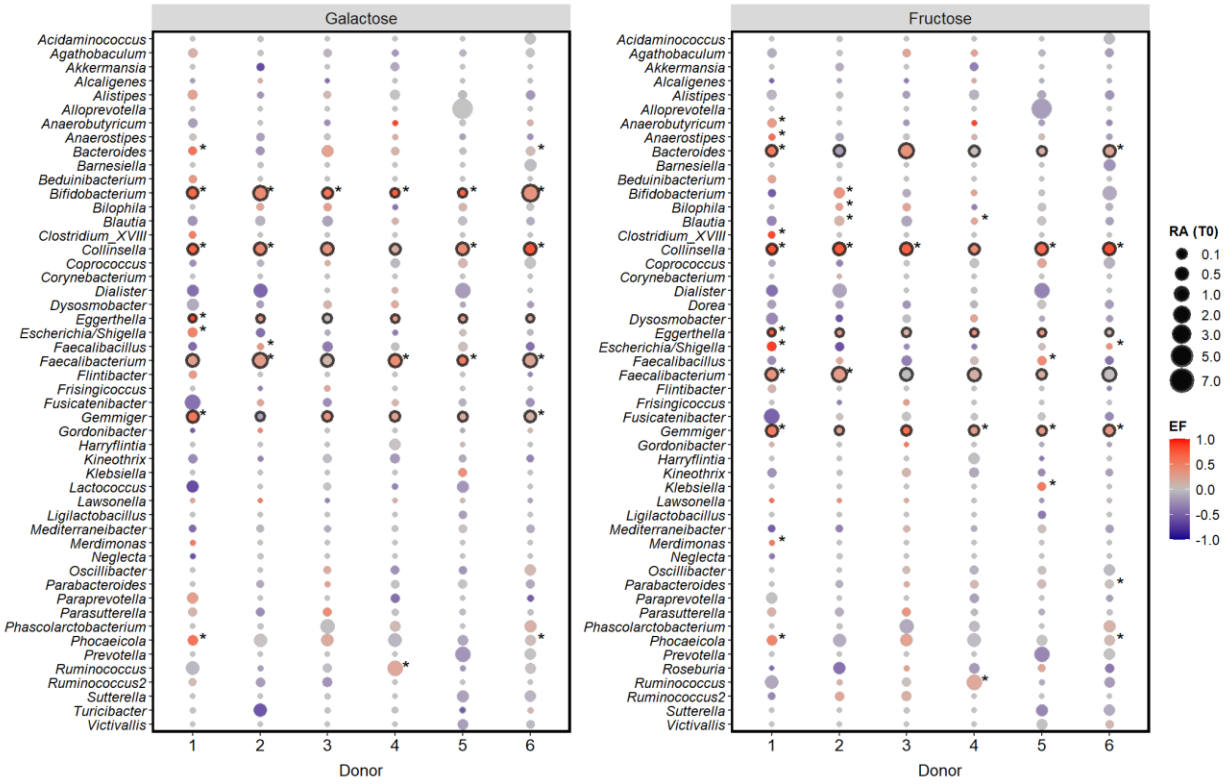

Supplementary Figure 4. Identification of translationally-active cells. Change in relative abundance of abundant bacterial genera after 6 h incubation in galactose- and fructose-amended samples. Bubble size indicates relative abundance (RA) at 0h. The difference in relative abundance of each genus between BONCAT-positive FACS-sorted cells of lactulose-amended samples and BONCAT-negative FACS-sorted cells of no amendment samples after 6 h incubation was calculated as a normalized and scaled enrichment factor (EF; see Materials and Methods) and is indicated by bubble color. Genera significantly enriched in individual donors are marked with an asterisk and those significantly enriched across all six donors (as determined with DESeq2) are outlined in black.

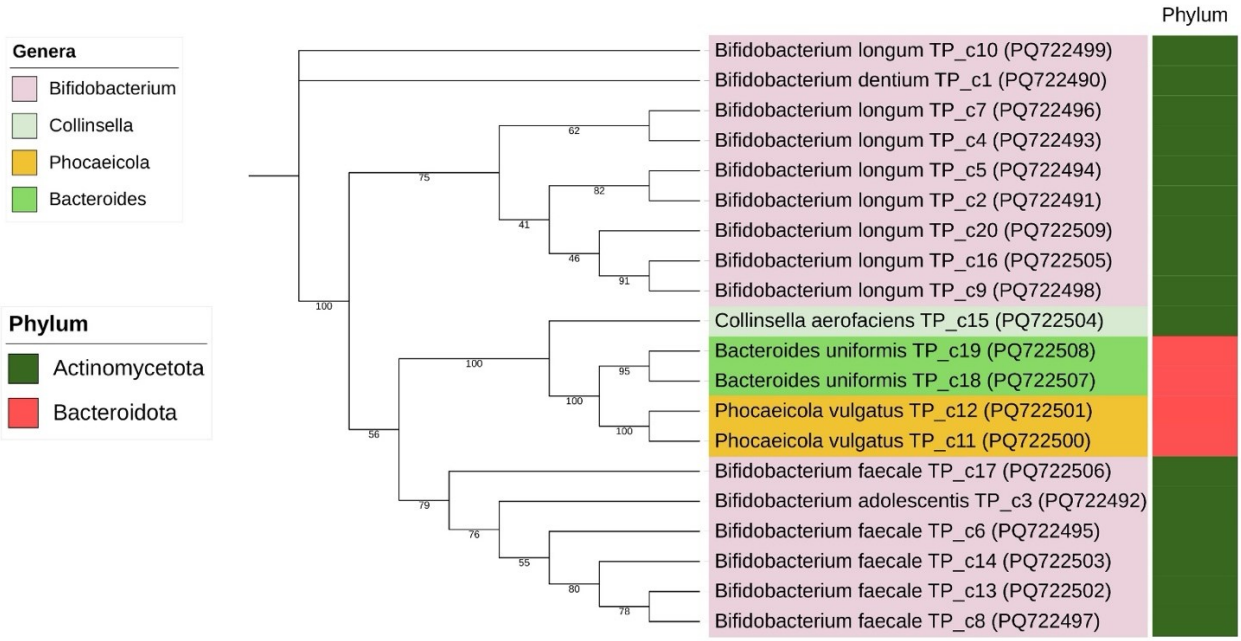

Supplementary Figure 5. Isolation of Lactulose-Utilizing Bacteria Using Direct Plating on YCFA-Lactulose Agar Plates. Phylogenetic tree showing the bacterial strains isolated from two fresh fecal samples grown on YCFA lactulose agar plates for 24 hours. The phylogenetic tree was constructed using the maximum likelihood algorithm in IQ-TREE and rooted at the mid-point, with branch support evaluated using 1000 ultrafast bootstrap replicates. The aligned sequences were used to generate the tree, which was then visualized and annotated in iTOL. Colonies were identified through colony PCR and Sanger sequencing.

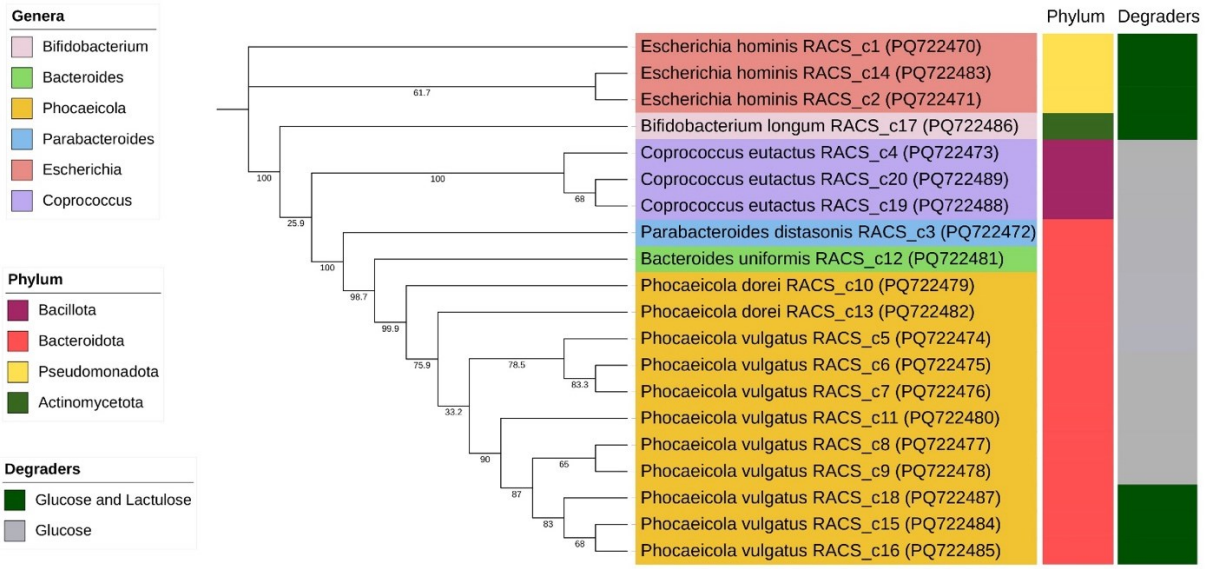

Supplementary Figure 6. Random Sorting by RACS. A random sorting experiment was used to capture all bacterial cells in the sample, regardless of their activity. Sorted cells were grown on YCFA Glucose agar plates and subsequently transferred to YCFA Lactulose agar to assess lactulose degradation. Green bars indicate strains capable of growing on both YCFA Glucose and YCFA Lactulose (lactulose degraders), while gray bars represent strains that failed to grow on lactulose. The phylogenetic tree was constructed using the maximum likelihood algorithm in IQ-TREE and rooted at the mid-point, with branch support evaluated using 1000 ultrafast bootstrap replicates. The aligned sequences were used to generate the tree, which was then visualized and annotated in iTOL.

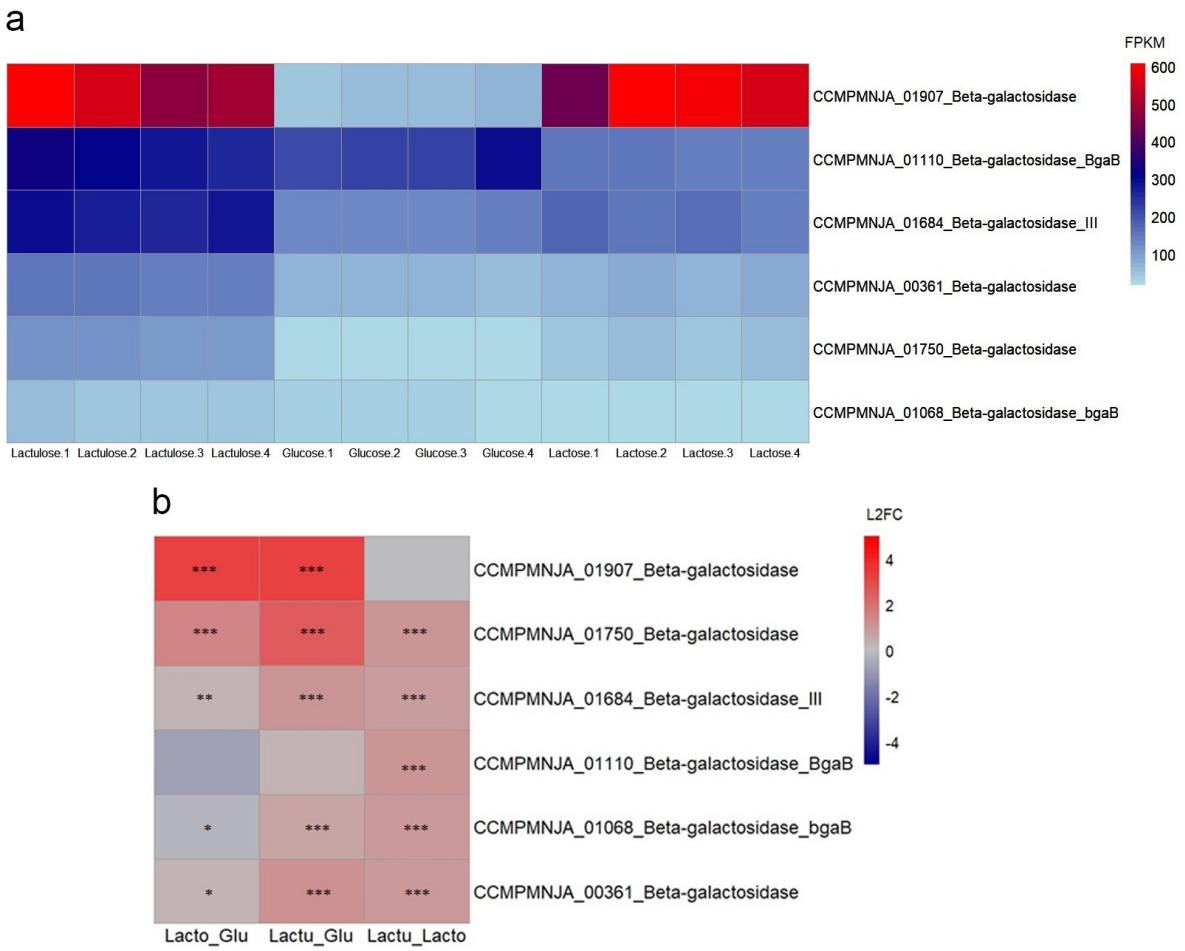

Supplementary Figure 7. Differential Expression of β-galactosidase Genes (a) Expression Levels of β-galactosidase Genes in *Bifidobacterium adolescentis* Under Lactulose, Lactose, and Glucose Conditions. Heatmap showing the expression levels (FPKM) of β-galactosidase genes in *B.adolescentis* grown in MRS media supplemented with Lactulose, Lactose, and Glucose. The x-axis represents four technical replicates for each condition. (b) Log2 fold change (L2FC) of β-galactosidase gene expression in *B. adolescentis* across three comparisons: Lactose vs Glucose (Lacto_Glu), Lactulose vs Glucose (Lactu_Glu), and Lactulose vs Lactose (Lactu_Lacto). Red indicates upregulation, while blue indicates downregulation. Asterisks denote significant changes based on the **Wald test (DESeq2)** (*** $p < 0.05$, ** $p < 0.01$, *** $p < 0.001$, n= 4).

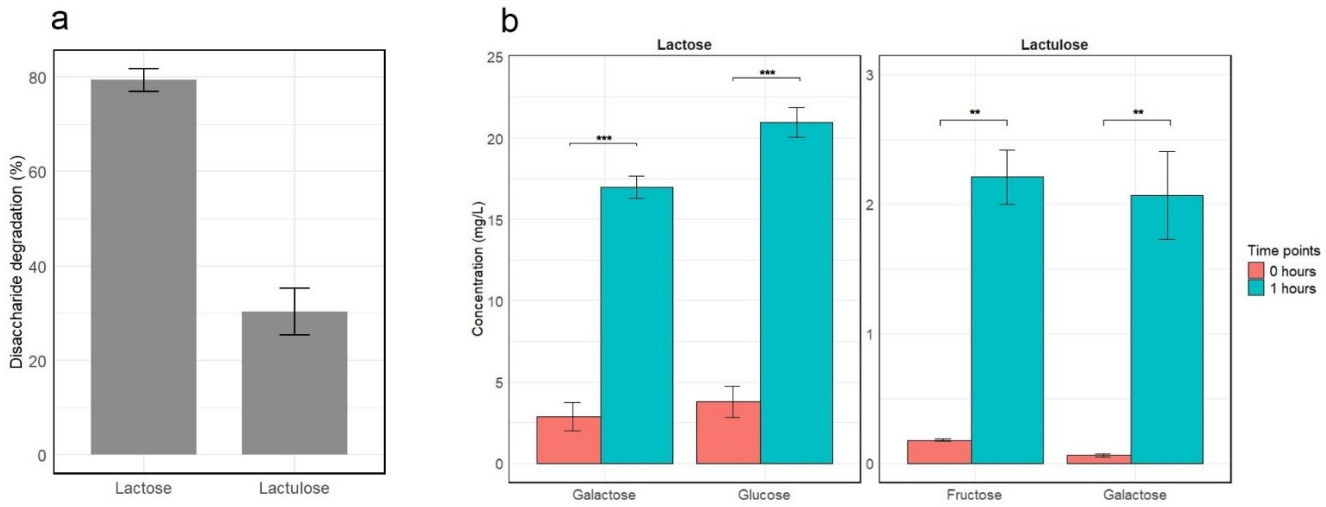

Supplementary Figure 8. Evaluation of β-galactosidase activity. (a) Percentage of lactose and lactulose degraded after 1 hour of incubation with commercial beta-galactosidase. (b) Detection of Monosaccharides hydrolyzed from lactose and lactulose by beta-galactosidase activity. The concentration of monosaccharides released after 1 hour of incubation with beta-galactosidase for lactose (left panel) and lactulose (right panel). The x-axis shows the detected monosaccharides (Galactose, Glucose, and Fructose), while the y-axis represents their concentration (mg/L). Red bars indicate 0 hours, and blue bars represent the values after 1 hour of incubation. A significant increase in glucose and galactose concentrations of lactose (Student's t-test, $p < 0.001$, $n = 6$) and in fructose and galactose concentrations of lactulose (Student's t-test, $p < 0.01$, $n = 6$) is indicated by asterisks.

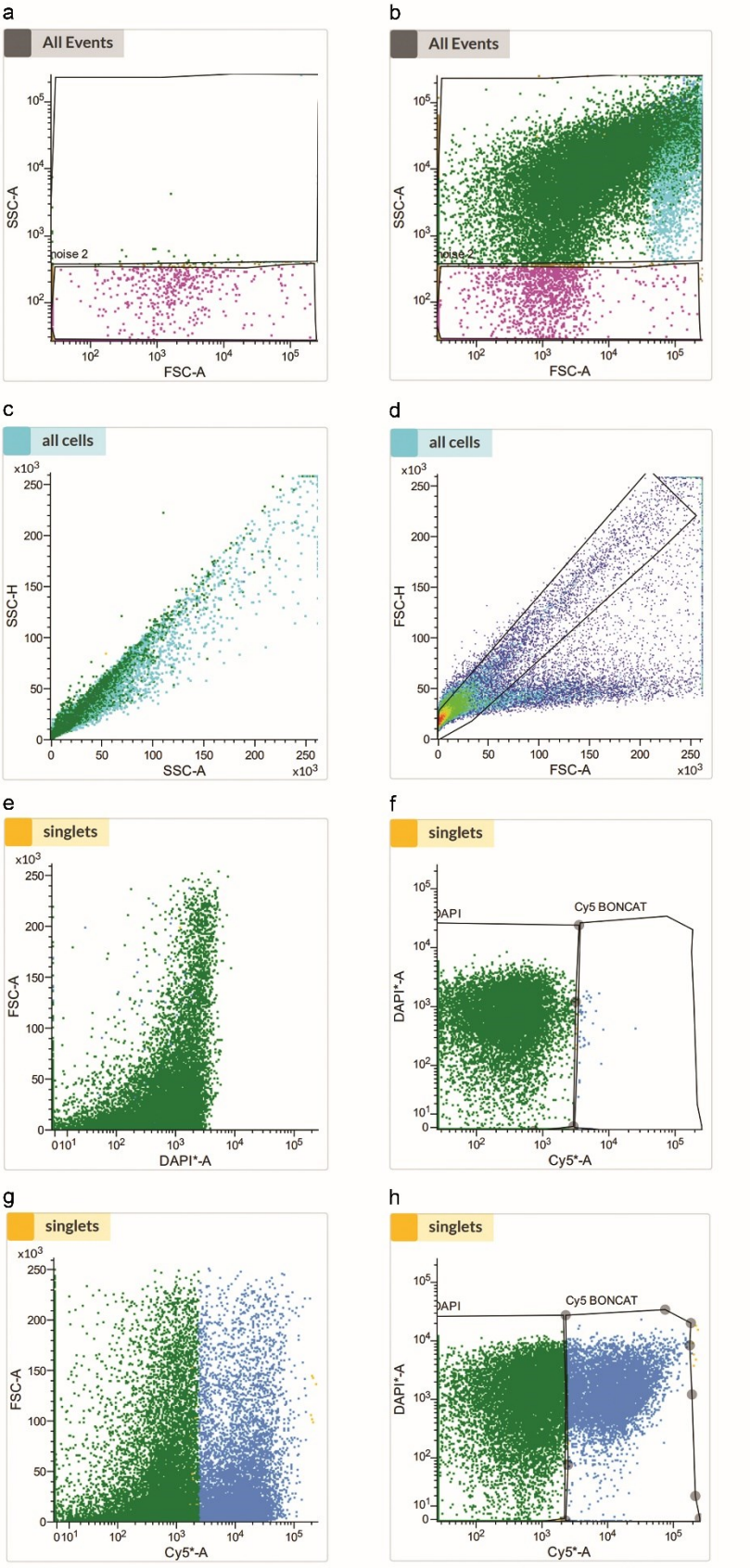
a
All Events
SSC-A
FSC-A
b
All Events
SSC-A
FSC-A
c
all cells
SSC-H
SSC-A
d
all cells
FSC-H
FSC-A
e
singlets
FSC-A
DAPI*-A
f
singlets
Cy5 BONCAT
DAPI*-A
Cy5*-A
g
singlets
FSC-A
Cy5*-A
h
singlets
Cy5 BONCAT
DAPI*-A
Cy5*-A

Supplementary Figure 9. **The full gating strategy** (a) All event: PBS blank sample. Forward scatter (FSC-A) vs. side scatter (SSC-A) plot of 1× PBS blank sample used to define background signal and set the threshold for debris exclusion. This control was used to gate out non-cellular noise from downstream cell sorting. (b) All event: sample, - DAPI, - AHA. A plot of a control sample without AHA and without DAPI staining, used to define the distribution of particles based on size and granularity and to identify background debris. (c–d) All cells: sample, - DAPI, - AHA. Doublet discrimination strategy using side and forward scatter properties of the control sample. (c) Side scatter area (SSC-A) vs. side scatter height (SSC-H) and (d) forward scatter area (FSC-A) vs. forward scatter height (FSC-H) plots were used to identify and exclude doublets. Events falling along the diagonal lines in plot were gated as single cells based on their proportional scatter signal profiles. (e–f) Singlets: sample, + DAPI, - AHA. Parent population gating strategy using control samples lacking AHA labeling. (e) Cells were visualized in a forward scatter area (FSC-A) vs. DAPI area (DAPI-A) plot to identify nucleic acid-containing events. (f) The same population was then plotted by DAPI*-A vs. Cy5*-A fluorescence, confirming the absence of BONCAT signal (Cy5-negative), which served as a baseline for setting the BONCAT-positive gate in AHA-treated samples. (g–h) Singlets: sample, + DAPI, + AHA. Gating strategy for BONCAT-labeled samples. Cells were incubated with AHA and labeled with Cy5 and DAPI to identify translationally active cells. (g) Cells were gated based on Cy5 fluorescence intensity (FSC-A vs. Cy5-A) to distinguish BONCAT-positive (blue) and BONCAT-negative (green) subpopulations. (h) A DAPI vs. Cy5-A plot was used to confirm DNA content and help separate active ($Cy5^{+}$) from inactive ($Cy5^{-}$) cells more clearly.

Supplementary material chapter 3

Supplementary figures 1 – 7

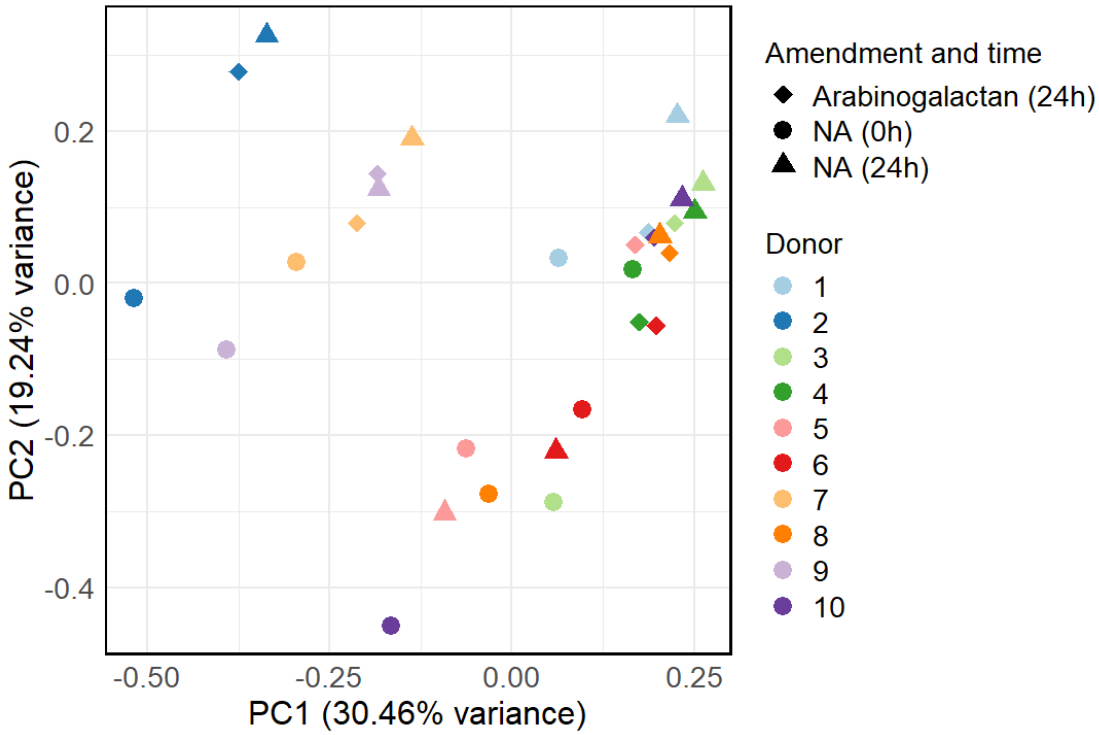

Supplementary Figure 1. Principal coordinate analysis (PCoA) ordination of genus-level microbiome profiles showing clustering of samples incubated with Arabinogalactan for 24 hours, compared to no amendment (NA) samples at 0 and 24 hours. Color and shape indicate donor identity and treatment condition, highlighting both individual and treatment-related differences.

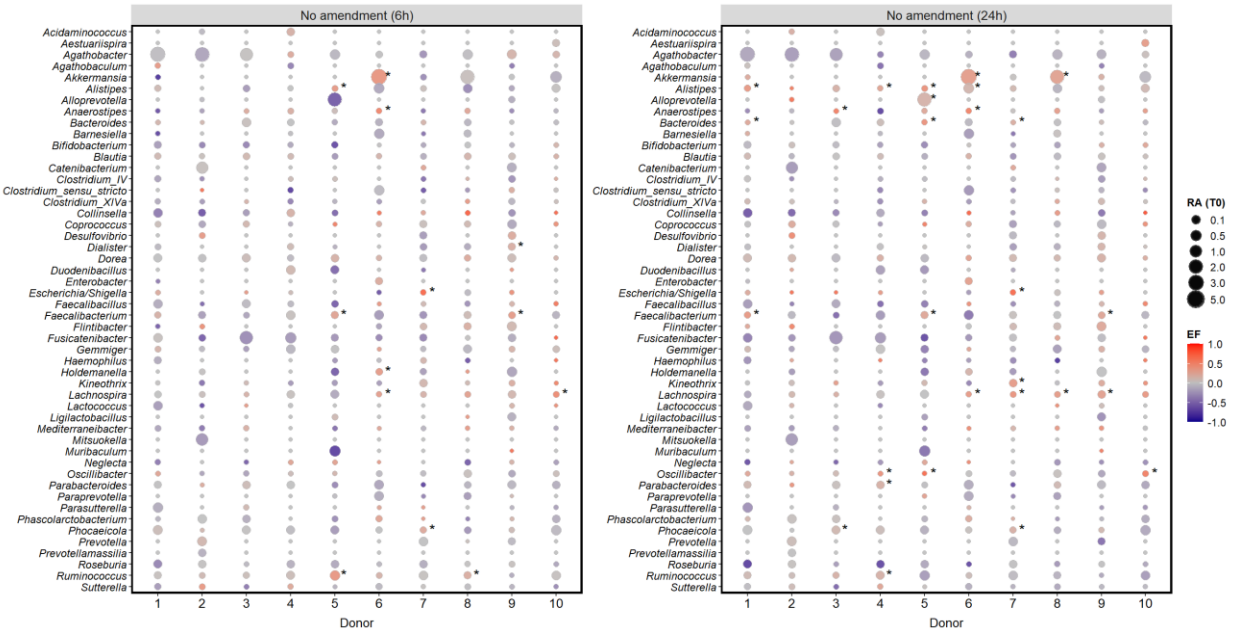

Supplementary Figure 2. No amendment controls (NA). Enrichment patterns of dominant bacterial genera after 6 and 24 h incubation in no amendment. Bubble size indicates the relative abundance at 0 h, and color indicates the scaled enrichment factor (EF), as described in the Materials and Methods section. Genera with significant enrichment in individual donors are indicated by an asterisk, while those consistently enriched across all donors are highlighted with a black outline (DESeq2, Wald Test p.adj < 0.05, n = 30 samples).

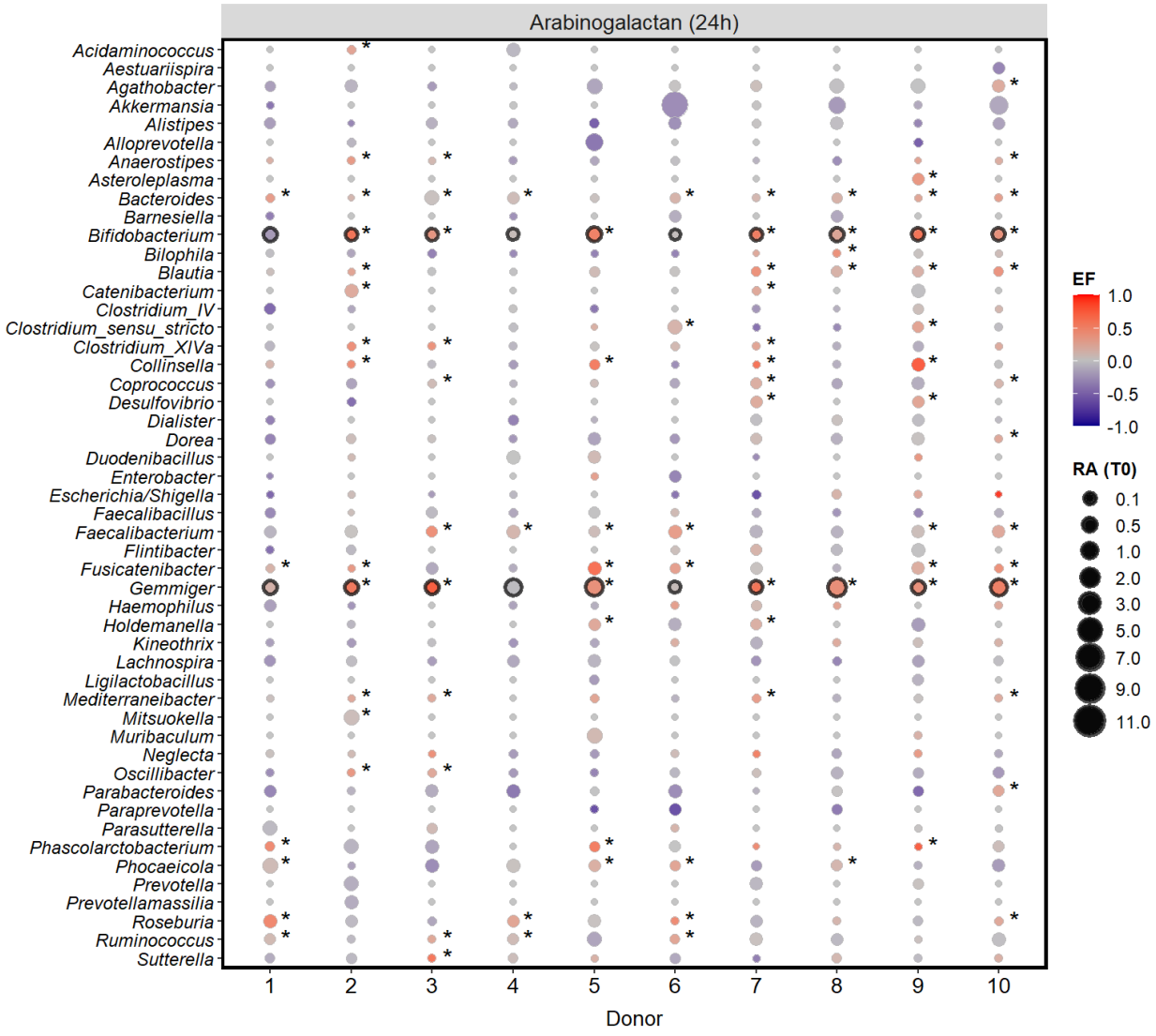

Supplementary Figure 3. Enrichment patterns of dominant bacterial genera after 24 h incubation with arabinogalactan. Bubble size indicates the relative abundance at 0 h, and color indicates the scaled enrichment factor (EF), as described in the Materials and Methods section. Genera with significant enrichment in individual donors are indicated by an asterisk, while those consistently enriched across all donors are highlighted with a black outline (DESeq2, Wald Test p.adj < 0.05, n = 30 samples).

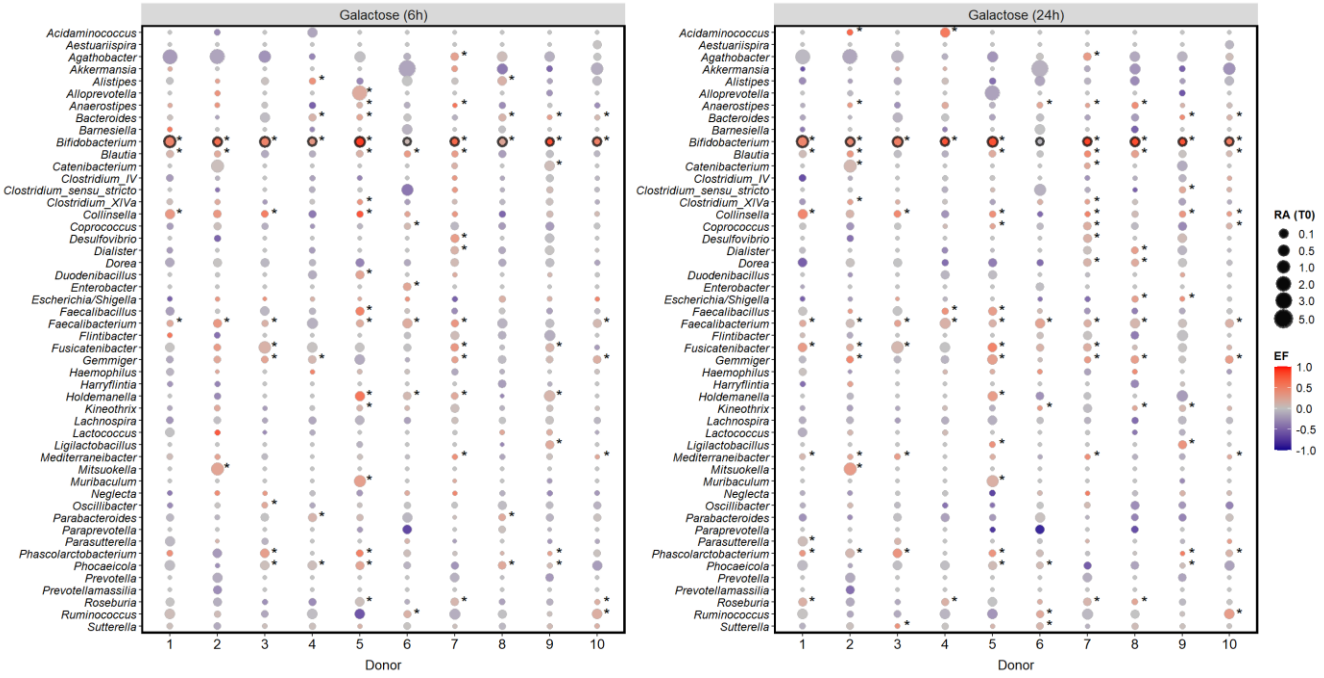

Supplementary Figure 4. Enrichment patterns of dominant bacterial genera after 6 and 24 h incubation with galactose. Bubble size indicates the relative abundance at 0 h, and color indicates the scaled enrichment factor (EF), as described in the Materials and Methods section. Genera with significant enrichment in individual donors are indicated by an asterisk, while those consistently enriched across all donors are highlighted with a black outline (DESeq2, Wald Test p.adj < 0.05, n = 30 samples).

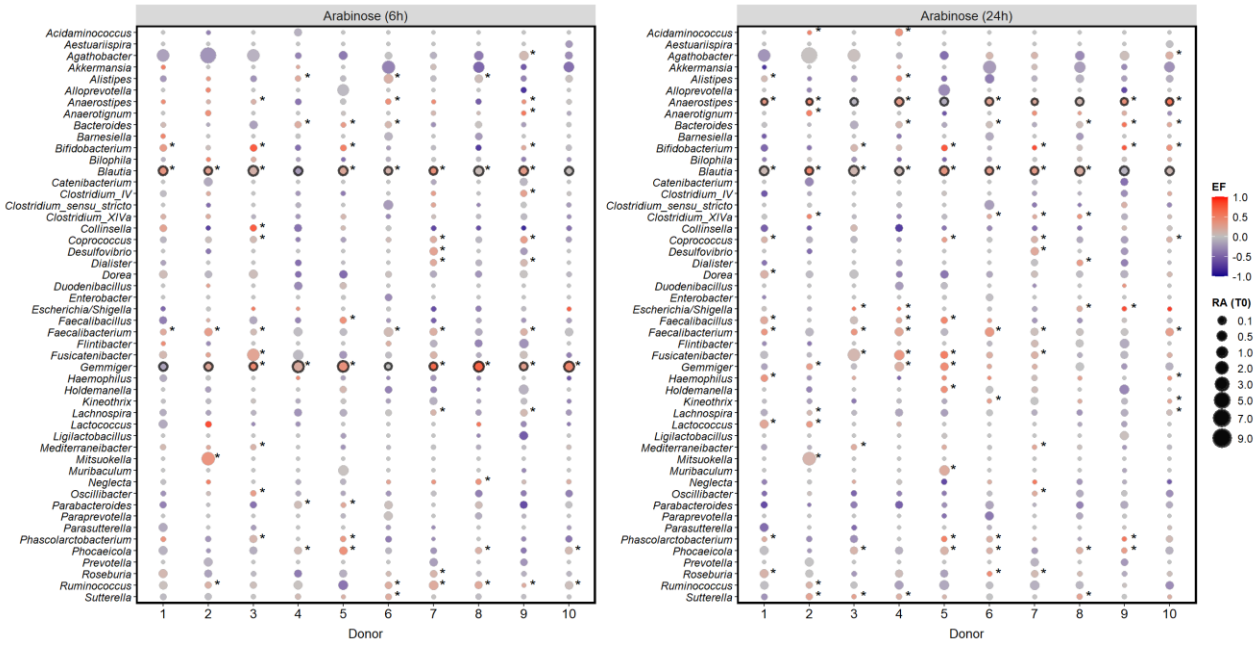

Supplementary Figure 5. Enrichment patterns of dominant bacterial genera after 6 and 24 h incubation with arabinose. Bubble size indicates the relative abundance at 0 h, and color indicates the scaled enrichment factor (EF), as described in the Materials and Methods section. Genera with significant enrichment in individual donors are indicated by an asterisk, while those consistently enriched across all donors are highlighted with a black outline (DESeq2, Wald Test p.adj < 0.05, n = 30 samples).

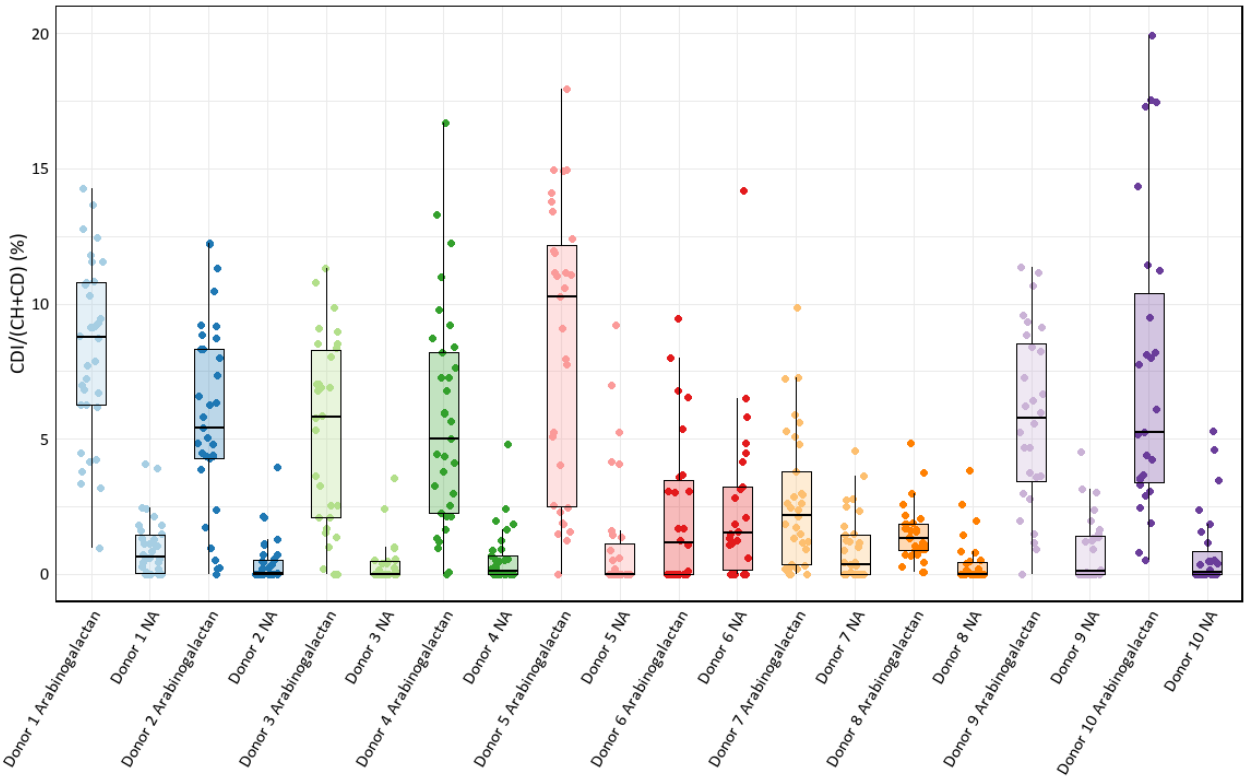

Supplementary Figure 6. Single-cell analysis of microbial metabolic activity in response to arabinogalactan. The percentage of deuterium incorporation (%CD) was measured in individual cells following 24 h incubation with D_2O, with or without arabinogalactan. The dots indicate single-cell measurements collected from each ten donors, while boxplots illustrate the spread of %CD values across conditions. Statistical testing across all donors revealed a significant increase in microbial metabolic activity following arabinogalactan treatment (ANOVA, $p<0.001$, $n=611$).

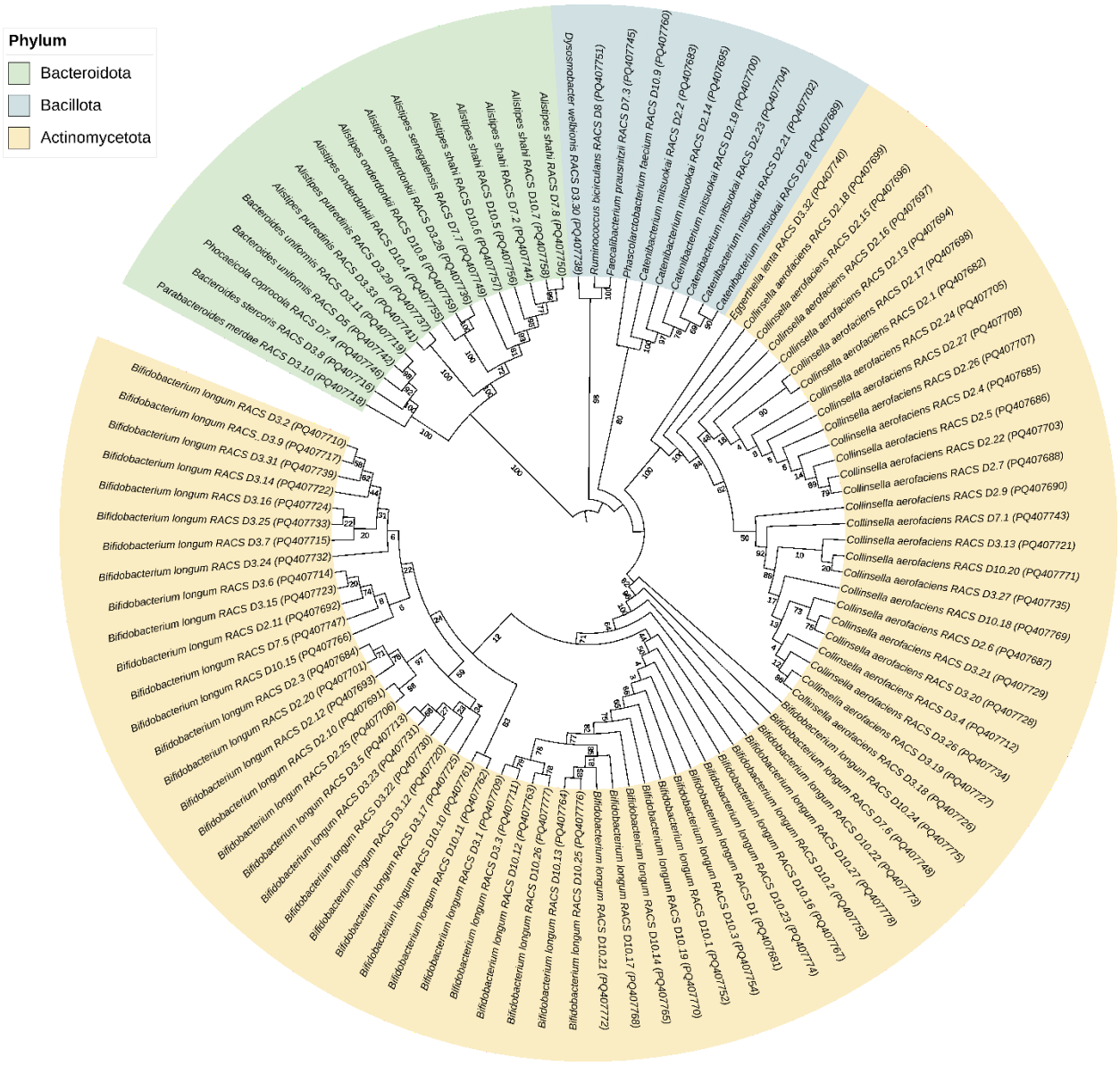

Supplementary Figure 7. Phylogenetic characterization of metabolically active cells sorted by RACS. Phylogenetic tree of 98 bacterial strains isolated using Raman-activated cell sorting (RACS) following 6 hours incubation with D_2O and Arabinogalactan. Isolates were classified based on near-full-length 16S rRNA gene sequencing and represent 16 species spanning three phyla: Actinomycetota (n = 72), Bacteroidota (n = 16), and Bacillota (n = 10). The phylogenetic tree was generated using the maximum likelihood algorithm in IQ-TREE, rooted at the midpoint, and branch support was calculated using 1000 ultrafast bootstrap replicates. Tree visualization and annotation were performed using iTOL, with phylum-level taxonomy indicated by branch color.

Supplementary table S1

Donor	1	2	3	4	5	6	7	8	9	10
Total analyzed cells (n)	821	798	239	174	182	843	169	548	192	782
D-labeled cells (n)	5	28	63	7	60	25	26	40	24	27
Labeled (%)	0.6	3.5	26.35	4.02	32.96	2.96	15.38	7.29	12.5	3.45
Colonies recovered (n)	1	27	33	0	1	0	8	1	0	27
Recovery rate (%)	20	96.4	52.3	0	1.6	0	30.76	2.5	0	100

Supplementary Table 1. Number of D-labeled and unlabeled cells analyzed during RACS for each donor following AG supplementation. The total number of sorted cells and the number of colonies recovered are shown. The recovery rate indicates the percentage of colonies obtained from the sorted D-labeled cells.